MORPHOLOGICAL AND BIOCHEMICAL CHARACTERIZATION OF REELIN-AMYLOID DEPOSITION IN THE AGING MOUSE BRAIN

Dissertation

zur

Erlangung der naturwissenschaftlichen Doktorwürde
(Dr. sc. nat.)

vorgelegt der

Mathematisch-naturwissenschaftlichen Fakultät

der

Universität Zürich

von

Jana Döhner

aus

Deutschland

Promotionskommitee:

Prof. Dr. Jean-Marc Fritschy (Vorsitz)

PD Dr. Irène Knüsel

Prof. Dr. Stephan Neuhauss

Prof. Dr. Roger M. Nitsch

Zürich, 2011

ACKNOWLEDGEMENTS

I am highly indebted to many people for their invaluable support, guidance and inspirations in successfully accomplishing my PhD work.

First I would like to sincerely thank PD. Dr. Irène Knuesel for the great opportunity to conduct my PhD in her group under her excellent and fair supervision. Without hesitation you introduced me patiently into the field of neuroscience, in particular in the diverse world of Alzheimer's disease, which has been a completely new subject for me, considering me having a degree in engineering. I highly profited from the confidence you gave me in accomplishing my thesis. Thank you for your intensive encouragement and having your door always open, having time to discuss whenever it was necessary, may it have been of scientific or personally need. Thank you as well for your critical and constructive feedback and the thorough proof-reading of my thesis. I can not imagine a better supervisor.

Further, I would also like to express my gratitude to Prof. Dr. Jean-Marc Fritschy for the opportunity to attend my PhD in his lab. During that time I profited a lot from your expertise in morphology and your great knowledge in any kind of microscopy. Thank you for introducing me in the amazing universe of electron microscopy, I am very grateful of having this chance to learn this kind of technique. Thank you for all the advice and professional support throughout my PhD, and the critical reviewing of my manuscript.

Another thank you goes to the members of my thesis committee, Prof. Dr. Roger M. Nitsch and Prof. Dr. Stephan Neuhauss for their scientific input in our meetings and the discussions about the project.

I would like to show my gratitude to all the people I have been working with in the past years.

First, I am deeply grateful to our mass spectrometric collaborators Dr. Bernd Wollscheid and Thomas Bock. Thanks for introducing me into the field of proteomics and the many discussions how we can improve our experimentations. Thank you for your support and this fruitful collaboration. Special thanks go to Thomas for investing a lot of time in the experimental part and the critical proof-reading and support while writing on this proteomic subject.

I am also indebted to our second collaborator Christel Genoud for her enthusiasm in performing and supporting our ultrastructural project. Without her experience and knowledge, and willingness to contribute to this project, we would not have gained so much insight in the Reelin granular structure.

Special thanks go to Corinne Sidler and Conny Schwerdel for their unlimited assistance and valuable technical support in the lab. You were/are always around and willing to help. Lots of thank yous.

It is a pleasure for me to thank the former and recent members of our "Reelin Group", today's also known as the "Reelin Girls and Dimitrije" (Amrita, Sandra, Prisca, Tina, Claudine, Karin Martina, Abigail, Samira, Mela) for your awesome team work, your continuous encouragement, the many scientific inspirations and your friendships. I learned from all of you in many different ways and the time would have been just half that nice and fun without you. A special Thank You goes to Amrita, who not became just a colleague during these years, but also a very great friend. I highly appreciated your scientific encouragement and introduction in the world of molecular biology. Many thanks as well for the thorough proof-reading of the manuscript. Thank you so much for your inspiring and illimitable friendship.

I would also like to thank my past and present office mates and the entire Fritschy Group for the nice environment, your helpful tips, your openness for scientific questions and discussions as well as your openness for chats about everything except science. It was always very nice to work with you. Thanks for the great time, good company and the pleasant atmosphere. Special thanks go the Rebecca, for being a great colleague as well an appreciable friend. Thanks for the many conversations, scientifically and non-scientifically, throughout your time in the lab and beyond.

Sincere thanks go to my friends for their continuous and unlimited support and friendship throughout the entire time of my PhD. Moreover, I would like to say thank you to my family, for their support and love during that time and letting me always freely choose the directions of my career. Finally I would like to thank my beloved boyfriend Patrick, who supported me in so many ways throughout my PhD. Thanks for always being there, your patience, your endless love and the encouragement to keep me going in times than things were not going the way they were supposed to.

TABLE OF CONTENTS

ZUSAMMENFASSUNG

Reelin ist ein grosses extrazelluläres Matrixprotein, welches essenziell für die korrekte neuronale Positionierung während der embryonalen/neuronalen Entwicklung ist. Dieselbe lipoprotein-vermittelte Signalkaskade reguliert die NMDA Rezeptor vermittelte Neurotransmission und moduliert synaptische Funktionen und Plastizität im adulten Gehirn. Dies geht einher mit der Tatsache, dass eine altersbedingte Reduktion der Reelin Expression zur kognitiven Beeinträchtigungen während des normalen Alterns beiträgt. Neueste experimentelle Erkenntnisse weisen auf die Beteiligung von dysfunktionalem Reelin in pathologischen Formen des Alterns hin, wie sporadische Alzheimer Demenz (AD), welche histopathologisch durch senile Plaques und Neurofibrillen charakterisiert ist. Da das Alter als Hauptrisikofaktor für die AD gilt, wurden die potentiellen Veränderungen in der Reelin Expression während normalem und pathologischem Altern untersucht. Diese Daten zeigten einen äußerst konsistenten altersbedingten Verlust von Reelin-exprimierenden Neuronen, begleitet von einer Anreicherung in extrazellulären Reelin-positiven amyloid-ähnlichen Ablagerungen im Hippokampus verschiedener alternder Spezies. Eine pränatale Immunstimulation durch Injektion der virus-ähnlichen Substanz Polyriboinosin-Polyribocytidil-Säure (PolyI:C) in Wildtyp Mäusen resultierte interessanterweise in früheren, sowie erhöhten und beständigeren Mengen dieser Ablagerungen. Dennoch bleibt der molekulare Mechanismus, durch welchen dieses konservierte extrazelluläre Glykoprotein zur Krankheitsentstehung von AD beiträgt, weitgehend unbekannt.

Das allgemeine Ziel dieser Arbeit war, die morphologischen, ultrastrukturellen und biochemischen Eigenschaften der Reelin Aggregate aufzuklären, um deren Herkunft und Bedeutung im Hinblick auf neurodegenerative Prozess im alternden Gehirn zu ermitteln. Auf diese Weise sollte eine potentielle molekulare Verbindung zwischen einer Reelin-Fehlfunktion und AD-assoziierter Neuropathologie untersucht werden. Dafür wurde zu Beginn ein immunohistochemisches Protokoll entwickelt, welches eine stringente und verlängerte Vorbehandlung mit der Endopeptitase Pepsin beinhaltete, um die Reelin-positiven Strukturen im Hippokampus alternder Wildtyp Mäuse optimal zu detektieren und zu charakterisieren. Diese Methode verbesserte die Reelin-Immunreaktivität (IR) merklich, was deutlich auf einen aggregierten und Protease-resistenten Zustand dieser Ablagerungen hinweist. Darüber hinaus ermöglichte diese Behandlung erstmals den spezifischen Nachweis verschiedener muriner

proteolytischer Amyloid-Precursor Protein (APP) Fragmente in alten Wildtyp Mäusen. Diese Untersuchungen zeigten, dass Reelin sehr selektiv mit fibrillären Amyloid-beta (Aβ) Spezies assoziiert, aber nicht vollständig co-lokalisiert ist. Auf der anderen Seite zeigten oligomere Aβ-Ablagerungen eine hohe Co-Lokalisationsrate mit Reelin, welches vorangegangene Untersuchungen mit transgenen AD-Mausmodellen bestätigt und erweitert. Diese immunhistochemischen Daten wurden mit ultrastrukturellen Untersuchungen ergänzt, welche die Präsenz von Reelin im extrazellulären Raum und im Somata von Interneuronen sowohl in jungen als auch alten Wildtyp Mäusen bestätigte. Zusätzlich wurde in alten Mäusen sowohl Reelin- als auch Aβ-IR in extrazellulären, granulären Ablagerungen detektiert und bekräftigte unsere vorangegangenen immunhistochemischen Resultate. Weitere Untersuchungen ergaben eine enge Assoziation der einzelnen Sphären mit Astrozyten beziehungsweise Mikroglia, was auf einen phagozytischen Prozess hindeutet. Interessanterweise waren diese Strukturen ebenfalls eng mit Dendriten verbunden, was auf eine intrazelluläre Herkunft der Ablagerungen hindeutet. Dies wurde ferner durch die immunhistochemischen Beobachtungen bekräftigt, welche Reelin in Axonen als auch axonalen Schwellungen aufzeigen. Dieses Phänomen beeinträchtigt möglicherweise die axonale Integrität und repräsentiert eine denkbare Herkunft der individuellen globulären Strukturen. Ultrastrukturelle Untersuchungen der PolyI:C-exponierten Mäuse zeigten signifikante Unterschiede in Bezug auf die Plaquemorphologie. Im Vergleich zur Kontrollgruppe (NaCl) zeigten die immunstimulierten Tiere (PolyI:C) grössere granuläre Ablagerungen, eine erhöhte Präsenz von Mitochondrien in diesen Strukturen, als auch degenerative Merkmale.

Um die Präsenz von Reelin und seinen proteolytischen Fragmenten in den granulären Strukturen nachzuweisen und zu bestätigen, wurde ein biochemischer und proteomischer Ansatz initiiert. Dafür wurde Laser-Mikrodissektion mit Massenspektrometrie kombiniert, um die Komposition und Herkunft der granulären Ablagerungen zu untersuchen. Obwohl dieser Ansatz noch weiterer technischer Verbesserungen bedingt, um die Plaque Komponenten mit hoher Genauigkeit zu charakterisieren, konnte die Anreicherung von Reelin als auch des N-terminalen Fragmentes mittels Western Blot bestätigt werden.

Weitere Untersuchungen über den Einfluss von Reelin auf die APP Prozessierung und Aβ-Produktion wurden in transgenen AD-Mäusen mit genetisch reduzierten Reelin Levels durchgeführt. Diese Ergebnisse lieferten den ersten Beweis verstärkter amyloidogener Prozessierung als auch beschleunigter Plaque Formation in den Doppel-Mutanten im Vergleich

zu den Kontrollmäusen und ergänzten jüngste *in vitro* Daten, welche eine Regulierung in der APP Prozessierung nach der Bindung von Reelin an dieses Membranprotein belegen. Darüber hinaus zeigten die Reelin-defizienten AD-Mäuse eine nachhaltig verstärkte Aβ-Plaque-Pathologie mit zunehmendem Alter. Dieses Phänomen war von erheblicher Mikro- and Astrogliose begleitet und einer beachtlichen Anreicherung phosphoTau-positiver Neuronen und Neurofibrillen um die Aβ-Ablagerungen im Hippokampus. Diese Studie liefert den ersten *in vivo* Support, dass eine Fehlfunktion in der Reelin-vermittelten Signalübertragung einen kritischen Einfluss auf die amyloidogene APP Prozessierung als auch Tau Hyperphosphorylierung hat.

Zusammenfassend liefert diese Arbeit wichtige neue Einblicke in die Funktion der Reelin-vermittelten Signalübertragung im erwachsenen und alternden Gehirn. Diese Beobachtungen heben Fehlfunktionen von Reelin als einen massgeblichen Initialfaktor hervor, der möglicherweise imstande ist, eine AD-ähnliche Neuropathologie auszulösen. Daraus folgt, dass eine fehlgeleitete Reelin Signalübertragung eine entscheidende treibende Kraft in der Verlagerung von Alterungsprozessen zu einer pathologischen, neurodegenerativen Krankheit darstellt. Dies beinhaltet die intrazelluläre abnormale Aggregation von Reelin, welche die Aβ- und Tau-Pathologie begünstigt und zu Neurodegeneration führen kann. Unsere Daten zeigen zudem, dass diese neuropathologischen Veränderungen durch eine pränatale, periphere Immunstimulation (PolyI:C) oder einer genetischer Reduktion von Reelin stark beschleunigt werden können.

SUMMARY

Reelin is a large extracellular matrix protein essential for mediating proper neuronal positioning during development. Employing the same lipoprotein-mediated signaling cascade, Reelin regulates NMDA receptor homeostasis and modulates synaptic function and plasticity in adult synapses. In line, aging-related reduction in Reelin expression has been shown to contribute to cognitive impairments during normal aging. Recent experimental evidence suggests an involvement of dysfunctional Reelin in pathological forms of aging, such as late-onset Alzheimer's disease (AD), which is characterized histopathologically by senile plaques and neurofibrillary tangles. Since aging is the major risk factor of AD, the putative changes in Reelin expression during normal and pathological forms of aging have recently been investigated. This data revealed a highly consistent age-related loss of Reelin-expressing neurons and concomitant accumulation in extracellular Reelin-positive amyloid-like deposits in the hippocampal formation of several aged species. Interestingly, a prenatal immune challenge in normal wild type mice using the synthetic viral mimic polyriboinosinic-polyribocytodilic acid (PolyI:C) resulted in earlier, higher and much more persistent levels of these Reelin-positive deposits in the hippocampal formation. However, the molecular mechanism by which this conserved glycoprotein contributes to the pathogenesis of AD remains still largely unknown.

Here, the general aim was to elucidate the morphological, ultrastructural, and biochemical properties of the Reelin aggregates in order to identify their origin and significance with respect to neurodegenerative processes characteristic of the aged brain. With that we aimed to provide a putative molecular link between Reelin dysfunction and AD-related neuropathology. To achieve these aims, we first developed an immunohistochemical protocol involving stringent and prolonged pretreatment with the endopeptidase pepsin to optimally detect and characterize Reelin-positive clustered structures in the hippocampal formation of aged wild type mice. This procedure markedly enhanced Reelin-immunoreactivity (IR) pointing to an aggregated and protease-resistant state of these deposits. Moreover, this treatment allowed for the first time the specific detection of several murine proteolytic amyloid precursor protein (APP) fragments in aged wild type mice. These investigations revealed that Reelin was selectively associated but not completely co-localized with fibrillary Aβ species. Oligomeric Aβ deposits on the other hand showed a very high degree of co-localization with Reelin, confirming and extending previous

findings involving transgenic AD mouse models. These data were complemented by ultrastructural investigations. We confirmed the presence of Reelin in extracellular space and somata of interneurons in young and aged wild type mice. In aged mice, Reelin- and amyloid-β-IR was detected in extracellular, spherical deposits, confirming our immunohistochemical data. Additional investigations revealed a close association of the individual granules with astrocytes and microglia, respectively, likely indicative of a phagocytic process. Interestingly, these granules were closely associated with dendritic processes confirming a putative intracellular origin. This was further confirmed by immunohistochemical observations, detecting Reelin in axons as well as Reelin aggregates in axonal swellings, likely affecting the axonal integrity and representing a possible origin of the individual granules. Ultrastructural investigations of PolyI:C exposed mice revealed significant differences with respect to plaque morphology following prenatal immune challenge compared to saline exposed mice, as indicated by a larger granule size, the increased presence of mitochondria in the granules, as well as degenerative features.

In order to confirm the presence of Reelin and its proteolytic fragments within these granular aggregates, we initiated a biochemical and proteomic investigation. We combined laser microdissection with mass spectrometry in order to investigate the granular composition and provide information on their origin. Although this current approach needs further technical improvement in order to characterize with high fidelity the plaque components, we confirmed the enrichment of full-length Reelin and its N-terminal fragment in these deposits by western blotting.

Further investigations on the involvement of Reelin in AD pathology included biochemical analyses on APP processing and amyloid-β peptide production in transgenic AD mice with genetically reduced Reelin levels. Our data provided first evidence of enhanced amyloidogenic processing and accelerated plaque formation in double-mutant as compared to control mice, complementing recent *in vitro* data showing modulation in APP trafficking and processing following Reelin binding to this membrane protein. Furthermore, we observed that the Aβ-plaque pathology was strongly aggravated in the Reelin deficient AD mice during aging, accompanied by significant micro- and astrogliosis and a striking accumulation of phospho-Tau positive neurons and neurofibrillary tangle-like structures around amyloid plaques in the hippocampal formation. This study provides the first *in vivo* support that dysfunctional Reelin-

mediated signaling is a critical upstream modulator of amyloidogenic APP processing and Tau hyperphosphorylation.

Taken together, we provide important novel insights into the function of Reelin-mediated signaling in the adult and aging brain. These observations highlight Reelin as an important upstream factor able to trigger AD-like pathology in the pathogenesis of sporadic AD. We propose dysfunctional Reelin signaling as an important driving force able to induce a shift from normal to pathological aging, including an intracellular and abnormal aggregation of Reelin, possibly leading to neurodegeneration. This gets accelerated by a prenatal peripheral immune challenge (PolyI:C), and increased Aβ- and Tau pathology due to genetic reduction of Reelin.

I. GENERAL INTRODUCTION

1. REELIN

Reelin, a large glycoprotein, is a major secretory protein with important roles during neurodevelopment in regulating neuronal migration and correct lamination of the cortex *(Cooper, 2008; D'Arcangelo et al., 1999; Forster et al., 2006; Frotscher et al., 2009; Rice and Curran, 2001)*. In the adult brain, Reelin plays a crucial modulatory role in the induction of synaptic plasticity and successful formation of long-term memory *(Herz and Chen, 2006)*.

1.1 THE REELIN PROTEIN AND ITS PROCESSING

Reelin, with a relative molecular mass of 450 kDa, consists of a highly glycosylated N-terminal region, containing a signal peptide and a sequence with 25 % F-spondin homology. This is followed by a central region containing eight unique repeats, each composed of two sub-repeats A and B with an EGF-like motif in between. The protein ends in a short highly charged C-terminal region. The protein is subjected to proteolytic cleavage in the extracellular and/or post-endoplasmic environment at the N- and C-terminus *(Kohno et al., 2009; Lambert de Rouvroit et al., 1999)* producing a total of 5 different fragments (**Fig. 1**). The physiological functions of the cleaved Reelin fragments are not fully understood. Current evidence suggests that the N-terminal region of Reelin is required for protein homodimerization and full signaling activity *(Kohno et al., 2009; Kubo et al., 2002)*; a process shown to be essential for postnatal dendritic maturation of cortical pyramidal neurons *(Chameau et al., 2009)*. The central region represents the minimal receptor-binding and signaling unit sufficient for normal cortical development *(Jossin et al., 2004, 2007)* and an amyloid precursor protein (APP) interaction domain *(Hoe et al., 2009b)*. The highly conserved C-terminal fragment appears to be required for protein secretion, and/or proper protein folding, as well as intracellular signaling activity *(de Bergeyck et al., 1997; Nakano et al., 2007)*. It has been shown by cell adhesion assays that processed Reelin can form large homomeric protein complexes *(Kubo et al., 2002; Utsunomiya-Tate et al., 2000)*. Dependent on processing, Reelin can form dimers or even oligomeric complexes, indicating an effect of the proteolytic processing of Reelin on its tertiary structure, which is required for its proper and stable assembly. Despite the pharmacological data that classified the Reelin proteases into the family of zinc-dependent disintegrin and metalloproteinases with or without

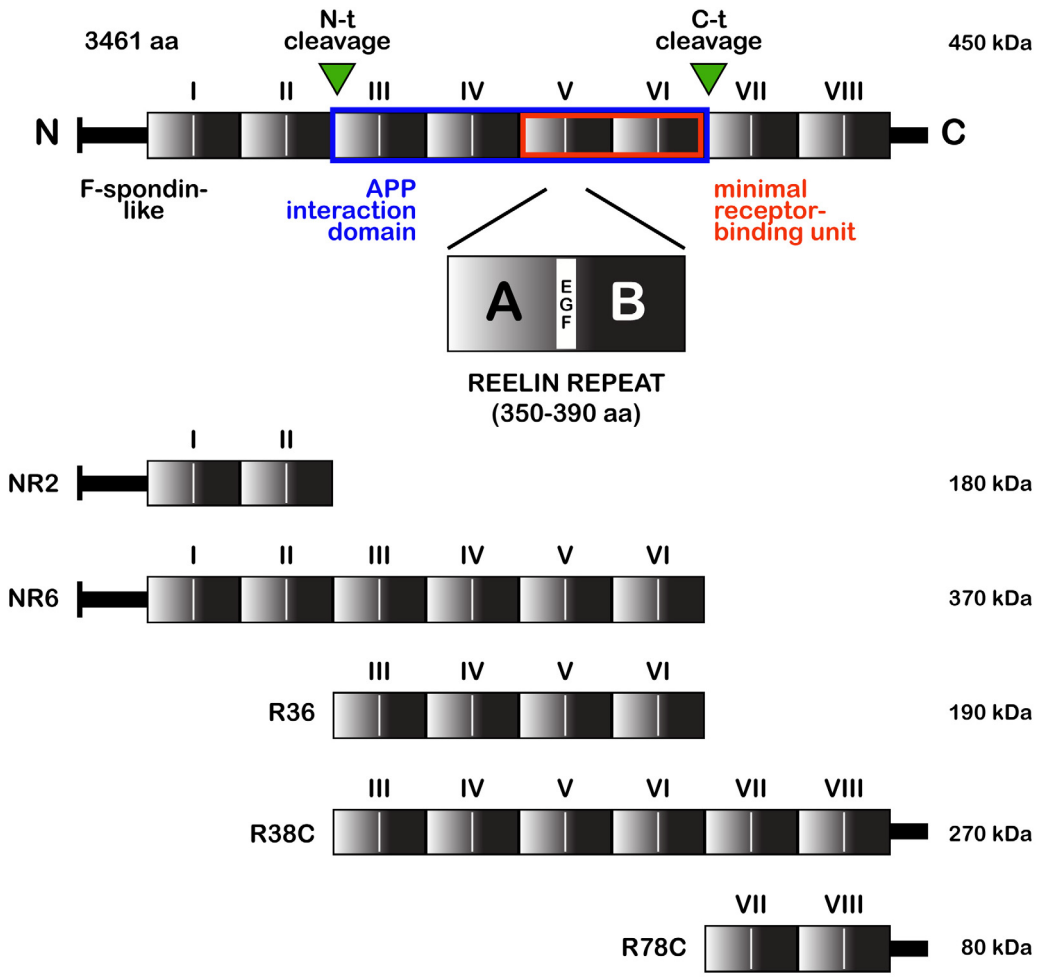

FIGURE 1: Reelin protein and its proteolytic processing
Reelin, with a relative molecular mass of 450 kDa, consists of a highly glycosylated N-terminal region, containing a signal peptide and a sequence with 25 % F-spondin homology. This is followed by a central region containing eight unique repeats, each composed of two sub-repeats A and B with an EGF-like motif in their center. The protein ends in a short highly charged C-terminal region. The protein is subjected to proteolytic cleavage, by so far unidentified proteinases, producing a total of 5 different fragments named after the position and number of repeats. The N-terminal cleavage site is located between the Reelin repeats 2B and 3A, whereas the cleavage site at the C-terminal region is located between the Reelin repeats 6B and 7A. The complete proteolytic cleavage results in the generation of 3 major fragments: the N-terminal (NR2; N –term to repeat 2 ~180 kDa), a central fragment (R36; repeats 3 to 6, 190 kDa) and the C-terminal fragment (R78C; repeat 7 and 8, 80 kDa). Further intermediate fragments as the 370 kDa fragment (NR6; N-term to repeat 6) and 270 kDa fragment (R38C; repeat 3 to 8) result from partial processing (*adapted from (Knuesel et al., 2009; Rice and Curran, 2001)*).

thrombospondin motifs (ADAM and ADAMTS *(Kohno et al., 2009; Lambert de Rouvroit et al., 1999)* the nature of the involved metalloproteinase is still not identified nor is it known whether it is involved in both the N- and C-terminal cleavage. Tissue plasminogen activator (tPA), a serine protease, has been suggested to degrade Reelin in the plasma *(Lugli et al., 2003)*. Our own research gives evidence that this protease is possibly involved in Reelin processing, cleaving at the C-terminal end (*D. Krstic, unpublished data*). Furthermore, ADAMTS-4 was found to be another protease likely being involved in cleaving Reelin at the C- and N-terminal ends

(*D.Krstic, unpublished data*). In addition, although processing of Reelin certainly modulates its signaling in the developing (and potentially also in the adult) brain, neither the biological significance nor the factors that modulate this process are known.

1.2 ROLE OF REELIN IN THE DEVELOPING BRAIN

The role of Reelin in the developing brain has been studied in great detail (for recent reviews, see *(Förster et al., 2010; Knuesel, 2010)*). During neuronal development, Reelin is secreted by Cajal-Retzius (CR) cells located in the marginal zone. Interestingly, there is recent evidence that Reelin can also be synthesized and secreted by oligodendroglial cells in the central nervous system (CNS) *(Siebert and Osterhout, 2011)*. The highly conserved protein is essential for neuronal migration and brain development *(Alcantara et al., 1998; Cooper, 2008; D'Arcangelo et al., 1995; Hirotsune et al., 1995)*. This is achieved through the activation of the apolipoprotein E receptor 2 (ApoER2) and very-low-density lipoprotein receptor (VLDLR, *(D'Arcangelo et al., 1995; Hiesberger et al., 1999; Howell et al., 1999; Trommsdorff et al., 1999)*; for review *(Reddy et al., 2011)*), which constitute the major Reelin receptors (**Fig. 2**). Reelin binding to these lipoprotein receptors induces their clustering and results in tyrosine phosphorylation of the adaptor protein Disabled-1 (Dab1) that interacts with conserved NPxY motifs in the cytoplasmic domains of VLDLR, ApoER2 and APP family members *(Hoe et al., 2006; Homayouni et al., 1999; Howell et al., 1999; Strasser et al., 2004; Trommsdorff et al., 1998, 1999)*. The phosphorylation of Dab1 results in the recruitment and activation of Src family tyrosine kinases (SFKs) and additional non-receptor tyrosine kinases *(Bock et al., 2003)*, which in turn trigger downstream cytosolic kinase cascades involving phosphatidylinositol-3-kinase (PI3K), Akt/PKB, mTor and the inhibition of Glycogen synthase kinase 3β (GSK3β) as well as cyclin-dependent kinase 5 (CDK5) *(Beffert et al., 2002, 2004)*. In line with this modulatory role, Reelin-deficient animals show hyperphosphorylation of the microtubule-associated protein Tau, which represents a major target of both latter kinases. Michael Frotscher and his group provided evidence that signaling molecules of the Reelin pathway involving Dab1, SFKs and PI3K are also involved in n-cofilin phosphorylation and actin cytoskeleton regulation *(Chai et al., 2009)*. Following phosphorylation of serine3, n-cofilin is unable to depolymerize F-actin and this in turn leads to a stabilization of the actin cytoskeleton. These results suggest a novel role of Reelin in controlling directional neuronal migration processes during development. Further support of Reelin in regulation of the cytoskeleton has been given by the group of Hans Bock *(Leemhuis et al., 2010)*, showing increased growth cone motility and filipodia formation after Reelin-induced

activation of Cdc42 (known for its role in neuronal morphogenesis, directed migration and cell cycle progression), promoting neuronal development.

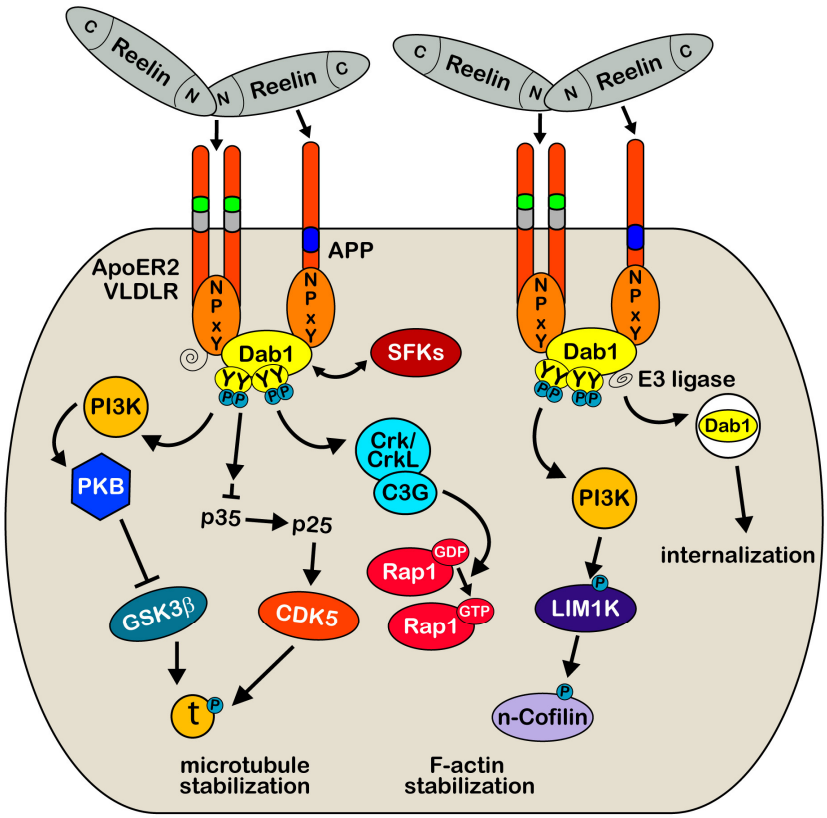

FIGURE 2: Reelin-mediated signaling during development
Binding of multimeric Reelin to VLDLR and ApoER2 induces their clustering and phosphorylation of the cytoplasmic adapter protein disabled 1 (Dab1) by the Src family tyrosine (SFKs) kinases Fyn and Src. Dab1 is initially phosphorylated on two (Tyr185, Tyr198) sites which seem to be required to permit transphosphorylation of adjacent Dab1 molecules at all four sites (Tyr185, Tyr198, Tyr220, Tyr232, *(Park and Curran, 2008)*). This leads to the recruitment and activation of additional activated non-receptor tyrosine kinases allowing the activation of cytosolic kinase cascades, involving Phosphatidylinositol-3-kinase (PI3K), Akt/PKB, and the inhibition of Glycogen synthase kinase 3β (GSK3β) as well as CDK5, two main kinases that phosphorylate the microtubule-stabilizing protein Tau *(Beffert et al., 2002, 2004)*. Phospho-Dab1 recruits also Crk/CrkL-C3G complexes which in turn stimulate Rap1 *(Park and Curran, 2008)*. The central Reelin domain also directly interacts with the E1 extracellular domain of APP; an interaction that appears to be necessary for proper neurite outgrowth both *in vitro* and *in vivo (Hoe et al., 2009b)*. Regulation of the actin cytoskeleton through the Reelin signaling cascade also involves activation of LIM1 kinase which results in increased n-cofilin phosphorylation in the leading processes of migrating neurons approaching the marginal zone *(Chai et al., 2009)*. Recruitment of ubiquitin ligases to phosphorylated Dab1 results in ubiquitination of the protein, which mediates the phosphorylation-dependent endocytosis of the entire Reelin signaling complex *(Bock et al., 2004; Suetsugu et al., 2004)*.

In agreement with the fundamental role of Reelin during neuronal development, impaired Reelin signaling has a devastating effect on the gross morphology of the hippocampus, cerebellum and neocortex, as evident by the abnormal cortical layering ("outside-in" instead of "inside-out") and neuronal positioning in Reelin homozygous knockout mice (*reeler*, **Fig. 3A**, *(Goffinet, 1984;*

Trommsdorff et al., 1999)), although the cortical neurons are generated normally. The *reeler* mutant mouse was first described in 1951 *(Falconer, 1951)*, holding an autosomal recessive mutation leading to the development of severe ataxia, tremor and a reeling gait. Reelin was discovered nearly 50 years later as the responsible gene for this phenotype *(D'Arcangelo et al., 1995)*. Also the hippocampus displays abnormal neuron disorganization (**Fig. 3B**) compared to wild type mice, evident by no compact granule cell layer in the dentate gyrus *(Lambert de Rouvroit and Goffinet, 1998; Weiss et al., 2003)* and the split in two layers of the pyramidal neurons (so-called double layered structure).

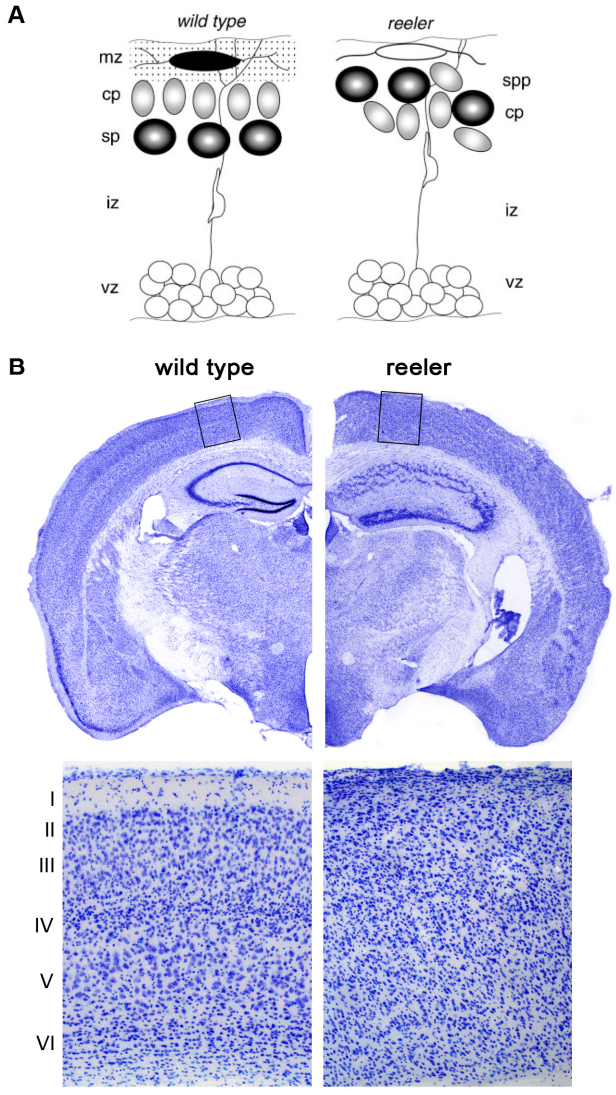

FIGURE 3: Role of Reelin in the cell lamination of cortex and hippocampus
Differences in cell layering in wild type and reeler mice. (**A**) During embryonic development the preplate is formed, consisting of Cajal-Retzius (CR) neurons in the marginal zone and subplate (sp) neurons. A first cohort of cortical plate neurons (gray) migrates along radial glia into the intermediate zone (iz) past the subplate level and stops beneath the Reelin producing (stipple) CR cells (black) in the marginal zone, a zone relatively cell-free in wild type mice. Following cells migrate past the older subplate neurons and insert themselves directly beneath the CR cells, resulting in the typical and normal layered pattern, where the cortical plate represents the prospective cortical layers II-VI and the marginal zone the future cortical layer I. In *reeler* mice, the cortical layering defect is apparent at the onset of the cortical plate formation as the first cohort of cortical plate neurons already fails to migrate past the subplate and accumulates instead in a disorganized fashion in the superplate (spp, cell-dense region), resulting in dispersed and inversed cellular layers, forming a so called "inverted cortex". (**B**) Brain slices of wild type and reeler mice showing differences in the histotypical appearance of cortical and hippocampal layering. Beside the abnormal inverted layering of the cortex in *reeler* mice, they also exhibit a failure in establishing a distinct granule cell layer in the dentate gyrus, showing intermingled granule cells and hilar mossy cells as compared to wild type mice. *vz* - ventricular zone; *CR* – Cajal-Retzius neurons; *SP* – subplate; *mz* – marginal zone; *spp* – superplate (*A obtained from (Rice and Curran, 2001)*.

Despite normal brain morphology, heterozygous *reeler* mice, expressing only 50 % of Reelin mRNA levels of wild type mice, show significant impairments in synaptic plasticity as well as

learning disabilities compared to wild type littermates *(Weeber et al., 2002)*. A *reeler* phenotype has also been described in mice with a loss of both Reelin receptors *(Trommsdorff et al., 1999)*, whereas single-mutants do not show the characteristic cortical disorganization. This indicates that ApoER2 and VLDLR can compensate for each other to a certain extent. However, novel evidence for divergent roles of the Reelin receptors has already emerged *(Hack et al., 2007; Hoe et al., 2006)*. These different functions might stem from either structural differences in the intracellular domains or selective localizations within distinct sub-domains in the plasma membrane. Support for the latter hypothesis has been provided by the recent study by Duit and colleagues *(Duit et al., 2010)*. Investigating the functional difference between the two Reelin receptors using a fibroblast cell culture system, they found that the endocytosis of Reelin is linked to specific sorting to raft versus non-raft domains of the plasma membrane. Duit and colleagues reported that VLDLR is present in non-raft domains and Reelin binding to this receptor results in fast endocytosis of the complex. Reelin is then targeted to the lysosome and the receptor recycled back to the cell membrane. Binding of Reelin to ApoER2, which is predominantly localized to raft domains of the plasma membrane, however, does not result in significant reduction of extracellular Reelin since this receptor-mediated endocytosis is rather slow. Activation of this pathway results in lysosomal sorting of both the ApoER2 and Reelin. Together with the Reelin-mediated ubiquitination and proteosomal degradation of Dab1 following receptor-mediated endocytosis, these differential processes provide not only an essential feedback mechanism and termination signal in the regulation of neuronal positioning *(Arnaud et al., 2003; Bock et al., 2004; Kerjan and Gleeson, 2007; Morimura et al., 2005)*, they likely also contribute to a highly selective and receptor-specific fine-tuning of the Reelin signal that is required for normal synaptic plasticity and learning in the adult brain.

1.3 REELIN-MEDIATED SIGNALING IN THE ADULT BRAIN

The studies focusing on developmental functions of Reelin clearly outnumber the investigations addressing the role of Reelin in the mature brain and we are just beginning to understand the implications of reduced Reelin expression during aging. Interestingly, the expression pattern of Reelin changes after the end of the neuronal migration phase *(Frotscher, 1998)*. In the adult brain, the Reelin-expressing CR cells are largely replaced by Reelin-expressing GABAergic interneurons that are dispersed throughout the forebrain (**Fig. 4**). Reelin is also expressed by glutamatergic pyramidal neurons in layer II of the entorhinal cortex, olfactory mitral cells and cerebellar granule cells *(Abraham and Meyer, 2003; Abraham et al., 2004; Alcantara et al.,*

1998; Baloyannis, 2005; Chin et al., 2007; Knuesel et al., 2009; Lacor et al., 2000; Miettinen et al., 2005; Pappas et al., 2003; Pesold et al., 1998a; Ramos-Moreno et al., 2006). ApoER2 and VLDLR and the adapter protein Dab1 also remain expressed in the adult brain. The distinct expression pattern of Reelin and its signaling members in brain regions implicated in mediating learning and memory *(Alcantara et al., 1998; Beffert et al., 2005; Cooper, 2008; Forster et al., 2002; Frotscher et al., 2003; Pesold et al., 1998a)* suggest that Reelin-mediated signaling in the adult brain is crucial for normal cognitive function.

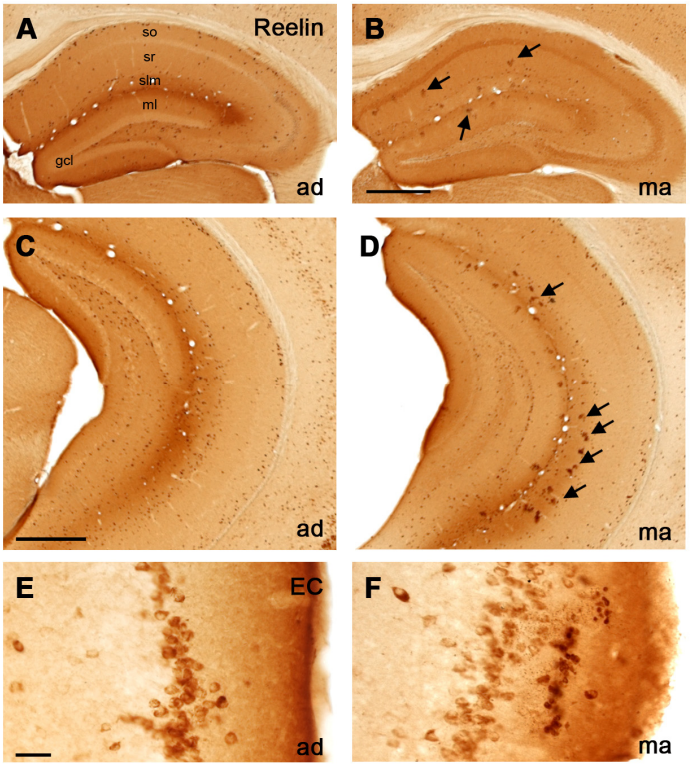

FIGURE 4: Reelin expression in the adult rodent brain
Immunoperoxidase staining showing the expression pattern of Reelin in the dorsal (**A, B**) and ventral (**C, D**) hippocampus and entorhinal cortex (**E, F**) in coronal brain sections obtained from adult (*ad*, 3 months, **A, C and E**) and mature (*ma*, 12 months, **B, D and F**) wild type mice. Reelin-IR is evident in the neuronal soma of GABAergic interneurons and in the neuropil throughout the hippocampus and cortex. The neuropil staining is especially dominant in the stratum lacunosum moleculare (slm) in *ad* subjects. **B, D**) In *ma* mice Reelin-IR is also present in plaque-like accumulations (arrows), restricted to the dorsal CA stratum oriens (so) and radiatum (sr) and outer dentate gyrus (DG) molecular layer (ml). In the ventral hippocampus they are strongly enriched in the slm and DG ml (arrows). **E, F**) High magnification images of the lateral entorhinal cortex (EC) of representative *ad* and *ma* mice. Reelin-IR was predominantly found in layers II and I. Age related plaques are found exclusively in layer I. Scale bars: **B, C** = 500 µm, **E** = 50 µm. (*adapted from (Knuesel et al., 2009)).*

Interestingly, a new role for Reelin in the healthy and injured adult brain was discovered recently *(Courtes et al., 2011)*, showing that Reelin signaling participates in spontaneous cell mobilization and post-lesional cell migration. This demonstrates how the developmental function of Reelin is reused in the adult brain to control regenerative processes.

1.3.1 THE ROLE OF REELIN IN SYNAPTIC PLASTICITY

First evidence that Reelin plays a role in synaptic plasticity came up in 2002 *(Weeber et al., 2002)*. The team of Joachim Herz demonstrated *in vitro* that application of recombinant Reelin can dramatically elevate the magnitude of long-term potentiation (LTP), a form of synaptic

plasticity induced by high frequency stimulations that results in a persisting increase in synaptic efficacy *(Bliss and Lomo, 1973)*. Using ApoER2- and VLDLR-deficient mice, they verified that high frequency stimulation results in reduced LTP induction in VLDLR-knockout mice and a pronounced decay in late-phase LTP in ApoER2-null mice *(Weeber et al., 2002)*. These findings are in line with the described hypomorphic phenotype of the single-mutants with developmental defects affecting mainly hippocampus and neocortex (ApoER2) or cerebellum (VLDLR), as well as the *reeler* phenotype in double-mutants *(Trommsdorff et al., 1999)*. Overall, the results provided the first experimental evidence for a critical role of Reelin in modulating synaptic function and enabling the formation of long-term memory. Other studies have confirmed the significant contribution of the Reelin signaling pathway to synaptic plasticity *(Beffert et al., 2005; Chen et al., 2005; Herz and Chen, 2006; Qiu et al., 2006a, 2006b)* by demonstrating that binding of Reelin to ApoER2 and VLDLR at postsynaptic sites controls glutamatergic neurotransmission through differential modulation of the activity of NMDA and AMPA receptors (**Fig. 5**). Similar to the signaling in the developing brain, the effect was dependent on Reelin-induced activity of SFKs that are involved in tyrosine phosphorylation of the NR2 subunits of the NMDA receptors *(Beffert et al., 2005; Chen et al., 2005)*. This in turn results in a potent enhancement of glutamate-stimulated Ca^{2+} influx that is required for LTP induction and maintenance *(Malenka, 2003)*. The Herz lab also established a molecular mechanism by which Reelin, in conjunction with alternatively spliced forms of ApoER2, regulates synaptic function and plasticity in the adult brain. They discovered that adaptor proteins binding to the exon 19-encoded intracellular domain of ApoER2 *(Gotthardt et al., 2000; Stockinger et al., 2000)* are necessary for transmitting the Reelin signal that is required to enhance LTP. Together, these results provided the first evidence for a physiological role of Reelin signaling in the control of NMDA receptor function and synaptic strength, suggesting that Reelin can physiologically modulate LTP through regulation of NMDA receptor activity.

All these findings implicate the influence of Reelin on postsynaptic functions; however no studies have been conducted to investigate the proteins effect on presynaptic functions. Very recently, first evidence for a role of Reelin at the presynaptic site was given by Hellwig and colleagues *(Hellwig et al., 2011)*. Their findings point to an altered vesicle fusion and neurotransmitter release in adult *reeler* mice, suggesting an involvement of Reelin in hippocampal presynaptic functions; however, the signaling pathway might not involve VLDLR and ApoER2.

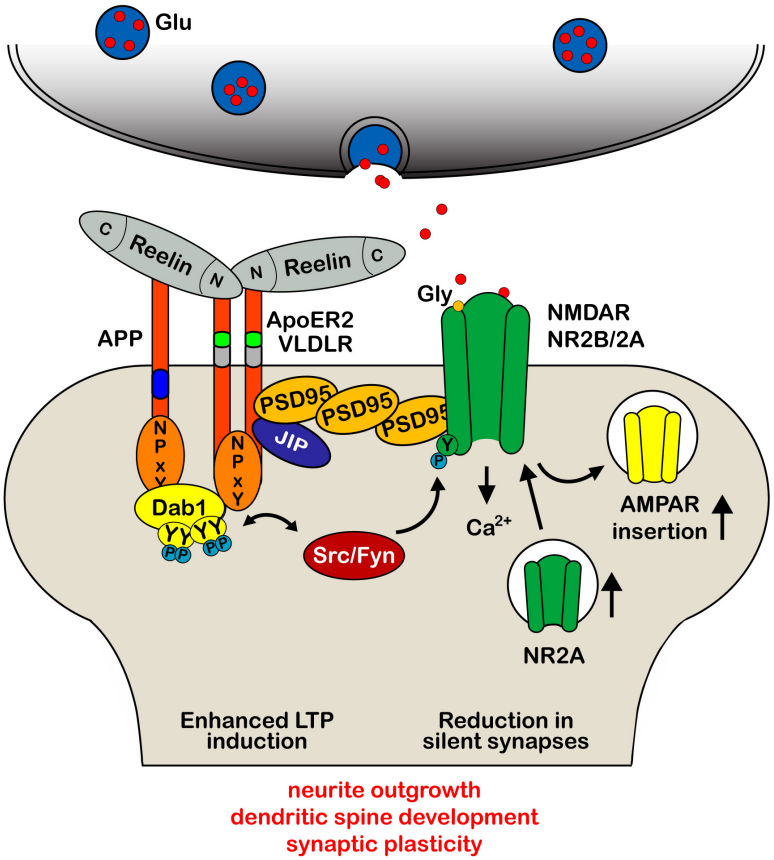

FIGURE 5: Reelin modulates synaptic plasticity and learning and memory.
Dab1 binding site and exon 19-encoded domain of ApoER2 are necessary for the Reelin-mediated increase in synaptic plasticity that allow the coupling of the Reelin receptor and the activated Dab1–Src/Fyn complex to the NR2A and NR2B subunit of the NMDA receptor for its subsequent tyrosine phosphorylation and Ca^{2+} entry in the postsynaptic density, PSD *(Beffert et al., 2005)*. Prolonged presence of Reelin at synaptic sites also modulates AMPA receptor-mediated responses, associated with an increased receptor number in the PSD *(Qiu et al., 2006b)* and reduction in the number of silent synapses that facilitated the developmental switch from NR2B to NR2A *(Qiu and Weeber, 2007)*. Reelin-induced augmentation of Ca^{2+} entry through NMDA receptors increases phosphorylation and nuclear translocation of the transcription factor cAMP-response element binding protein (CREB), indicating that Reelin may physiologically modulate learning and memory by modulating NMDA receptor functions *(Chen et al., 2005)*. These data fit with the observations that in the absence of Reelin or the Reelin receptors, neurons exhibit stunted dendritic growth, a reduction in dendritic branches and significantly fewer spines *(Borrell et al., 1999; Borrell et al., 2007; Del Rio et al., 1997; Niu et al., 2004, 2008; Qiu and Weeber, 2007; Trommsdorff et al., 1999)*.

1.3.2 REELIN AND ITS IMPACT ON DENDRITE AND SPINE FORMATION, MODULATION AND MAINTENANCE

One critical aspect of synaptic adaptations associated with LTP involves the changes in dendritic spine morphology. Similarly to the situation during development where Reelin-dependent signaling is required for the outgrowth of dendrites and the formation of dendritic spines *(Chameau et al., 2009; Jossin and Goffinet, 2007; Matsuki et al., 2008; Niu et al., 2004, 2008)*, the Reelin signaling cascade is used in adulthood to regulate plasticity-induced morphological changes of dendritic spines. First evidence to support a role for Reelin in this process has been

provided by the work of Stanfield and Cowan *(Stanfield and Cowan, 1979a, 1979b)*. They reported altered dendritic morphology and orientation in the cortex and hippocampus of adult *reeler* mice. In line, heterozygous *reeler* mice exhibited reduced spine density, as well as defects in the molecular composition of the synapses in the hippocampus and cortex that was accompanied by impaired performance in certain learning and memory tasks *(Liu et al., 2001; Pappas et al., 2001; Qiu et al., 2006a; Tueting et al., 1999; Ventruti et al., 2011)*. In the absence of Reelin or its receptors, Dab1-expressing neurons also exhibited stunted dendritic growth and reduction in dendritic branches *(Niu et al., 2004)*. It has been further shown that application of recombinant Reelin can reverse this deficit in neuronal cultures lacking one or both *Reelin* genes *(Niu et al., 2004, 2008; Qiu et al., 2006a)*. The rescue was again dependent on the activation of the downstream tyrosine kinase-dependent signaling pathway, as shown for the regulation of neuronal migration and adult synaptic plasticity. In addition, data showed that stimulation of cultured hippocampal neurons with Reelin leads to enhanced dendritogenesis *(Matsuki et al., 2008)*. This effect was blocked by reduced expression of Crk family proteins, suggesting that Dab1-binding proteins are important downstream components of the Reelin signaling pathway in regulating hippocampal dendritogenesis. Altogether, these studies demonstrate that constitutive levels of Reelin and its receptors are required for correct formation and maintenance of dendritic structures that are crucial for normal information processing in adult synapses.

Recently, the group of Eduardo Soriano addressed for the first time the impact of Reelin overexpression on synaptic plasticity and associated morphological changes *(Pujadas et al., 2010)*. They reported that adult generated neurons in the dentate gyrus of transgenic mice exhibit an increased complexity in their developing dendrites that was accompanied by a significant enlargement of dendritic spines and an increase in the number of synaptic contacts. Furthermore, the overexpression evoked a dramatic increase in LTP induction and maintenance as compared to controls. They also discovered that overexpression of Reelin leads to dispersion, impaired migration and abnormal positioning of adult-generated neurons, indicating that adequate levels of Reelin above and below a certain threshold are required for successful neuronal migration, dendritic development and morphological adaptations that are associated with processes underlying synaptic plasticity and learning and memory *(Pujadas et al., 2010)*. Taken together, these results suggest that Reelin and its lipoprotein receptors participate in the control of developmental processes that are fundamental for proper synaptic and neuronal functioning in the adult brain.

1.3.3 REELIN EXPRESSION IN HUMANS

In the developing human brain, CR cells in the marginal zone also constitute the main source of Reelin as described in rodents and non-human primates *(Meyer and Goffinet, 1998; Ogawa et al., 1995)*. However, besides the well-characterized human developmental disorder, Lissencephaly, which is caused by dominant mutations in the *Reelin* gene in humans *(Hong et al., 2000)*, relatively little information is available on the expression and localization of Reelin in the healthy adult and aged human brain. Reelin-positive CR cells can still be detected in the neo- and entorhinal cortex of adult and aged humans *(Belichenko et al., 1995; Martin et al., 1999; Mikkonen et al., 1997; Riedel et al., 2003)*, but they appear to decline during pathological aging *(Baloyannis, 2005)*. In 2005, Roberts and colleagues reported the first ultrastructural localization of Reelin in postmortem human brain samples *(Roberts et al., 2005)*. Reelin-IR was readily detected in the neocortex; being present both in interneurons and glia cells. In the neuropil, Reelin-IR was found in small axons, axon terminals, dendrites and postsynaptic spines. These results are consistent with immunohistochemical studies involving postmortem brain tissue obtained from rodents *(Knuesel et al., 2009; Ramos-Moreno et al., 2006)*, ferrets *(Martinez-Cerdeno et al., 2003)*, primates *(Abraham and Meyer, 2003; Martinez-Cerdeno et al., 2002)* as well as humans *(Abraham and Meyer, 2003; Deguchi et al., 2003; Guidotti et al., 2000; Impagnatiello et al., 1998)*. The data fit with the important role of Reelin in normal synaptic function, including synaptic plasticity and dendritic remodeling in the adult brain in several species. However, it is currently unknown whether Reelin expression changes across aging in humans. Recent genome-wide SNP association studies revealed that polymorphisms in the *Reelin* gene (especially in and near the promoter region) are associated with Alzheimer's disease (AD) neuropathology *(Kramer et al., 2010; Seripa et al., 2008)*, suggesting that putative alterations in Reelin expression levels correlate with aging-associated mental decline and contribute to a pathological mechanism involving AD-associated neuropathology.

2. REELIN AND ALZHEIMER'S DISEASE

In line with the previous hypothesis and the critical role of Reelin in synaptic transmission and learning and memory, several recent findings suggest that alterations in Reelin expression and abnormal Reelin signaling may contribute to neuronal dysfunction associated with AD. In addition, several studies have investigated the molecular mechanism by which Reelin, its

receptors and downstream signaling proteins may contribute to the etiology of this progressive neurodegenerative disease.

2.1 ALZHEIMER'S DISEASE

AD is the most common form of age-related dementia; approximately 10 % of people over 65 of age are affected, with rates doubling every five years from that age on (*Source: AlzForum, 2010; (Querfurth and LaFerla, 2010)*), turning AD into a major health problem. AD is an incurable disease, clinically characterized by progressive decline in memory and cognition, disorientated behavior, altered personality, difficulties with language and impaired movements, leading to death within 3-9 years after diagnosis *(Hirtz et al., 2007)*. The entorhinal cortex, the basal forebrain and the hippocampus are primarily affected by the disease *(Braak and Braak, 1991)*; specialized brain regions playing a critical role in encoding, storage and retrieval of episodic memory (reviewed in *(Eichenbaum, 2004)*).

AD can be divided into two forms: the rare early-onset familial AD (EOAD) and the common late-onset AD (LOAD). The familial form accounts for only a small proportion of all known AD cases and usually affects people younger than 65 years *(Schellenberg, 1995)*. Dominant genetic effects induced by mutations located in genetic loci encoding proteins involved in the amyloidogenic APP processing (app, presenilin-1 (PSEN1) and presenilin-2 (PSEN-2)) are responsible for the early-onset form of the disease *(Bertram et al., 2010; Bird, 2008)*. All these mutations enfavor amyloidogenic APP cleavage and, therefore, amyloid-β (Aβ) production *(Goate et al., 1991; Levy-Lahad et al., 1995; Rogaev et al., 1995a; Sherrington et al., 1995).* One current hypothesis known as the "amyloid hypothesis" postulates that the imbalance between production and clearance of Aβ, the transformation of Aβ to its toxic forms, and the direct toxic effect of aggregated Aβ, result in the formation of aggregated Aβ deposits leading to AD neuropathology *(Hardy and Selkoe, 2002)*; accompanied by a series of downstream events (synapse loss, plaque deposition, inflammation, vascular damage, tangles).

The sporadic late-onset form of AD occurs after the age of 65, and accounts for the majority of all AD cases *(Bertram et al., 2010; Bertram and Tanzi, 2009)*. Even though the prevalence is much higher, the cause of the late-onset form remains largely unknown. Although, genome-wide association studies (GWAS) performed in humans in the last years revealed several candidate genes that potently increase the risk to develop LOAD *(for review Bertram et al., 2010; Hollingworth et al., 2011; Naj et al., 2011)*, beside the so far strongly confirmed genetic risk factor apolipoprotein E (ApoE) ε4 *(Bertram et al., 2010; Bertram and Tanzi, 2008; Corder et al.,*

1993; Schmechel et al., 1993; Strittmatter et al., 1993). However, the details of the process through which ApoE contributes to the induction and progression of AD pathology remains still largely unclear *(Kim et al., 2009)*. Further, regarding the amyloid cascade hypothesis, sporadic AD has been hypothesized to develop after a failure of Aβ clearance, a gradual rise of $A\beta_{42}$ in the brain and deposition in the form of plaques at a certain point. Hence, the sporadic form appears to follow the same pathway as the familiar form of AD, although they differ in their initiation/onset.

2.1.1 NEUROPATHOLOGICAL HALLMARKS

The histopathological hallmarks of AD comprise neurofibrillary tangles (NFTs), consisting of hyperphosphorylated Tau *(Grundke-Iqbal et al., 1986)* and the formation of senile plaques, primarily composed of Aβ peptides, a hydrophilic peptide of 39–43 amino acids *(Glenner and Wong, 1984; Haass and Selkoe, 2007)*. In parallel, the disease is also defined by neuronal and synaptic loss, brain atrophy, and inflammation.

APP AND AMYLOID-β

Aβ peptides are the amyloidogenic cleavage product of APP, a transmembrane protein playing a major role in the nervous system and is involved in synapse formation or stabilization as well as synaptic plasticity *(Gralle and Ferreira, 2007; Hoe et al., 2009a; Wang et al., 2009)*. The amyloid-β peptides result from the sequential cleavage by β- and γ-secretases *(Estus et al., 1992; Haass et al., 1992)*, also termed as amyloidogenic processing (**Fig. 6**). β-secretase, also termed as BACE1, catalyses the initial step in the amyloidogenic processing, generating two fragments: an N-terminal soluble fragment (sAPPβ) and a C-terminal membrane bound fragment (C99). C99 is further processed by γ-secretase, a large protein complex consisting of nicastrin, anterior pharynx-defective phenotype-1 (APH-1), PS enhancer 2 (PEN-2) and PSENs, within its transmembrane domain *(Steiner et al., 2008)*, generating an APP intracellular domain (AICD) and Aβ species, mainly $A\beta_{40}$ and $A\beta_{42}$, being the most prone to aggregate *(Jarrett et al., 1993)*. Due to an imbalance between formation and clearance of these peptides, Aβ starts to accumulate in the brain, forming oligomers, fibrils or even insoluble fibers assembling into senile plaques in AD. This abnormal amyloidogenic Aβ processing and formation of amyloid-β plaques have been suggested to lead to synaptic dysfunction, synapse loss, and ultimately to neuronal death. The

alternative non-amyloidogenic processing of APP occurs by the subsequent cleavage through α- and γ-secretase, preventing the formation of Aβ.

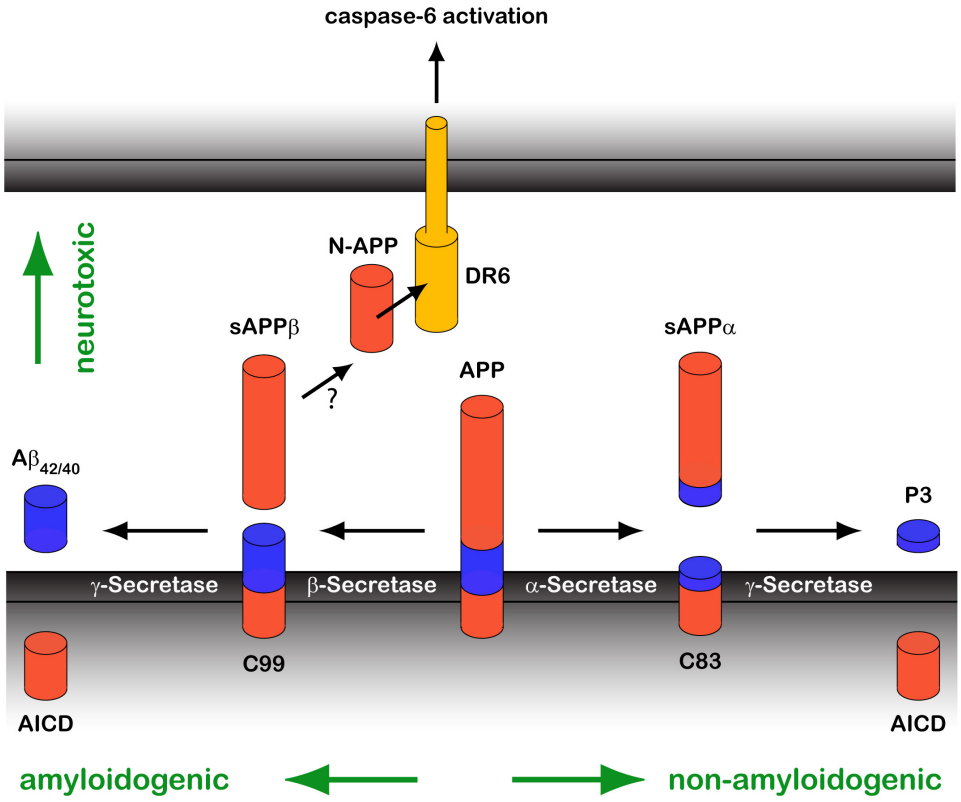

FIGURE 6: The two alternative processing pathways of Amyloid precursor protein (APP).
Senile plaques are primarily composed of amyloid-β (Aβ) peptides, which result from sequential cleavage of APP by β- and γ-secretases *(Estus et al., 1992; Haass et al., 1992)*, also termed amyloidogenic processing. This results in an extracellular N-terminal fragment (sAPPβ), and intracellular AICD domain and several amyloid peptides. The main amyloid peptides released by this cleavage are $A\beta_{40}$ and $A\beta_{42}$ being the most prone to aggregate *(Jarrett et al., 1993)*. Non-amyloidogenic processing by cleavage through α- and γ-secretase in turn results in the production and release of a large N-terminal extracellular fragment (sAPPα) and smaller, membrane-bound C-terminal fragments (P3 and AICD) with putative neuroprotective and transcriptional functions. Recently, an additional disease-modifying, N-terminal fragment of APP that acts as ligand of the death receptor 6 (DR6, a member of the tumor necrosis factor receptor superfamily) has been discovered. This fragment is produced upon growth factor withdrawal by β-secretase cleavage plus an additional, as yet unidentified, protease *(Knuesel, 2010)*.

α-secretase cleaves in between the Aβ domain, yielding a large soluble N-terminal extracellular fragment (sAPPα) and a smaller, membrane-bound C-terminal fragment (C83). The latter one is further processed by γ-secretase, generating a non-amyloidogenic 3 kDa peptide (P3) and as well AICD with putative neuroprotective and transcriptional functions *(Furukawa et al., 1996; Gao and Pimplikar, 2001; von Rotz et al., 2004)* (**Fig. 6**). AICD has also been suggested to play an important role for APP in early neurodevelopment *(Konietzko, 2011)*. Lately, the team of

Tessier-Lavigne discovered an additional disease-modifying, N-terminal fragment of APP that acts as a ligand of the death receptor 6 (DR6, a member of the tumor necrosis factor receptor superfamily). This fragment is produced upon growth factor withdrawal by β-secretase plus an additional, as yet unidentified, protease and has been shown to induce Caspase-6-mediated axonal degeneration *(Nikolaev et al., 2009)* (**Fig. 6**) a process involved in axonal pruning during development.

TAU

Neurofibrillary tangles, the second neuropathological hallmark of the disease, comprise neuronal filamentous inclusions of aggregated hyperphosphorylated Tau (pTau) *(Grundke-Iqbal et al., 1986)*. Under physiological conditions, Tau is an abundant soluble axonal protein, promoting assembly and stability of microtubules and is responsible for axonal vesicle transport and neurite outgrowth *(Binder et al., 1985*; *for review Morris et al., 2011)*. In physiological equilibrium, Tau undergoes site-specific phosphorylation events regulated by several phosphatases and kinases (mainly GSK3β and CDK5). In AD, Tau phosphorylation is elevated, leading to insoluble pTau. In turn, Tau detaches from the microtubules, due to highly decreased affinity, and gets delocalized from axonal in somatodentritic compartments, leading to instability of the microtubule network *(Ballatore et al., 2007; Brunden et al., 2009; Ittner et al., 2010; Lee et al., 2001*; *for review Morris et al., 2011)*. Factors which trigger this imbalance in the progression of this pathology are so far unknown. Experimental evidence indicates that Aβ is one of these factors driving Tau aggregation *(Gotz et al., 2001; Hardy and Selkoe, 2002; Lewis et al., 2001)*, or the other way around - that Tau enables the pathogenic effects of Aβ *(Ittner et al., 2010; Roberson et al., 2011; Roberson et al., 2007)*. In addition, the activity of the Tau specific kinases resulting in increased Tau phosphorylation can be also modulated by cytokine-mediated signaling, e.g. through the p35/MAPK pathway activated by IL-1β, highly overexpressed in AD brains *(Li et al., 2003; Sheng et al., 2001; Sheng et al., 2000)*. Further, IL-6 levels are also correlating with increased Tau phosphorylation *(Jones et al., 2009; Luterman et al., 2000; Quintanilla et al., 2004)*. These results suggest that abnormal neurodegeneration associated with AD might be due to inappropriate activation or reactivation of a developmental pathway in the aged brain.

3. THE MOLECULAR LINK BETWEEN REELIN DYSFUNCTION AND AD-RELATED NEUROPATHOLOGY

Current experimental evidence supports that altered Reelin expression and abnormal Reelin signaling are contributing to the etiology of AD:

1) Besides binding to the intracellular domain of ApoER2, it was already shown that intracellular Dab1 binds also to the cytoplasmic NPxY motif of APP *(Homayouni et al., 1999; Trommsdorff et al., 1998)*, affecting directly the trafficking and processing of ApoER2 and APP. This was tested *in vitro* by the group of Rebeck and Hoe *(Hoe et al., 2006)* demonstrating that Reelin significantly increased the intracellular interaction of Dab1 with both ApoER2 and APP, promoting their surface localization and favoring non-amyloidogenic APP processing. Both groups also provided first evidence of a direct interaction between Reelin and the extracellular domain of APP *(Hoe et al., 2009b)*, appearing to be necessary for proper neurite outgrowth. In addition, other results showed in turn that the extracellular N-terminal fragment of APP induces axon pruning and neuron death following growth factor withdrawal *(Nikolaev et al., 2009)*.

2) One Reelin-mediated signaling pathway involves the suppression of the major downstream kinases GSK3β and CDK5, the key mediators in Tau phosphorylation *(Gonzalez-Billault et al., 2005; Hiesberger et al., 1999)*. Thus, Reelin-mediated signaling reduces Tau phosphorylation by downregulating these kinases, as also confirmed by elevated levels of pTau in *reeler* and *apoer2/vldlr* double knockout mice *(Beffert et al., 2004; Hiesberger et al., 1999; Ohkubo et al., 2003)*. Therefore, abnormal Reelin-mediated signaling could promote NFT formation and potentially neuronal cell death.

3) AD patients show decreased Reelin levels in the entorhinal cortex compared to non-demented individuals *(Chin et al., 2007)*.

4) Another critical role of Reelin and its associated signaling cascade in AD-associated neuropathology is given by identifying AD-related polymorphism (SNPs) in the Reelin locus *(Kramer et al., 2010; Seripa et al., 2008)*.

5) The human ApoE comprises 3 different isoforms, which differentially compete with Reelin for binding and activation of VLDLR and ApoER2 receptors *(Chen et al., 2010;*

D'Arcangelo et al., 1999). In the case of ApoE ε4, this leads to impaired Reelin-mediated synaptic plasticity and phosphorylation of NMDA *(Chen et al., 2010)*.

Furthermore, novel insights into the pathophysiology of Aβ suggested a potent negative impact of Aβ oligomers on synaptic functions that may underlie impairments in long-term synaptic plasticity *(Lacor et al., 2004; Lambert et al., 1998; Selkoe, 2002)*. Incubation of hippocampal neurons with Aβ oligomers lead to intracellular trapping or functional impairment of AMPA and NMDA receptors *(Hsieh et al., 2006; Kamenetz et al., 2003; Snyder et al., 2005)*, thereby decreasing LTP *(Lacor et al., 2004; Lambert et al., 1998; Shankar et al., 2007; Shankar et al., 2008; Townsend et al., 2006; Walsh et al., 2002)*. As already mentioned, several studies showed an increase in LTP following Reelin application to hippocampal slices *(Weeber et al., 2002)*, demonstrating that Reelin has an opposite effect on synaptic function compared to Aβ oligomers. A study conducted in Joachim Herz' lab demonstrated that Reelin could indeed antagonize the suppressive effects of Aβ oligomers on synaptic NMDA receptor-mediated neurotransmission *(Durakoglugil et al., 2009)*. They demonstrated that Reelin signaling in excitatory synapses could restore oligomeric Aβ-induced impairments in synaptic plasticity to normal levels. Activation of SFKs by Reelin through ApoER2 and VLDLR binding was necessary for neutralizing the Aβ-mediated suppression, supporting again the crucial role of Reelin-mediated signaling for normal synaptic function.

The group of Saez-Valero has addressed the putative link between abnormal Reelin levels and AD pathogenesis. They analyzed the expression and glycosylation pattern of Reelin in the cerebrospinal fluid (CSF) and cortical tissue extracts obtained from AD patients and non-demented controls *(Botella-Lopez et al., 2006, 2010; Saez-Valero et al., 2003)*. They reported abnormal glycosylation of Reelin as well as a preferential up-regulation of the N-terminal 180 kDa Reelin fragment in the CSF and frontal cortex of AD patients. Full-length and other proteolytic fragments of Reelin remained unaltered in control and AD subjects *(Botella-Lopez et al., 2006)*, suggesting alterations in Reelin processing and signaling in AD. Another study showed that the N-terminal fragment of Reelin can be generated within the endosomes after internalization of the full-length form *(Hibi and Hattori, 2009)*, pointing to the possibility that, in AD patients, the endosomal recycling and re-secretion of this fragment into the extracellular space could also be significantly affected.

Studies performed in our lab provide an alternative explanation for the selective increase in the N-terminal Reelin fragment. We have previously observed that Reelin accumulates in oligomeric amyloid-like plaques in the hippocampal formation (**Fig. 4**) of several aged species *(Knuesel et al., 2009)*, indicating that the N-terminal fragments may preferentially oligomerize and aggregate in the extracellular matrix during aging. Further experimental support for Reelin being involved in AD pathology is given by Wirths and colleagues, showing the presence of Reelin in amyloid plaques involving transgenic AD mouse models *(Wirths et al., 2001)*. To address the putative functional implications, we have investigated whether early accumulations of extracellular protein deposits in the projection areas of subcortical neurons can act retrogradely to induce degeneration of cholinergic neurons in the basal forebrain *(Madhusudan et al., 2009)*, known to be affected early in AD pathogenesis and significantly contributing to the progressive hippocampus-dependent memory impairments *(Gold, 2003)*. Considering the highly consistent finding of aging-related Reelin plaque deposition in target areas of cholinergic neurons, such as the hippocampus, entorhinal and piriform cortices, we reasoned that these plaques could impair the integrity of axonal terminals, potentially resulting in or contributing to the degeneration of basal forebrain projection neurons. We found that the age-related neuropathological changes in the target areas of these neurons were indeed accompanied by abnormal axonal varicosities and altered expression profiles of calcium-binding proteins in plaque dense areas. Moreover, we reported a significant reduction in the number of parvalbumin-positive GABAergic as well as choline acetyltransferase-positive cholinergic projection neurons in several basal forebrain areas. No Reelin deposits were found in these regions, suggesting that the loss of projection neurons was not due to adverse effects of local protein deposition and plaque formation. Altogether, our findings suggest that the elevated Reelin plaque load in the projection areas of afferent subcortical GABAergic and cholinergic neurons affects the axonal integrity and survival of these neurons, potentially also contributing to the cognitive impairments observed in aged wild type mice.

Although all these data strongly imply an involvement of the Reelin signaling cascade in the neuropathology of AD, the molecular mechanisms through which this glycoprotein participates in the pathogenesis of AD is still unknown.

4. THE ROLE OF INFLAMMATION IN ALZHEIMER'S DISEASE

Since the first suggestion that inflammation might play a role in the pathogenesis of AD was made about 20 years ago, neuroinflammation is increasingly accepted to be associated with the onset and/or progression of the disease *(Lucin and Wyss-Coray, 2009)*. Even recent GWAS revealed that immune system members show a strong association with sporadic AD *(Lambert et al., 2009)*. Chronic activation of inflammatory pathways can be detrimental and promote degeneration, as suggested by the accumulation of activated microglia and astrocytes in the vicinity of senile Aβ plaques and neuronal lesions (for review, *(Lucin and Wyss-Coray, 2009)*. It has become apparent that the inflammatory mediators, including cytokines, chemokines, prostaglandins, free oxygen radicals and complement activation components, are not only produced in the circulating leukocytes and peripheral immune organs, but are also generated locally in the brain; most of them by the activated glial cells, but many of them also by neurons *(Lucin and Wyss-Coray, 2009)*. Beside the activation of these inflammatory modulators, numerous human postmortem studies have also shown that the initial pathological stages in the hippocampus and entorhinal cortex in AD include a pronounced up-regulation of cell cycle and cell adhesions proteins *(Parachikova et al., 2007)*, hypothesized to reflect an initial regenerative response of neurons to the presence of diffuse Aβ plaques and oligomeric or protofibrillic forms of Aβ peptides *(Hoozemans et al., 2006; Salminen et al., 2009)*. Later stages are characterized by the widespread deposition of Aβ plaques and NFTs, with their focal complement activation and accumulation of activated glial cells. Under these chronic insulting conditions, the efficiency of the innate immune system appears to fluctuate and it has been suggested that an unwanted potentiation of pro-inflammatory responses could turn the beneficial innate immunity into a negative driving force in AD pathogenesis by inducing autotoxicity *(McGeer and McGeer, 2002; Salminen et al., 2009; Wyss-Coray, 2006)*. On the other hand, another study revealed that the formation and maintenance of Aβ plaques in transgenic AD mouse models was independent from the presence of microglia *(Grathwohl et al., 2009)*, challenging our view of the role of inflammatory mediators derived from activated microglia cells. Clearly, more information is needed to understand the role of activated glia cells and to support an adverse, and potentially early-misregulated innate immunity defense in AD pathogenesis. Consequently, treating AD using an anti-inflammtory strategy is complicated due to the contradictory role of microglia.

Clinical evidence for a critical role of inflammation in the disease is given by several epidemiological studies. Individuals suffering from a chronic inflammatory disease such as rheumatoid arthritis showed a considerable reduced risk of developing AD after a regularly long-

term nonsteroidal anti-inflammatory agents (NSAIDs) administration/medication *(McGeer et al., 1996; Stewart et al., 1997)*, supporting the hypothesis of an inflammatory background in AD. Interestingly, a novel hypothesis includes the statement that normal aging itself is attended by a chronic upregulation of certain inflammatory responses such as cytokine production and microglia activation. This phenomenon is also termed "inflammaging" and refers to an over-active innate immunity in some elderly people *(Giunta et al., 2008)*. Importantly, this phenomenon can be found in both healthy and pathological aging. Although all these findings support an active involvement of the immune system in the etiology of sporadic AD, experimental evidence is still lacking.

5. PRENATAL BRAIN INFLAMMATION AND ITS IMPACT ON REELIN-MEDIATED SIGNALING

In addition to regulating inflammatory responses induced by neurodegenerative processes, cytokines released from both astrocytes and microglia have also critical effects on synaptogenesis and contribute to the targeting of synapses for elimination, thereby representing important modulators of neuronal activity, differentiation, and survival during neurodevelopment, as well as synaptic strength and plasticity in adulthood *(for review, Deverman and Patterson, 2009)*. These cytokine-mediated developmental processes are highly susceptible to disruption by immune dysregulation. Overexposure to cytokines, for example, during early brain development in mice has been shown to strongly affect cell migration, neuronal differentiation, and synaptogenesis, leading to multiple morphological and neurochemical defects which result in disturbances of homeostatic neuronal network activity and subsequent behaviour and cognitive functions in the adult offspring *(Deverman and Patterson, 2009)*. In line with these data obtained from animal studies, elevation of inflammatory cytokines in the maternal serum has been associated with an increased risk factor for neuropsychiatric disorders in the offspring *(Patterson, 2009; Penner and Brown, 2007)*. Our own recent findings provide first support for a comparable relationship for neurodegenerative diseases like AD. We have previously demonstrated that systemic administration of the synthetic cytokine releaser and viral mimic polyriboinosinic-polyribocytidilic acid (PolyI:C) in mice provides convincing support to the link between maternal infection during pregnancy and behavioral and neurochemical abnormalities in the adult offspring *(Meyer et al., 2005; Shi et al., 2003; Zuckerman et al., 2003)*. We have shown that the middle and late gestation periods correspond to

two windows of enhanced vulnerability to inflammatory cytokines, leading to an acute response in the fetal brain and delayed brain neuropathology, including defective Reelin expression, apoptosis in early adolescence *(Meyer et al., 2006)*, as well as pronounced changes in the GABAergic, glutamatergic, and dopaminergic system in limbic structures in the adult brain (**Fig. 7**, *(Meyer et al., 2008a; Meyer et al., 2008b; Nyffeler et al., 2006)*.

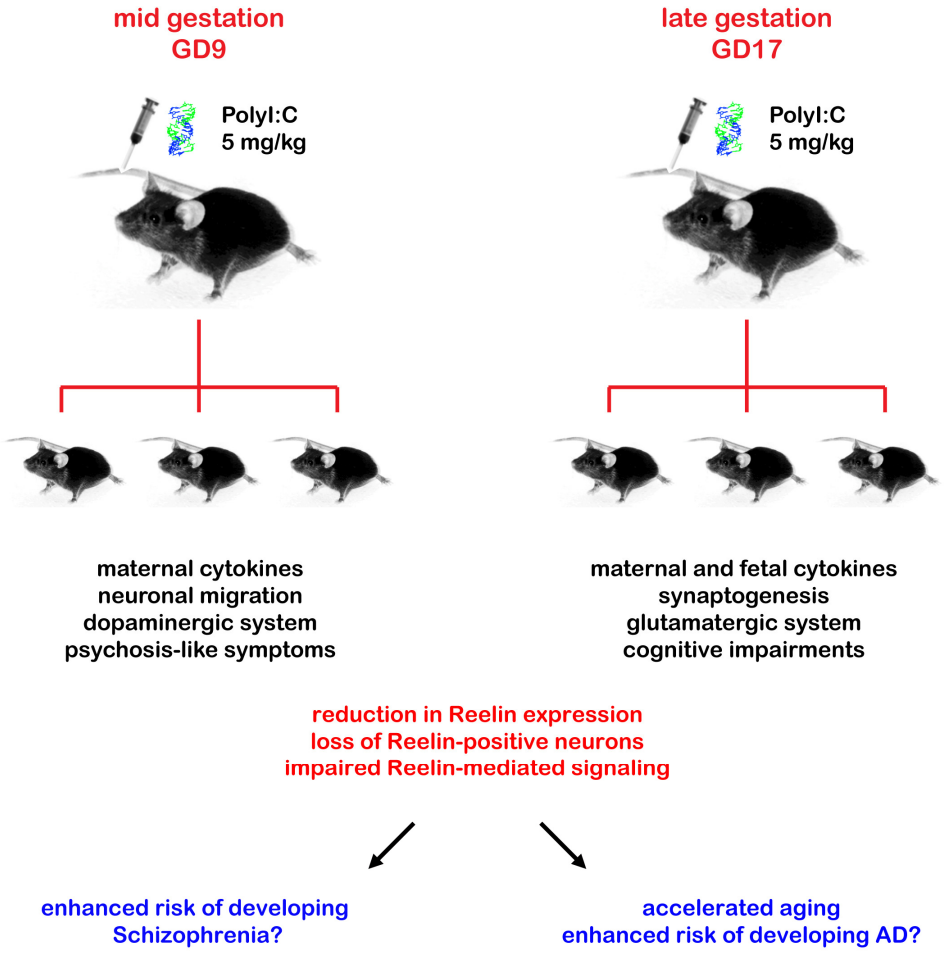

FIGURE 7: Animal models of neuropsychiatric and neurodegenerative diseases
The time of maternal immune challenge critically determines the patterns of fetal immunological, juvenile neurochemical, as well as adult behavioural abnormalities displayed by the offspring. An acute systemic challenge of the viral mimic polyriboinosinic-polyribocytodilic acid (PolyI:C), a synthetic analog of double-stranded RNA and cytokine releaser, during mid-gestation (gestational day, GD9) results in a behavioural profile that mimics certain aspects of psychotic symptoms in the adult offspring, potentially linked to the pronounced impact of this treatment on the dopaminergic system. Late-gestational (GD17) immune challenge results in a behavioural phenotype characterized primarily by cognitive impairments, accompanied by a strong imbalance in the glutamatergic neurotransmitter system. The fetal brain can directly contribute to the specific changes in inflammatory cytokine protein levels at a late-gestational but not mid-gestational immune challenge, suggesting a close correlation between acute immunological modulators and histopathological changes in the adult offspring. Although both mid- and late gestational PolyI:C treatments are equivalently effective in reducing the number of Reelin-positive neurons, the time of the maternal immune challenge is expected to determine whether the reduction in Reelin-mediated signaling primarily affects proper neuronal migration or impairs synaptogenesis. This might further contribute to the distinct symptom clusters characteristic of the adult offspring born to mid- or late-gestational immune challenged dams.

Moreover, our studies demonstrated for the first time that this prenatal viral–like infection in wild type mice significantly accelerates the reduction in Reelin-expressing interneurons and its accumulation in extracellular amyloid-like plaques, a phenomenon consistently seen in aged subjects across species and correlating with the cognitive performance *(Knuesel et al., 2009)*.

Taken together, these findings suggest that prenatal exposure to infection is not only an important factor in the segregation of symptom clusters in neuropsychiatric disorders but does also represent a critical driving force of aging-related neurodegenerative processes. Moreover, the acceleration of senescence after early brain inflammation confirms the critical role of non-genetic components as major risk factors of LOAD.

II. AIM OF THE THESIS

Previous studies performed in our lab suggest that Reelin aggregates into abnormal oligomeric or protofibrillary deposits during aging, potentially creating a precursor condition for Aβ plaque formation in animal models of sporadic AD. The overall aim of this thesis was to elucidate the significance of this neuropathology and to identify the role of abnormal Reelin-mediated signaling in the etiology of the more common late-onset form of the disease. Therefore, we focused on the following four specific aims:

STUDY I **Do Reelin and APP associate in the hippocampus of aged wild type mice?**

We previously reported an age-related decline in Reelin-expressing interneurons, accompanied by an accumulation in amyloid-like plaques in the hippocampal formation of aged mice *(Knuesel et al., 2009)*. Further, Reelin was found to closely associate with fibrillary Aβ-plaques in transgenic AD mice. The question here was whether there is also a close correlation between APP and Reelin in the amyloid-like plaques, potentially mimicking neuropathological changes in the prodromal phase of AD. Therefore, we aimed to explore the immunohistochemical properties of Reelin-positive plaques by adapting an optimized immunohistochemical protocol involving pepsin pre-digestion to investigate their potential to sequester murine proteolytic APP species in wild type mice across aging. Moreover, we aimed to clarify whether these aggregates are extra- or intracellular and investigate their potential association with glia cells and the cerebral vasculature.

STUDY II **Are there ultrastructural differences in the Reelin-positive granule morphology after a prenatal immune challenge?**

Recent studies from our group revealed that a prenatal immune challenge using the viral mimic PolyI:C results in significant acceleration of aging-associated neuropathological alterations in wild type mice, including precocious accumulation of the Reelin-positive clusters. These findings suggested that a prenatal immune challenge represents a critical driving force of aging-related neurodegenerative processes and confirms a role of dysregulated components of the innate immune system as major risk factor of sporadic AD. Here, we were interested to elucidate

whether Reelin-positive deposits in the hippocampal formation differ in size, density and ultrastructural properties between immune challenged compared to saline treated subjects.Moreover, employing a longitudinal immuno-electron microscopy study, we aimed to characterize the temporal and spatial properties, as well as their potential intracellular origin that may be indicative of degenerative processes. Another aspect of this study was the clarification of whether these observed granular clusters share similarities to the polyglycogen bodies (PGs) described by several research groups.

STUDY III Is Reelin present in the granular structures and can they be analyzed by a mass spectrometric approach?

In order to confirm our immunohistochemical and ultrastructural data, we also wanted to characterize the protein composition of the clustered granular plaques characteristic of aged wild type mice using a biochemical approach. The first question to be solved was the confirmation of Reelin, potentially its proteolytic fragments and also proteolytic fragments of APP being actually present in these age-related deposits. This was accomplished by using laser microdissection (LMD) to isolate these accumulations from the hippocampal formation of wild type mice and processed further for western blot analysis. Secondly, would a precise proteomic analysis be achievable with this small amount of sample? To address this issue, we chose a proteomic approach combining the LMD with mass spectrometry. We hypothesized that a systematic analysis of the protein composition associated and enriched in the extracellular deposits could shed light on potential signaling pathways that govern their formation, potentially even allowing a prediction on critical determinants involved in plaque initiation and maintenance.

STUDY IV Influence of reduced Reelin expression on APP processing and Tau pathology

Besides the fundamental roles of Reelin in the developing and adult brain, it has been suggested that alterations in Reelin mediated signaling contribute to neuronal dysfunction associated with AD *(Beffert et al., 2002, 2004; Hiesberger et al., 1999; Hoe et al., 2006, 2009b)*. Based on *in vitro* data from the group of Rebeck *(Hoe et al., 2006)* as well as on our previous findings on age-associated aggregation of Reelin *(Knuesel et al., 2009; Madhusudan et al., 2009)* we hypothesized that reduced Reelin-mediated signaling represents a critical upstream factor in

initiating both amyloidogenic APP processing and pTau/NFTs formation. We aimed to decipher the putative association of Reelin and its functional signaling in amyloid plaque formation as well as its influence on Tau pathology *in vivo*. We crossed heterozygous Reelin knock-out mice (*reeler*) into a transgenic AD background and tested the hypothesis that the AD-like neuropathology accelerates and aggravates during aging in the transgenic offspring expressing only 50 % of the *reeler* gene in comparison to the control. To address this issue I employed immunohistochemical and biochemical methods.

III. RESULTS

1. STUDY I: CO-LOCALIZATION OF REELIN AND PROTEOLYTIC AβPP FRAGMENTS IN HIPPOCAMPAL PLAQUES IN AGED WILD TYPE MICE

Jana Doehner[a], Amrita Madhusudan[a], Uwe Konietzko[b], Jean-Marc Fritschy[a] and Irène Knuesel[a]

[a] Institute of Pharmacology and Toxicology, University of Zurich, Switzerland

[b] Divison of Psychiatry Research, University of Zurich, Switzerland

Published in the Journal of Alzheimer's Disease 19 (2010) 1339-1357.

My contributions to this publication were the EM preparations, TEM Imaging, and most of the immunofluorescence images. I also wrote part of the manuscript.

1.1 ABSTRACT

Reelin is a large extracellular glycoprotein required for proper neuronal positioning during development. In the adult brain, Reelin plays a crucial modulatory role in the induction of synaptic plasticity and successful formation of long-term memory. Recently, alterations in Reelin-mediated signaling have been suggested to contribute to neuronal dysfunction associated with Alzheimer's disease (AD). We previously reported that aging in several species is characterized by a decline in Reelin-expressing interneurons and concomitant accumulation in amyloid-like plaques in the hippocampal formation, significantly correlating with cognitive impairments. In transgenic AD mice, we detected Reelin in oligomeric amyloid-β aggregates and in tight association with fibrillary plaques. Here, we used immunohistochemistry at the light and electron microscopy level to characterize further the morphology, temporal and spatial progression, as well as the potential of Reelin-positive plaques to sequester murine amyloid-β peptides in wild type mice across aging. We developed a new immunohistochemical protocol involving a stringent protease pretreatment which markedly enhanced Reelin-IR and allowed specific detection of variable shapes of murine anti-amyloid beta precursor protein (AβPP)-IR in plaques in the hippocampus, likely representing N-terminal fragments and amyloid-β species. Ultrastructural investigations confirmed the presence of Reelin in extracellular space, somata of interneurons in young and aged wild type mice. In aged mice, Reelin- and amyloid-β-IR was detected in extracellular, spherical deposits; likely representing small intermediates or fragments of amyloid fibrils. Our results suggest that Reelin itself aggregates into abnormal oligomeric or protofibrillary deposits during aging, potentially creating a precursor condition for fibrillary amyloid-β plaque formation.

1.2 INTRODUCTION

Many age-associated degenerative diseases are associated with abnormal proteinaceous aggregates, often in the form of amyloid deposits. In Alzheimer's disease (AD), amyloid-β (Aβ) peptides, the β- and γ-secretase-mediated cleavage product of amyloid beta-precursor protein (AβPP), are the major plaque components *(Glenner and Wong, 1984)*. Besides cerebrovascular amyloid deposits, non-vascular Aβ-plaques are highly abundant in neocortex and hippocampal formation of AD patients, typically referred to as "senile plaques" with different morphologies and protein contents, assumed to reflect different temporal and spatial aggregation states *(Fiala, 2007; Thal et al., 2006)*. The linkage of rare familial AD mutations which all affect the proteolysis of AβPP, leading to increased production of aggregation-prone Aβ peptides, supports a central role of Aβ in AD pathophysiology *(Hardy and Selkoe, 2002)*. However, it is currently unknown which type of Aβ aggregate plays a primary causative part and whether the underlying mechanisms are identical in familial and sporadic AD. Growing experimental evidence suggest that soluble Aβ species in the form of pre-fibrillary oligomers may be important in initiating neuronal malfunction and cell death *(Glabe, 2008)*. Moreover, it has been reported that soluble Aβ correlates better with dementia than insoluble fibrillary deposits *(McLean et al., 1999)*. Experimental support has been provided by numerous cell culture models of Aβ aggregate neurotoxicity *(Dahlgren et al., 2002; Hartley et al., 1999; Lambert et al., 1998; Zhang et al., 2002)* as well as administration of non-fibrillary Aβ oligomers to hippocampal slice cultures and live animals *(Cleary et al., 2005; Klyubin et al., 2005; Knobloch et al., 2007a; Knobloch et al., 2007b; Walsh et al., 2002)* that produced deficits in long-term potentiation and cognition.

Amyloid-β plaques also commonly occur in absence of disease, injury or dementia in elderly humans, aged primates and many non-primate species *(Fiala et al., 2007; Giannakopoulos et al., 1997; Peters, 2002; Price et al., 1991)*. Despite numerous investigations reporting AD-like neuropathology in aged rodents *(Armstrong et al., 1988; Jucker and Ingram, 1997; Jucker et al., 1994a; Lamar et al., 1976; Mandybur et al., 1989; Vaughan and Peters, 1981)* the development of transgenic AD mouse models focusing on genetic factors resulted in decreasing interest in this topic. However, the recent implications of soluble Aβ species in AD pathophysiology prompted us to investigate aging-related neuropathological changes in wild type rodents and non-human primates to re-evaluate abnormalities in protein expression and aggregation, expected to provide important information regarding early markers of sporadic AD-like neuropathology *(Knuesel et*

al., 2009). We reported that normal aging is accompanied by the occurrence of amyloid-like plaques in hippocampus, entorhinal and piriform cortex. These extracellular, glial-associated deposits are positive for Reelin, a conserved glycoprotein with fundamental roles during neurodevelopment *(Rice and Curran, 2001)*. The full-length form of Reelin is a 3,461 amino acid protein with a relative molecular mass of about 400 kDa. The N-terminus is glycosylated and shares 25 % identity with that of F-spondin. The central sequence consists of eight "Reelin repeats" containing an intermediate EGF-like motif *(D'Arcangelo et al., 1995)*. This is followed by a highly charged C-terminus which appears to be essential for both secretion and signal transduction *(D'Arcangelo et al., 1997; de Bergeyck et al., 1997; Nakano et al., 2007)*. In the extracellular matrix, Reelin is processed proteolytically at two sites to produce a total of six different fragments *(Lambert de Rouvroit et al., 1999)*. In the adult brain, Reelin is produced by GABAergic interneurons and expressed in layer II glutamatergic pyramidal cells in the entorhinal cortex *(Herz and Chen, 2006; Knuesel et al., 2009)* locally modulating neurotransmission in the hippocampus *(Herz and Chen, 2006)*. This is achieved via the same signaling cascade as used in the developing brain, involving binding of Reelin to its receptors, the ApoE receptor 2 (ApoER2) and very low density lipoprotein receptor (VLDLR), and the activation of an intracellular signaling cascade involving Dab1, Src and Fyn tyrosine kinases that modulate NMDA receptor-dependent synaptic plasticity and learning *(Beffert et al., 2006a, 2005; Chen et al., 2005)*. In line, we recently reported that the age-related decline in Reelin expression was accompanied by significant impairments in episodic-like memory in aged mice *(Knuesel et al., 2009)*. Moreover, recent findings describing direct binding of Reelin to the N-terminus of AβPP *(Hoe et al., 2009b)*, an involvement of Reelin in AβPP processing in-vitro *(Hoe et al., 2006)*, in Tau phosphorylation *(Beffert et al., 2004; Hiesberger et al., 1999; Ohkubo et al., 2003)* as well as binding-competition with ApoE to ApoER2 and VLDL receptors *(D'Arcangelo et al., 1999)* point to a critical function of this signaling cascade in AD pathogenesis. Here, we explored the biochemical and ultrastructural properties of Reelin-positive plaques by adapting a novel immunohistochemical protocol involving pepsin pre-digestion and preembedding immuno-electron microscopy (IEM) to investigate their potential to sequester murine proteolytic AβPP species.

1.3 METHODS AND MATERIALS

EXPERIMENTAL ANIMALS

All procedures were approved by the local authorities of the Cantonal Veterinary Office in Zurich. Female wild type mice were obtained from our in-house C57BL/6J(FUE) breeding colony (RCC Ltd, Fuellinsdorf, Switzerland). Transgenic AD mouse models included the following lines: 1) Mice overexpressing human $A\beta PP_{695}$ containing the Swedish (K670N+M671L) and Arctic (E693G) mutations in a C57Bl/6 background under the control of the prion protein promoter (PrP); named ArcAβ mice *(Knobloch et al., 2007b)*. These mice show intracellular Aβ deposition that coincides with behavioral deficits around 6 months of age before the onset of β-amyloid plaque formation and cerebral amyloid angiopathy, which starts around 9 months *(Knobloch et al., 2007b)*. 2) Mice with a complete inactivation of the mouse amyloid precursor protein gene ($A\beta PP^{-/-}$) were obtained from The Jackson Laboratory, Bar Harbor, Maine, USA (Strain: B6.129S7-*App*^{tm1Dbo}*/J*; Stock Nr. 004133). The deletion encompasses a 3.8 kb sequence encoding the promoter and the first exon, which encodes the ATG translation initiation codon and the signal peptide of the murine amyloid precursor protein *(Zheng et al., 1995)*. Neither AβPP mRNA nor protein can be detected in the mutant animals. The homozygous $A\beta PP^{-/-}$ mice are viable and show no physical or behavioural abnormalities at birth, but have a lower body mass, decreased locomotor activity, and compromised neuronal and muscular functions at 14 weeks of age *(Zheng et al., 1995)*. Finally, for antibody specificity controls, 4 female *reeler orleans* ($Reln^{rl\text{-}orl}$) mice aged 15 months were obtained from Jessica Maas, Forschungszentrum Jülich GmbH, Jülich, Germany. The $Reln^{rl\text{-}orl}$ mice, which in contrast to the original *reeler* ($Reln^{J}$) mice survive into adulthood and old ages, harbor a L1 transposable element near the 3' end of the gene that causes the skipping of a 220-bp exon *(Bar et al., 1995; Hirotsune et al., 1995)*. This deletion results in a frame shift that alters the predicted amino acid sequence of the C-terminus of Reelin; allowing the production but not the secretion of the C-terminally truncated protein *(de Bergeyck et al., 1997; Takahara et al., 1996)*. All animals were housed in same sex groups of 3 - 4 in an optimized hygiene area (OHB, University of Zurich Irchel, Switzerland) under 12-h light-dark cycle and ad libitum food and water. For the immunohistochemical examinations we employed wild type mice of 1, 2, 3, 9, 12 and 15 months of age (n = 3-5 per age), as well as 15 month-old transgenic ArcAβ and $A\beta PP^{-/-}$ mice (n = 3 per transgenic line). For the ultrastructural investigations, we included in total of 3 young (2 mo) and 3 aged (9 and 12 mo) C57Bl/6 wild type mice. Finally, for the western blotting we included brain

hippocampal lysates obtained from 15 month-old C57Bl/6 mice (n = 3). All experiments were repeated 2 (western blotting) or 3 times (EM, IHC).

TISSUE PREPARATION

Paraformaldehyde-fixation: Animals were anesthetized (Nembutal™; 4 ml/kg body weight; i.p.) and perfused with 4 % paraformaldehyde and 15 % saturated picric acid in PBS buffer and the brain tissue processed as described *(Knuesel et al., 2009)*. Serial coronal sections (40 µm) starting at Bregma level -0.82 to -3.40, or serial transverse sections starting from lateral level 2.4 to 0.48 *(Paxinos and Franklin, 2001)* were cut on a sliding microtome, collected and stored at -20°C in cryoprotectant solution until further processing. Immunohistochemical stainings were performed on either free-floating or air-dried mounted sections. *Paraffin-embedding:* The preparation of brain sections from 15 mo old ArcAβ mice (5 µm thick) was performed by Marlene Knobloch, Division of Psychiatry Research, University of Zurich, as described *(Knobloch et al., 2007b)*. Microwave pretreatment (10 min in 85°C citrate buffer), followed by a 5 min submersions in 95 % formic acid, 10 min incubation in 3 % H_2O_2 in MeOH, and blocking in 4 % BSA, 5 % goat serum and 5 % horse serum at RT for 1 h was done before the immunostaining. *Cryotissue*: Mice were decapitated, the dissected brains rapidly frozen on powdered dry ice and cut coronally (12 µm) on a cryostat, mounted on gelatinized glass slides and fixed in 70 % ice-cold acetone for 1 min.

PEPSIN PRETREATMENT

Prior to conventional immunohistochemical incubations, paraformaldehyde- and acetone-fixed brain sections were treated with pepsin (DAKO, Carpinteria, CA). Frozen aliquots containing 3 mg/ml of pepsin solution in 0.2 N HCl were thawed immediately before use and added to 0.2 N HCl to a final pepsin concentration of 0.15 mg/ml. Free-floating perfusion-fixed or mounted acetone-fixed brain sections were then incubated with the pepsin solution at 37°C. After 10, 30 (cryotissue) or 60 min (paraformaldehyde-fixation) incubation, sections were briefly washed with phosphate-buffered saline (PBS, pH 7.4) and processed for immunohistochemistry.

IMMUNOHISTOCHEMICAL PROCEDURES

Reelin immunoperoxidase stainings without pepsin pretreatment were performed on wild type brain sections as described previously *(Nyffeler et al., 2007)*. Paraffin-embedded and pepsin-treated brain sections were incubated overnight at 4°C in the primary antibody solutions diluted

in PBS containing 2 % normal goat serum and 0.2 % Triton X-100. The antibodies and dilutions used in this study are summarized in **Table 1**. After three washes in PBS, tissue sections were incubated for 30 min at room temperature (RT) in corresponding secondary antibodies coupled to Alexa488 (diluted 1:1000; Molecular Probes, Eugene, OR), Cy3 (diluted 1:500) and Cy5 (diluted 1:200; Jackson ImmunoResearch Laboratories) and processed as described *(Nyffeler et al., 2007)*. Thioflavin-S counterstaining involved a 10 min incubation in filtered 1 % aqueous Thioflavin-S (Sigma-Aldrich, Buchs, Switzerland) solution at RT, followed by 2 washes for 5 min in 80 % EtOH, 5 min wash in 95 % EtOH, and 3 times 5 min washes in distilled water. Brain sections were then air-dried in the dark and mounted with aqueous permanent mounting medium (DAKO).

TABLE 1: Primary antibodies used in this study

Antigen	Immunogen	Manufacturer, Species, type, cat.no	Dilution
Reelin, clone G10	Rodent Reelin, amino acid residues 164-496	Chemicon (Millipore, Billerica, MA) mouse monoclonal, #MAB5364	1:1000 (IHC) 1:1000 (IEM)
Amyloid-$\beta_{1\text{-}40/42}$	Synthetic $A\beta_{1\text{-}40}$ conjugated to BSA. The immunogenic peptides shows a high degree of homology with human/mouse $A\beta_{1\text{-}40}$ and $A\beta_{1\text{-}42}$	Chemicon (Millipore, Billerica, MA) rabbit polyclonal, #AB5076	1:5000 (IHC) 1:1000 (IEM) 1:1000 (WB)
Amyloid-β, clone 6E10	Human Aβ protein, amino acid residues 1-17	Chemicon (Millipore, Billerica, MA) mouse monoclonal, #MAB1560	1:500 (WB)
Amyloid-β protein precursor (AβPP A4, clone 22C11)	Bacterial recombinant AβPP (pre-AβPP695) fusion protein, human amino acid residues 66-81 (N-terminus)	Chemicon (Millipore, Billerica, MA) mouse monoclonal, #MAB348	1:1000 (IHC) 1:1000 (WB)
Amyloid-β protein precursor (C-terminus)	Nine amino acid peptide from the C-terminus of human AβPP (YKFFEQMQN)	Chemicon (Millipore, Billerica, MA) rabbit polyclonal, #AB5352	1:500 (IHC) 11000 (WB)
α1-syntrophin	Synthetic peptide (CRQPSSPGPQPRN LSEA), Rat amino acid residues 191-206 *(Haenggi et al., 2005)*	Affinity purified polyclonal rabbit serum	1:500 (IHC)

IHC: Immunohistochemistry; IEM: Immuno-electron Microscopy; WB: Western Blotting

ANTIBODY CHARACTERIZATION

The anti-Reelin, clone G10 antibody recognizes the full-length (~400 kDa) protein and two N-terminal products (~300 and ~180 kDa) on Western blot of wild type but not Reelin knockout (*reeler*) mouse tissue *(Lambert de Rouvroit et al., 1999)*. On brain tissue sections obtained from mouse, rat, monkey and postmortem human samples, the G10 antibody shows highly selective somatic IR in GABAergic interneurons throughout the forebrain, as well as granule cells in the

cerebellum, mitral cells in the olfactory bulb, pyramidal neurons in entorhinal and piriform cortex; which is absent on brain tissue collected from *reeler* mice *(Chin et al., 2007; Knuesel et al., 2009; Miettinen et al., 2005; Pappas et al., 2001, 2003; Ramos-Moreno et al., 2006)*. All the studies revealed that the G10 antibody additionally shows a distinct neuropil staining, particularly prominent in the CA1 stratum lacunosum-moleculare and outer molecular layer of the DG, likely reflecting the secreted protein located in the extracellular matrix. The immunohistochemical staining described here is highly comparable to the published studies mentioned above. In addition, we confirmed the specificity of the G10 antibody on perfused brain tissue obtained from aged $Reln^{rl\text{-}orl}$ mice which revealed only intraneuronal but no extracellular IR (data not shown).

The rabbit polyclonal antibody beta-amyloid Aβ1-40/42 was raised against a synthetic BSA-conjugated peptide corresponding to the beta-amyloid 1-40 and recognizes the β- and γ-secretase-mediated proteolytic cleavage product of AβPP, Aβ1-40/42, the major component of human senile amyloid-β plaques *(Glenner and Wong, 1984)*. According to the manufacturer's technical information, the immunogenic peptide shows a high degree of homology between human and mouse, and correspondingly, the antibody recognizes the human and mouse AβPP, β-stubs (β-secretase-cleaved C-terminal fragments), and the fully cleaved Aβ peptides, in line with the immunohistochemical and western blot data described here and our previous study *(Knuesel et al., 2009)*.

The mouse monoclonal antibody β-amyloid clone 6E10 was raised against amino acid residues 1-17 of the beta-amyloid protein and reacts with human but not mouse full-length AβPP on paraffin-embedded and perfusion-fixed brain tissue, as well on brain lysates of transgenic (overexpressing mutant human AβPP), but not wild type mice *(Knobloch et al., 2007b; Mayeux et al., 1999; Van Dooren et al., 2006)*. The mouse monoclonal 22C11 anti- AβPP (N-terminus) was raised against a bacterial recombinant amyloid precursor protein (AβPP A4) fusion protein (human AβPP695). The antibody recognizes amino acids 66-81 of the N-terminus of the full-length AβPP molecule *(Hilbich et al., 1993; Knobloch et al., 2007b)* and detects all three isoforms of AβPP in rodent and human tissue: the mature form of ~130 kDa, the secretory N-terminal fragments s AβPP of ~120 kDa, the immature AβPP of ~110 kDa *(Knobloch et al., 2007b)* as well as the newly described N-terminal fragment of ~35 kDa *(Dooley et al., 1992; Nikolaev et al., 2009)*.

The rabbit anti-AβPP polyclonal antibody was raised against a nine amino acid peptide from the C-terminus of AβPP. According to the manufacturer's technical information, the immunogenic peptide shows a high degree of homology between human and monkey, and correspondingly, the antibody shows reactivity in both species. This antibody has also been used in numerous murine studies, and was shown to recognize full-length AβPP, C-terminal fragments resulting from cleavage by secretases by both immunoblotting and immunocyto- and histochemistry *(Chang et al., 2004; Muresan and Muresan, 2004)*.

The affinity-purified rabbit polyclonal α1-syntrophin antibody was raised against a peptide sequence derived from the first pleckstrin-like domain of the rat syntrophin α1 gene *(Haenggi et al., 2005)* α1-syntrophin is a member of the dystrophin-associated protein complex and localized to cellular membranes in skeletal muscles, kidney, liver, and brain, including the postsynaptic density of glutamatergic synapses as well as astrocytic endfeet *(Haenggi and Fritschy, 2006)*. Specificity of the antibody has been demonstrated using tissue from α1-syntrophin knockout mice, as well as in preadsorption experiments incubating primary antibodies with peptide antigen, which resulted in a dose-dependent loss of specific IR *(Haenggi et al., 2005)*.

PREEMBEDDING IMMUNO-ELECTRON MICROSCOPY

Mice were anesthetized as described above and perfused with a fixative containing 4 % paraformaldehyde, 0.2 % picric acid and 0.1 % glutaraldehyde in 0.1 M phosphate buffer, pH 7.4. The tissue was postfixed for 5 h at 4°C, washed and stored in phosphate buffer overnight. Coronal sections (70 μm) were cut with a Vibratome, the hippocampus dissected and cryoprotected in 30 % sucrose overnight. The sections were then processed for anti-Reelin and -Aβ immunohistochemistry using DAB immunoperoxidase reactions (secondary goat-anti mouse/anti rabbit, conjugated to biotin, 1:250; Jackson ImmunoResearch Laboratories Inc., West Grove, PA) or secondary immunogold-conjugated antibodies (1:200; Alexa Fluor-488-Fluoronanogold-Fab, Nanoprobes Yaphank NY, USA). The latter immunoprobe consists of a 1.4 nm gold particle conjugated with goat-anti mouse F_{ab} fragment and fluorescein.

The DAB reaction product was silver-intensified and gold-toned according to *(Sassoe-Pognetto et al., 1994)*. Briefly, sections were incubated in a solution containing 2.8 % hexamethylenetertramine (Merck, Darmstadt, Germany), 0.2 % silver nitrate (Merck) and 0.02 % disodium tetraborate (Merck) for 10 min at 60°C. The sections were then rinsed in distilled water and treated for 2 min with gold chloride (0.05 % in distilled water, Merck).

Finally the sections were rinsed in distilled water and incubated for 2 min in sodium thiosulfate (2.5 % in distilled water, Merck).

Optimal visualization of the 1.4 nm gold-particles (FNG-labeled tissue samples) at the electron microscopic level required gold enhancement. The specimens were incubated with a commercially available kit (GOLDENHANCE^{TM}-EM, Nanoprobes, Yaphank NY, USA) containing four vials with solutions called enhancer (solution A), activator (solution B), initiator (solution C) and buffer (solution D). Equal volumes of each solution were mixed to form the final reagent. The samples were then immersed in 300 µl of this solution and incubated for 7min at RT. After the enhancement for both procedures, samples were kept in Na-cacodylate buffer (0.1 M, pH 7.4) overnight. Finally, sections were postfixed in 0.5 % OsO4 (on ice), counterstained with 1 % uranyl acetate, dehydrated in acetone and embedded in Epon 812. Ultrathin sections (50 nm) were collected on adhesive-coated nickel grids (300 mesh) and examined using a Philips 208 transmission electron microscope equipped with a side mounted digital camera (4k x 3k; Gatan GmbH, Munich, Germany).

REELIN-POSITIVE PLAQUE ESTIMATES AND QUANTIFICATION OF REELIN-Aβ CO-LOCALIZATION

The immunoperoxidase stainings were analyzed with bright-field microscopy and digital images acquired using a color digital camera (AxioCam, Zeiss, Jena, Germany) controlled by AxioVision 4.1 software (Zeiss). Quantification of Reelin-positive plaques in the dorsal hippocampus, cerebellum, and olfactory bulb were performed on transverse sections obtained from young (3 mo; n = 3) and old (15 mo; n = 5) wild type mice on 4-5 sections per subject. They were counted exhaustively, i.e. involving all and not only a representative sample of the immunoreactive plaques labeled within the outlined brain regions using the 40x objective (NA 1.3). The total number of plaques was estimated according to the formula $P_{tot} = \sum P \times 1/ssf$, where $\sum P$ is the sum of plaques, and ssf = the section sampling fraction (1/6). Qualitative evaluations of immunofluorescence labelings were done with confocal microscopy (LSM-710, Zeiss) using either 40x (NA1.3) or 100x objectives (NA1.4). Double-immunofluorescence stainings were visualized using sequential acquisition of each channel. The pinhole aperture was set to 1.0 Airy unit for each channel. Stacks of consecutive optical sections (3-6; 512 x 512 pixels, spaced 1 µm in z) were acquired at a magnification of 0.11-0.22 µm/pixel. For visual display, Z-sections of all channels were projected in the z-dimension (maximal intensity), and merged using the image analysis software Imaris (Bitplane, Zurich, Switzerland). Cropping of

images, adjustments of brightness and contrast were identical for each labeling using electron microscopy, bright field or epifluorescence microscopy and done using Adobe Photoshop (Adobe Systems, San Jose, CA). Reelin- and Aβ–immunoreactive signals in amyloid-like plaques were quantified on projected z-sections acquired in CA1 stratum radiatum and lacunosum-moleculare obtained from paraformaldehyde-fixed brain tissue. Red and green channels were first individually segmented and analyzed in regard to pixel brightness (area and integrated density), as well as pixel overlap between Reelin- and Aβ-IR within outlined plaques using a co-localization plug-in of ImageJ (NIH, http://rsbweb.nih.gov/ij/). A total of 6-10 plaques collected from 3-7 perfusion-fixed sections per animal (n = 4; 15 month old wild type mice) and treatment (no pepsin, 60 min pepsin pre-incubation) were included in this quantitative analysis.

STATISTICAL ANALYSIS

The analysis was performed with the software StatView version 5.0 (Abacus Concepts, Inc., Berkeley, CA). Nonparametric Mann-Whitney *U* tests were used to statistically compare the estimated total number of Reelin-positive plaques in young (3 mo, n = 3) versus aged (15 mo, n = 5) wild type mice for each brain region separately. The same test was also used for the quantification of the difference in immunofluorescence staining intensity of Reelin IR and Reelin-Aβ co-localized signals (total area and integrated density of individually labeled plaques) with or without pepsin pretreatment (n = 4 animals per treatment group). Statistical significance was set at $p < 0.05$.

1.4 RESULTS

AGING-RELATED ACCUMULATIONS OF REELIN-POSITIVE PLAQUES CORRELATE WITH THE EXPRESSION PATTERN OF REELIN

Young and aged wild type mice (3 and 15 mo) were employed in an immunohistochemical evaluation without pepsin pretreatment to confirm the aging-associated changes in Reelin expression and to investigate the spatial profile of Reelin-positive plaque deposition in the murine brain. Anti-Reelin immunoperoxidase stainings confirmed our previous findings of a pronounced age-associated reduction in Reelin-immunoreactivity (IR) in GABAergic interneurons and neuropil of the hippocampus, particularly prominent in the CA1 stratum lacunosum-moleculare (slm) and outer molecular layer of the DG (**Fig. 1A-B**). Reelin-positive plaques were detected at comparable densities, layer-specific locations, as well as in close vicinity to Reelin-expressing neurons in aged individuals (**Fig. 1C-D**) as described previously *(Knuesel et al., 2009)* confirming the consistency and robustness of this age-related pathology. Moreover, we found a pronounced reduction in Reelin-IR in cerebellar granule cells, accompanied by plaque depositions around Purkinje cells (**Fig. 1E**), and prominent accumulations in the main and accessory olfactory bulb (**Fig. 1F**); all areas with high densities of Reelin-secreting cells in adulthood, indicating a close association between extracellular Reelin levels and plaque deposition. Counterstaining using Thioflavin-S to detect β-sheet containing proteinous aggregates revealed a high degree of co-localization between Reelin-IR and Thioflavin-S staining in extracellular plaques in 15 month old subjects (**Fig. 1G**), confirming the presence of amyloid-like depositions in aged wild type mice. Thioflavin-S staining was not detectable in 3 month old mice (data not shown), in line with the absence of Reelin-positive plaques at this age (**Fig. 1A**). Stereological estimates of the number of Reelin-positive plaques in these areas revealed significant differences in the total number of plaques in the cerebellum (3 mo: median = 72; 15 mo: median = 522; Mann–Whitney $U = 15.5$, $p = 0.02$) and hippocampus (3 mo: median = 48; 15mo: median = 684; $U = 15.1$, $p = 0.03$). In the olfactory bulb, the difference in distribution of the plaque density between the two groups closely approached significance ($U = 13.5$, $p = 0.057$; **Fig. 1H**).

To examine the relationship between Reelin- and β-amyloid plaques in aged transgenic ArcAβ AD mice, we performed double-immunofluorescence staining using anti-Reelin and anti-amyloid-β antibodies (rabbit anti-Aβ1-40/42, **Table 1**). Reelin-positive plaques were detected in the hippocampus and cortex (**Fig. 2A**), showing similar granular morphologies as described in

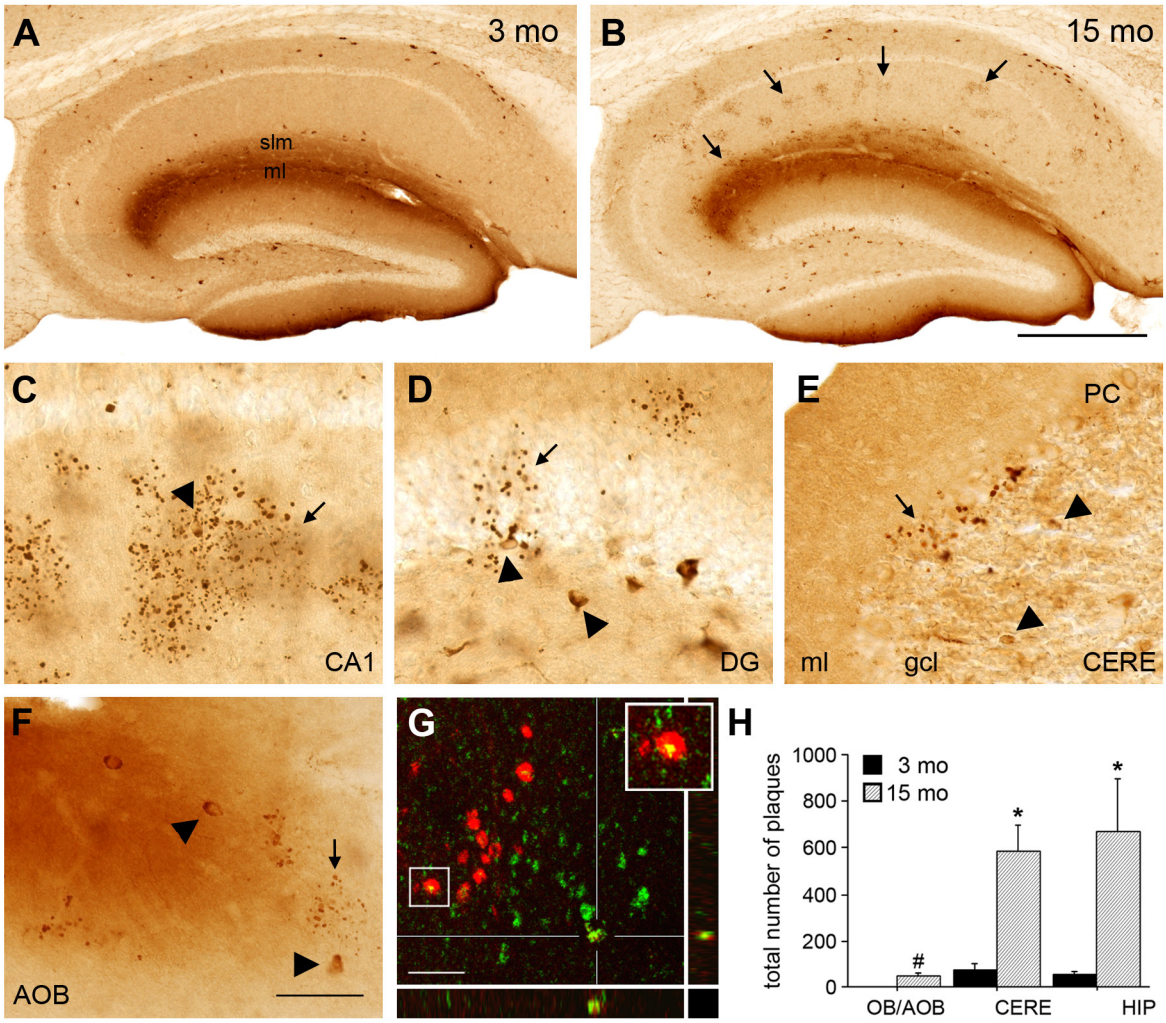

FIGURE 1: Accumulation of Reelin in extracellular plaques in the aged brain. A-B) Immunoperoxidase staining using anti-Reelin antibodies on brain sections of young (3 mo) and old (15 mo) wild type mice (n = 3 per age). Note the reduction in IR in Reelin-expressing interneurons and neuropil, particularly prominent in CA1 stratum lacunosum-moleculare (slm) and outer molecular layer (ml) of the DG; concomitantly with the striking high density of Reelin in amyloid-like plaques (arrows) in aged compared to young mice. **C-D**) Higher magnification of Reelin-positive plaques (arrows) located in the CA1 and DG. Most of these aggregates are detected around or in close proximity to Reelin-expressing neurons (arrowheads). **E**) A high density of Reelin-positive deposits was also evident in the cerebellum (CERE), precisely surrounding Purkinje cells (PC, arrow) and again closely associated with Reelin-producing cerebellar granule cells (arrowheads). **F**) Similar observations were done in the main (OB) and accessory olfactory bulb (AOB), with many amyloid-like plaques (arrow) centered around Reelin-expressing interneurons (arrowheads). **G**) Thioflavin-S counterstaining (green) confirms the amyloid-like nature of the Reelin-positive plaques (red) in the hippocampus of 15 mo-old mice. Note the dense aggregated core that contains both Reelin-IR and Thioflavin-S stainings (yellow signal, box is enlarged in the upper right corner). Crossed lines indicate the levels of the xz- and yz-view of one individual granule positive for Reelin and Thioflavin-S. **H**) Stereological estimates of the total number of Reelin-positive plaques in the olfactory bulb, cerebellum and hippocampus of young and aged wild type mice. $*p < 0.05$; $\#p = 0.056$, statistical significance based on Mann-Whitney *U* test. Abbreviations: ml, molecular layer; gcl, granular cell layer. Scale bars: **B** = 500 µm, **F** = 50 µm, **G** = 10 µm.

old wild type mice. Interestingly, Reelin-IR was closely associated but never completely co-localized with fibrillary Aβ plaques (**Fig. 2B-D**), suggesting a tight association between Reelin- and amyloid-β plaques in transgenic AD mice with ~6-fold overexpression of human $A\beta PP_{swe,arc}$

(Knobloch et al., 2007b). Human and rodent AβPP not only share >96 % amino acid sequence identity, the Aβ peptides also have highly similar biophysical properties with respect to their ability to form congophilic filaments and amyloid fibers *(Fung et al., 2004; Hilbich et al., 1991b)*. However, immunohistological investigations so far failed to confirm the presence of fibrillary amyloid plaques in aged rodents.

PEPSIN PRETREATMENT ENHANCES REELIN-IMMUNOREACTIVITY AND ENABLES THE DETECTION OF DISTINCT MURINE AβPP-DERIVED IMMUNOREACTIVITY

To test whether Reelin-positive plaques may also serve as a nucleation site for murine amyloid plaques in aged wild type rodents, we optimized our protocols to better visualize rodent AβPP, putative N-terminal fragments and Aβ peptides and their association with Reelin-positive plaques in aged subjects. Immunostaining using cryotissue allows the detection of Reelin both intraneuronally and extracellularly in plaques (**Fig. 3A**). However, background labeling especially in the cerebral vasculature suggests reduced antigenicity due to tissue fixation. We therefore decided to apply an antigen retrieval step, based on the protocol of Watanabe and colleagues *(Watanabe et al., 1998)*. They applied short pepsin pretreatment to improve the epitope accessibility and immunohistochemical detection of postsynaptic proteins. Here, we extended the protease pretreatment up to 60 min at 37°C (**Fig. 3**), which allowed us to significantly enhanced immunodetection and visualization of Reelin-IR in neurites, particularly prominent in axonal projections (**Fig. 3B''**) as compared to non-treated brain sections. Importantly, the prolonged pepsin pretreatment significantly reduced background staining as well as IR of soluble intraneuronal Reelin and allowed a visual enrichment of aggregated Reelin in both cryotissue (**Fig. 3A**) and perfusion-fixed brain (**Fig. 3B**) sections, pointing to an aggregated and protease-resistant state of the deposits. For the perfusion-fixed tissue, we obtained a 3-fold increase in total area (Mann-Whitney U, $p = 0.01$) and 8-fold increase in brightness (integrated density, Mann-Whitney U, $p < 0.0001$) covered by immunoreactive signals within the amyloid-like plaques following a 60-min pepsin treatment as compared to no pepsin. Control treatments using solvent solution (0.2 M HCl in PBS) alone, did not effect the intensity and density of Reelin-immunoreactive signals (**Suppl. Fig. 1 online**), indicating that the proteolytic activity of pepsin and not the acidic environment is responsible for the antigen-retrieval effect.

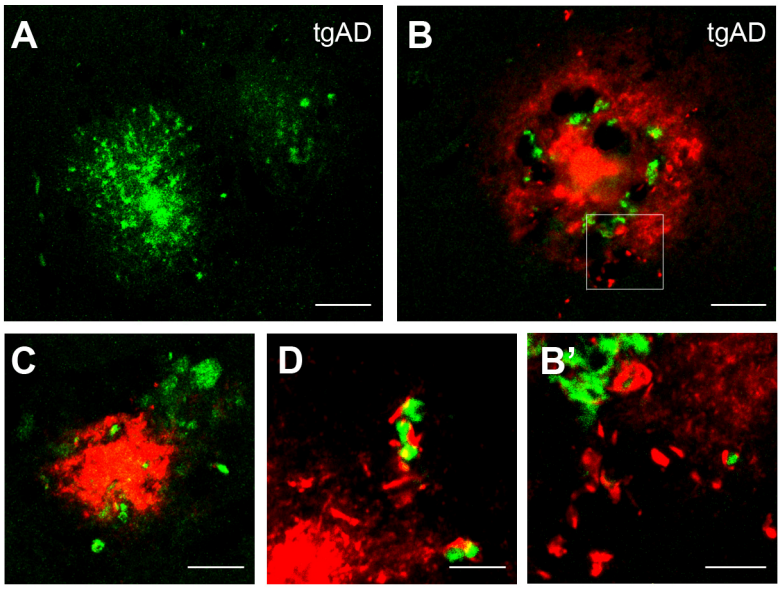

FIGURE 2: Reelin-positive plaques associate with amyloid-β in AD mice. Representative confocal images of immunofluorescence stainings of brain tissue obtained from 15 mo old transgenic ArcAβ mice (n = 3) using mouse anti-Reelin and rabbit anti-Aβ1–40/42 antibodies. **A-B**) Granular Reelin-positive deposits (green) were detected at high densities and close association with amyloid-β plaques (red) throughout the hippocampus. **B'** shows a higher magnification of the boxed area outlined in **B**. Note the lack of co-localization between the two markers. **C-D**) Tight linkage between Reelin- and fibrillary Aβ-immunoreactive signals was evident in numerous amyloid-β plaques, most prominently at the edge of the extracellular deposits. Scale bars: **A-B** = 30 μm, **C-D** = 15 μm, **J, B'** = 5 μm.

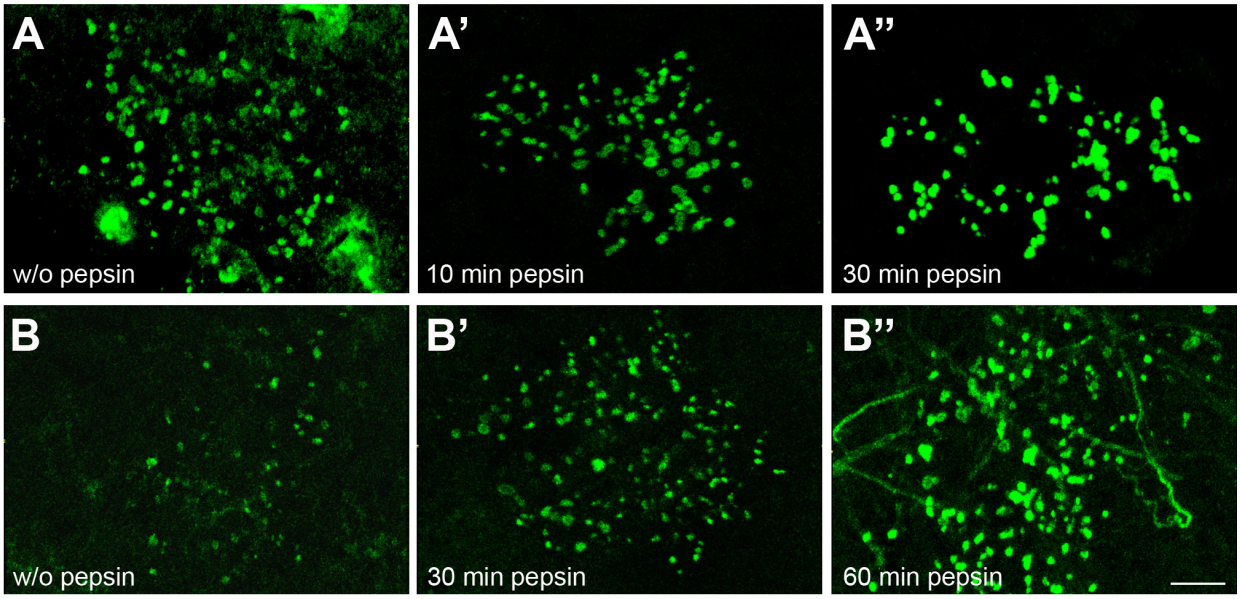

FIGURE 3: Pepsin pretreatment strongly enhances Reelin-immunoreactivity in extracellular deposits. Anti-Reelin immunohistochemistry using aceton-fixed cryosections (**A**) and paraformaldehyde perfusion-fixed sections (**B**) of 15 mo old wild type mouse brain tissue (n = 4 animals per treatment) processed with or without pepsin pretreatment for 10, 30 or 60 min. Note the pronounced treatment effect in terms of reduction of the background staining and the visual enhancement of Reelin-IR in amyloid-like plaques and axonal projections (**B"**). Scale bar: **B"** = 15 μm.

Our pepsin-pretreatment protocol allowed for the first time the specific detection of rodent anti-$A\beta_{1\text{-}40/42}$–IR in granular Reelin plaques in aged wild type mice, which was not possible without pepsin pretreatment (**Fig. 4**). With the conventional protocol, anti-Aβ-IR was readily detectable in neuronal somata (**Fig. 4A**) and to some extent also in neurites throughout the brain, likely representing full-length AβPP. Following 60 min pepsin pretreatment, the intraneuronal IR was lost but extracellular aggregates were clearly detectable (**Fig. 4B**), indicating that intraneuronal, soluble AβPP is degraded while extracellular, aggregated Aβ is not, likely due to its protease-resistant state. Since the Aβ-specific antibody also detects full-length AβPP and the soluble sAβPP α/β fragments, we included additional antibodies raised against the N- (N-AβPP) and the C-terminus of AβPP (C-AβPP) to characterize further the plaque components. Without pepsin pretreatment, both antibodies revealed again strong IR in neuronal somata and neurites in both young and old wild type mice, confirming the presence of full-length AβPP (data not shown). As described for the Aβ- and Reelin-IR, pepsin treatment resulted also in a strong reduction of intraneuronal fluorescence but at the same time it strongly enhanced extracellular IR using antibodies against the N-terminus (**Fig. 4C**). This was not seen using an antibody raised against the C-terminus of AβPP (**Fig. 4D**), suggesting the presence of either the 35 kDa N-terminal fragment *(Nikolaev et al., 2009)* and/or soluble s AβPP α/β ectodomains. Although the presence of low levels of full-length AβPP cannot be completely ruled out, the absence of immunoreactive signals within the extracellular deposits using C-terminus-specific AβPP antibodies suggest that proteolytic cleavage products rather than the full-length form of AβPP preferentially accumulate in these plaques. Importantly, the same pepsin treatment of brain sections obtained from young (1 month old) mice did not yield any extracellular immunoreactive signals (data not shown), pointing to the possibility that aggregated Reelin deposits might act as a seed for murine amyloid-β and N-terminal AβPP fragments. Support for this hypothesis is provided by our observations that variable shapes of the Aβ-IR in extracellular plaques located around Reelin-positive deposits were detected in aged wild type mice after pepsin pretreatment. Their morphology included both typical granular but also fibrillar features (**Fig. 4E**), which closely resembled the amyloid-β plaques in transgenic ArcAβ mice. Reelin was again associated but not co-localized with Aβ–IR in fibrillary plaques (**Fig. 4E''**). Control stainings using brain sections of age-matched AβPP knockout mice incubated with the same antibody dilutions confirmed the specificity of the immunoreactive signals (**Fig. 4F**), suggesting the presence of murine Aβ peptides and N-terminal AβPP fragments in granular and fibrillary amyloid-like plaques in aged

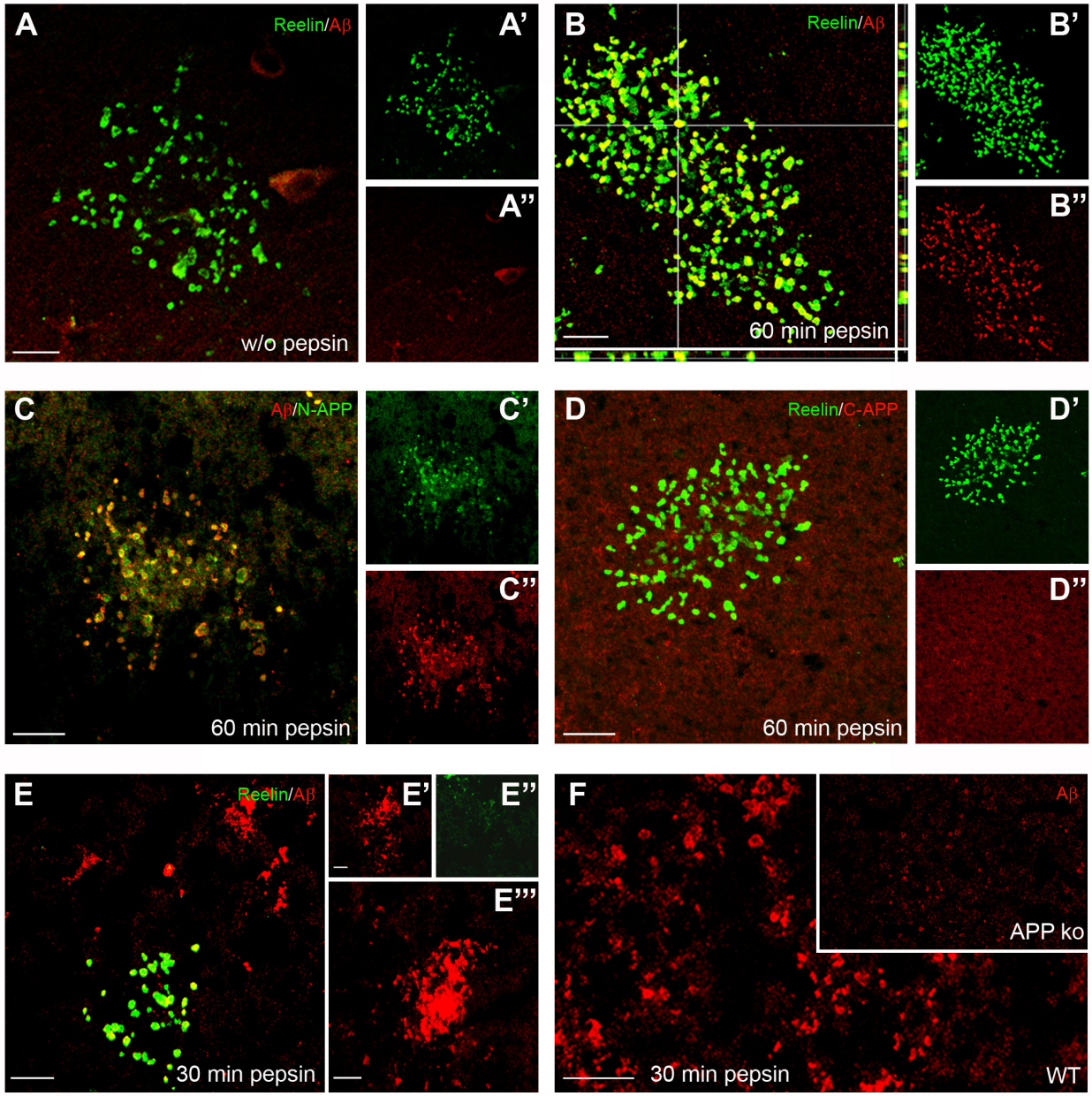

FIGURE 4: Pepsin pretreatment enables the detection of murine Aβ and N-terminal AβPP fragments. Double-immunofluorescence stainings of perfusion-fixed (**A-D**) and fresh frozen (**E-F**) wild type mice brain sections using anti-Reelin (green: **A, B, D, E**), anti-Aβ1-40/42 (red: A-C, E-F), anti-N-AβPP (green: **C**) and anti-C-AβPP (red: **D**) antibodies following a 60 min or 30 min pepsin pretreatment reveals murine Aβ- and N-terminal AβPP IR in Reelin-positive plaques in the hippocampus of aged wild type mice (12 mo, n = 3). **A**) Without pepsin pretreatment, murine Aβ–IR is not detectable in plaque-like deposits. **B**) Note the co-localization of Reelin and Aβ (yellow signal) in a subfraction of individual granules on pepsin pre-treated sections. **C**) Pepsin pretreatment also revealed immunoreactive signals in the extracellular granules using an N-terminus-specific AβPP antibody, but not with the antibody raised against the C-terminus of AβPP (**D**). Control stainings using 1 month-old wild type mice did not yield any extracellular IRs (data not shown). **E**) Prolonged pepsin pretreatment on cryotissue even allowed the visualization of fibrillary Aβ (red) plaques in close vicinity to Reelin (green) plaques. In line with findings from transgenic brain sections, fibrillary Aβ plaques (**E'-E'''**) showed no co-localization with Reelin-IR (**E''**). **F**) Representative images of control labelings using identically processed sections from age-matched wild type and AβPP knockout mice (n = 3 per mouse line). No specific anti-Aβ IR (red) was evident in mutants as compared to control subjects. Scale bars: **A-E, F** = 15 µm, **E'**= 10 µm, **E'''**= 7 µm.

wild type mice. Quantification of the co-localization of Reelin- and Aβ-IR within granular plaques confirmed these observations and revealed significant differences following pepsin pretreatment as compared to the non-treated brain sections in the total area covered (w/o pepsin: median = 1.01 μm^2; w pepsin: median = 160.3 μm^2, Mann–Whitney $U = 15.1$, $p = 0.02$), as well as the integrated pixel brightness, combining both size and staining intensity of the co-localized immunoreactive signals (w/o pepsin: median = 650.2; w pepsin: median = 3180.6, Mann–Whitney $U = 15.2$, $p = 0.03$).

ULTRASTRUCTURAL PROPERTIES OF REELIN-POSITIVE PLAQUES IN AGED WILD TYPE MICE

To characterize the ultrastructural features of the Reelin-positive deposits and their potential association with rodent Aβ, brains of young and aged wild type mice were analyzed using IEM. We detected specific Reelin-IR in the soma of interneurons in CA1 stratum lacunosum-moleculare (slm), particularly prominent in the smooth endoplasmatic reticulum (**Fig. 5A,** arrows, enlarged in **A'**). Importantly, it was not associated with the highly abundant intracellular lipofuscine deposits, characteristic of aged cells (**Fig. 5A,** asterisks, enlargement in **A''**) as described in detail elsewhere *(Peters et al., 1991*; *Harris and Spacek*, *Synapse Web* http://synapses.clm.utexas.edu). Reelin-IR was also highly enriched in the extracellular space in aged individuals as compared to young mice (**Fig. 5B-C**), potentially representing preliminary stages of protein aggregates. In addition, we found prominent accumulations of Reelin-IR in astrocytic end-feet enclosing cerebral blood vessels (**Fig. 5D-E**), highly similar to the close association of Reelin plaques with the vasculature as shown by immunohistochemical stainings using the end-feet marker, α1-syntrophin (**Fig. 5F**). These findings point to putative clearance pathways of the extracellular deposits that might be less effective in aged compared to young individuals.

Our ultrastructural investigations confirmed the presence of Reelin in amyloid-like plaques, again highly selectively abundant in the CA1 slm of aged wild type (**Fig. 6**). The stained globular structures very likely represent the individual granules of the Reelin deposits. They were typically surrounded by discontinuous membranes, indicative of extracellular localizations. Surprisingly, they exhibited a distinctive ultrastructure; with the center of the granule containing mostly fibrillary material and being free of any normal cell organelles (**Fig. 6**). Reelin-IR was detected in these membranes and fibrillary components. With immunoperoxidase reactions (DAB), the core of the granules was usually homogenously covered and the underlying structures difficult to identify (**Fig. 6A-D**).

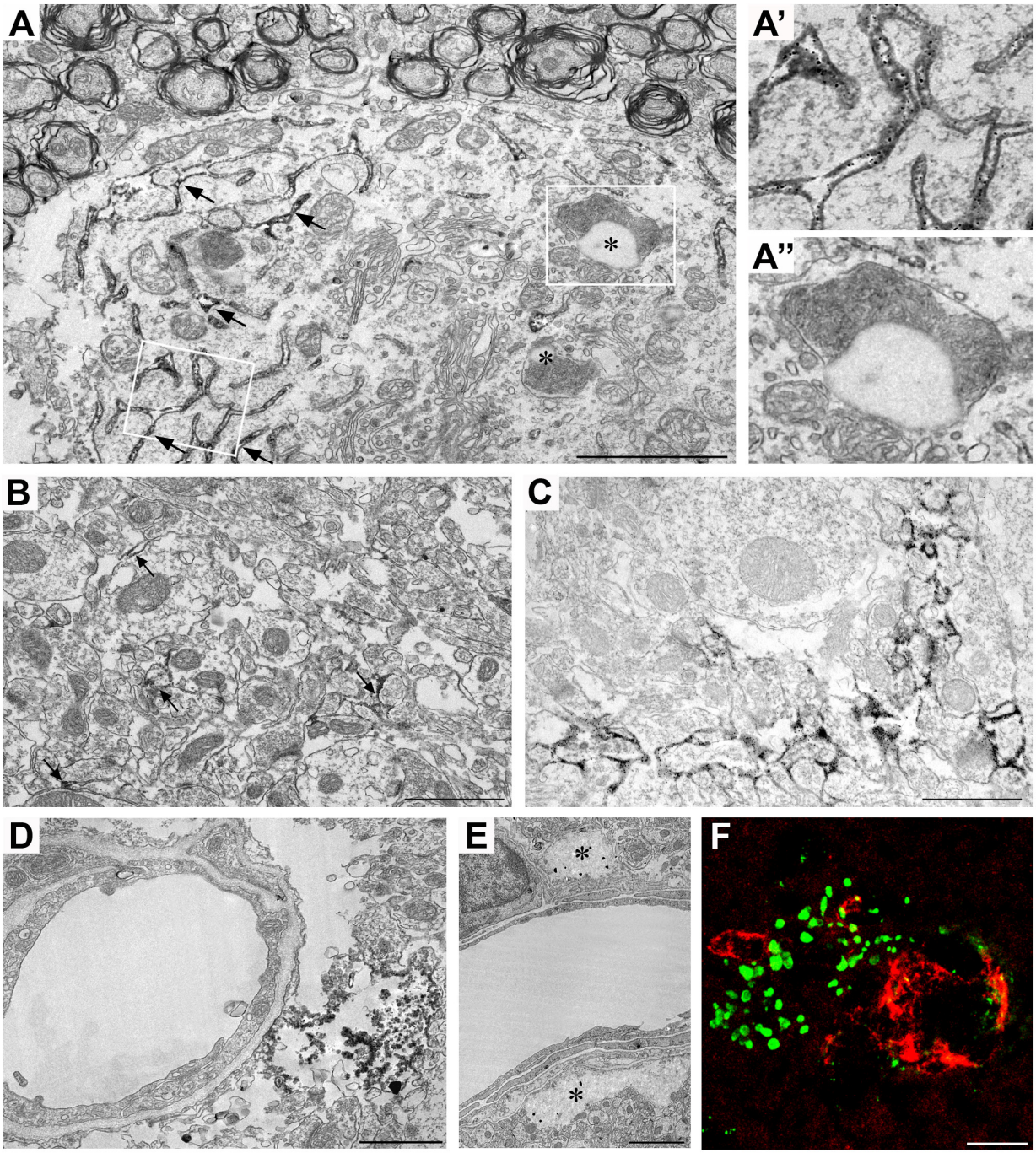

FIGURE 5: Immuno-electron microscopy using anti-Reelin antibodies in CA1 stratum lacunosum-moleculare. Sections from young (2 mo; **B**) and aged (9 mo: C; 12 mo: **A, D-E**) wild type mice (n = 3 animals per age group) were processed using 3,3'-Diaminobenzidine (DAB) immunoperoxidase reactions (**A-D**) or Fluoronanogold-conjugated antibodies (**E**). **A**) Representative image of the soma of a Reelin-expressing interneuron showing Reelin-IR in the smooth endoplasmic reticulum (**A**, arrows, white box is enlarged in **A'**). Intraneuronal lipofuscine deposits, which are indicative of aged cells, were devoid of Reelin-IR (**A**, asterisks, enlarged in **A''**). **B-C**) Reelin-IR in the extracellular space was much denser in aged (**C**) compared to young mice (**B**, arrows). **D-F**) Reelin-IR in granular deposits was also associated with astrocytic endfeet enclosing the cerebral blood vessels, as shown with DAB labeling (**D**) as well as Fluoronanogold-conjugated antibodies (**E,** asterisks). **F**) The strong accumulation of Reelin-positive deposits in astrocytic endfeet is also observed in immunohistochemical stainings using the same anti-Reelin antibody (green), as confirmed in double-immunofluorescence labelings with the astrocytic endfeet marker, α1-Syntrophin (red). Scale bars: **A, E** = 2 μm, **B-D** = 1 μm, **F** = 15 μm.

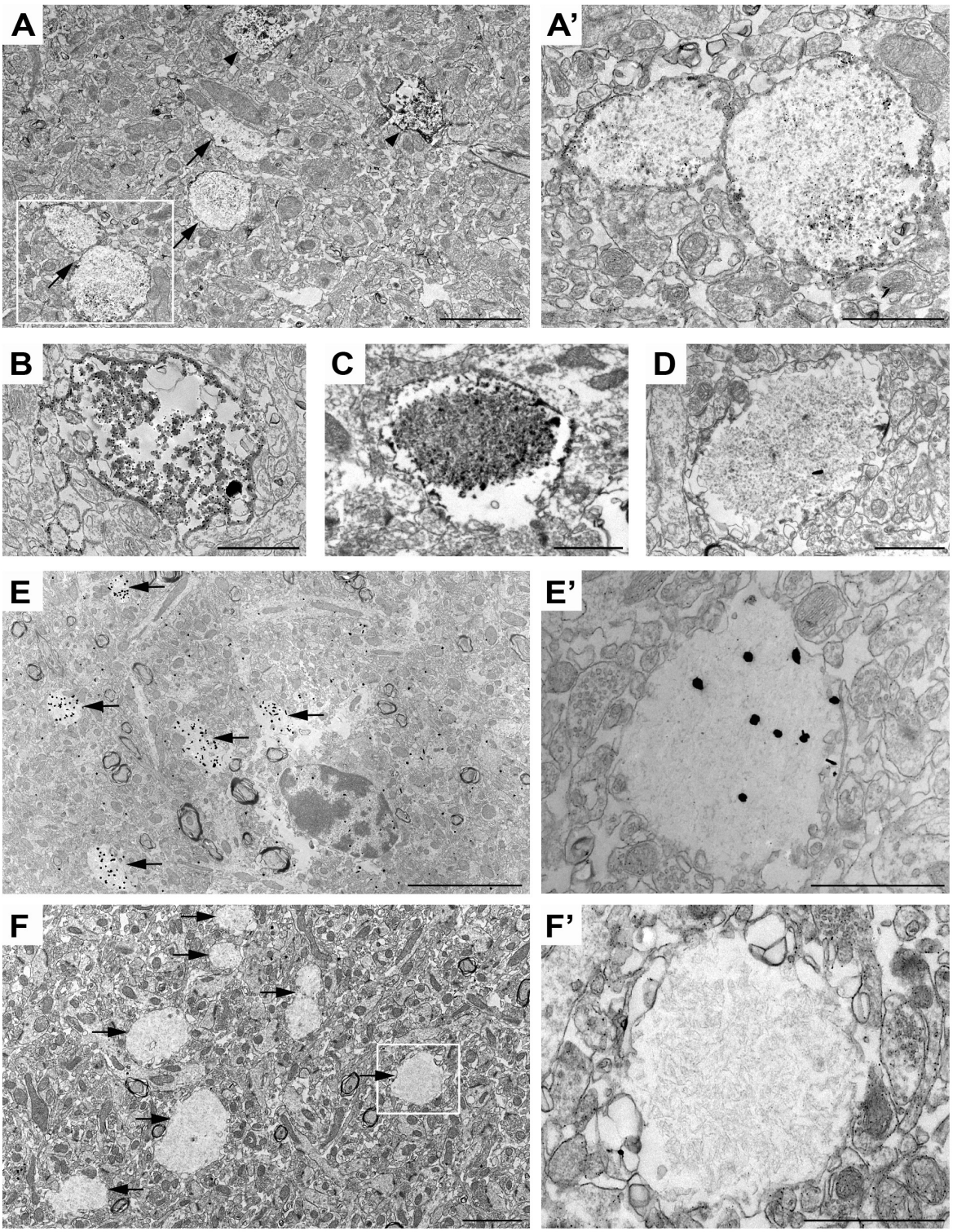

FIGURE 6: Ultrastructural characterization of Reelin plaques in CA1 stratum lacunosum-moleculare. Representative electron micrographs taken from DAB- (**A-D**), Fluoronanogold- (**E**) and non-stained (**F**) brain sections of aged wild type mice (12 mo, n = 3). Individual Reelin-positive granules revealed a distinct fibrillary structure with varying staining intensities, from partial-light (**A**, arrows, **D**) to full-dark stainings (**A**, arrowheads, **B**, **C**). **A'**) The enlarged area in **A** (box) show the selective and specific anti-Reelin IR in two of the light-stained granules. **E**) A similar picture was also evident using Fluoronanogold-conjugated antibodies, showing a dense array of Reelin-immunoreactive granules with fibrillar morphologies in the neuropil of CA1 slm, as shown at higher magnification in **E'. F**) Granular plaques filled with fibrillar material were also easily detectable without immunostaining. F' shows the enlargement of the boxed area in F. Scale bars: **A, F** = 2 μm, **A'-D, E', F'** = 1 μm, **E** = 5 μm.

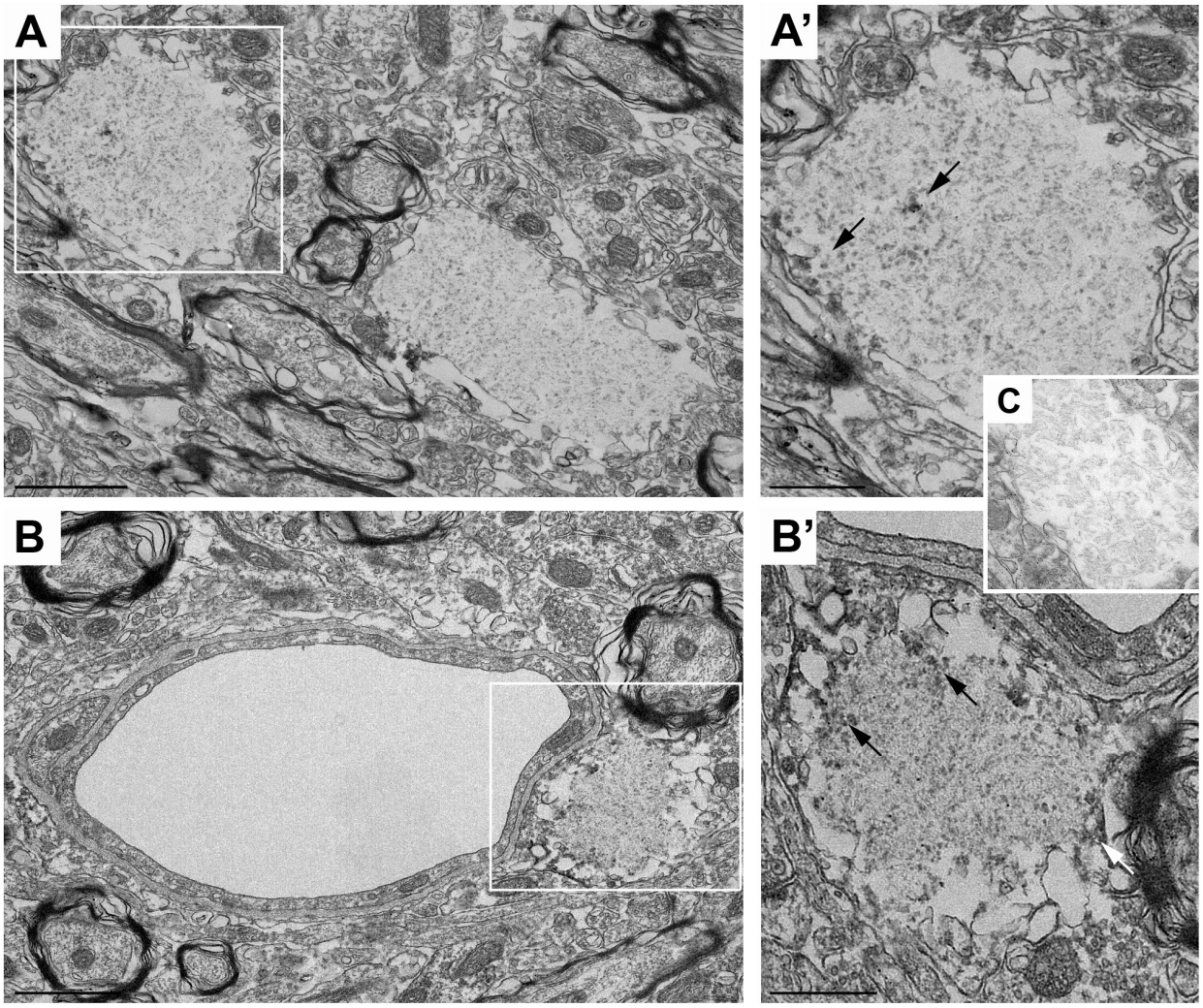

FIGURE 7: Ultrastructural characterization of murine amyloid-β–immunoreactivity in CA1 stratum-lacunosum-moleculare. Representative electron micrographs taken from DAB-stained brain sections of aged wild type mice (12 mo, n = 3). **A**) Aβ-IR was detected in a subpopulation of granular plaques in the neuropil showing highly similar shapes and morphologies as described for the Reelin-positive deposits. **A'** shows the enlargement of the outlined granular plaque in **A**. Arrows point to the few but distinct immunoreactive signals in the center and edge of the plaque. Note the difference of the labeled compared to the unlabeled (**C**) deposits. **B**) Numerous Aβ-immunoreactive granules were detected in astrocytic endfeet, closely opposed to the endothelial cells of brain capillaries. B' shows an enlarged view of the outlined area in **B**. Scale bars: **A, B** = 1 μm, **A',B'** = 500 nm.

The immunolabeled granules displayed a wide spectrum of staining patterns and intensities, potentially reflecting different stages of protein aggregations or technical limitations due to antibody penetration (**Fig. 6A-D**). Tissue sections stained with Fluoronanogold-coupled antibodies (**Fig. 6E**), displayed enrichments of gold-particles in the fibrillary area of the granules. This method allowed a much better identification of the ultrastructure of the individual granules as compared to the immunoperoxidase reaction. To characterize their morphology even better, we also analyzed tissue without anti-Reelin immunostaining (**Fig. 6F**). Pale fibrillary structures identical to the Reelin-positive granular plaques described above were detected in

these brain sections (**Fig. 6F'**), confirming that they are extracellular deposits of fibrillary proteinous material and devoid of organelles or cytoskeletal elements. Finally, immunostaining with the anti-$A\beta_{1\text{-}40/42}$ antibody revealed specific labelings of a subfraction of pale granules with the same morphology and ultrastructure. The reaction product was most prominent at the edges but also seen over the entire surface of these plaques (**Fig. 7A-B**). In line with the localization of the Reelin deposits, we found a considerable fraction of Aβ-positive granules associated with astrocytic end-feet (**Fig. 7B-B'**), suggesting again a potential clearance mechanism of aggregated protein depositions. Compared to the Reelin-labeling, the intensity of the anti-Aβ-immunoreactive signals was much lower, which is in agreement with our immunofluorescence stainings. On the other hand, the signal was clearly much stronger when compared with non-labeled deposits seen without primary antibodies (**Fig. 7C**), pointing to the presence of murine amyloid-β species in extracellular plaques in aged wild type mice.

1.5 DISCUSSION

The present study provides first ultrastructural and immunohistochemical evidence that age-related neuropathological changes involve the accumulation of murine AβPP-derived proteolytic peptides, likely including the N-terminal fragments s AβPPα/β; and potentially also N-AβPP and amyloid-β species in a subset of Reelin-positive plaques in aged wild type mice. While we do not have direct biochemical evidence of the presence of Aβ1-40 or 42 species, the distinct fibrillar structure labeled by the anti-Aβ antibody using IEM points to a specific accumulation of these highly aggregation-prone peptides in the aged murine hippocampus.

IR was only detectable after prolonged protease pretreatment, suggesting that the unmasking of epitopes is a prerequisite to detect rodent proteolytic AβPP species in amyloid deposits in aged rodents. The same treatment in young wild type and aged AβPP knockout mice did not reveal any comparable staining pattern, confirming the specificity of the IR. Moreover, our investigations using this adapted immunohistochemical protocol allowed the detection of fibrillary Aβ deposits as seen in transgenic AβPP mice, indicating that similar aging-related pathophysiological changes occur in wild type mice, pointing to the usefulness of non-transgenic animals in addressing certain aspects of early molecular mechanisms of Aβ plaque deposition that may potentially underlie the shift from normal to pathological forms of aging.

Interest in neuropathological studies in aged wild type rodents aimed at identifying possible markers and models of AD rapidly declined after the successful production of transgenic AD mouse models that recapitulated amyloid-β plaque and neurofibrillary tangle formation, the two major neuropathological hallmarks of AD. The observations that amyloid-like deposits described in aged mice did not resemble senile human AD plaques and did not stain with monoclonal antibodies to Aβ *(Jucker et al., 1994a)* reinforced the view that wild type rodents were not useful to study amyloid-β plaque formation. However, AβPP in mouse, rats, monkeys and humans share >96% amino acid sequence identity *(Shivers et al., 1988; Yamada et al., 1987)* and only 17 amino acid distinguish mouse AβPP from its human homolog. Three of amino acid substitutions are located within the N-terminal domain of the Aβ peptide, a region thought to be important for the specificity of interaction between Aβ peptides, whereas the highly conserved hydrophobic C-terminal sequence governs the rate of Aβ aggregation *(Hilbich et al., 1991b; Jarrett and Lansbury, 1993)* espite these three amino acid substitutions, *in-vitro* studies using synthetic Aβ peptides revealed no difference in the ability of rodent and human peptides to form congophilic

filaments in aqueous buffers and they can also co-aggregate in solution to form mixed Aβ fibers *(Fung et al., 2004; Hilbich et al., 1991a)*. Due to technical limitations including the availability of rodent-specific anti-Aβ antibodies, the precise amino acid composition and size of these peptides are currently unknown. However, due to the sequence homology and the ultrastructural properties described here (see below) it is likely that the antibody employed (anti-$A\beta_{1\text{-}40/42}$) indeed recognizes the corresponding rodent peptides. Interestingly N-terminus-specific AβPP antibodies also revealed comparable enrichments in extracellular plaques, indicating that other proteolytic cleavage products accumulate in these aging-associated proteinous deposits. Based on their biochemical properties it is, however, unlikely that these N-terminal fragments form fibrils. Rather, they might associate with the aggregated Reelin oligomers. Putative N-terminal AβPP components include the recently described 35 kDa N-AβPP peptide *(Nikolaev et al., 2009)* and the α- and β-secretase produced soluble sAβPPα and sAβPPβ fragments. Based on the recent report of Hoe et al. *(Hoe et al., 2009b)* demonstrating direct binding of the central Reelin repeats (R3-6) to the N-AβPP domain it is tempting to speculate that Reelin co-aggregates and sequesters N-terminal AβPP fragments, potentially preventing the production and/or allowing the elimination of potentially neurotoxic fragments that have been shown to trigger death receptor 6-mediated caspase-6 activation and axonal degeneration following trophic factor withdrawal *(Nikolaev et al., 2009)*. Finally, based on a lack of C-terminal-specific immunoreactive signals in these plaques, we consider it unlikely that the extracellular plaques also contain full-length AβPP.

Altogether, our data, obtained with an adapted pepsin pretreatment protocol originally developed by Watanabe and colleagues *(Watanabe et al., 1998)* to improve of detection of synaptic proteins, suggest that the failure so far to detect amyloid pathology in rodents is likely due to masking of antibody epitopes. Support for an enhancement of staining specificity rather than increase in unspecific detection is provided by the visualization of Reelin-positive axons, which were not visible following standard immunohistochemistry protocols. In addition, control experiments in young wild type as well as aged AβPP knockout mice revealed no specific extracellular anti-Aβ or anti-N-AβPP stainings, demonstrating that the immunoreactive signals reported here are specific and not caused by fixation- or staining artifacts. Similarly, the treatment with solvent alone did not have any effect on the staining intensity as well as the detectability of murine N-AβPP/Aβ-IR, suggesting that pepsin is responsible for the antigen retrieval effect. Pepsin is a member of the aspartyl proteases with broad structural specificity. However, they are known to cleave specific dipeptide bonds as well as beta-methylene groups in

their substrates (MEROPS Peptide database). Pepsin in particular elicits a preference for those amino acid residues composed of Phe and Tyr amino acid residue *(Ryle and Auffret, 1979)* indicating that the mechanism of action of pepsin is to break methylene cross-links created by binding of formaldehyde to these amino acid residues occurring during the fixation process, resulting in an unmasking of the epitope and better accessibility of the antibody. However, considering the broad substrate specificity and the high homology to other members of the aspartyl protease family, i.e. β-secretase BACE1 *(Dunn, 2002)* we cannot exclude that pepsin may promote the proteolytic processing of AβPP. Our biochemical investigations in fact show that in isolated brain lysates and cell extracts obtained from AβPP-transfected HEK cells pepsin is able to completely proteolytically digest AβPP *in vitro*; starting from the N-terminal side (**Supplementary Methods and Fig. 1**). The control conditions using HCl only again did not reveal any proteolytic cleavage of AβPP, indicating that indeed pepsin digests AβPP in a time-dependent process starting from the N-terminus into 12-15 kDa fragments in-vitro (**Supplementary Fig. 1**). The situation in fixed brain sections, however, appears to be quite different. Instead of a reduction in the abundance of small AβPP fragments, likely due to complete proteolytic digestion, we observe a significant increase in extracellular IR, again supporting our hypothesis of an epitope unmasking effect. It is also rather unlikely that the pepsin pretreatment is responsible for the acute increase in amyloid-β peptides in the extracellular matrix: The paraformaldehyde- or acetone-fixed brain sections are incubated at a very acidic pH that is expected to fully inactivate γ-secretase activity; occluding the production of Aβ peptides. Moreover, one would not expect to see this phenomenon in selected layers of the hippocampus and entorhinal cortex in the aged brain, but rather in a widespread fashion correlating with the expression pattern of rodent AβPP in young, adult and aged subjects.

Further support for an antigen retrieval effect of the pepsin treatment on perfusion-fixed brain sections is provided by our IEM data. We observed distinct but rather weak immunoreactive signals using the anti-$A\beta_{1\text{-}40/42}$ peptides on ultrastructural sections as compared to immunofluorescence, likely due to suboptimal antibody penetration and/or epitope accessibility in tissue processed for electron microscopy. Nevertheless, the immunoreactive signals were clearly identifiable in similar extracellular fibrillary granules as observed with the G10 anti-Reelin antibody. This antibody worked very well using IEM and allowed the specific localization of Reelin in neuronal somata of interneurons and in the extracellular space, in close agreement with previous ultrastructural investigations *(Pappas et al., 2001; Roberts et al., 2005)*. We were also able to confirm ultrastructurally the presence of Reelin-positive plaques in CA1

stratum lacunosum-moleculare using both immunoperoxidase and Fluoronanogold labeling. The individual granules displayed an unique fibrillary structure, potentially representing spherical protofibrils; small intermediates or fragments of amyloid fibrils *(Caughey and Lansbury, 2003)*. These types of small oligomers were all surrounded by discontinuous membranes pointing to their potential to compromise membrane integrity in ways that could lead to cellular stress and or/apoptosis. The pronounced Reelin-IR in some of these individual granules suggests that Reelin forms abnormal oligomers in aged individuals. This hypothesis is in line with the Thioflavin-S-positive stainings of the core of Reelin-positive plaques on perfusion-fixed tissue sections (**Fig. 1G**), confirming the amyloid-like nature of the extracellular deposits. Further support for this hypothesis is provided by cell adhesion assays demonstrating that secreted Reelin can form large homomeric protein complexes via the CR-50 epitope in the N-terminal domain, either forming disulfide-linked dimers or larger oligomeric complexes with truncated fragments *(Kubo et al., 2002; Utsunomiya-Tate et al., 2000)*. It has also been proposed that the multimerization of Reelin is necessary for the clustering and activation of the VLDLR and ApoE receptor 2 *(D'Arcangelo et al., 1999; Hiesberger et al., 1999; Strasser et al., 2004; Yasui et al., 2007)*. It is therefore conceivable that the proteolytic processing of Reelin may be altered during aging and that this affects the tertiary structure required for the proper and stable assembly/dimerization necessary for receptor activation. As a consequence oligomerization will be favored and higher-order multimerization and formation of fibrillary aggregations could occur as a result of aging-related impairments in clearance and proteasomal degradation of these deposits. On the other hand, the aggregated granular and fibrillar material could also be a result of degenerative processes, or reflect relatively inert dumping grounds for misfolded proteins.

Our findings of a pronounced accumulation of Reelin-positive as well as Aβ-positive plaques in astrocytic end-feet are in line with this hypothesis and suggest that aging-related deficits in protective clearance pathways may allow abnormal protein aggregation that eventually spiral out and result in full-blown amyloid-β plaque pathology in aged individuals. While Reelin expression has been studied in human AD subjects, the putative presence of Reelin-positive plaques has not been investigated in postmortem tissue yet. Wirths and colleagues reported in a transgenic AD mouse model the presence of Reelin-IR in the neuritic component of amyloid β plaques *(Wirths et al., 2001)*. However, the resolution of these investigations does not allow a precise identification of the localization and morphology of the Reelin-immunoreactive signals. With respect to changes in Reelin levels and AD, no coherent picture has emerged yet: While Riedel and colleagues *(Riedel et al., 2003)* reported only marginal changes in Reelin levels in

Cajal-Retzius cells in the entorhinal cortex of AD subjects as compared to normal aging, Baloyannis *(Baloyannis, 2005)* and Chin et al. *(Chin et al., 2007)* on the other hand reported a dramatic decline in the number of Cajal-Retzius cells and layer II pyramidal cells in the entorhinal cortex, respectively, in early cases of AD. Evidence from Saez-Valero's group also suggests a link between abnormal Reelin levels and AD pathogenesis. Using a biochemical approach, they reported altered glycosylation and increased levels of the N-terminal 180 kDa Reelin fragment in the CSF and frontal cortex brain extracts of AD patients as compared to non-demented control subjects *(Botella-Lopez et al., 2006; Chin et al., 2007; Saez-Valero et al., 2003)*. Interestingly, Reelin mRNA was elevated in the frontal cortex but this did not translate into increased levels of full-length or the 310 kDa forms in AD compared to control, suggesting a compensatory increase in transcription and/or altered proteolytic processing of the full-length protein in the diseased stage. The conflicting data may likely be due to methodological reasons, including differences in tissue quality and processing, age and cognitive status of the subjects. With respect to cell number estimates in postmortem human AD and control tissue samples, not all of the studies mentioned above respected the criteria of unbiased stereological counting principles. Moreover, biochemical analyses of the Reelin expression do not differentiate between the physiological, soluble (intracellular or secreted) and the putative non-physiological, aggregated forms. It will be therefore very important to investigate in the human hippocampal formation whether Reelin-positive plaques can be detected in early stages of AD using a pepsin-pretreatment approach, whether their density and localization differs from non-demented individuals, and if they associate and/or co-localize with amyloid-β IR.

In conclusion, our immunohistochemical and ultrastructural data provide first evidence that the formation of granular and fibrillary amyloid-β plaques is a common neuropathological phenomenon in the hippocampus of aged wild type mice, confirming previous biochemical and biophysical investigations revealing the same ability of rodent and human Aβ peptides to form congophilic filaments and amyloid fibers *(Fung et al., 2004; Hilbich et al., 1991a)*. The observation that these amyloid-β plaques can only be detected using immunohistochemical methods with stringent epitope-unmasking suggests that peptide and plaque densities in short-living animals remain much lower compared to humans, potentially due to higher protein turnover, less impaired clearance pathways and/or more efficient proteasomal degradation mechanisms in short-living laboratory mice. On the other hand, the fact that aged rodents do form spontaneous protein aggregations allows the investigations of the role of oligomers or

spherical protofibrils in neuronal malfunction and degeneration in a much more physiological context compared to transgenic AD animals overexpressing large amounts of foreign protein.

1.6 ACKNOWLEDGEMENTS

The present study was supported by SNF Grant Nr. 3100AO-100309 and Swiss National Competence Centre in Neural Plasticity and Repair (NCCR). We are grateful to Kofi Kyere, Institute of Pharmacology and Toxicology, UZH for animal husbandry and care. A special thank goes to Prof. Dr. Roger M. Nitsch, Division of Psychiatry Research, UZH for his continuous support and for providing us the transgenic AD mice. Finally, we thank Dr. Marlen Knobloch, Division of Psychiatry Research, UZH for her generous supply of ArcAβ mouse brain sections.

1.7 SUPPLEMENT MATERIAL

Supplement Figures can be found on the enclosed DVD or online.

2. STUDY II: ULTRASTRUCTURAL INVESTIGATION OF REELIN-POSITIVE GRANULAR DEPOSITS IN THE NORMAL AND PATHOLOGICAL AGED BRAINS OF WILD TYPE MICE – A PRECURSOR CONDITION FOR ALZHEIMER'S DISEASE?

Jana Doehner[1], Christel Genoud[2], Claudine Imhof[1] and Irène Knuesel[1]

[1] Institute of Pharmacology and Toxicology, University of Zurich, Switzerland

[2] Electron Microscopy Facility, Friedrich Miescher Institute, Basel, Switzerland

Unpublished data

My contribution to this work was the whole tissue preparation for ultrastructural analysis, the transmission electron microscopy imaging and the analysis of the images and quantifications. I wrote the whole manuscript.

2.1 ABSTRACT

Reelin is a large extracellular matrix protein essential for mediating proper neuronal positioning during development. In adult brain, Reelin plays a crucial modulatory role in the induction of synaptic plasticity and successful formation of long-term memory. Alterations in Reelin-mediated signaling have been suggested to contribute to neuronal dysfunction associated with Alzheimer's disease (AD). Aging in several species is characterized by a decline in Reelin-expressing interneurons and concomitant accumulation of Reelin in amyloid-like deposits in the hippocampal formation. Previous studies of these deposits in wild type mice using electron microcopy revealed extracellular round to ovoid spherical deposits showing a fibrillary center surrounded by a discontinuous membrane and being free of any normal cell organelles. These data likely indicate that the investigation of dysfunctional Reelin signaling in normal aged wild type mice may provide us some insights into the molecular mechanism of late-onset AD. This data is in line with several ultrastructural investigations describing clustered structures - so called polyglycogen bodies (PGs) – that are highly similar to our granular structure regarding morphology and localization. Interestingly, a prenatal immune challenge by systemic administration of the synthetic cytokine releaser and viral mimic polyriboinosinic-polyribocytidilic acid (PolyI:C) in mice during late gestation results in significant acceleration of these extracellular protein depositions in the adult wild type offspring. Here, immuno-electron microscopy was employed to elucidate whether morphological differences exist in the hippocampal formation between immune challenged mice (PolyI:C) compared to saline treated (NaCl) subjects. Moreover, we aimed to gain more information about the ultrastructural properties, the localization and origin of these granules as well as to clarify whether these granular structures are equal to the PGs described earlier by other groups. For that, we employed serial sectioning using serial block face scanning electron microscopy (SBF-SEM), allowing us to perform 3D-reconstructions of these Reelin-positive amyloid-like deposits. Using 2D-EM, we found differences with respect to plaque morphology following prenatal immune challenge compared to saline exposed mice, as indicated by the larger size and the increased presence of mitochondria in the granules of PolyI:C exposed subjects, as well as degenerative features. Surprisingly, after close examination of these granules, we found that these structures are not completely of extracellular origin, but closely associated with neurites and glia cells. This was further supported by SBF-SEM, demonstrating that the granules are not individual structures, but likely be connected with each other. Altogether, these results indicate that these clustered

deposits represent an aging phenomenon that is accelerated and exacerbated by a prenatal immune challenge, likely linked to dysfunctional Reelin signaling and processing. Therefore, it is conceivable, that these deposits represent critical early markers of pathological forms of aging, eventually leading to AD in aged individuals.

2.2 INTRODUCTION

Reelin is a large neuronal glycoprotein, first identified in 1995, that plays a critical role in cortical development, including proper neuronal migration *(D'Arcangelo et al., 1995; Frotscher, 1998)*. Employing the same lipoprotein-mediated signaling cascade, Reelin regulates NMDA receptor homeostasis and modulates synaptic function and plasticity in adult synapses *(Beffert et al., 2005; Weeber et al., 2002*; for review see also *Doehner and Knuesel, 2010)*. Interestingly, the expression pattern of Reelin changes after the end of the neuronal migration phase *(Frotscher, 1998)*. In the adult brain, the Reelin-expressing Cajal-Retzius cells are largely replaced by Reelin-expressing GABAergic interneurons *(Qiu et al., 2006b)*. Although Reelin continues to be expressed in the adult brain, its complete function and changes throughout aging remains poorly understood, as most studies have been conducted in mouse embryos. The distinct expression pattern of Reelin in the adult brain and its signaling members in brain regions implicated in mediating learning and memory *(Alcantara et al., 1998; Beffert et al., 2005; Frotscher et al., 2003; Pesold et al., 1998a)* suggest that Reelin-mediated signaling in the adult brain is crucial for normal cognitive function. Human studies in the elderly imply that the hippocampal region, the area important for learning, and memory, is highly susceptible to normal aging and neurodegenerative diseases, like Alzheimer's disease (AD). Putative changes in Reelin expression during normal and pathological forms of aging have recently been investigated *(Knuesel et al., 2009)*. These data reported that normal aging in several species is accompanied by loss of Reelin-expressing neurons and concomitant accumulation of Reelin- and Aβ-positive granular aggregates in the hippocampal formation *(Doehner et al., 2010; Knuesel et al., 2009)*. The specificity of this phenomenon was further confirmed by investigating aged Reelin knock-out mice, which do not show any Reelin-positive granular deposition. Our findings so far provide important information regarding putative temporal processes underlying the transition from normal to pathological aging *(Knuesel et al., 2009)*; whereby the reduced density of Reelin expressing interneurons appears to be a consistent feature of normal aging. In line with these data and the critical role of Reelin in synaptic transmission and learning and memory, several recent findings suggest that alterations in Reelin expression and abnormal Reelin signaling may contribute to neuronal dysfunction. Although recent experimental evidence from our group as well as of several other research groups suggests this involvement of dysfunctional Reelin in pathological forms of aging, such as late-onset AD *(Botella-Lopez et al., 2006; Doehner et al., 2010; Durakoglugil et al., 2009; Madhusudan et al., 2009; Motoi et al., 2004; Saez-Valero et al.,*

2003; Wirths et al., 2001), the molecular mechanism by which this conserved protein contributes to the pathogenesis of AD remains still largely unknown. Our recent experimental approach provides the first evidence that a prenatal immune challenge during late gestation using the viral mimic and cytokine releaser polyriboinosinic-polyribocytidilic acid (PolyI:C) results in significant acceleration of aging-associated neuropathological alterations in non-transgenic wild type mice, involving reduced Reelin expression and precocious accumulation of Reelin-positive deposits *(Knuesel et al., 2009)*.

To investigate the role of Reelin and its aggregates in more detail in the aging brain and its possible role in neurodegenerative diseases like AD, we already started to investigate the localization and distribution of this highly conserved protein at the subcellular level in wild type mice using electron microscopy *(Doehner et al., 2010)*. Several ultrastructural studies focusing on Reelin have been already performed in several mammalian species, including mice *(Pappas et al., 2001)*, rats *(Pesold et al., 1998a)*, non-human primates *(Martinez-Cerdeno et al., 2003; Pesold et al., 1998b; Rodriguez et al., 2000)*, ferrets *(Martinez-Cerdeno et al., 2003)* and human brain *(Roberts et al., 2005)*. In these studies, Reelin has been detected in the extracellular space, neuronal somata, axonal processes, dendrites and spines *(Derer et al., 2001; Martinez-Cerdeno et al., 2003; Pappas et al., 2001, 2003; Pesold et al., 1998a; Pesold et al., 1998b; Roberts et al., 2005; Rodriguez et al., 2000)*. The presence of Reelin-Immunoreactivity (IR) at synaptic sites fits with the important role of Reelin in normal synaptic function, including synaptic plasticity and dendritic remodeling in the adult brain in several species *(Chameau et al., 2009; Jossin and Goffinet, 2007; Niu et al., 2004, 2008)*. Although none of these studies focused on Reelin-positive deposits, one ultrastructural study gave evidence of intra-axonal accumulation of Reelin *(Derer et al., 2001)*, with elevated appearance in *reeler orleans* mice. In addition, extracellular structures morphologically similar to our Reelin-positive granules have been already described earlier at the subcellular level in SAMP8 and B6 mice *(Akiyama et al., 1986; Jucker and Ingram, 1994; Jucker et al., 1992, 1994a)*. They are as well suggestive of an age-induced phenomenon, and being positive for heparan sulfate proteoglycan (HSPG) and laminin. Reelin as a major component of these structures was not described until recently *(Doehner et al., 2010; Knuesel et al., 2009)*. Therefore, it would be of interest to decipher if the Reelin-positive structures described by us are the same age-dependent phenomenon as the ones described earlier.

Based on all these data and the increasing evidence of dysfunctional Reelin-mediated signaling as an important etiological factor in age-dependent neurodegenerative diseases, we challenged

non-transgenic mouse dams with PolyI:C or NaCl at gestation day 17 (GD17) and analyzed the appearance of the granules in the hippocampal formation across adulthood and aging using EM. We aimed to elucidate the ultrastructural properties of the Reelin-positive deposits and investigate whether morphological differences between immune challenged mice compared to saline treated subjects exist. Moreover, we aimed to gain more precise insights into the ultrastructural appearance, localization and origin of these granules to clarify if these granular structures are equal to the fibrillary granules described earlier *(Akiyama et al., 1986; Jucker and Ingram, 1994; Jucker et al., 1992, 1994a)*. Besides immuno-electron microscopy (IEM) we also employed serial sectioning using serial block face scanning electron microscopy (SBF-SEM) *(Denk and Horstmann, 2004; Leighton, 1981)* for a 3D-reconstruction of the Reelin-positive amyloid-like deposits.

2.3 MATERIALS AND METHODS

ANIMALS

All procedures were approved by the local authorities of the Cantonal Veterinary Office in Zurich and are in agreement with the Principles of Laboratory Animal Care (NIH publication No. 86-23, revised 1985). All animals were housed in same sex groups of 3-4 in an optimized in-house hygiene area (OHB, University of Zurich Irchel, Switzerland) under 12-h day-night cycle and *ad libitum* food and water. C57BL/6J mice were obtained from the breeding facility of the Institute of Laboratory Animal Science, University of Zurich (LTK Fuellinsdorf).

POLYI:C INJECTIONS

Pregnant mouse dams of the C57Bl/6J strain were given a single intravenous injection of 5 mg/kg polyriboinosinic-polycytidilic acid (PolyI:C potassium salt, Sigma-Aldrich, Buchs, Switzerland, P9585-50mg) dissolved in 0.9 % saline with an injection volume of 5 ml/kg body weight or an equivalent volume of saline at gestation day 17 (GD17). The animals were mildly restrained during the injection procedure using an acrylic mouse restrainer and immediately returned to their home cage. The offspring was weaned at 3 weeks of age and housed in groups of 4-5 siblings of the same sex. Brain tissue was collected at the age of 6~ (n = 2), 9~ (n = 2-3) and 15 month (n = 3) per treatment group for the immunohistochemical and ultrastructural characterization of Reelin-positive plaques.

PREEMBEDDING IMMUNO-ELECTRON MICROSCOPY

One single wild type mouse (10 mo) and two to three animals per age group (6, 9 and 15mo) and treatment (NaCl, PolyI:C) of both gender were anesthetized as described above and perfused with a fixative containing 4 % paraformaldehyde, 0.2 % picric acid and 0.1 % glutaraldehyde in phosphate buffer (PB; 0.1 M, pH 7.4). The brains were removed and post-fixed in the same fixative for 5 h at 4°C, washed and stored in PB over night. Coronal sections (70 μm) were cut on a Vibratome, the hippocampi were dissected and cryoprotected in 30 % sucrose in 0.1 M PB over night at 4°C.

To enhance antibody penetration, the sections were frozen and thawed rapidly 3 times in the same sucrose solution by using liquid nitrogen. They were then collected and washed in Tris-buffered saline (TBS, pH 7.49) and blocked for 2 h in TBS containing 10 % normal goat serum at room temperature (RT). The sections were then processed for immunohistochemistry using

DAB immunoperoxidase reactions or Fluoronanogold. Labeling was done using primary antibodies against mouse anti-Reelin (clone G10, 1:1000, Millipore, MAB5364) and rabbit anti-$A\beta_{1-40/42}$ (1:1000, Chemicon, AB5076) diluted in TBS containing 3 % normal goat serum and 0.05 % sodium azide was applied for 72 h at 4°C under constant agitation. After washing in TBS sections were either incubated in secondary goat anti-mouse/anti-rabbit antibodies conjugated to biotin (1:250; Jackson ImmunoResearch Laboratories Inc., West Grove, PA) or secondary immunogold-conjugated antibodies (1:200; Alexa Fluor-488-Fluoronanogold-Fab, Nanoprobes Yaphank NY, USA) diluted in TBS containing 3 % of NGS over night at 4°C. The latter immunoprobe consists of a 1.4 nm gold particle conjugated with goat-anti mouse F_{ab}-fragment and fluorescein. The DAB reaction product was silver-intensified and gold-toned as described previously *(Sassoe-Pognetto et al., 1994)*. Briefly, sections were incubated in a solution containing 3 % hexamethylenetetramine (Merck, Darmstadt, Germany), 0.25 % silver nitrate (Merck), and 0.025 % disodium tetraborate (Merck) for 10 min at 60°C. The sections were then rinsed in distilled water and treated for 2 min with gold chloride (0.05 % in distilled water, Merck). Finally, the sections were rinsed in distilled water and incubated for 2 min in sodium thiosulfate (2.5 % in distilled water, Merck). Optimal visualization of the 1.4 nm gold-particles (FNG-labeled tissue samples) at the electron microscopic level required as well gold enhancement. The specimens were incubated with a commercially available kit (GOLDENHANCETM-EM, Nanoprobes, Yaphank NY, USA) containing four vials with solutions called enhancer (solution A), activator (solution B), initiator (solution C), and buffer (solution D). Equal volumes of each solution were mixed to form the final reagent. The samples were then immersed in 300 μl of this solution and incubated for 7 min at RT. After the enhancement for both procedures, samples were kept in Na-cacodylatebuffer (0.1 M, pH 7.4) overnight. Finally, sections were post-fixed for 15 min in 0.5 % OsO4 (on ice), counterstained with 1 % uranyl acetate for 30 min at RT, dehydrated in graded acetone and flat embedded in Epon812 (Science Services). The Epon812 polymerization was achieved by incubation for at least 48 h at 60°C. Ultrathin sections (50 nm) were cut on an ultramicrotome (Leica EM UC6, Leica Microsystems) and collected on adhesive-coated nickel grids (300 mesh). In addition, to better describe the ultrastructure of the individual granules, some sections were processed without any immuno-labeling. For that the mice were perfused as explained above. After cutting and dissecting the hippocampi, the sections were directly collected in Na-Cacodylate buffer, and processed without staining as described before. Before imaging, ultrathin sections were further contrasted in a 2 % lead-citrate solution for 10 min at RT. Ultrathin sections were examined

using a Philips CM100 transmission electron microscope equipped with a side mounted CCD camera (4k x 3k; Gatan Bioscan GmbH, Munich, Germany) and images acquired with the software program Digital Micrograph (Gatan Inc.). Cropping of images and adjustments of brightness and contrast was processed using Adobe Photoshop (Adobe Systems, San Jose, CA).

QUANTIFICATION OF GRANULAR SIZE AND APPEARANCE OF MITOCHONDRIA

The quantitative analyses of the area size of the Reelin-positive granules and the amount of granules associated with mitochondria were done on randomly selected granules from 4 to 6 EM-micrographs of 3 to 4 animals per treatment group (NaCl, PolyI:C). A total of 50 to 55 granules per treatment group were outlined and the area measured using ImageJ software. In addition to the size, the granules were also evaluated regarding the presence of mitochondria. Histograms and pie charts were composed using Microsoft Office Excel. The Box Plot graph was created in StatView (Abacus Concepts, Inc. Berkeley, CA).

STATISTICAL ANALYSIS

The analysis was performed using the software StatView version 5.0 (Abacus Concepts, Inc. Berkeley, CA). The nonparametric Kolmogorov-Smirnov test was used to statistically compare the size distribution of the granules and the Mann-Whitney *U* test was used to statistically compare the ratio of mitochondria in the granules between the PolyI:C and NaCl group. Statistical significance was set at $p < 0.05$.

TISSUE PREPARATION FOR SBF-SEM

To perform 3D reconstruction of the granular structure the mentioned EM protocol was slightly adjusted. 15 month old PolyI:C exposed mice were perfused with a fixative containing 4 % paraformaldehyde, 0,2 % picric acid and 2 % glutaraldehyde in phosphate buffer (PB; 0.1 M, pH 7.4). The brains were removed and post-fixed in the same fixative for 3 h at 4°C, washed and stored in PB over night. Coronal sections (70 µm) were cut on a Vibratome, the hippocampi were dissected and washed in Na-Cacodylate buffer (0.1 M, pH 7.4). The sections were then postfixed in reduced osmium (1.5 % KFeCN, 1 % OsO4 in 0.1 M cacodylate buffer) for 30 min at RT, followed by post fixation in 1 % osmium diluted in 0.1 M cacodylate buffer for 30 min at RT. Subsequently, the sections were subjected to a counterstaining in 1 % uranyl acetate solution for 30 min at RT, dehydrated in increasing acetone concentration and flat embedded in Durcupan ACM (Science Services, Munich, Germany). The Durcupan polymerization was achieved by

incubation for at least 24 h at 60°C. The ultrastructure of the granules was investigated using serial block-face scanning electron microscopy (SBF-SEM), which is particularly suited to fast data collection from larger samples. The region of interest was mapped by light microscopy, cut out of the resin and mounted on a Plexiglas stub. The block was trimmed to obtain a trapezoid block of maximally 500 x 500 µm of size and placed in the SBF-SEM, consistent of a microtome (3VIEW, GATAN, Pleasanton, CA, USA) mounted in a scanning electron microscope (Quanta200VP-FEI, Endhoven, Netherlands). The surface of the block was imaged and cut by a diamond knife in alternation in order to obtain a stack of images. Once the surface was scanned 80 nm of tissue was removed and the fresh surface imaged. In the present work, imaging was performed at an accelerating voltage of 4.5 kV (spot size 3) in low vacuum mode (0.25 Torr water pressure) and images were taken as a mosaic of 3x3 fields of view (2048 x 2048 pixel) with an overlap of 10 %. For control, ultrathin sections (50 nm) were collected on adhesive-coated nickel grids (300 mesh) and examined using a Philips CM100 transmission electron microscope equipped with a side mounted CCD camera (4k x 3k; Gatan Bioscan GmbH, Munich, Germany). All images were acquired and equalized for contrast in Digital Micrograph (GATAN, Pleasanton, CA, USA). Cropping of images and adjustments of brightness and contrast was done using ImageJ software and Adope Photoshop (Adobe Systems, San Jose, CA).

TISSUE PREPARATION AND IMMUNOHISTOCHEMISTRY

Wild type animals (15 mo) exposed prenatally either to PolyI:C or saline were deeply anesthetized (Nembutal™; 40 mg/kg body weight; i.p.) and transcardially perfused through the ascending aorta with 4 % paraformaldehyde and 15 % saturated picric acid in phosphate buffered saline (PBS). After postfixation in the same fixative for 4 h at 4°C, the brains were cryoprotected in 30 % sucrose, frozen and stored at -80°C until further processing. Free floating sections (40 µm) were cut coronally on a sliding microtome and stored at -20°C in cryoprotectant solution until immunohistochemical evaluations. A 10 min pepsin pretreatment (0.15 mg/ml in 0.2 N HCl at 37°C) was applied to all free-floating sections and subsequently employed for double-immunofluorescence staining as described previously *(Kocherhans et al., 2010)* using the following antibodies: mouse anti-rodent Reelin (clone G10; Millipore; MAB5364; 1:1000) and rabbit anti myelin-basic protein (MBP; Chemicon, AB980, 1:200). Brain sections were incubated over night at 4°C in the primary antibody solution diluted in PBS containing 2 % normal goat serum and 0.2 % Triton X-100. After three washes in PBS, tissue sections were incubated for 30 min at RT in the corresponding secondary antibodies conjugated to Alexa488 (1:1000;

Molecular Probes, Eugene, OR) and Cy3 (1:500) and processed as described *(Kocherhans et al., 2010)*. Brain sections were then mounted and air-dried in the dark and cover slipped with aqueous permanent mounting medium (Dako).

Double immunofluorescence labelings were visualized by confocal microscopy (LSM-710, Zeiss, Jena, Germany) using a 40x (NA 1.3) and 63x (NA 1.4) objective and sequential acquisition of separate channels. Z-stacks of consecutive optical sections (1024 x 1024 pixel, spaced 0.5 -1 μm in z) were acquired. For visual display, Z-sections of all channels were summed and projected in the z-dimension (maximal intensity) and merged using the image analysis software Imaris (Bitplane, Zurich, Switzerland). Cropping of images and adjustments of brightness and contrast were identical for each labeling and done using Adobe Photoshop.

SILVER STAINING

For the detection of dystrophic neurites, extracellular and intracellular proteinaceous aggregates, we used the FD NeuroSilver Kit II (FD NeuroTechnologies Inc., Ellicott City, MD). Free floating perfusion-fixed brain slices (40 μm) prepared for normal immunohistochemistry were processed according to the manufacturer's instruction with slight modifications. Here, mounted sections were employed and washing was carried out in PBS instead of ddH_2O to prevent shriveling of the tissue sections.

2.4 RESULTS

Detailed knowledge of the ultrastructural properties of the Reelin-positive granules as well as their origin and association with other cellular structures is expected to shed light on their possible function in the aging brain. Therefore, we employed electron microscopy to study the granules in the subcellular range to discern where the protein is localized. For this, we employed 2 to 3 animals per age and treatment (PolyI:C/NaCl; 6, 9 and 15 months) group of both gender. Only the hippocampal formation was dissected for examination, as the plaque appearance is a highly consistent feature detectable in this region of aged animals.

STRUCTURAL PROPERTIES OF AGING-ASSOCIATED REELIN-POSITIVE GRANULES

The Reelin-positive granules have been already intensely investigated by light microscopy by our group *(Doehner et al., 2010; Knuesel et al., 2009; Kocherhans et al., 2010; Madhusudan et al., 2009)*. These deposits are an age-dependent phenomenon starting at an age of 9 to 12 months, primarily appearing in the hippocampal formation (**Fig. 1A,** arrows, adapted from *(Doehner et al., 2010)*). Moreover, first ultrastructural investigations of these Reelin-positive granules in wild type mice have been recently obtained in our lab *(Doehner et al., 2010)*. These ultrastructural data confirmed the presence of Reelin in 1-3 μm sized extracellular spherical deposits in the hippocampal formation (**Fig. 1B,** green), most likely representing individual Reelin granules of the clustered amyloid-like deposits investigated already by light microscopy. Individual granules were typically surrounded by a discontinuous membrane (**Fig. 1B-D**), indicative of extracellular localization. Their ultrastructure exhibits distinct fibrillary material in the center of each granule and being largely free of any other organelles (**Fig. 1C**). Interestingly, observing these granules in more number and detail, mitochondria could be observed in a small portion of investigated granules (**Fig. 1D,** black arrows). Moreover, these globular structures were also positive for $A\beta_{1-40-42}$ *(Doehner et al., 2010)* confirming previous immunohistochemical staining. Still, the precise origin, if they are developing extra- or intracellular and the induction of these described granules has not been deciphered yet.

REELIN GRANULES MIGHT BE OF DEGENERATIVE ORIGIN

The accumulation of Reelin in this clustered granular structure might lead to degeneration of the surrounding tissue, or might itself be of degenerative origin. Evidence that Reelin might

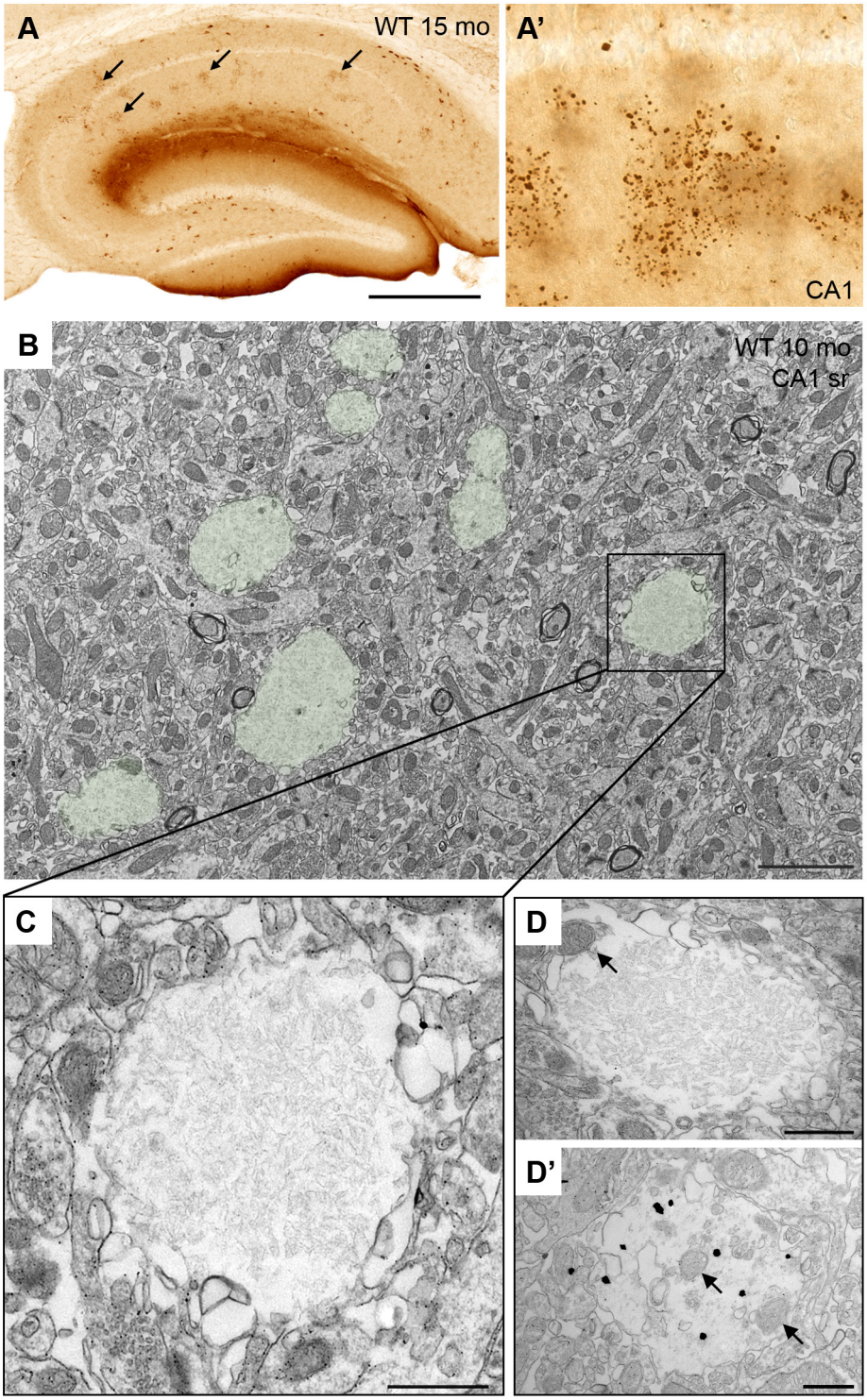

FIGURE 1: Structural properties of aging-associated Reelin-positive granules. Reelin forms clustered granular deposits in the aging hippocampus. **A**) Immunoperoxidase staining using anti-Reelin antibodies (G10) on a brain section of an old (15 mo) wild type mouse. Note the high density of Reelin in amyloid-like plaques (arrows) mainly in the CA1 sr and slm. **A')** Higher magnification of a single representative Reelin-positive granular deposit (adapted from *(Doehner et al., 2010)*). **B-D**) Ultrastructural characterization of Reelin-positive plaques (green) in the CA1 sr of an aged wild type mouse (10 mo). **B**) Representative electron micrograph taken from a non-stained brain section. Individual granules revealed a distinct fibrillary structure. **C**) Higher magnification of one individual granule of the marked area in (**B**). **D**) Interestingly, in a small subset of deposits mitochondria could be observed within the granules (arrows). Scale bars: **A** = 500 µm, **B** = 2 µm, **C, D, D'** = 500nm.

accumulate in some dendrites is given by the observation of Reelin-positive staining (**Fig. 2A and C**) and the same fibrillary ultrastructure in dendritic processes (**Fig. 2B and C**).

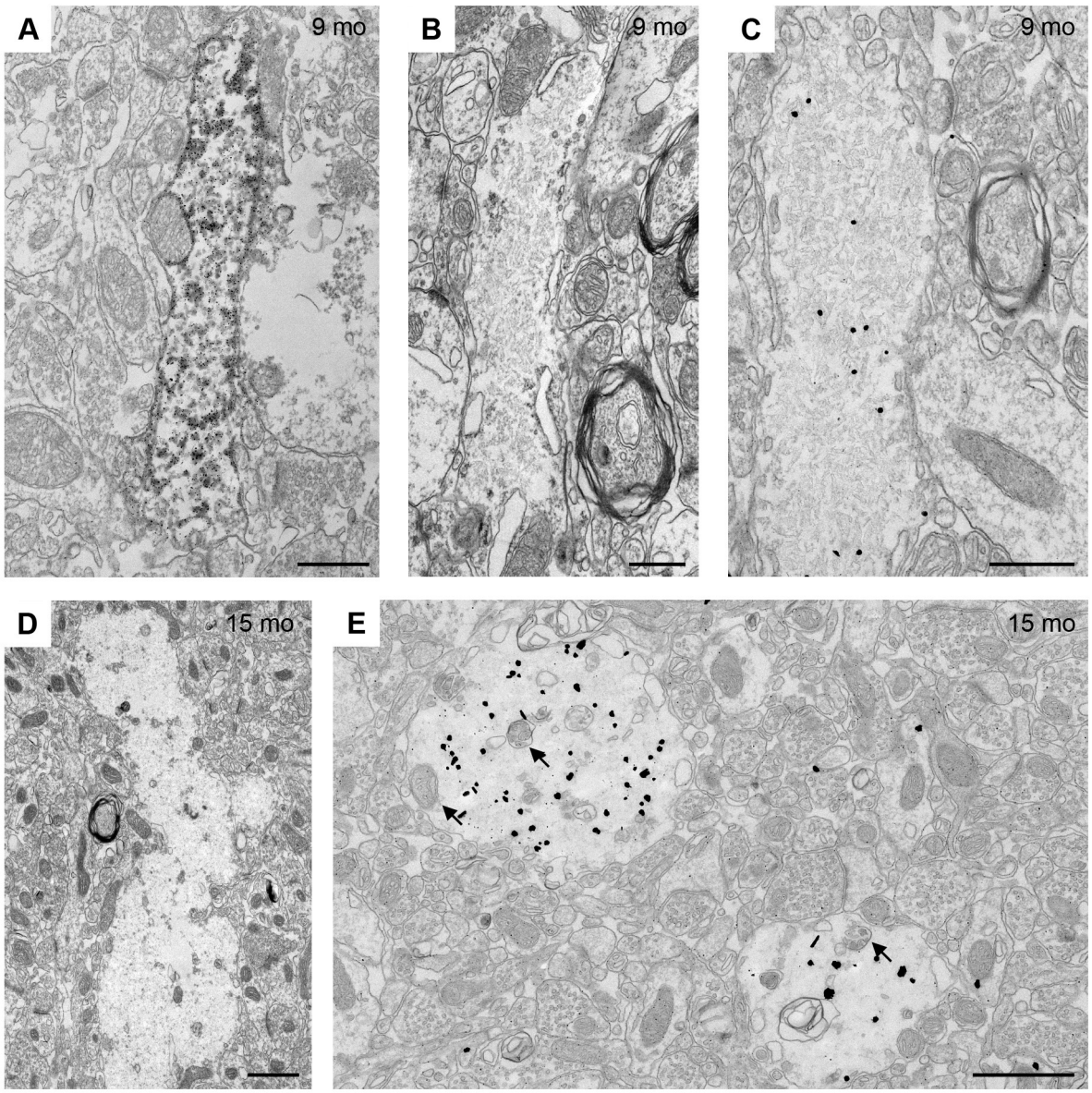

FIGURE 2: Reelin granules: Linked to degenerating dendrites? Representative immuno-electron micrographs taken from immunoperoxidase stained (**A, D**), Fluoronanogold labeled (**C, E**) and non-labeled (**B**) hippocampal brain sections using the anti-Reelin antibody (G10) of 9 months (**A-C**) and 15 months (**D and E**) old NaCl subjects. The presence of Reelin-positive staining (**A, C**) and the highly similar fibrillary ultrastructure within the dendritic processes as seen in extracellular granules (**B**) provides evidence that Reelin potentially aggregates in dendritic processes. **D**) Signs of neurodegeneration were evident by disintegrated/dystrophic dendrites. **E**) Presence of cell debris-like structures in the granules (arrows), indicative of a degenerating process. Scale bars: **A, B, C** = 500 nm, **D, E** = 1 μm.

Signs of neurodegeneration were evident by the presence of distinct ultrastructural changes: this included disintegrated/dystrophic dendrites (**Fig. 2D**), cell debris, swollen vacuoles, dispersed neurofilaments and other undefined structures indicative of neuronal degeneration. In addition,

evidence of ongoing neurodegeneration was given by the disrupted membranes of individual granules, as well as the presence of cell-debris-like structures in the granules (**Fig. 2E,** arrows).

3D RECONSTRUCTION OF THE REELIN-POSITIVE GRANULES

To get a better understanding of the 3-dimensional (3D) -structure of the Reelin-positive deposits we performed serial block-face scanning electron microscopy (SBF-SEM) *(Denk and Horstmann, 2004; Leighton, 1981)*. By approaching the level of macromolecular dimensions *(Baumeister et al., 1999)*, a 3D-reconstruction allows a more detailed view of the cellular and organelle structures. In particular, visualization and reconstruction the 3D anatomical structure of the individual granules *in situ* is crucial to clarify their origin as well determine the source of organelles and debris in order to understand their possible role in the aging central nervous system. For this, we used differently preserved (see materials and methods) and unlabeled tissue. The 2D investigations of the stronger fixed and higher contrasted tissue samples showed an amplified preservation of the subcellular structures (**Fig. 3A**). Furthermore, granules could be detected even without labeling and it appeared that the membrane surrounding the fibrillary structure was more continuous (**Fig. 3B**). Here, the fibrillary structure of the granules appeared much darker and denser compared to the previous tissue sections involving only 0.1 % Glutaraldehyde (see materials and methods; **Fig. 3B, Fig. 1**). This likely also stems from the extended osmium treatment and the embedding in a different resin. In **Figure 3C,** a sequence of 24 serial sections obtained by SBF-SEM experiments is documented, showing the appearance of two granules (**Fig. 3C,** outlined in green**; supplement material**). Going through the sequence it appeared that these granules fused at some point (**Fig. 3C10**) and separated again. This indicates that the granules might not be individual round/ovoid shaped structures, but are more likely connected with each other. This in turn, supports the hypothesis that they might origin from axons and/or dendrites through a mechanism involving some “budding”-like events.

FIBRILLARY GRANULES ARE ASSOCIATED WITH GLIAL CELLS

The fine fibrillary structure of the granules might well be of membranous origin or an aggregation of glial filaments, which would be in line with the close association with glia as previously described by immunohistochemistry as well ultrastructurally *(Doehner et al., 2010; Knuesel et al., 2009)*. Reelin-positive granules have been observed around blood vessels, suggesting a tight association of the granules with perivascular astrocytic end-feet *(Doehner et al., 2010; Knuesel et al., 2009)*, and pointing to a selective clearance of Reelin deposits through

the brain vasculature. Here, we extended this examination to the putative association with astrocytes and microglia and provide more evidence on the presence of fine gliofilaments in the periphery of some granules (**Fig. 4A,** gf) and bundles of glial filament processes/astrocytic processes passing around individual granules (**Fig. 4B and C,** gf), in aged individuals. In some instances, granules were also observed in the somata/cytoplasm of or in close association with glial cells (microglia, astrocytes) (**Fig. 4D and E**).

ULTRASTRUCTURAL APPEARANCE OF THE GRANULES IN POLYI:C VERSUS NACL EXPOSED MICE

In the present study, we aimed to investigate, if a prenatal immune challenge causes morphological differences in the granules ultrastructure and in the surrounding neuropil in comparison to aged matched NaCl exposed mice.

TREND TOWARDS LARGER GRANULE SIZE IN THE IMMUNE CHALLENGED MICE

Unfortunately, the 6 month old animal group (n = 2 per treatment) did not exhibit any granular structures in the hippocampal region, whereupon we were not able to investigate possible granular differences in this age group. It needs to be stressed, that normal wild type mice exhibit plaque deposition at an age of 9-12 months, whereas immune challenged mice show these granular structures already at an age of 6 months, indicative of premature aging in the hippocampal formation. However, since this marks the beginning of the extracellular deposition, some animals are expected to show no or very few Reelin-positive granules. This decreases of course the chances to detect these structures with an ultrastructural analysis. Therefore, more animals of this age group need to be investigated in order to capture the starting phase of plaque deposition. Apart from the increased numerical density, ultrastructural analysis of the granular structure in the 9 month old subjects revealed no overt difference between the two treatment groups (**Fig. 5**).

FIGURE 3: 3D-preparation of the granular structure
To visualize and reconstruct the 3D anatomical structure of the individual granules *in situ* we used differently preserved and unlabeled tissue. **A**) 2D investigations using transmission electron microscopy of the stronger fixed and higher contrasted tissue samples showed an amplified preservation of the subcellular structures. **B**) Higher magnification of an individual granule. Using this protocol the membrane surrounding the fibrillary structure was

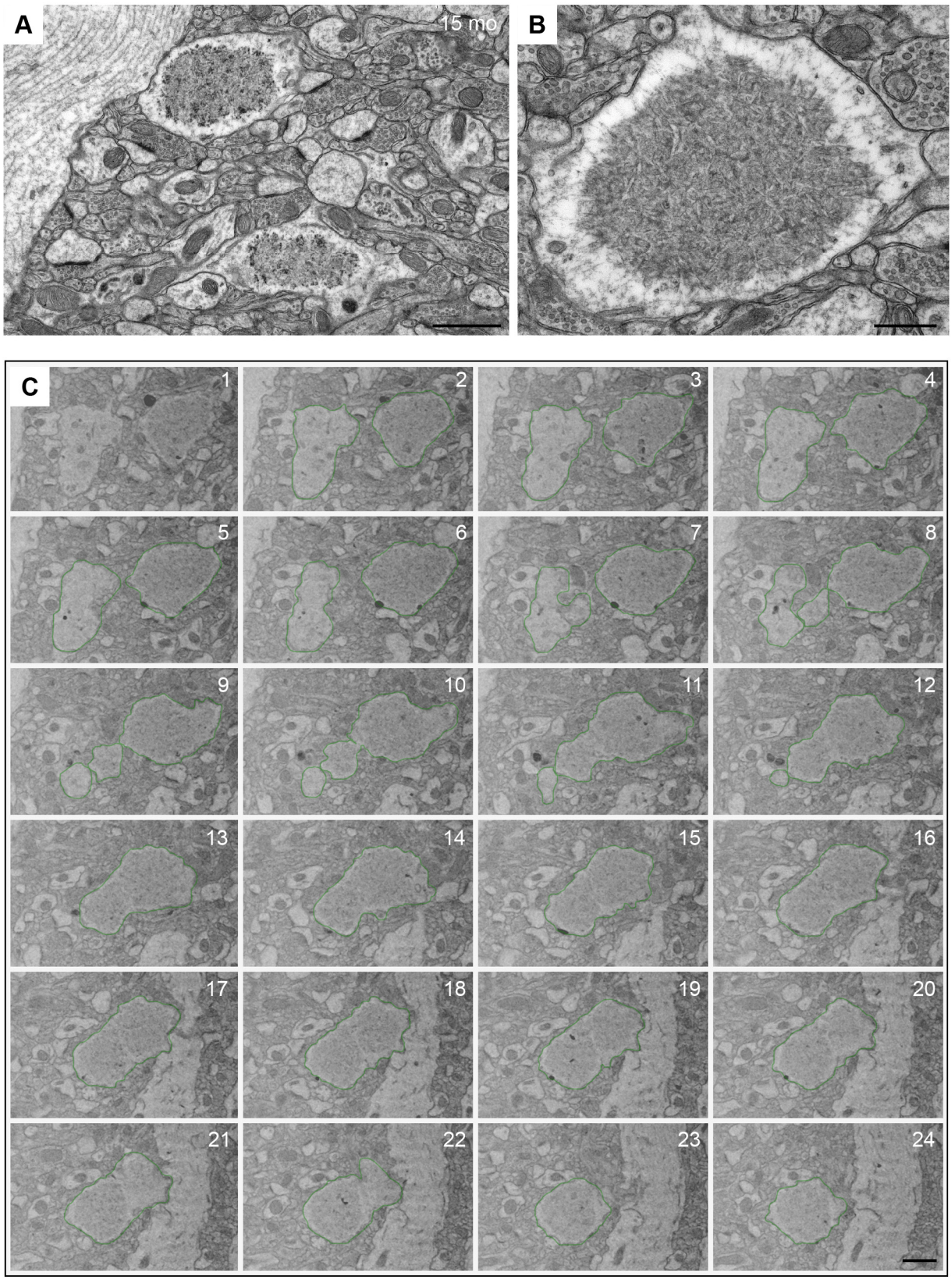

almost continuous and the typical fibrillary structure in the center of the granules appeared much darker and denser. **C**) Twenty-four consecutive sections through the CA1 sr region of the hippocampus obtained by SBF-SEM showing the appearance of two granules (outlined in green), which seem to fuse at some point (C10) and separate again. Scale bars: **A, C** = 1 μm, **B** = 500 nm.

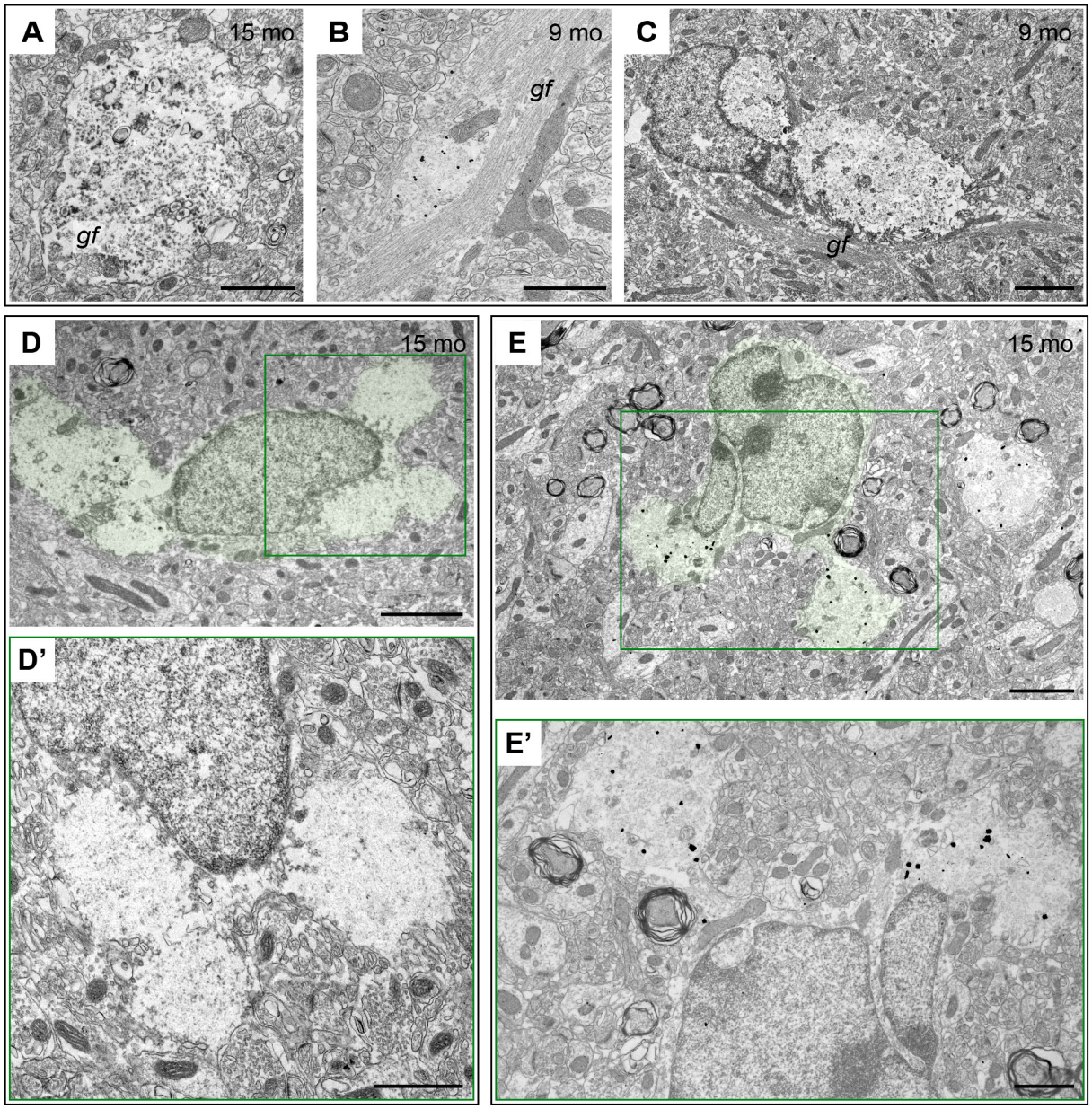

FIGURE 4: Fibrillary granules are associated with glial cells. Ultrastructural investigation of the association of Reelin-positive granules with astrocytes and microglia. Note the presence of fine gliofilaments (gf) in the periphery of a granule of NaCl exposed mice (15 mo) processed for immunoperoxidase staining (**A**) and the presence of glial filament bundles (gf) processes/astrocytic processes passing around individual granules of NaCl processed for Fluoronanogold labeling (**B**) and PolyI:C subjects (9 mo) processed for immunoperoxidase staining (**C**). In some instances, granules were also observed in the somata/cytoplasm of glial cells of old (15 mo) NaCl (**D**) as well as PolyI:C (**E**) subjects (green). **D'** and **E'**) Enlarged views of the boxed areas (green) in **D** and **E**, respectively, showing two fibrillary granules in the cytoplasm of glia cells. Scale bars: **A, B, D', E'** = 1 μm, **C, D, E** = 2 μm.

Nonetheless, fibrillary granules in the PolyI:C treated subjects appeared bigger in size compared to the control (**Fig. 5,** higher magnification). However, no statistical analysis has been performed for this age group due to the low sample size.

The same structures with their distinct fibrillary features were also observed in 15 month old animals (**Fig. 6A**). Morphological evaluation of the granules revealed a trend towards a larger

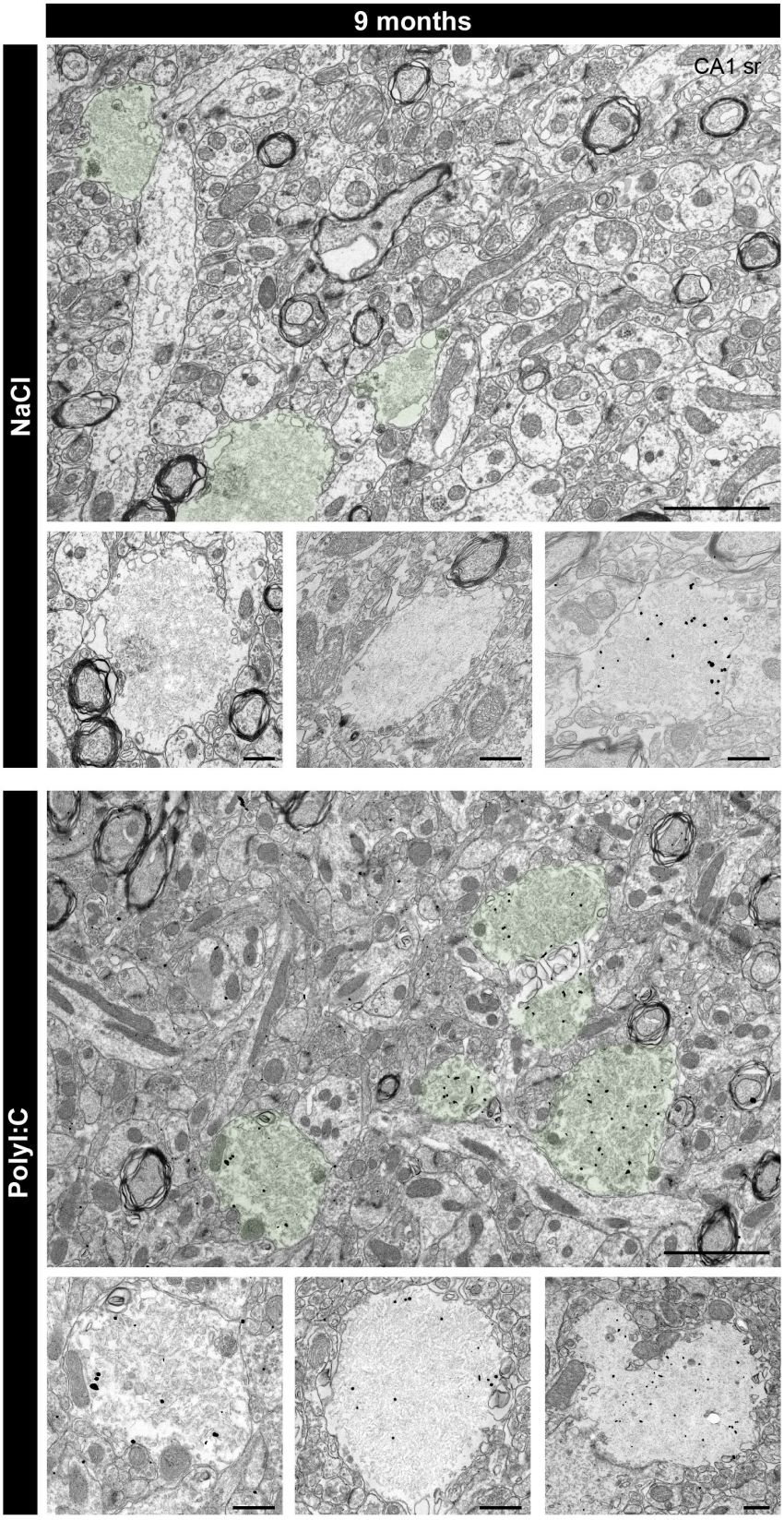

FIGURE 5: Comparison of the Reelin-positive granules of 9 month old mice.
Immuno-electron microscopy of hippocampal brain tissue obtained from NaCl- and PolyI:C-exposed mice at 9 months of age (green) processed for Fluoronanogold labeling. A gallery of individual granules obtained from several (n = 3) mice with a single prenatal virus-like infection (PolyI:C) or saline (NaCl) is shown below each overview, respectively. Scale bars: overviews = 2 μm, small images = 500 nm.

size in the immune challenged cohort (PolyI:C), compared to the saline exposed group. In line, statistical analysis showed that in the NaCl group the highest frequency was at a size of 5 to 10 μm^2, whereas in the PolyI:C group the area size was between 10 to 15 μm^2 (**Fig. 6B**). This analysis closely reached statistical significance ($p = 0.0672$; **Fig. 6B**). Initially, we described the morphology of the granules on the subcellular level free of any organelles *(Doehner et al., 2010)*. However, we observed in the PolyI:C subjects the presence of cellular organelles in these granules. Closer examination of the NaCl and aged wild type mice revealed these features also in these subjects. However, these cellular organelles, mainly mitochondria (**Fig. 6A,** higher magnifications lower panel, arrowheads), seem to be more frequently associated with the deposits in the immune challenged mice (PolyI:C) (**Fig. 6C**). This was confirmed by statistical analysis and yielded a nearly significant treatment effect ($p = 0.0771$). In NaCl subjects the number of individual granules (50-55 per treatment) containing mitochondria was maximally 25 %. In PolyI:C mice, more than the double amount of granules (52 %) were associated with mitochondria. Interestingly, the mitochondria look healthy in their appearance (**Fig. 6A,** higher magnifications lower panel, arrowheads). However, their abundant presence following a prenatal immune challenge suggests elevation or dysfunction in autophagy, a cellular process required for efficient clearance of non-functioning organelles. In line with this hypothesis, degenerative changes were seen in some neurons, evident by their dark appearance due to electron dense cytoplasm and numerous fibrils in the cytoplasm and shrunken cell body and pyknotic nucleus respectively (**Fig. 8A** and **B**); they are so called dark neurons. These cells were more frequently observed in PolyI:C exposed mice, mainly surrounded by swollen hydropic astrocytic processes (**Fig. 8A** and **B,** asterisks).

FIGURE 6: Comparison of the Reelin-positive granules of 15 month old mice
A) Immuno-electron microscopy of hippocampal brain tissue obtained from NaCl- and PolyI:C-exposed mice at 15 months of age (green) either processed for Fluoronanogold labeling or immunoperoxidase reaction (lower left image). The effect of PolyI:C administration prenatally on granule morphology was evident in a pronounced increase in size and the elevated presence of mitochondria associated with the granules (lower panel, black arrowheads). This morphological evaluation was confirmed by statistical analysis (**B**), which yielded a treatment effect that approached closely statistical significance ($p = 0.0672$). The analysis showed that in the NaCl group the highest frequency was at a size of 5 to 10 μm^2, whereas in the PolyI:C group the area size was between 10 to 15 μm^2 (**B**). The summary of the analysis is displayed in a box plot graph. The dimensions of the box are defined by the 75th (top) and 25th percentile (bottom) and the median line. The upper and lower error bars indicate the 90th and 10th percentile, respectively. All observations above 90th and below 10th are represented as black dots. **C**) The increase in size was accompanied by elevated appearance of mitochondria in these granules. They seem to be more frequently associated with the deposits in the immune challenged mice (PolyI:C) compared to saline (NaCl) exposed granules (50-55 per treatment) containing mitochondria was maximally 25 %. In PolyI:C mice, more than the double amount of granules (52 %) were associated with mitochondria (table). Scale bars: overviews = 2 μm, small images = 500 nm.

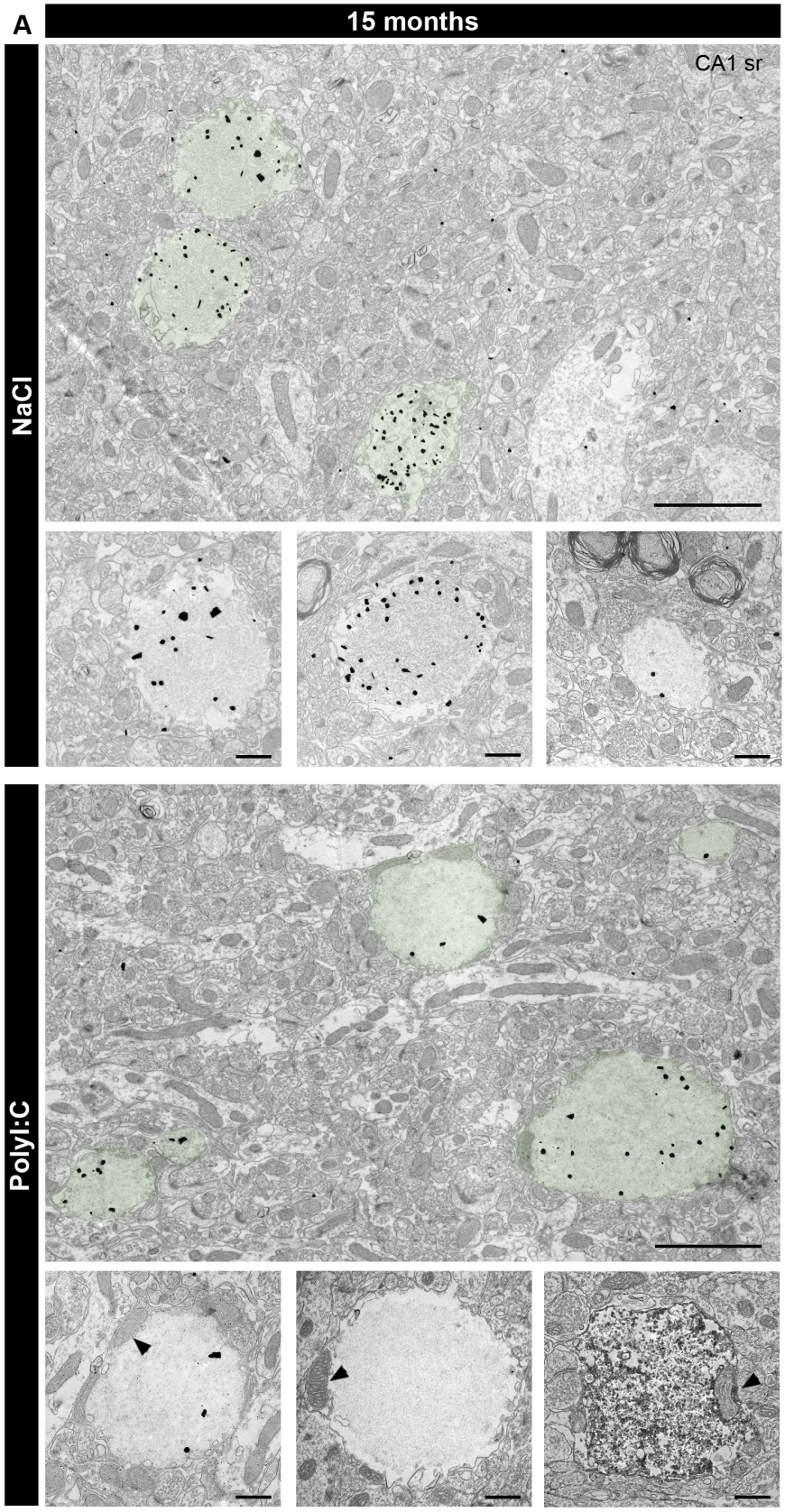

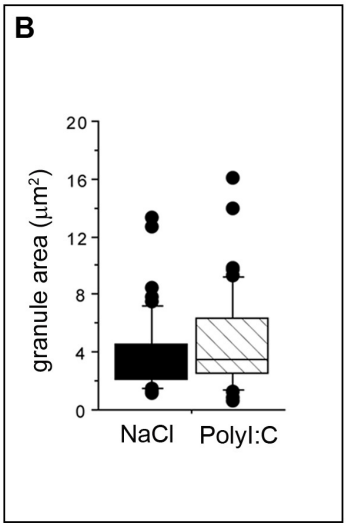

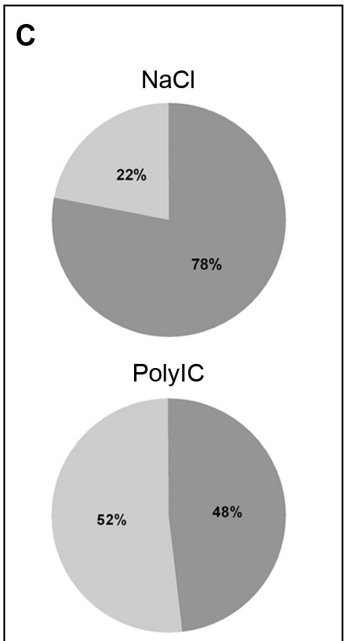

Animal	granules with mito / total analyzed granules	
NaCl -1	3 / 22	11/50
NaCl - 2	3 / 10	
NaCl - 3	5 / 18	
PolyI:C - 1	2 / 7	28/55
PolyI:C - 2	4 / 12	
PolyI:C - 3	11 / 15	
PolyI:C - 4	11 / 21	

Degeneration of synapses, as already described subcellularly in degenerative diseases, i.e. prion diseases *(Gray et al., 2009*; for review see *Perry and O'Connor, 2010)* have not been observed yet in the immune challenged mice. Further investigations have to be done to elucidate if a prenatal immune challenge has a detrimental effects on synapse morphology in the adult brain.

REELIN IS OBSERVED IN MYELINATED AXONAL PROJECTIONS

To test whether the putative elevation or dysfunction in the autophagosome formation was accompanied by axonal degeneration, we performed double immunofluorescence staining of myelin basic protein (MBP) and Reelin. We found that the matrix protein was strongly enriched in myelinated axons in the immune challenged animals (**Fig. 7B**), whereas no Reelin-IR could be detected yet in the axons of saline treated mice (**Fig. 7A**). This indicates that Reelin is either present in very low levels in these axons, or the myelin sheaths might be still intact in the saline treated mice, and therefore the epitope for the Reelin antibody is not accessible. Support for the latter hypothesis is given by our previous findings in aged wild type mice *(Doehner et al., 2010)*, showing axonal Reelin-positive staining after extensive pepsin treatment (60 min). It confirms that prolonged protease treatment is required to likely disrupt the myelin sheaths that in turn allows the detection of Reelin in the axonal projections even in non-immune challenged mice. Here, the pepsin treatment was only applied for 10 min, minimizing its effect on the myelin sheaths, but rather supporting an alteration of the myelin sheath due to the long-term effects of a prenatal infection. Note the appearance of the granular structures at the terminals of the axonal projections, indicating that they might be formed within the axonal compartments (**Fig. 7C,** magnified image, white arrowhead). Ultrastructurally, Reelin was not observed in myelinated axons yet. However, distinct granular appearances along unmyelinated axonal processes were detected in PolyI:C exposed mice (**Fig. 7D,** granule in green, axon in red), indicative of an axonal swelling or "budding" event. This would be in line with our 3D preparations (**Fig. 3C**).

FIGURE 7: Reelin can be detected in myelinated axons
A-C) Representative confocal images of double-immunofluorescence staining of brain sections obtained from old (15 mo) NaCl and PolyI:C subjects using mouse anti-Reelin (red) and rabbit anti-MBP (myelin basic protein, green) antibodies. **A**) No Reelin-IR was observed in axonal projections in saline (NaCl) treated mice. **B**) The matrix protein Reelin was strongly enriched in myelinated axons in the immune challenged animals. Note the appearance of the granular structures at the terminals of the axonal projections, indicating that they might be formed within the axonal compartments (**C**). **C'** shows higher magnification of the boxed area outlined in **C**. **D**) Ultrastructurally, distinct granular appearance (green) along unmyelinated axonal processes (red) were detected in PolyI:C exposed mice, indicative of an axonal swelling or "budding" event. Scale bars: **A, B, C** = 10 μm, **A', B'** = 5 μm, **D** = 1 μm.

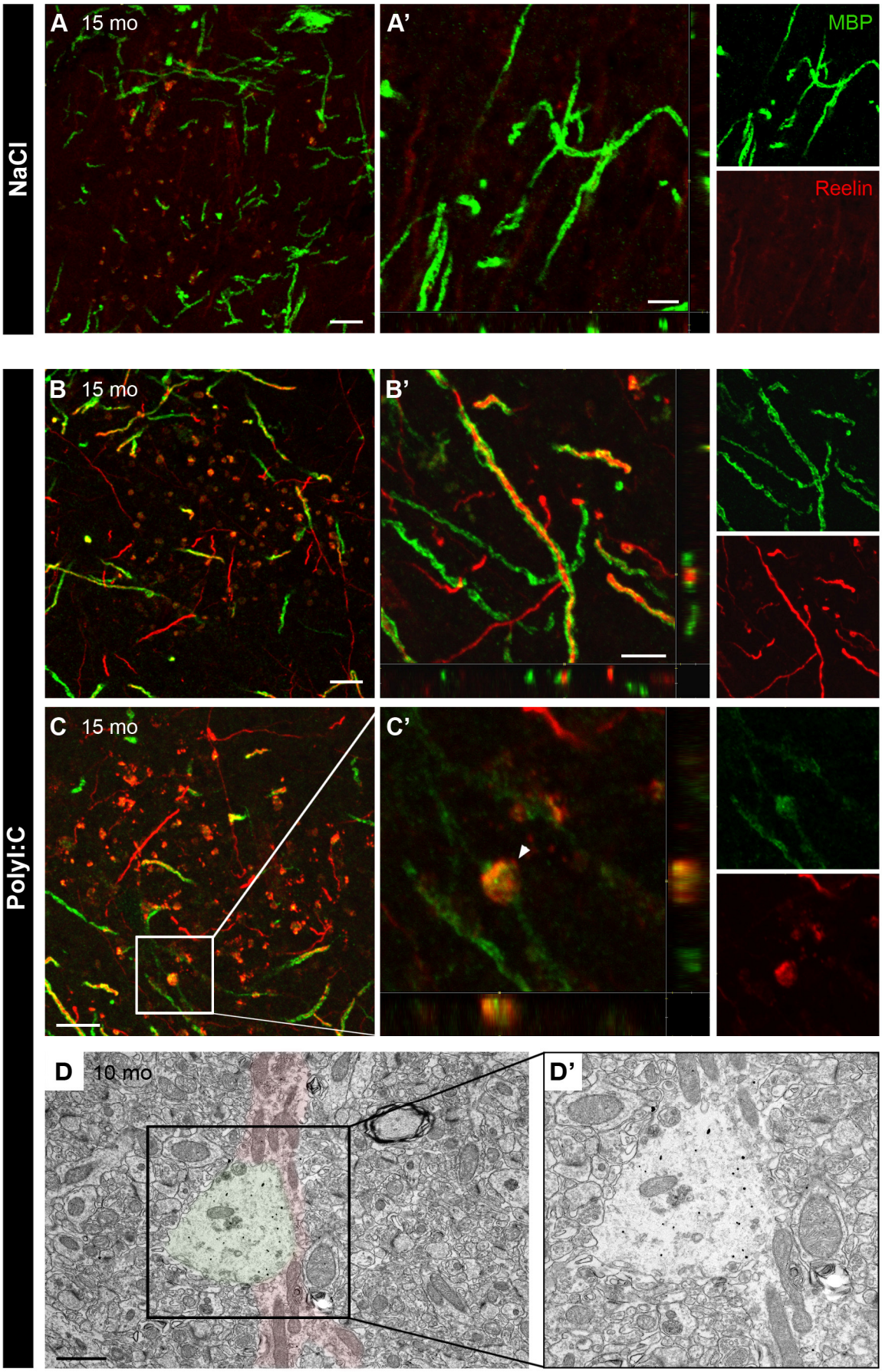
NaCl
A 15 mo
A'
MBP
Reelin
Poly I:C
B 15 mo
B'
C 15 mo
C'
D 10 mo
D'

REELIN GRANULES MIGHT BE OF DEGENERATIVE ORIGIN

To confirm the degenerative features, we also performed silver staining in 15 month old NaCl and PolyI:C exposed animals. In line with our EM data the Reelin-positive deposits in the immune challenged mice exhibit a distinct grayish pattern mainly in the periphery of the granules (**Fig. 8C** and **D,** arrows), suggestive of dystrophic neurites, whereas in the control animals (NaCl) a considerably weaker pattern could be observed. This supports the hypothesis, that a prenatal immune challenge accelerates degenerative effects. However, no overt progressive and widespread neurodegeneration was evident at the time points investigated in these mice. Nevertheless, the degenerative features in PolyI:C subjects appeared to be restricted to the plaque areas, as discernible by the grayish granular pattern.

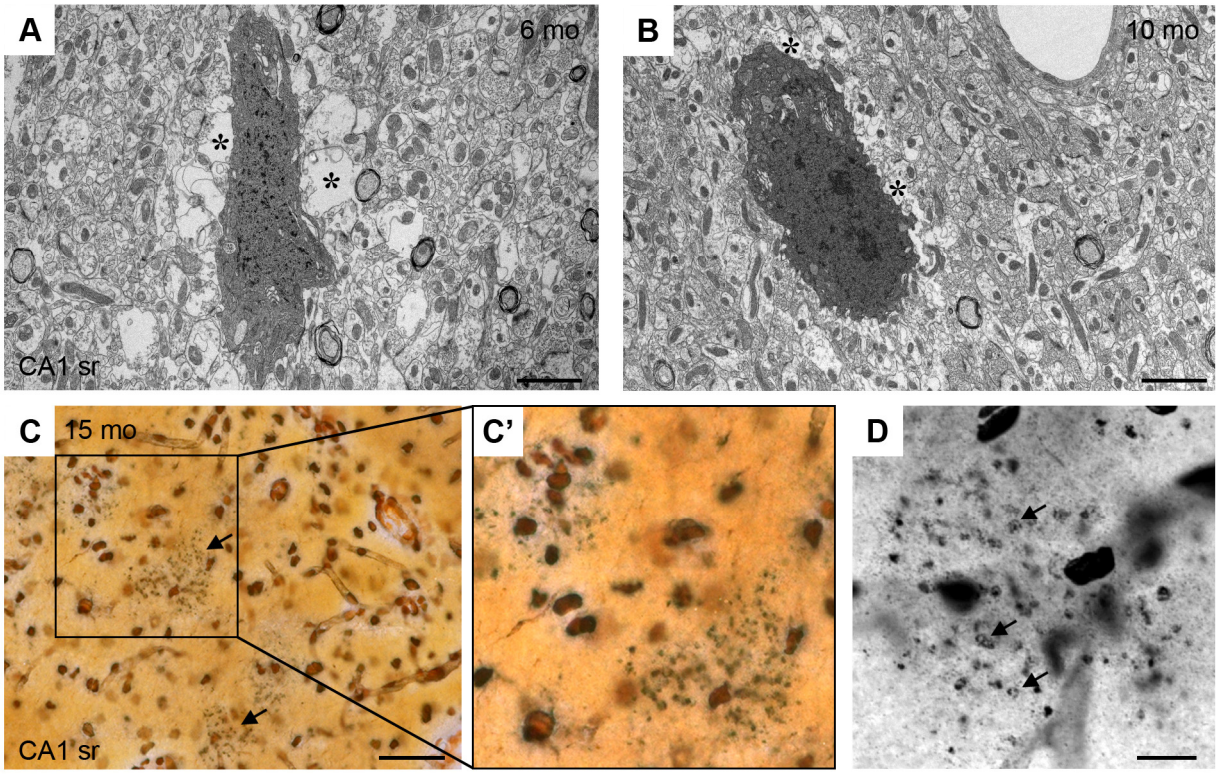

FIGURE 8: Increased neurodegeneration after prenatal PolyI:C exposure
Electron micrographs of degenerating neuronal cells in the hippocampus obtained from 6 month (**A**) and 10 month (**B**) old PolyI:C exposed mice. These neurons, evident by their dark appearance and the pyknotic nucleus are more frequently observed in aged PolyI:C exposed mice compared to saline (NaCl) subjects, mainly surrounded by swollen hydropic astrocytic processes (asterisks). **C, D**) To confirm the degenerative features, brain sections obtained from 15 month old PolyI:C exposed animals were processed for silver staining. This revealed a distinct grayish pattern mainly in the periphery of the granules (arrows), indicative of degeneration. Scale bars: **A, B** = 2 µm, **C** = 50 µm, **D** = 10 µm.

2.5 DISCUSSION

In summary, our electron microscopy revealed a trend towards larger granules and a significantly higher number of mitochondria in the granules after prenatal PolyI:C exposure. This was accompanied by distinct degenerative features including shrunken neurons, axonal varicosity and the extracellular deposits. In the following sections, these observations, as well as the possible origin of these granules will be discussed in more detail

ULTRASTRUCTURAL APPEARANCE OF THE REELIN DEPOSITS

In the 80s, Periodic acid-Schiff (PAS) positive granules were discovered in aged SAMP8 and B6 mouse brains, which were primarily found in the hippocampus and the cerebellum, quantitatively increasing with age *(Akiyama et al., 1986; Jucker and Ingram, 1994; Jucker et al., 1992, 1994a; Lamar et al., 1976; Mandybur et al., 1989; Mitsuno et al., 1999)*. Our observations of the Reelin-positive granules are in some aspects comparable with the studies referring to these structures as polyglycogen bodies (PGs) in aged mice *(Akiyama et al., 1986; Corsetti et al., 2008; Del Valle et al., 2010; Jucker et al., 1994a)*, concerning their morphological appearance, size, localization and age dependency. The granules have been identified as mouse-strain specific, age-associated deposits of fibrillary material *(Jucker et al., 1992)*. Clustered PGs in humans have been reported to be linked to several disorders *(McMaster et al., 1979; Sugiyama et al., 1993)* and have been suggested to be involved in human neurodegenerative diseases *(Nakamura et al., 1995)*. These human PGs referred to be fairly similar to murine PGs regarding size, staining properties and ultrastructural features; though they differed in their anatomical distribution (human: eg. palladium, substantia nigra, hypothalamus; murine: eg. hippocampal formation). It was thought that the rodent PGs might be related to the human Corpora amylacea *(Adams, 1984; Alder, 1953; Ramsey, 1965)*. Although they exhibit intriguing similarities like being PAS positive and of polysaccharide nature, important differences have been noted *(Jucker and Ingram, 1994)*: including their ultrastructural appearance, conventional staining properties and distribution. The fibrillary granules observed in rodents appear in clusters primarily in the hippocampal formation, cerebellum and piriform cortex, whereas human corpora amylacea are more widely and randomly distributed and occur most frequently in the subpial region. A positive PAS reaction is suggestive of the presence of matrix proteins, proteoglycans and glycogen in this clustered granular structure. Therefore, it has been shown that these granules are positive for heparan sulfate proteoglycan (HSPG), an extracellular matrix (ECM) protein *(Kuo et al., 1996)*. Previous

research findings indicate that ECM molecules, in particular HSPG co-exist with Aβ in the cores of many senile plaques found in AD brain *(Armstrong, 2006; Narindrasorasak et al., 1991; Snow et al., 1988; Snow and Wight, 1989; Su et al., 1992)* and the deposition of such molecules might be a prerequisite for amyloidogenesis *(Snow and Wight, 1989)*. Therefore, considering Reelin as a possible proteoglycan, which is defined by heavy glycosylation, would support our hypothesis that these clusters may mimic a precursor condition for amyloid deposition, as also supported by our positive labeling for Aβ *(Doehner et al., 2010)*. On the other hand, it is well known, that several HS chains are attached in close proximity to extracellular matrix proteins *(Lyon et al., 2000)*, suggesting that several HS chains trigger the aggregation of Reelin in this granules and facilitating Aβ or proteolytic fragments of APP to bind to this structure additionally. Nevertheless, although these data state a strong analogy of our observed deposits to the earlier described PGs based on their age dependency, clustering and localization primarily in the hippocampal formation, it is not deciphered yet if the Reelin-positive granules which we investigated are of the same origin as all the PGs described above. It is still an open question, whether the granules investigated by the several research groups are the same structures or may be indicative of different neuropathologies. One major difference, for example, to the structures described by Jucker *(Jucker and Ingram, 1994; Jucker et al., 1992, 1994a)* is the appearance of mitochondria in our investigated granular clusters. Indeed, Kuo and coworkers *(Kuo et al., 1996)* describe mitochondria or other organelles in the outer "submembrane space" of the granules. Further, both groups did not show any association of these fibrillary structures with axons, whereby we observed such a phenomenon in our lab. Until today, these structures were claimed as being extracellular. Results of the SBF-SEM approach applied in this present study, suggest that the granular structures are not simply round and ovoid individual structures, but that they are connected to each other and potentially remnants of represent dendritic or axonal compartments; indicative of intracellular origin. These slightly varying characteristics indicate that the structures described in our study are different from the granules observed by others, and likely describe a different pathological feature. In a recent paper described, similar granular structures in SAMP8 mice were also positively identified by different antibodies like Tau 5 (total tau), Aβ specific ones, MAP2 and syndecan-2 *(Del Valle et al., 2010; Kern et al., 2011; Manich et al., 2011)*, the key players in AD. This is suggestive of a very complex mixture of proteins in the granules. However, to entirely differentiate between the observed granules in our lab and the previously described PGs, additional stainings for the particular proteins need to be performed to better characterize these structures.

REELIN IS CLOSELY ASSOCIATED WITH GLIAL CELLS

Our results obtained Reelin-IR or Reelin-positive granules in astrocytic processes, in the soma or in close vicinity of glia cells. This is in line with findings from several research groups *(Akiyama et al., 1986; Jucker et al., 1994b; Kuo et al., 1996; Roberts et al., 2005)*. Roberts and Colleagues *(Roberts et al., 2005)* have described Reelin in the human cortex, finding Reelin-IR in the somata of glia cells as well as in small astrocytic processes. The reported association of the proteoglycan (PGs) bodies with astrocytes is in conflict with a recent study *(Kern et al., 2011)*, reporting that there is no evidence of any association of the granules with neuronal and astrocytic processes, as their observed Tau/Reelin granules, similar to the previously described structures were negative for MAP2 and GFAP. Indeed, immunohistochemical and ultrastructural investigations of several research groups including ours showed a close association of granules with astrocytes or being even localized in astrocytic processes and/or somata and astrocytic endfeet *(Akiyama et al., 1986; Del Valle et al., 2010; Doehner et al., 2010; Jucker et al., 1992, 1994b; Knuesel et al., 2009; Kuo et al., 1996; Manich et al., 2011; Mitsuno et al., 1999)*, which is consistent with our ultrastructural observations. This close association of the granules with glial cells likely indicates that the aggregated material is either produced or phagocytosed by astrocytes. If the granules are of astrocytic origin, one would hypothesize that they are a degenerative processes likely yielding to the aggregation of glial filaments, explaining the fibrillary appearance of the granules. Moreover, the localization around blood vessels is also consistent with an astrocytic origin, as is the evidence for HSPG like and laminin like molecules in the fibrillary material, as these are known to be secreted by astrocytes and expressed in activated glia cells in AD brains upon CNS injury *(Ard and Bunge, 1988; Liesi et al., 1984; Snow et al., 1988)*. Further, a very recent study by the group of Vilaplana *(Manich et al., 2011)* suggests that their described granular structures in SAMP8 mice – mimicking our granular clusters - are not of astrocytic origin, although a few were closely associated this, the majority of the deposits were not. They note these clusters are suggestive of a neuronal origin as they are positive for NeuN. Further support of the idea that the granules might be of neuronal origin came from the research by Irino and coworkers *(Irino and Fujita, 1994)*, reporting that similar granular structures can represent enlarged presynaptic terminals. Another supportive aspect that the granules might closely arise from neurons and/or glia came from the group of Hosokawa *(Nakamura et al., 1995)*. They found monoamine oxidase-B-positive granular structures (MGS) in the hippocampus of old SAMP8. These structures were equal to the PAS positive granules described earlier *(Akiyama et al., 1986)* and therefore highly similar to the structures described

here. Monoamine oxidase is usually bound to the outer membrane of mitochondria, found in neurons and astroglia. MGS was in close anatomical relationship with astrocytic processes, thereby a monoamine oxidase-positive astrocyte was observed in the central area of each cluster of MGS *(Nakamura et al., 1995)*. As already well described, cerebral MAO-B activity increases with aging and during the development of several kind of neurodegenerative disorders such as AD *(Fowler et al., 1980; Gottfries, 1990; Jellinger and Riederer, 1984; Mann et al., 1980)*. This increase may be linked to the presence of MAO-B-rich reactive astrocytes and glial cells *(Gottfries, 1990; Riederer et al., 1987)* in response to neuronal degeneration as well as early infection. These data further support the assumption that the granules are of astrocytic or neuronal origin as this catalase could be observed in these structures.

WHICH POSSIBLE ROLE DOES REELIN PLAY IN NEURODEGENERATION?

Studies from Jucker and Kuo *(Jucker and Ingram, 1994; Jucker et al., 1994a; Kuo et al., 1996; Mitsuno et al., 1999)* reported that their subcellular structure could not be observed in detail, as these granules were surrounded by electron-lucent halos, suggestive of a degenerative condition of axonal and dendritic processes. In our study, no such observations were recognized. The surrounding tissue of the granules appeared healthy without any sign of neurodegeneration in the close proximity of the clustered structures. In contrast, our silver staining is suggestive of the granules most likely representing a degenerative event on its own, whereby - as evident by ultrastructural investigations - the core containing cellular organelles without overt evidence of ongoing neurodegeneration in the surrounding.

As already mentioned before, the PGs were specifically labeled for HSPG *(Kuo et al., 1996)*. Kuo and co-workers discussed that the aggregated granular and fibrillary material might be the result of a degenerative process. HSPG appeared only at the periphery of these granules, suggesting that the periphery of the granule might be the active site of degeneration, and that HSPG may be involved in the degenerative process. The mechanism of this degenerative process and the cellular compartment where the degenerative process occurs were not clear. However, declaring the periphery of the granules as the active site of degeneration would in fact be in line with our investigations, observing silver labeling as well mainly in the periphery of these granules. In addition, ultrastructural analyses done by some research groups suggest that small quantities or fractions of microtubule-associated protein (MAP2) and Glial fibrillary acidic protein (GFAP) may be present as dystrophic processes in and around the granules *(Kuo et al.,*

1996; Mitsuno et al., 1999), supporting the idea, that the granules are possible degenerative or of axonal as well neuronal origin.

REELIN IN AXONAL PROCESSES

Reelin was also found in the close proximity of axons. Further support is given by our own recent immunohistochemical investigations of Reelin-IR in spherical structures found in human brain areas *(unpublished data),* which potentially originate from axonal swellings. These results are supported by several studies. Indeed, ultrastructural deposition of Reelin inside axonal processes has already been described in rodents and non-human primates *(Derer et al., 2001; Martinez-Cerdeno et al., 2003; Pappas et al., 2001)*. Derer and his group *(Derer et al., 2001)* present morphological evidence that Reelin is indeed secreted from local, specialized compartments in the axons of the Cajal Retzius (CR) cells, which look like axonal beads displayed throughout their length in a size of 0.5-3 μm, each containing a smooth spheroidal cistern or reservoir filled with fibrillar Reelin-positive material named as "axonal Reelin reservoirs". They propose that Reelin and possible other products are synthesized and distributed in the neuropil at this sites along the axonal projection. This indicates that such an arrangement may favor the wide diffusion of Reelin and other factors in extracellular channels or induces abnormal axonal varicosities and/or degeneration. The work of Derer and Goffinet *(Derer et al., 2001)* and another recent research done by the group of Phelps *(Kubasak et al., 2004)* suggest that Reelin is likely to be secreted from varicose axons. Furthermore, in 1998 it has been described that Reelin can be transported along cell axons *(Pesold et al., 1998a)*, even long distances, explaining the appearance of the Reelin protein in the neuropil of some certain brain areas. The two previous studies were done in the context of development, one might consider that this axonal swellings filled with Reelin may also occur in the adult/aged brain in the axonal projection from the entorhinal cortex to the slm region of the hippocampus, as well as from GABAergic neurons in the hippocampal formation and not only being restricted to CR cells, likely explaining the Reelin positive clusters in exact these brain regions. They might as well be originating due to an axonal transport dysfunction yielding to the aggregation of the preserved matrix protein, finally leading to a disintegration of the axons. These studies and the hypothesis would be in agreement with our previous study *(Madhusudan et al., 2009)*, centering around the hypothesis that early accumulations of Reelin deposits in the projection areas of subcortical neurons could impair the integrity of axonal terminals, potentially resulting in degeneration of cholinergic neurons in the basal forebrain, known to be early affected in AD. The occurrence of

Reelin labeling throughout axonal processes strongly suggests that Reelin can be transported long distances through axonal tracts *(Derer et al., 2001; Martinez-Cerdeno et al., 2003; Perez-Costas et al., 2002; Roberts et al., 2005)*.

Furthermore, in our study we have challenged wild type mice prenatally with a viral-like infection. The applied PolyI:C is a ligand for the Toll-Like Receptor 3. TLRs are having emerging roles in neurodegenerative and demyelinating diseases (for review *(Okun et al., 2011)*). This is in line with our immuno-staining of MBP and Reelin, showing a disruption of the myelin sheaths in the immune challenged mice (PolyI:C). One might ask, if it is possible that a prenatal infection is capable of disrupting the myelin sheaths around axons in the adult brain? It is well known that for example myelin components concentrations decrease throughout the pathology of AD (reviewed in *(Gottfries, 1990)*). Based on these results, it can be hypothesized that a prenatal immune challenge might have a degenerative and/or disintegrating impact on the myelination of certain axons, likely triggering alterations in axonal transport as well as already inducing age-related neuropathology. This in turn might be the potential region where aggregated Reelin develops swellings and subsequently gets secreted in the neuropil, explaining the increased density of clustered Reelin-positive deposits in these mice. The swellings might as well be a budding event of degenerative material formed in the axon – maybe as a consequence of abnormal Reelin signaling - which then get removed and form the described granules. Further, this budding might also be a protective event, to save the neuritic processes from degeneration. A recent paper by Nixon *(Lee et al., 2011)* described abnormal accumulation of lysosomes and autolysosomes causing axonal swellings, due to lack of the AD-linked protein presenilin. It is known, that in AD focal swellings can develop along the axons and dendrites of neurons throughout affected brain regions, like the hippocampal formation or cortex *(Nixon, 2007; Nixon et al., 2005; Shacka et al., 2008; Yu et al., 2005)*. These swellings comprise typically accumulated organelles specifically related to the autophagic-lysosomal pathway likely reflecting a disruption of axonal transport *(Morfini et al., 2009)*, as also recently supported by ultrastructural observations *(Nixon et al., 2005)*, strongly implying a defect in the proteolytic clearance of this undigested protein accumulation. This might also support that the aggregation of Reelin forming clustered granules might derive from inappropriate clearance of the protein. In the case that lysosomal proteolysis is inhibited, the axonal transport is slowed down, most likely resulting in their accumulation and forming of axonal swellings *(Lee et al., 2011)*. Based on these findings, it can be suggested that impaired lysosomal proteolysis and the aggregation of the matrix protein could be a basis for leading to neuritic dystrophy. Therefore, it will be

interesting to determine if lysosomal markers are present in the Reelin deposits or are formed to be closely associated with them.

THE ROLE OF INFLAMMATION IN THE DEVELOPMENT OF THE REELIN-POSITIVE GRANULES

In the last decades, there is accumulating evidence that inflammation contributes to AD pathology and can exacerbate the course of the disease *(Akiyama et al., 2000; Hoozemans et al., 2006; Lucin and Wyss-Coray, 2009; Parachikova et al., 2007; Salminen et al., 2009; Wyss-Coray, 2006)*. Despite the growing number of studies linking inflammatory responses to AD pathogenesis, very little information is available on early inflammatory processes which might possess stronger disease-modifying potential than the Aβ-plaque associated inflammatory response. Systemic inflammation by peripheral administration of PolyI:C to pregnant dams may evoke pathological alterations in the brain of mice via cytokines, complement and several signaling molecules. However the effect of systemic inflammation on the CNS is not fully understood. Our recent experimental approach provides the first evidence that a prenatal immune challenge during late gestation using PolyI:C results in significant acceleration of aging-associated neuropathological alterations in non-transgenic wild type mice, involving, reduced Reelin expression and precocious accumulation of Reelin-positive deposits *(Knuesel et al., 2009)*. This prenatal immune challenge suggests a role for early neurodevelopmental and immunological abnormalities underlying aging-related neuropathology. In addition, recent results *(unpublished data)* indicate that a prenatal viral-like immune challenge induces long-term alterations in critical immune modulators that potentially underlie abnormal Reelin signaling and proteolytic processing. This may favor the production of Aβ-peptides, impair their clearance and result in elevated levels of phosphorylated Tau. These changes are seen in animals as young as 3 months of age and aggravate throughout aging. Granules also start to appear much earlier in the immune challenged mice compared to the saline treated ones. Evaluating all these differences by biochemical and immunohistochemical investigations, we further wanted to elucidate if PolyI:C induces differences on the subcellular level. We therefore conducted electron microscopy. Morphological difference between the granules of PolyI:C and NaCl exposed mice were evident by a trend towards larger size in the immune challenged animals accompanied by an increased association with mitochondria. It still needs to be elucidated if the appearance of mitochondria correlates with the size of the granule. However, the presence of mitochondria is indicative of a degenerative process of cellular structures forming these granules, going in line with the previous discussed data. This also indicates that PolyI:C accelerates this age effect and thus,

triggers neurodegeneration events, supporting our hypothesis that the granular formation likely results from degeneration events. Although, the phenomenon was amplified due to PolyI:C exposure, the origin of the granules seems to be still the same. For a definite conclusion more granules and animals need to be investigated and quantitatively analyzed, as granules are cut differently while processing and the analysis therefore might not give an appropriate estimate of size and amount of mitochondria associated between these two groups. A more precise analysis could be accomplished by volumetric measurements of the whole granules for defining possible differences between the two treatment groups. Moreover, the immune challenged mice revealed some substructural alterations in the form of neurodegenerative events. Some groups have discovered that the granular structures appear in increased numbers in the brain of SAMP8 mice *(Akiyama et al., 1986; Del Valle et al., 2010)*. It is known that these mice are deriving from selective inbreeding of AKR/J strain of mice, which are viremic from birth on. This unfolds a role of inflammation background in these SAMP8 mice, supporting our data, that early infection accelerates the formation of these particular deposits.

CONCLUSION AND FUTURE PERSPECTIVES

Our current data suggest that the Reelin-positive granules are pathological, emerging as a function of advanced age and as a consequence of axonal degeneration *(Kern et al., 2011; Knuesel et al., 2009; Kuo et al., 1996; Mitsuno et al., 1999)*. However, the exact nature/etiology of these deposits needs to be further elucidated by additional labelings with specific markers to clarify which precise cell-type or cellular compartment is involved in the formation of these granules. Further, it would be crucial to define their putative pathophysiological significance in relation to neurodegenerative disorders, especially AD. Altogether, the observed and extensively investigated granular structure might represent the focal deposition of ECM molecules that could function as an initial step in the pathogenesis. Therefore, it is of high interest to extend the three dimensional (3D) reconstructions approach to fully define the deposits function and possible origin.

2.6 ACKNOWLEDGEMENTS

We are extremely grateful to Corinne Sidler and Cornelia Schwerdel for their excellent technical support and help with histology. We also thank Prof. Jean-Marc Fritschy and Dr. Patrizia Panzanelli for the help in establishing the electron microscopy. The present study was supported by the SNF Grant Nr. 310 000 – 117806.

2.7 SUPPLEMENT MATERIAL

Full datasets of the SBF-SEM experiments can be found on the enclosed DVD.

3. STUDY III: ESTABLISHING A PROTOCOL FOR THE BIOCHEMICAL INVESTIGATION AND CHARACTERIZATION OF REELIN-POSITIVE GRANULAR DEPOSITS IN THE AGED BRAIN OF WILD TYPE MICE

Jana Doehner[1], Thomas Bock[2], Bernd Wollscheid[2] and Irene Knuesel[1]

[1] Institute of Pharmacology and Toxicology, University of Zurich, Switzerland

[2] Institute of Molecular Systems Biology, ETH Zurich, Switzerland

Unpublished data

In this study my contribution was the preparation of the brain tissue, their labeling, laser microdissection, IHC, western blotting and the silver stainings. Further I helped by processing the samples for MS. I also wrote the manuscript.

3.1 ABSTRACT

Reelin is a major extracellular matrix glycoprotein required for proper neuronal positioning during brain development. In adulthood, Reelin is crucial for synaptic plasticity and successful formation of long-term memory. Changes in Reelin-mediated signaling have been suggested to contribute to the neuropathology of late-onset Alzheimer's disease (AD). Since aging is the major risk factor in AD, the putative changes in Reelin expression during normal and pathological forms of aging have been recently investigated in our laboratory. These data showed that aging in several species is characterized by a marked reduction of Reelin-expression and concomitant accumulation of Reelin in amyloid-like deposits in the hippocampal formation. Observations further revealed that these deposits showed a very high degree of co-localization with proteolytic APP fragments including Aβ-peptides, indicating a potential seeding effect of the Reelin deposits. The molecular mechanism underlying Reelin aggregation and its putative link to the pathogenesis of AD remains largely unknown. A systematic analysis of the biochemical nature of the Reelin-positive deposits in both normal and accelerated forms of aging should shed light on the potential signaling pathways that govern plaque initiation, formation and maintenance in mice. Therefore, in order to identify critical determinants that are potentially involved in the early stages of aggregation, a proteomic analysis, including mass spectrometry (MS), was applied. Our specific objective was to develop an efficient protocol to extract and identify proteins enriched and associated with Reelin-positive plaques. Here, we show that fluorescently labeled Reelin deposits can be isolated from fresh frozen brain sections of wild type mice by using laser microdissection. Furthermore, extracted proteins were systematically identified following western blotting and high accuracy mass spectrometry (LC-MS/MS). Our results revealed that the low protein amount isolated constitutes a major challenge for mass spectrometric detection. However, the protocol established here provides a suitable approach to identify larger protein deposits in tissue sections. To this end, herein we will discuss successively each step on our way of protocol establishment.

3.2 INTRODUCTION

Reelin is a major extracellular matrix glycoprotein secreted by Cajal-Retzius cells and required for proper neuronal positioning during brain development *(D'Arcangelo et al., 1999; Rice and Curran, 2001)*. In the adult brain, Reelin is crucial for synaptic plasticity and successful formation of long-term memory *(Herz and Chen, 2006)* through phosphorylation-dependent regulation of NMDA receptors *(Beffert et al., 2005; Chen et al., 2005)*. Alterations in Reelin-mediated signaling have been suggested to contribute to neuronal dysfunction associated with Alzheimer's disease (AD) *(Botella-Lopez et al., 2006, 2010; Durakoglugil et al., 2009; Hiesberger et al., 1999; Hoe et al., 2006, 2009b; Nikolaev et al., 2009; Seripa et al., 2008)*. This disease is characterized by progressive loss of cognitive abilities and severe neurodegeneration *(Abraham and Meyer, 2003; Savla and Palmer, 2005)*. Histopathologically, AD is manifested by the extracellular aggregation of amyloid plaques, mainly composed of amyloid-β peptides (Aβ) and the intraneuronal neurofibrillary tangles (NFTs), consisting of hyperphosphorylated Tau *(Glenner and Wong, 1984; Grundke-Iqbal et al., 1986)*. Since aging is the major risk factor in AD, the putative changes in Reelin expression during normal and pathological forms of aging have been recently investigated *(Knuesel et al., 2009)*. This study revealed that aging in several species is characterized by a marked reduction of Reelin-expression and concomitant accumulation of Reelin in amyloid-like deposits in the hippocampal formation. Further observations indicated that these Reelin deposits show a very high degree of co-localization with proteolytic APP fragments, including Aβ peptides *(Study I; (Doehner et al., 2010)),* confirming and extending previous findings involving transgenic AD mouse models *(Motoi et al., 2004; Wirths et al., 2001)*. Although all these findings imply an involvement of the Reelin signaling cascade in amyloid plaque deposition and potentially neurodegeneration *(Durakoglugil et al., 2009; Hiesberger et al., 1999; Hoe et al., 2006)*, the molecular mechanism through which this conserved protein contributes to the pathogenesis of AD remains largely unknown. Moreover, knowledge on the detailed molecular mechanism of Reelin signaling and its mechanism to form aggregates in the aging brain is lacking. Although it has been described using immunohistochemistry that Reelin is one of the main components in these granular deposits *(Knuesel et al., 2009)*, their proteomic composition is unknown. Specifically, it is currently unclear which fragments of Reelin and APP are present in these deposits and whether these granules are related to a similar structure described 20 years ago in aged mice *(Jucker and Ingram, 1994; Jucker et al., 1992, 1994a)*. These structures were described positive for laminin

and heparin sulfate proteoglycan, but were also claimed that many antibodies, primary of polyclonal origin, bind unspecific to this particular deposits. We find that Reelin-IR is not exclusively detected in the granules, but also in close proximity, likely indicating that the structures observed in our laboratory are not exactly equal to the earlier described granules *(see also Study II)*. Nevertheless, data suggest that these extracellular deposits might represent focal deposition of other proteins and suggesting a role as initiator of the pathogenesis of amyloid-plaque formation. Hence, elucidating the identity and role of the granules components that may act synergistically or competitively with Reelin in aggregation and deposition would allow us to better understand early stages of plaque deposition during aging. Therefore, to investigate the critical processes that govern the formation of these deposits, we aimed at isolating the deposits from brain sections and analyzing them using a mass spectrometric based proteomic approach. This technique allows the comprehensive study of gene and cellular functions at the protein level *(Aebersold and Mann, 2003)*. However, the analysis of proteins isolated from cells or tissue typically create challenges due to the high degree of complexity of cellular proteomes and low abundance of many of these proteins. Therefore, a highly sensitive analytical technique is required to analyze complex protein samples. To isolate the desired areas from tissue sections laser microdissection represents a powerful technique facilitating rapid and precise isolation of morphological or immunohistochemical defined structures from heterogeneous tissue sections *(Curran et al., 2000; Johann et al., 2009; Lu et al., 2008; Simone et al., 1998; von Eggeling et al., 2007)*. This technique was first described in 1996 by the group of Liotta *(Emmert-Buck et al., 1996)* and has since become an extensively used technique to analyze DNA and gene expression at the mRNA level *(Fend et al., 1999; Goldsworthy et al., 1999; Parlato et al., 2002; Stagliano et al., 2001)*,, as well as for subsequent protein analysis *(Patel et al., 2008; Rodriguez et al., 2008)*. Additionally, laser microdissection approaches have also been extensively used in the pathogenesis of AD evaluating desired regions in the hippocampal formation, neurons and senile plaques *(Aoki et al., 2008; Fernandez-Medarde et al., 2007; Hutchinson et al., 2005; Liao et al., 2004a; Wilson et al., 2005; Zellner et al., 2009)*. Although, the subsequent analysis is vaguely limited by the low amount obtained by this technique, this can be overcome by the employment of liquid chromatography combined with tandem mass spectrometry (LC-MS/MS) *(Aebersold and Mann, 2003; Washburn et al., 2001)*, a technique facilitating sensitive and reliable examination of the small sample amount provided by laser microdissection, indicating its high potential for comprehensive proteomic analysis *(Schad et al., 2005)*.

The Reelin positive aggregates described above have been best investigated by immunohistochemistry and electron microscopy. Based on our previously obtained data and the increasing evidence of dysfunctional Reelin-mediated signaling as an important etiological factor in age-dependent neurodegenerative diseases such as AD, it is of high interest to perform a proteomic approach to further characterize the biochemical nature of the Reelin-positive deposits in order to identify critical determinants of plaque initiation, formation and maintenance. Hence, the aim of this study was to establish a suitable protocol to systematically analyze the protein composition of these structures in order to elucidate the potential signaling pathways that govern the formation of these granular structures during normal aging and following chronic neuroinflammatory conditions.

3.3 MATERIALS AND METHODS

ANIMALS

All procedures were approved by the local authorities of the Cantonal Veterinary Office in Zurich and are in agreement with the Principles of Laboratory Animal Care (NIH publication No. 86-23, revised 1985). All animals were housed in same sex groups of 3 - 4 in an optimized in-house hygiene area (OHB, University of Zurich Irchel, Switzerland) under 12 h day-night cycle and *ad libitum* food and water. C57BL/6J mice were obtained from the breeding facility of the Institute of Laboratory Animal Science, University of Zurich (LTK Fuellinsdorf). For the protocol establishment and immunohistochemical investigations we employed wild type mice of 15 months of age exposed prenatally to polyriboinosinic-polycytidilic acid (PolyI:C), mice that show accelerated aging and significant enrichment of the Reelin deposits *(Knuesel et al., 2009)*. In addition, mice exposed to saline (NaCl) at GD17 or 2 month old subjects were used as controls.

BRAIN TISSUE PREPARATION FOR LASER CAPTURE MICRODISSECTION (LCM)

The mice were decapitated and their brains snap frozen on powdered dry ice and stored at -80°C until further processing. Frozen brain tissue was cut coronally on a cryostate (Microm HM 560) and serial sections were collected throughout the hippocampal formation at 12 µm thickness, adhered to SuperFrost glass slides (Superfrost® Plus, Thermo Scientific, Menzel GmbH, D) and kept in -20°C until the cutting session was completed. Thereafter, slides were placed in a plastic slide box and stored at -80°C until processing for LCM.

Immunohistochemical staining procedure: Upon removal from -80°C, slides were allowed to thaw for 5 to 10 min at room temperature (RT). Brain sections were outlined with a Pap Pen (LucernaChem) and fixed in 70 % acetone (4°C) for 1 min, briefly washed with phosphate-buffered saline (PBS, pH 7.4) and processed immediately for immunofluorescence staining. Sections were incubated for 2 h at RT in primary anti-Reelin antibody solution (mouse anti-rodent Reelin, clone G10; Millipore; MAB5364; 1:1000) diluted in PBS containing 2 % normal goat serum and 0.2 % Triton X-100. After three washes in PBS, tissue sections were incubated for 30 min at RT in goat anti-mouse secondary antibody coupled to Alexa Fluor 488 (1:1000; Molecular Probes, Eugen, OR). Immediately after immunostaining, sections were dehydrated in the following series of solutions: 70 % EtOH (30 sec), 96 % EtOH (30 sec), 100 % EtOH (30 sec), cleared for 2 min in xylene and air dried. To ensure efficient dehydration, fresh

solutions and anhydrous alcohols prior to xylene treatment were used as recommended by Ball and colleagues *(Ball et al., 2002)*.

LASER CAPTURE MICRODISSECTION (LCM)

Tissue sample retrieval was achieved by the gentle cutting process and clean processing procedure provided by the Arcturus Biotec LCM System (Bucher Biotec AG) and was performed on the same day of immunostaining. Before performing LCM, tissue slides were cleaned from dust particles and loose tissue by the use of an adhesive Strip (Prep Strip™ from Arcturus, Bucher Biotec AG). Individual Reelin plaques were then microdissected onto a CapSure Macro LCM cap (Bucher Biotec AG) using only the IR laser with the following settings: 7.5 μm laser spot size, power range of 60 mW and pulse duration of 10 μs. This combination of parameters allowed the efficient retrieval of the tissue samples and minimizing the area lifted per laser shot. On average, approximately 200 to 300 Reelin positive plaques were procured from 4 to 6 brain sections per cap. Directly after capturing the caps were placed onto 0.5 ml microcentrifuge tubes containing 30 μl of lysis buffer for protein extraction.

PROTEIN EXTRACTION

Immediately following LCM, proteins were extracted from the Macro Caps using the following buffers summarized in **Table 1**: RIPA Buffer (20 mM Tris pH 7.2, 150 mM NaCl; 1 % Triton X-100; 1 % DOC; 0.1 % SDS), extraction buffer adapted from Liao and colleagues (*(Liao et al., 2004a)* PBS pH 7.2; 2 % SDS; 10 % Glycerol, 10 mM DTT, 1 mM EDTA) both containing protease (Roche, mini complete tablets™) and phosphatase inhibitors (Sigma-Aldrich), or directly SDS sample buffer (150 mM Tris, pH 6.8, 2 % SDS, 30 % glycerol, bromophenol blue, 15 % βME). For MS sample preparation, a 50 mM ammonium bicarbonate (Sigma-Aldrich) buffer containing the MS compatible 0.1 % RapiGest detergent (kindly provided by Dr. B. Wollscheid, ETH Zurich, Switzerland) was used for protein extraction. To solubilize the captured material, the tube was inverted to cover the cap surface with lysis buffer and incubated for 30 min at RT while gently mixing the cap every five minutes so that the extraction buffer moved over the cap surface. Subsequently, the lysates were collected using a brief centrifugation (12'000 rpm for 1 min) and stored at -80°C until further processing.

TABLE 1: Protein Extraction buffers.

Buffer	Content	Application
RIPA buffer	20 mM Tris pH 7.2, 150 mM NaCl; 1 % Triton X-100; 1 % DOC; 0.1 % SDS Protease and phosphatase inhibitor	IB
Buffer adapted from Liao and coworkers *(Liao et al., 2004a)*	PBS pH 7.2; 2 % SDS; 10 % Glycerol, 10 mM DTT, 1 mM EDTA Protease and phosphatase inhibitor	IB
SDS sample buffer	150 mM Tris, pH 6.8, 2 % SDS, 30 % glycerol, bromophenol blue, 15 % βME	IB
0.1 % RapiGest	0.1 % RapiGest^{TM} in 50 mM NH_4HCO_3	MS

IB: Immunoblotting; MS: mass spectrometry

PROTEIN SEPARATION BY GEL ELECTROPHORESIS

Silver staining: Extracted protein samples were mixed with SDS-sample buffer (250 mM Tris-HCl pH 6.8; 10 % SDS, 30 % glycerol, bromophenol blue; 5 % βME) and boiled at 90°C for 5min. A volume of 15 µl of each sample was resolved electrophoretically on a 8 % SDS-polyacrylamid gel with 5 % stacking gel in SDS-running buffer (25 mM Tris, 192 mM glycine and 0.1 % SDS, pH approx. 8.6) at 25°C. An initial current of 100 V constant was applied for the first 20 min, and the separation was run at 150 V constant for 45 min. Subsequently, the gels were subjected to silver staining, which was performed according to the SilverQuest^{TM} Silver Staining kit compatible for MS (Invitrogen) with slight modifications. Briefly, after a short rinse in ultrapure water, the gel was fixed for 20 min (40 % EtOH, 10 % acetic acid in ddH2O), washed in 30 % EtOH, incubated for 10 min in sensitizer solution (Invitrogen), followed by two washing steps in 30 % EtOH and ultrapure water. Due to the low protein content obtained by LCM, the silver incubation was extended to 2 1/2 h. The gel was shortly washed in ultrapure water followed by incubation in developing solution (Invitrogen) until bands started to appear. After the desired intensity was reached, the reaction was stopped, once more washed in ultrapure water and either dried on a gel dryer (Bio-Rad) or processed for in-gel digest as described in the MS sample preparation section.

Immunoblotting: Western blots were performed using the following antibodies (**Table 2**): mouse anti-amyloid precursor protein A4 (close 22C11, Millipore, 1:1000; recognizing full-length APP, the soluble α- or β-secretase cleaved APP ectodomain (sAPP), as well as a shorter N-terminal fragment of 36 kDa), mouse anti-β-amyloid (1-17, clone 6E10, Covance, 1:500, recognizing Aβ peptides and the β-cleaved C-terminal APP fragments (15 kDa), mouse anti-rodent Reelin (clone

G10, Millipore; 1:500, recognizing the full-length of 400 kDa and the two N-terminal products of 300~ and 180 kDa) and rabbit anti-β-actin (A2066, Sigma-Aldrich, 1:5000).

TABLE 2: Primary antibodies used in this study

Antibody	Manufacturer	Species, type, cat.no	Dilution
β-Actin	Millipore, Billerica, MA, USA	mouse monoclonal, clone 4, #MAB1522	1:5000 (WB)
α-Synuclein	Abcam, Cambridge, UK	rabbit polyclonal, #Ab52168	1:1000 (IHC) 1:500 (WB)
APP (A4)	Millipore, Billerica, MA, USA	mouse monoclonal, clone 22C11, #MAB348	1:500 (WB)
Amyloid-$\beta_{1\text{-}17}$	Covance, Princeton, NJ, USA	mouse monoclonal, clone 6E10, #MAB5075	1:500 (WB)
Reelin	Millipore, Billerica, MA, USA	mouse monoclonal, clone G10, #MAB5364	1:1000 (IHC) 1:500 (WB)

IHC: Immunohistochemistry; WB: Western blotting

For Reelin immunoblotting, extracted protein samples were mixed with NuPAGE LDS sample buffer (Invitrogen, LA0041, Carlsbad, CA) and NuPAGE sample reducing agent (Invitrogen, NP0004) and boiled at 90°C for 5 min. Samples were then separated by SDS-PAGE using 3-8 % Tris-Acetate gels (NuPAGE Invitrogen, Carlsbad, CA) in Novex Tris-Acetate SDS running buffer (Invitrogen) applying 150 V constant for 1h. Separated proteins were transferred (25 mM Tris, 190 mM glycine, 20 % MeOH) onto PVDF (Amersham Hybond^{TM}-P) applying 30 V constant at 25°C for 90 min. For Aβ and APP immunoblotting, extracted protein samples were mixed with SDS-sample buffer (250 mM Tris-HCl pH 6.8; 10 % SDS, 30 % glycerol, bromophenol blue; 5 % βME) and boiled at 90°C for 5 min. A volume of 15 µl of each sample was resolved electrophoretically on 10-20 % Novex NUPAGE Tris-Tricine gels (Invitrogen, Carlsbad, CA) in Novex Tris-Tricine SDS running buffer (Invitrogen) applying 125 V constant for 90 min. Separated proteins were transferred (25 mM Tris, 190 mM glycine, 20 % MeOH) onto Protran 0.1 µm nitrocellulose membranes (Sigma-Aldrich) applying 30 V constant at 25°C for 90 min. Both types of membranes were then blocked in TBS containing 5 % western blocking reagent (Roche) for 30 min. Primary antibodies (**Table 2**) were incubated over night at 4°C. The next day the membranes were washed in TBS, probed with conjugated secondary antibody (HRP conjugated 1:15'000) diluted in TBS containing 5 % western blocking reagent for 45 min at room temperature (RT). Bands were visualized by the enhanced chemiluminescence reaction (Amersham Biosciences Europe, Freiburg, Germany). To verify the presence of protein and their amount, the same blots were stripped (100 mM Tris-HCl pH 7.5,

2 % SDS) at 56°C for 30 min and probed with anti-actin antibody (**Table 2**) according to the protocol described before.

SAMPLE PREPARATION FOR MASS SPECTROMETRY

In gel digest: In-gel digestion of proteins for MS characterization was performed in principle as described elsewhere *(Shevchenko et al., 2006)*. In brief, after the silver staining the gel was washed thoroughly with ultrapure water. The gel was placed on a clean glass plate and the entire lanes were carefully excised into 8 pieces using a clean scalpel, cut into small pieces of approximately 1 mm in size and transferred into 1.5 ml sterile microcentrifuge tubes. Destaining was performed according to the SilverQuest^{TM} Silver Staining kit (Invitrogen). Once the destaining was completed, the gel pieces were dehydrated in 100% acetonitrile (ACN) for 10 min at 25°C. The procedure was repeated until the gel pieces were hard and white. After drying the sample in a vacuum concentrator, the gel pieces were rehydrated in reduction buffer (10 mM DTT in 50 mM ammonium bi-carbonate [ABC]) sufficient to cover the gel pieces and incubated at 56°C for 1 h to remove disulfide bridges. The DTT solution was replaced by the same volume of alkylation buffer (55 mM iodoacetamide [IAA] in 50 mM ABC) and incubated in the dark at 25°C for 45 min to alkylate cysteines. After discarding the liquid, the gel pieces were washed in digestion buffer (50 mM ABC in water, pH 8.0) for 10 min at 25°C. The gel pieces were dehydrated twice in 100 % ACN for 10min at 25°C. Following that, they were dried in a vacuum concentrator and rehydrated in trypsin solution (12.5 ng/µl in 50mM ABC) at 37°C over night. The digestion was stopped by adding 10 % TFA (trifluoroacetic acid). The samples were briefly vortexed and centrifuged at maximum speed. The liquid was transferred to a fresh sterile tube. Peptides were extracted from the gel matrix by incubating the gel pieces twice with extraction buffer (3 % TFA, 30 % ACN) at 25°C under vigorously shaking for 10 min. After each extraction cycle the samples were centrifuged and the supernatant was combined with the one already obtained. The gel pieces were dehydrated twice in 100 % ACN under vigorously shaking at 25°C for 10 min and the supernatant was combined with the previous ones. Finally, the peptide mixture volume was reduced to approximately 5 µl in a vacuum concentrator. Buffer A (2 % ACN, 0.1% formic acid, in HPLC grade H_2O) was added to the nearly completely dried sample and the peptide mixture was solubilized by indirect sonication (Hielscher) for around 10 seconds. The sample was centrifuged (14680 rpm, 16000 g respectively) for 10 min and the supernatant was kept at -20°C until further analysis.

In solution digest: In solution digest was performed for 2-3 Macro Caps at a time and digested peptide mixtures pooled for further MS analysis. For the removal of disulfide bridges the lysates were incubated with 5mM TCEP (tris-2-carboxyethyl-phosphine) in ABC at RT for 5 min. After briefly vortexing and 30s centrifuging at maximum speed, samples were subjected to carbamidomethylation by adding 10mM IAA in water to each tube and incubated in the dark at 4°C for 10 min. First enzymatic digestion (predigest) was carried out by adding 0.1 µg of the serine protease Lys-C (Wako) at pH 7.8 and 37°C for 3 h. Subsequently, 1 µg sequencing grade trypsin (Promega) was added to the solution and incubated over night at 37°C. Trypsin was heat inactivated by incubation at 95°C for 10 min. For the reversed phase purification, the plaque digests were pooled. Each single tube was then washed with 50 µl of HPLC-A buffer (2 % ACN, 0.1% formic acid) and combined with plaque digest. The peptide mixture was desalted on a Ultra MicroTIP C18 column (The Nest Group) and further dried in a vacuum concentrator. Purified peptides were solubilized in LC-MS grade water (Fisher Scientific) containing 2 % ACN (Fisher Scientific) and 0.1 % Formic Acid (Merck) prior to MS-Analysis.

MASS SPECTROMETRIC ANALYSIS

The plaque derived peptide mixture was analyzed on a LTQ-Orbitrap XL mass spectrometer (Thermo Scientific). Peptides were retained on a 10cm RP-HPLC column of 75µm diameter packed with Magic C18 AQ 3µm stationary phase (Michrom Bioresources) and eluted over a linear gradient of 60 min from 5 % -30 % Buffer B (2 % H_2O, 0.1 % Formic Acid in ACN) in Buffer A (2 % ACN, 0.1 % Formic Acid, in H_2O) at 0.3 µl flow per minute into the mass spectrometer. Peptide ion mass to charge range (m/z) of 350-1600 was monitored in one high resolution (60000) MS1 scan followed by five MS2 fragmentation scans on the most intense ions in collision induced dissociation (CID) mode. Singly charged ions were excluded from CID analysis. Precursor ion masses were dynamically excluded from fragmentation after CID for 30 seconds. The peptide mixture was analyzed in triplicates. The MS was operated in two different analysis modes. For first and second injection a data dependent acquisition (shotgun mode) was used for analysis. For the second injection, additionally theoretical Reelin peptide masses were included as preferred masses for fragmentation. Reelin peptide masses were derived by *in silico* digest from the ExPASy proteomics server *(http://expasy.org/cgi-bin/peptide-mass.pl)*. The third injection exclusively used the theoretical Reelin peptide masses in targeted mode. The *in silico* tryptic digest was performed by the use of the UniProt sequence of Reelin (RELN_MOUSE) allowing for carbamidomethylated cysteines and one missed

cleavage. Peptides with a monoisotopic mass range of 800-4000 Da were considered in the targeted mode. Targeted Reelin peptide masses are listed in the inclusion list in **Suppl. Table 1**.

MS DATA SEARCH AND ANALYSIS

RAW data files were converted to the open mzXML data format *(Pedrioli et al., 2004)* and searched with the Sorcerer™-SEQUEST® platform against the mouse UniProt/SwissProt protein database *(Apweiler et al., 2010; Jain et al., 2009)* (version 57.15) containing common contaminants and reversed sequence entries search. The search allowed for a 40 ppm mass window and stable amino acid modification of cysteine (carbamidomethylation: +57.021464 Da) and variable modification of methionine (oxidation: +15.994915 Da). Semitryptic peptide isoforms and two missed cleavages were allowed for the search.

Peptide search results were statistically evaluated using software tools from the Trans Proteomic Pipeline (TPP) *(Keller et al., 2005)* including Peptide Prophet *(Keller et al., 2002)* and Protein Prophet *(Nesvizhskii et al., 2003)* for determination of correct peptide and protein identification. A peptide and protein false discovery rate (FDR) of 1% was used for the overall data set. Plaque derived proteins were grouped into protein classes according to the PANTHER database *(www.pantherdb.org) (Mi et al., 2005; Thomas et al., 2003)*.

IMMUNOHISTOCHEMICAL EVALUATION

A 10min pepsin pretreatment (0.15 mg/ml in 0.2 N HCl at 37°C) was applied to perfusion fixed (4 % Paraformaldehyde, 0.2 % picric acid in 0.1 M phosphate buffer, pH 7.4) free-floating sections and subsequently employed for double-immunofluorescence staining as described previously *(Kocherhans et al., 2010)*. Brain sections were incubated over night at 4°C in the primary anti-α-synuclein antibody solution (**Table 2**) diluted in PBS containing 2 % normal goat serum and 0.2 % Triton X-100. After three washes in PBS, tissue sections were incubated for 30 min at RT in corresponding to secondary antibodies coupled to Alexa488 (1:1000; Molecular Probes, Eugene, OR) and Cy3 (1:500) and processed as described *(Kocherhans et al., 2010)*. Brain sections were then mounted and air-dried in the dark and cover slipped with aqueous permanent mounting medium (Dako).

3.4 RESULTS

Here we are going to explain in detail the most relevant steps in the protocol establishment and optimization steps achieved so far as well discuss major problems faced during accomplishment, concerning sample preparation, protein extraction and final mass spectrometric analysis.

A first set of experiments was performed on 15 month old wild type mice prenatally exposed to NaCl. As the amount of captured protein was not sufficient, and the whole protocol still needed to be established, PolyI:C exposed wild type mice were employed, as they show a higher Reelin plaque load *(Knuesel et al., 2009)* and hence, enriched protein samples were captured per sample.

One key factor in biochemical and molecular research is sample purity and the preparation and staining of the sample are highly critical processes for reliable proteomic analyses. For the successful analysis of the Reelin deposits, they needed first to be isolated from the neuropil. Indeed, isolation of low density and protease-resistant plaques and proteins to homogeneity from heterogeneous tissue specimen is a fairly challenging task. For the extraction of proteins used for proteomic analysis, it is required to obtain the desired sample free of contamination and preservation of the material should be guaranteed. Therefore, laser microdissection is an uncomplicated technique that allows the collection of specific tissue regions. There are several different systems for laser microdissection commercially available. Considering a gentle isolation process, good sample retrieval, qualitative preservation of the tissue and low risk of contamination we chose the Arcturus from Bucher Biotec, which is based on capturing the sample (laser capture microdissection – LCM) (**Fig. 1**). Importantly, this apparatus allowed the isolation of mounted tissue directly from glass slides. An additional infrared (IR) laser beside an ultraviolet (UV) laser facilitated a more precise dissection. The cap is placed directly on the tissue and hence, not exposed to the environment for long times which would enhance the risk of dust and Keratin contamination. Employing the IR laser, the thermoplastic film on the surface of the cap is annealed to the desired areas of interest of the specimen. Upon removal of the cap, the marked desired tissue samples get isolated from the whole specimen and can then be processed for extraction (**Fig. 1A**). Although the system consists of two lasers, sample achievement was already sufficient by using the IR laser alone in this study. This method creates a gentle, non-

damaging microdissection that preserves the integrity of the captured material, as the film absorbs the laser radiation.

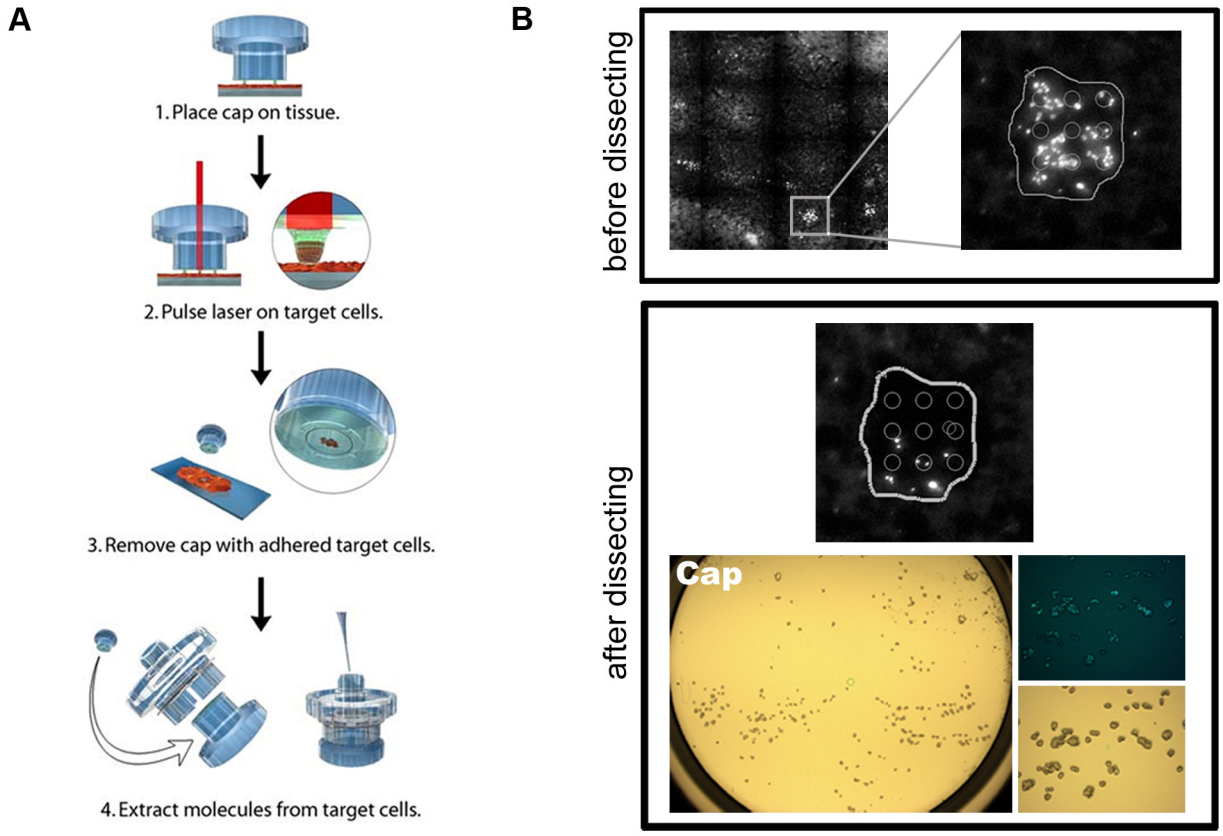

FIGURE 1: The Arcturus system – laser capture microdissection (LCM) technology
(**A**) Schematic four-step representation of the laser capture microdissection process. The cap is placed directly on a targeted area of the tissue fixed onto a glass slide and the low power IR laser melts the thermoplastic film on the lower surface of the cap directly to the desired areas of interest of the specimen. The region of interest is lifted from the section upon removal of the cap, and can be retrieved for subsequent analysis (*Diagram obtained from Arcturus Engineering, Inc.; www.arctur.com*). (**B**) Isolation of Reelin-positive granular clusters by LCM. As the sample was fluorescently labeled, a tiled image of the whole hippocampal area was taken and the selection of desired areas was accomplished on the offline image to prevent bleaching of the sample. The fluorescently labeled granular clusters were easily distinguishable under the microscope attached to this LCM system. The circles in the target area represent the IR annealing points. The "after image" demonstrates that the capturing with the IR laser alone is sufficient to capture the outlined tissue. After collecting all the plaques, the cap was observed in the control station to verify the capturing process. The isolated plaques were attached to the cap as shown in the lower panel. The higher magnification images using brightfield or epifluorescence microscopy were used to visualize and identify the captured material on the cap.

1. STEP: OPTIMIZATION OF TISSUE SAMPLE PROCESSING AND LCM

For the proteomic analysis special requirements have to be taken into account for the sample preparation. Antibodies or other staining components most likely complicate MS analysis because they introduce additional complexity to the sample due to their high abundance.

Therefore, in order to obtain high purity samples, one way to do so is to cut individual plaques from unstained sections. An adjacent antibody-labeled section could serve as a reference in order to identify the precise localization and cutting position. Unfortunately, this serial sectioning is not applicable with the chosen Arcturus System. Thus, the tissue sections were fluorescently labeled using an antibody against Reelin, as the granular structures were not discernible without any staining. Despite dehydration and no cover slipping, which significantly decrease the optical resolution, the plaques were easily distinguishable under the microscope attached to this LCM system (as also demonstrated in **Fig. 1B**). We adjusted the immunohistochemical protocol to a one day procedure, to capture as fresh material as possible. Briefly, the 1st antibody incubation was reduced to 2h at RT instead of an over night incubation at 4°C. With that the preparation, capturing and protein extraction could be accomplished in one day, which was necessary to gain qualitative and quantitative adequate results for the proteomic analysis. The staining procedure was then followed by a dehydration step, which is another significant factor in sample preparation when working with the Arcturus system, thereby facilitating efficient capturing. Without clearing in xylene, we were not able to detach the desired tissue from the glass slides, as xylene provides sufficient desiccation of the section to achieve effective lifting of the targeted tissue. After dehydration the sample was directly processed for LCM. Importantly, keeping the dehydrated slides for longer at RT or placing them back into -20°C will rehydrate them slowly and interfere later with the dissection process; re-dehydration does not work as efficiently anymore. Approximately every third time of dehydration, fresh solutions were prepared, to guarantee proper dehydration. Subsequently, after ensuring clean processing, dust and loose tissue was easily removed from the slides before capturing by using Prep Strips. After LCM, the caps containing the retrieved tissue were directly subjected for protein extraction. The lysates then could be stored for several days and months at -80°C as confirmed by silver stainings and western blotting.

2. Step: Applying Silver Staining for Optimization of Protein Extraction sampling different Lysis Buffers

Dissected Reelin positive granules from the hippocampus of mouse brain sections by LCM were then processed for biochemical/proteomic analysis to determine the plaque components. Therefore, an efficient protein extraction protocol was established regarding buffers and processing conditions. The total extracted protein samples captured by LCM were first resolved by SDS-PAGE (**Fig. 2A, C**). Subsequently, silver staining was applied to the SDS-gels for

visualization of the protein content of the isolated material to determine the extraction efficiency and to further optimize the protocol. As the protein amount captured by LCM was very low and was below detection limit of standard protein determination assays, we loaded at least half of the lysis volume (15 µl) on the gels. The silver staining method was chosen as it is more sensitive than the colloidal Coomassie blue (detection limit: 50-100 ng). Silver staining has a detection limit between 1 and 10 ng *(Kocherhans et al., 2010; Rabilloud, 1990, 1992; Switzer et al., 1979)*. Notwithstanding, the low amount of the protein captured prompted us to prolong the silver incubation time to 2 ½ h.

Applying RIPA-buffer for protein extraction from the microdissection caps did not yield efficient results, as tissue was still present on the cap surface. Correspondingly, very weak to no protein bands were visible in the silver stained gels (**Fig. 2A,** lane 5). Different extraction times and temperatures did not reveal any improvement of protein yield using this buffer. After several and different trials of extraction with RIPA-buffer, we adapted a lysis buffer from Liao and his group *(Liao et al., 2004a)*, who were using this buffer for extraction of Aβ-plaques after LCM. Working on extraction times and temperatures, it turned out that 30 min at RT were already sufficient. Comparing different extraction methods, using the buffer adapted from the group of Peng *(Liao et al., 2004a)*, RIPA-buffer or directly 2x SDS sample buffer for 30 min at RT, neither RIPA-buffer nor SDS sample buffer were working sufficient as visualized by silver staining after SDS-PAGE (**Fig. 2A,** lane 1, 2 and 5). Best results were gained by using the lysis buffer adapted from Liao and collegues *(Liao et al., 2004a)* as can be seen in the silver stained SDS-gel (**Fig. 2A,** lane 3 and 4). As control for non-specific protein contamination (i.e. Keratin), the different sample buffers were also separated alone by SDS-PAGE, without any protein lysed. Silver staining did not reveal any protein contamination of the lysis buffers (data not shown).

The silver staining of the extracted proteins revealed some distinct protein bands, confirming that the tissue collection and current protein extraction worked. However, checking the captured caps under a microscope revealed that a small amount of tissue still remained on the cap. Therefore, the extraction protocol was extended by pipetting approximately 10 µl of the already applied lysis buffer on the cap surface and gently scratching the membrane surface with the pipette tip without destroying the membrane. Subsequently, the lysis buffer used was pipetted up and down in the microfuge tube, to ensure no protein was left in the pipette tip and the whole sample was finally centrifuged again. This additional step should remove remaining material from the cap leading to higher extraction efficiency. This was further confirmed by microscopy showing the

caps free of any captured material as illustrated in Figure 2 (**Fig. 2B**). After establishing a sufficient extraction method different amounts of captured protein were separated by SDS-PAGE and subsequently silver stained (**Fig. 2C**). It can be demonstrated that a higher amount of protein yielded stronger protein bands in the silver stained gel. Further, in the first two lanes, protein samples originated from an over night sample preparation. The adjustment to a one day procedure resulted in much better protein recovery, as can be seen in Figure 3C (**Fig. 2C,** lane 3). As already mentioned, silver staining of the gels revealed many but clear bands. Accumulation on top of the gel and bands in the high mass range might correspond to full-length Reelin, N-terminal fragments or even aggregated portions of the protein (**Fig. 2A and C,** arrows). Moreover, the dense strong band at around 50-68kD across the gel (**Fig. 2A and C,** arrowhead) might either originate from Keratin contamination, or more likely the heavy chain of the antibody IgGs used for tissue staining.

3. STEP: EVALUATION OF THE EXTRACTED PROTEINS BY WESTERN BLOTTING

Having established an efficient protein extraction, a selected number of Reelin positive plaques excised by LCM was further processed for western blotting using the buffer adapted from the group of Peng *(Liao et al., 2004a)*. Albeit the protein amount was very small, full-length Reelin (420 kDa) and the N-terminal fragment (N-R2, 180 kDa) could be detected in these extracted samples (**Fig. 2D**). Furthermore, biochemical analysis of the extracted samples revealed that APP can be also found in this granular structure or in close vicinity, as western blots show a double band at 110 kDa corresponding to the immature and full developed APP, detected by the N-terminal specific antibody 22C11 (**Fig. 2E**). Although, no results have been obtained by probing these samples for other APP fragments using antibodies displayed in **Table 2**, it can not be ruled out that other proteolytic fragments of APP are present in these granular structures. The low amount of captured material is rather the limiting factor here. Actin was used as a loading control, to verify if protein was present in the sample and how the samples differentiate in protein amount, representing the success of the protein extraction from the captured material (**Fig. 2D, E**).

4. STEP: SAMPLE PREPARATION FOR MASS SPECTROMETRIC ANALYSIS

Western blotting confirmed the presence of Reelin and even APP in the dissected material, demonstrating that the capturing and protein extraction was satisfactory to process these samples further for mass spectrometric analysis. Therefore, 0.1 % RapiGest^{TM} in 50 mM ABC was used

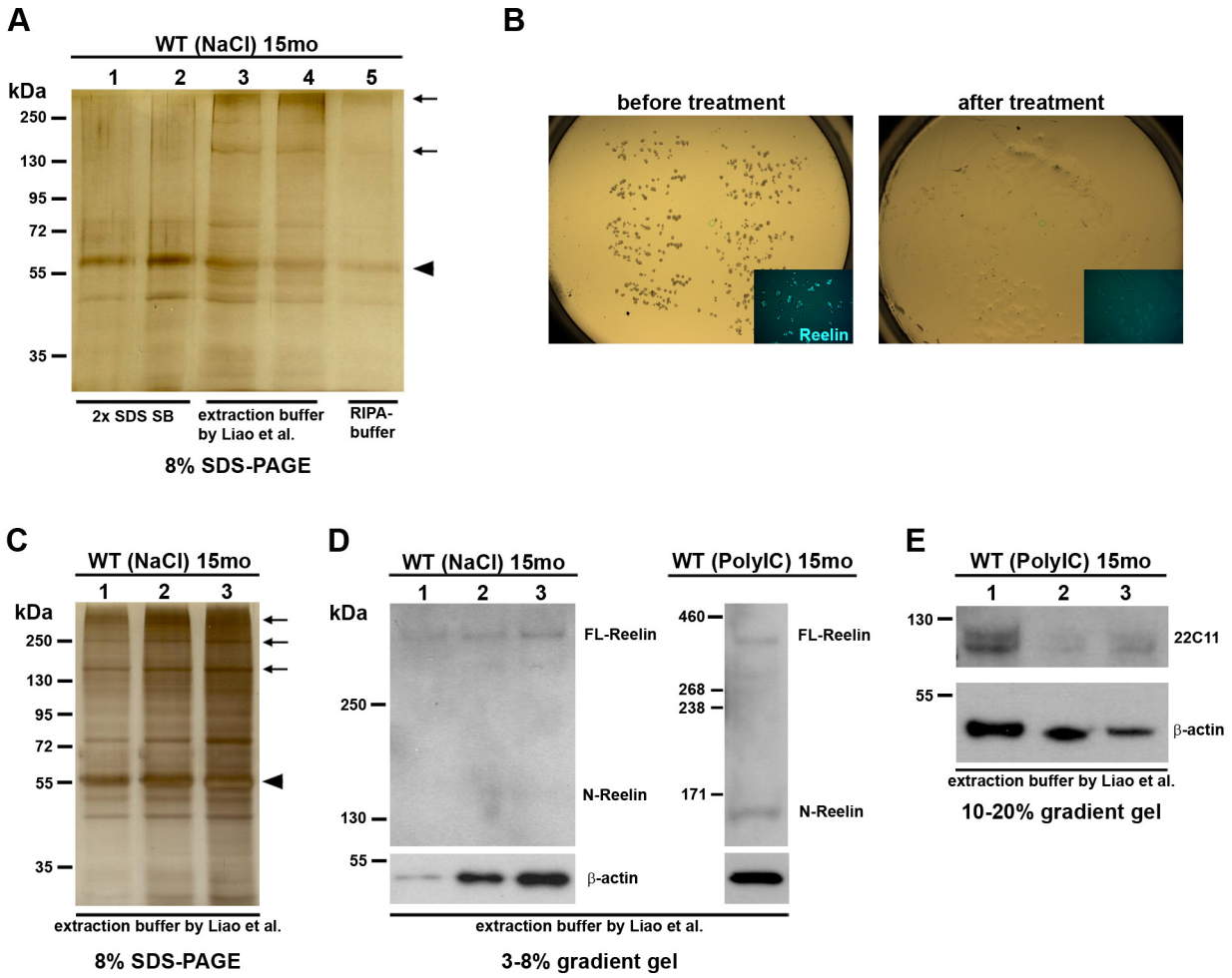

FIGURE 2: Biochemical investigation and evaluation of the captured material
(**A**) The total extracted protein samples captured by LCM were first resolved by SDS-PAGE and subsequently silver stained. Applying RIPA-buffer for protein extraction yielded very weak to no protein bands (lane 5; 30min extraction). Further, extraction by SDS sample buffer (SB) did not reveal any protein bands or very weak ones (lane 1, 30min extraction; lane 2, 2½ h extraction). Best results were obtained by using the lysis buffer adapted by Liao and collegues *(Liao et al., 2004a)*, showing no overt difference in extraction time (lane 3, 2½ h; lane 4, 30min). (**B**) View from the control station following the capturing of Reelin-positive clusters from the hippocampal formation before and after the protein extraction directly from the cap. Note the almost empty surface after the extraction using the buffer adapted by Liao and collegues; caps were free of any captured material. (**C**) SDS-PAGE of different amounts of captured Reelin plaques with subsequent silver staining (lane 1 = protein recovered from 1540 laser shots, lane 2 = 3170 laser shots, lane 3 = 2106 laser shots lane 1 and 2 sample preparation overnight, lane 3 sample preparation in one day). (**A and C**) Accumulation on top of the gel and bands in the high mass range might correspond to full-length Reelin, N-terminal fragments or even aggregated portions of the protein (arrows). The dense band appearing at 50-68 kDa across the gel (arrowhead) might either originate from Keratin contamination, or the heavy chain of the antibody IgGs used for tissue staining. (**D**) Anti-Reelin western blot (left) of proteins extracted from individual caps with different amounts of captured material (lanes corresponding to the silver stained samples in **C**). Anti-Reelin western blot (right) of a PolyI:C exposed 15 month old wild type mouse; sample was pooled from 3 caps (protein recovered from 10957 laser shots). Albeit the protein amount was very small, full-length Reelin (420 kDa) and the N-terminal fragment (N-R2, 180 kDa) could be detected in these extracted samples. Molecular mass was estimated by using pre-stained markers. (**E**) APP can be also found in this granular structure or in close vicinity, as western blots show a double band at 110 kDa corresponding to the immature and full developed APP, detected by the N-terminal specific antibody 22C11.

for protein extraction. RapiGest™ is a MS-compatible detergent because it can be easily removed before sample analysis in the MS. It further enhances enzymatic digestion without inhibiting enzyme activity, as well as not modifying peptides or suppression of endoprotease activity.

For a first mass spectrometric pilot experiment, laser microdissection was carried out on PFA fixed brain tissue. Around 500 deposits were collected per animal. Reelin itself could not be detected in the spectrogram, likely due to irreversible and covalent protein-protein cross links *(Fox et al., 1985)* and the high molecular weight of Reelin. Furthermore, the tissue might have not come off the Capture Cap. Checking these caps under a light microscope revealed that still fluorescent tissue could be detected on these caps. Finally, as formalin fixed tissue is not easily applicable for MS spectrometry and complicating protein extraction and analysis respectively *(Ahram et al., 2003)*, albeit several studies have already been achieved using fixed tissue in combination with MS analysis *(Crockett et al., 2005; Hwang et al., 2007; Patel et al., 2008; Rodriguez et al., 2008; Scicchitano et al., 2009)*, further experiments were carried out using fresh cryotissue. An overview of the different preparative steps for the following mass spectrometric analysis, which will be explained in more detail in the following sections, are outlined in a workflow chart (**Fig. 3**).

Here, for one experimental trial, the proteins extracted by RapiGest™ were separated electrophoretically, subsequently visualized by the MS-compatible silver stain method and the entire gel lanes of one sample were processed for in-gel digest (**Fig. 4A**), followed by tryptic digestion to be subsequently analyzed by MS. One advantage of conducting in-gel digest MS is that the molecular weight of the proteins in the chosen areas is known, providing further information for the data analysis and it is quite resistant towards impurities. The eight excised areas were chosen randomly, depending on the density of protein bands and the potential presence of Reelin (expected in the excised areas 1-4) (**Fig. 4A**). Additionally, and for comparison, MS analysis has been performed in parallel on a sample processed for in-solution digest. Indeed, this MS trial with the captured and extracted material of fresh tissue processed either by in-gel~ or in-solution digestion did not reveal any Reelin spectra in any of the nine samples; however a high amount of Keratin was detected once more. If not present endogenously, Keratin is often introduced during sample preparation as an external contaminant.

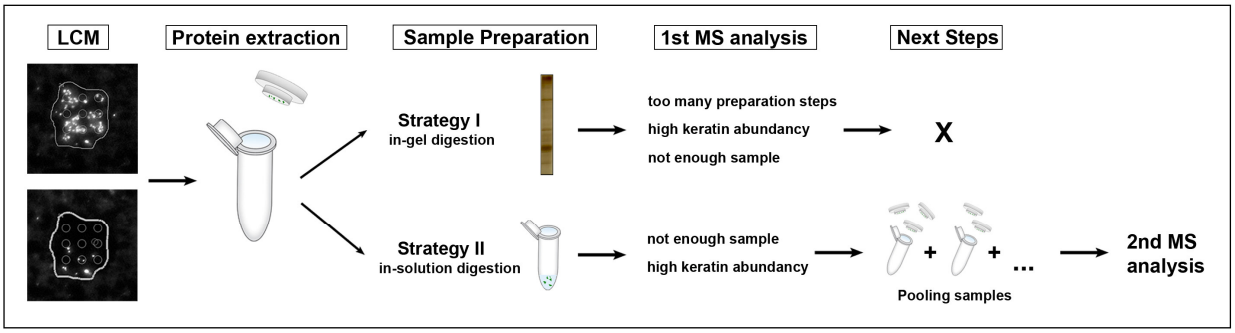

FIGURE 3: Workflow of the proteomic approach
An overview of the different preparative steps for the mass spectrometric analysis is outlined in this workflow chart. After LCM, the captured material was subjected to protein extraction with RapiGest^{TM}, compatible for MS. In the first MS trial, two strategies were pursued. Either the proteins were separated by SDS-PAGE and prepared for MS by in-gel tryptic digestion, or the extracted proteins from one cap were directly digested by trypsin and subsequently analyzed by MS. Since the in-gel digest was more prone to contamination, the second strategy was chosen. As the protein amount was not sufficient in the first run, samples and caps were pooled for the second MS run.

It mostly comes from dust particles, human hair or skin. As previously described for the MS-compatibility of affinity reagents such as antibodies, Keratin likewise complicates MS analysis by adding a high layer of complexity to the sample due to its high abundance. Keratin abundance in every sample of the gel excised bands is illustrated as a bar chart (**Fig. 4B**), demonstrating that no conclusion on any protein amount and presence in this sample could be drawn due to this high abundance of contamination. Detected protein signals were significant low (detection below 10 %) and thus, not evaluable. Hence, no data interpretation was possible, as either the contaminant or the complexity of the sample highly suppressed lower signals of proteins of interest. Comparing this Keratin contamination of the in-gel digested samples to the contamination in the in-solution processed one no quantitative conclusion could be drawn, as preparation steps are completely different regarding time and handling steps. But as the processing time in the latter one is much shorter, the likelihood of Keratin contamination decreases. Reasons for Reelin not being identified in these samples might include: 1) the amount of captured protein was too low, as indicated by the disproportionate contaminations of Keratin. The Keratin contamination was higher in the in-gel digested samples compared to the in solution digest, which might indicate that contamination occurred throughout the sample processing steps as already outlined above. 2) Since Reelin is a very large protein and highly accumulated in these deposits, the Reelin granules might have not been sufficiently solubilized during the extraction step and therefore the following tryptic digestion of the sample could have been insufficient, whereupon a complete trypsin digest is a prerequisite for optimal MS analysis. To assess the efficiency of tryptic digestion small samples were taken before and after the digestion, separated

by SDS-Page and processed for silver staining. No protein bands were detectable after the digestion, confirming the efficiency of the used protease. Additionally, Reelin consists of sufficient Arginin and Lysin, therefore enough detectable peptides should have been generated. 3) Moreover, a loss of protein during the sample processing might have occurred, and it needs to be stressed that the amount of protein is already rather low. 4) Further, the high contamination might be due to many sample processing steps in the in-gel digest. Additionally, the fact that the recovery of peptides is much lower in in-gel digest preparations compared to an in-solution digest, lead us to the conclusion that in-solution proteolytic digestion was the most preferable approach for the MS experiments.

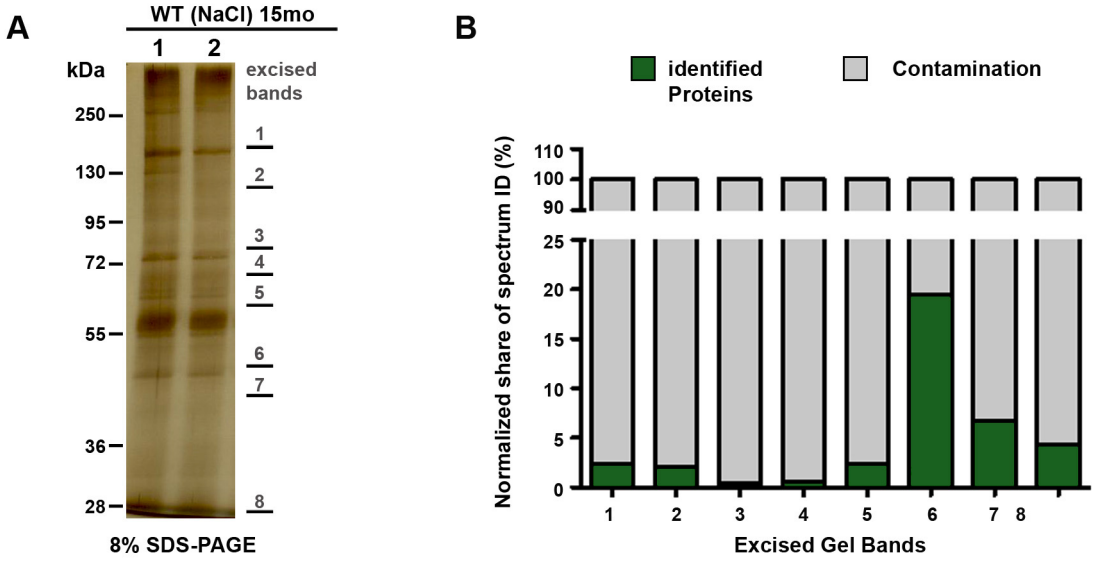

FIGURE 4: In gel-digestion mass spectrometry
(**A**) The protein in the captured plaques was extracted by 0.1% RapiGest^{TM}, run on a SDS gel (8%) followed by an MS-compatible silver staining. Each sample lane was cut into 8 pieces that were subsequently subjected to in-gel trypsin digestion and MS based analysis. The eight excised areas were chosen randomly, depending on the density of protein bands and the potential presence of Reelin (expected in the excised areas 1-4). The sample loaded contained protein recovered from 2 caps (2862 laser shots). (**B**) The contamination density in every gel sample is illustrated in the bar charts. High contamination prevented gel-based Reelin analysis by MS. High amounts of Keratin contaminants (> 75 % in all samples) preclude the meaningful analysis of the protein content in the SDS-PAGE gel.

Another critical and also limiting factor in this analysis was the protein amount captured by LCM. Therefore, to achieve higher quantity of protein, MS was carried out by pooling the samples from several captures (**Fig. 3**). This was easily accomplished by extracting proteins from 2 to 3 caps using the same 30µl of lysis buffer. Additionally, several extracted samples were later combined during the final preparations steps for MS (explained in detail in the material and methods sections). Additional care was taken during the complete preparation steps to reduce

Keratin contamination by using nitril gloves, cleaning working areas with 100 % EtOH or MeOH as well as using single packed microfuge tubes, which are generally used for RNA extraction. Moreover, observing these higher concentrated samples by silver staining, denser protein bands were detected despite increased background (as seen in **Fig. 2C**), most likely resulting from the still low protein load and the increased silver incubation time as explained previously. However, this demonstrated that the protein amount was increased in the pooled samples compared to single samples and increased the likelihood to identify the desired proteins by MS.

Mass spectrometric analysis of the in-solution sample revealed that the purified plaque samples still consisted of a very complex protein mixture, with the majority belonging to intracellular compartments. Entirely, 448 mouse proteins from 1636 tryptic peptides were identified throughout three technical replicates (detailed description in material and methods) on a high mass accuracy MS instrument (LTQ-Orbitrap XL). A list of the total identified proteins can be found in the **supplement material**. The identified proteins were classified into multiple categories based on protein and gene ontology analysis (PANTHER functional protein database), as demonstrated in **Fig. 5 A and B**. The large diversity in protein function and protein location reveals a still high complexity of the plaque-enriched sample. Moreover, the Keratin amount detected was low and therefore, remained in a negligible range (**Fig. 5C**), meaning that this contamination was not an issue anymore in the analysis. Nevertheless, mouse derived Reelin could not be identified in the pooled sample via MS analysis, although an inclusion list for inclusion list for theoretical peptides of Reelin was applied to boost sensitivity of the analysis by a targeted MS strategy. This might have several reasons: 1) It needs to be stressed, that the analyte not only consists of plaque material, but also of attached debris/cytoskeleton which is surrounding the individual granules. This might have added a high layer of complexity to the in-solution MS sample as cytoskeleton and cytoplasmic proteins are usually of very high abundance compared to membrane associated proteins such as Reelin. The attached debris therefore might have partly foiled our efforts to highly purify for the low abundant Reelin protein by LCM. Although we enriched for low abundant plaques by LCM, the MS sample was still too complex for a positive identification, even in an inclusion list targeted mode. 2) One other possibility might be that the Reelin peptides are poorly digested or do not fly well in the Mass spectrometer. However, predicting from the *in-silico* digestion, the chance that no suitable Reelin peptide exists is rather low. 3) Reelin is not present in the sample, which, taking the western blot results into account, was very unlikely to be the case, as Reelin fragments were well detectable in the

captured material. Additionally, although, the whole protocol from staining to the point of protein extraction was performed at RT, it can be excluded that Reelin was degraded over time and therefore not detected anymore in the MS, as it was recently confirmed by us that Reelin is stable at 37°C for several days *(D. Krstic, unpublished data)*. Beside, the database search for APP and its proteolytic fragments did not reveal any positive results, either. However, a specific database search after MS analysis revealed a positive identification for the axonal protein α-synuclein.

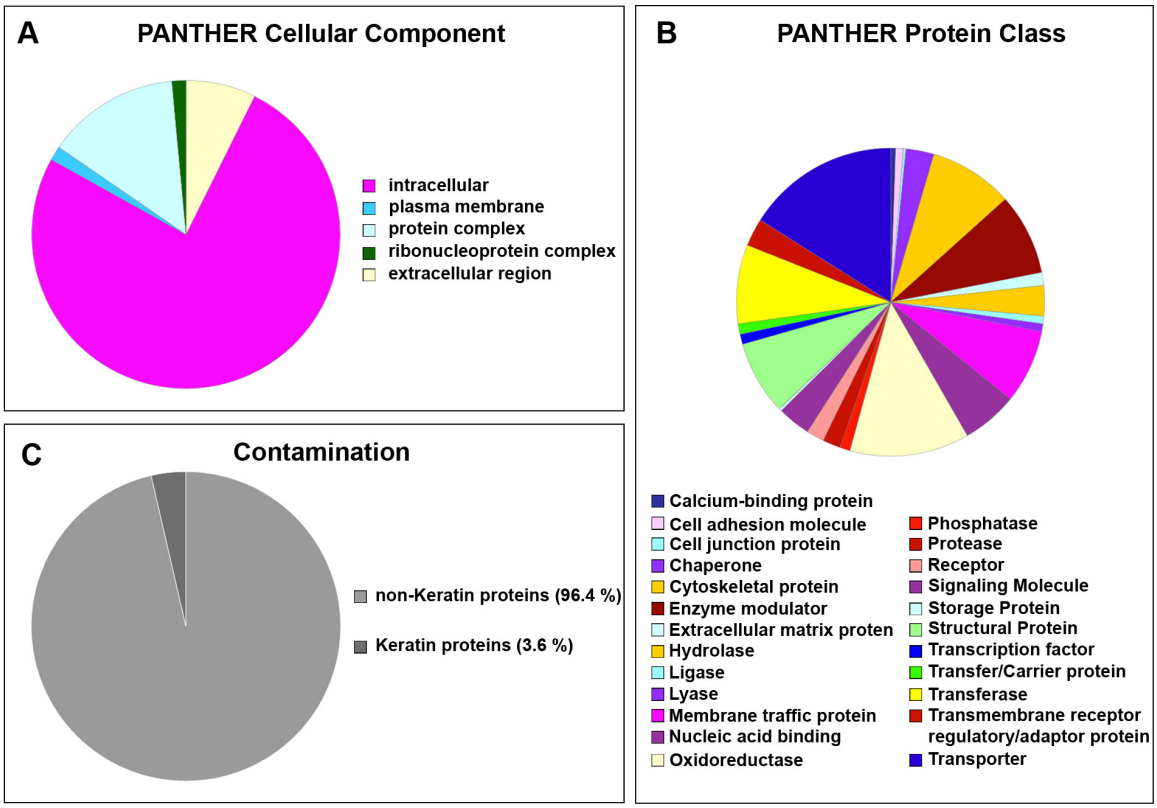

FIGURE 5: Distribution of proteins identified from the pooled captured samples
Illustration of the protein annotation by the PANTHER functional protein database: (**A**) protein classification by cellular component, (**B**) classification by protein class. The large diversity in protein function and protein location reveals a very high complexity of the Reelin plaque enriched sample. In total, 448 mouse proteins from 1636 tryptic peptides were identified. (**C**) Although the sample was highly complex, the amount of keratin was low, remaining in an acceptable range in MS-based experiments, as illustrated in the pie chart, with light gray demonstrating the non-keratin proteins identified in the samples and the dark grey the keratin proteins. The sector size is the sum of percentage share of spectrum identifications normalized to proteins filtered with 1 % false discovery rate. The sample applied to LC-MS/MS contained protein recovered from 35'548 laser shots.

5. STEP: IMMUNOHISTOCHEMICAL CONFIRMATION AND EVALUATION

As α-synuclein was detected in the dissected granular structure by MS and our latest investigations on human tissue showed a co-association of this protein with Reelin *(unpublished*

data), we performed a double labeling in brain tissue of wild type mice. Double-immunofluorescent stainings of Reelin and α-synuclein showed that the latter one can also be found in these particular granular structures in the mouse brain hippocampal formation (**Fig. 6**), as well as in close proximity, supporting the findings by MS.

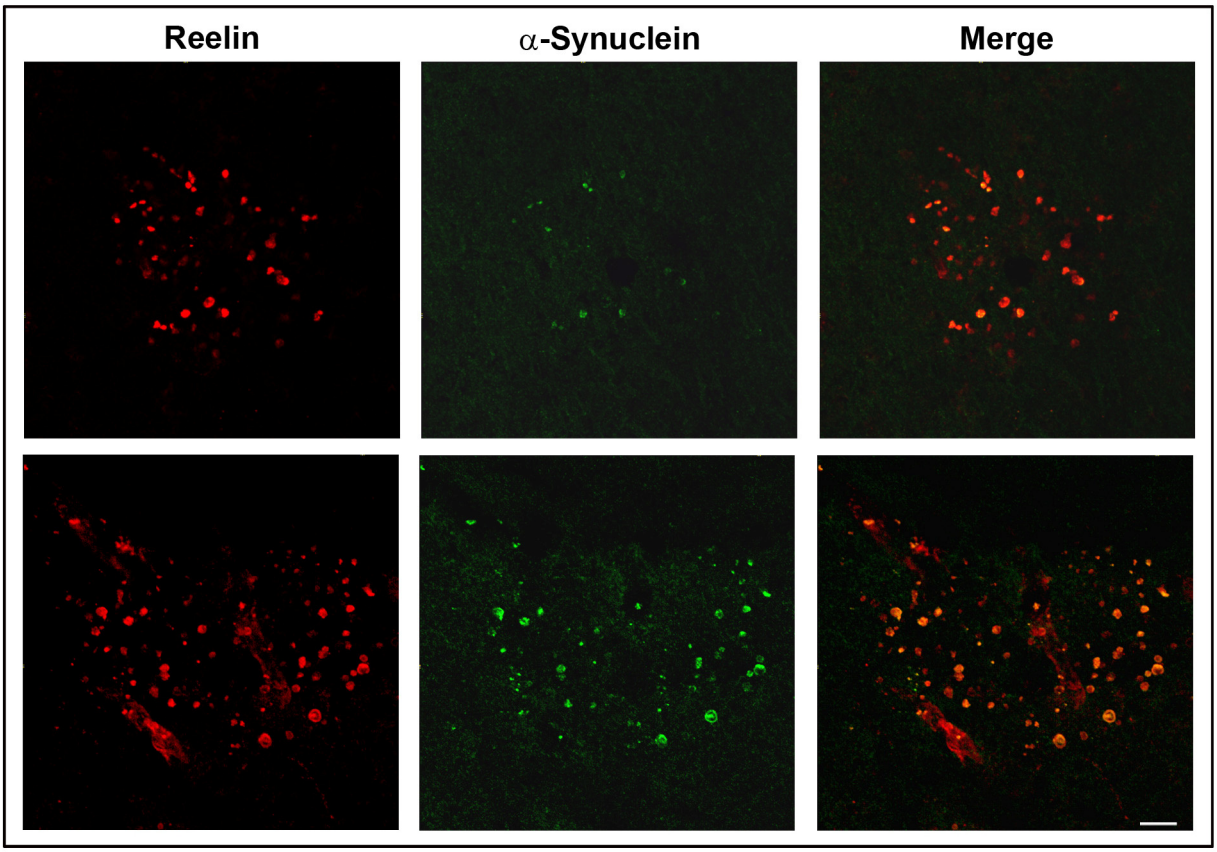

FIGURE 6: α-synuclein partially co-localizes with the Reelin-positive granular structures
Representative confocal images of hippocampal brain sections obtained from wild type mice (12 months), processed for double-immunofluorescence staining using anti-Reelin (red) and anti-α-synuclein (green) antibodies. Note the partial co-localization of α-synuclein in two different Reelin-positive granules. Scale bar = 10 µm.

6. STEP: MS RESULTS AND POSSIBLE OPTIMIZATION STEPS – TECHNICAL DISCUSSION

An essential factor in MS-based molecular research is sample purity, implying low levels of dust/Keratin contamination. However, the introduction of significant amounts of plaque surrounding tissue (neuropil, cytoskeletal molecules) to the sample could not be avoided by the methods used in this study. Unfortunately, our proteomic analysis was hampered by the difficulty in obtaining homogenous and highly enriched Reelin deposits in adequate amounts, explaining its limited abundance in the MS analysis compared to the cytoskeletal components/proteins detected. Although, the Reelin plaques look very dense, the size of the

applied laser spot in the LCM exceeded the size of the individual granule and the material between each is enormous, as clearly seen by ultrastructural investigations *(Study II; Study I (Doehner et al., 2010))*. Thus, the amount of granular material was most likely much lower compared to the amount of the neuropil coming along with the granules during capturing. The identification of a variety of cytoskeletal molecules in the second MS analysis (**Fig. 5A, B**) reflects the previous statement and confirming the very complex protein mixture captured by LCM. Nevertheless, it can not be excluded that this detected cellular structural elements might be as well components of these deposits, as already discussed in chapter II *(Study II)*.

The problem we faced in analyzing the captured material by MS was the lack of identifying Reelin. Though, it should be stressed, that not identifying Reelin in all the tested samples does not imply that the protein is not present in the captured material due to the discovery-driven mode of operation (shotgun analysis), keeping clearly in mind the positive detection via western blotting. We believe that two main factors were a major challenge in our approach and interfered with a positive MS-identification of Reelin: 1) general low abundance of the Reelin protein, 2) still too high complexity of the study material after purification for shotgun analysis. However, even a targeted inclusion list based MS approach did not successfully lead to Reelin identification, most probably due to the still high complexity and high dynamic range of the peptide mixture after isolation by LCM. Although various sample preparation efforts were performed to reduce the sample complexity, the remaining high presence of multiple abundant protein species might have interfered with a successful identification of the lower abundant Reelin protein, as MS-based shotgun approaches are generally biased towards high abundant molecules. An additional disproportionate level of sample complexity was further introduced by contaminations of Keratin. Human Keratins which mainly originate from chemicals and/or sample handling often become ubiquitous at these low protein levels and it is not predictable how much Keratin will be included in the sample throughout preparation steps. It is common that the Keratin-polluted environment necessarily leads to contamination of the samples and hence, creates a significant problem for the analysis of low abundance proteins as it emerged in our study. Therefore, it was and is a prerequisite to work as clean as possible.

Successful mass spectrometric analysis of proteins in protein mixtures is dependent on sample complexity and sufficient presence of study material. For low abundant proteins, the reduction of sample complexity is a prerequisite for a successful analysis. Protein characteristics such as hydrophobicity and solubility have to be taken into account during sample preparation to minimize losses of the protein of interest. Even a small loss of sample during processing can

decide about success or failure of the whole analysis. Taking the second MS analysis into account (**Fig. 5**), despite pooling many samples to increase protein amount, it seems that either the quantity of captured Reelin protein was still not sufficient and/or in combination, the high complexity of the sample might have suppressed the low abundant, present Reelin peptide ions from identification. Comparing the amount of sample processed in our study with other studies using LCM followed by MS, it appears they have applied much higher amounts for such an approach. For instance, one study performed by Miravella and colleagues *(Miravalle et al., 2005)* captured a total of about 100'000 amyloid plaques for MS analysis and around 2500 for WB analysis. In our study, only 5000 Reelin positive plaques (approx. 35'000 7.5µm laser shots) were captured for the last MS trial. Cheng and his group *(Cheng et al., 2008)* claim that at least 20'000 to 25'000 cells are considered to be necessary to perform western blotting *(for review Mustafa et al., 2008)*. Therefore, achieving a more complete view of the granular structure, a specific enrichment after LCM is highly required to significantly increase the amount of protein. Taken together, isolating the Reelin deposits by laser microdissection and applying them subsequently to MS might not be feasible in the current state. Additional purification steps need to be involved, as a pull-down assay using anti-Reelin antibodies, sorting the proteins with the COPAS technology (Complex parametric analyzer and sorter – cytometric sorting) or by magnetic beads (e.g. Dyna beads), or applying ultracentrifugation to separate the sample into soluble and insoluble fractions. One might also consider, after increasing the protein amount to detectable levels, to adapt a pepsin pretreatment *(Doehner et al., 2010)* prior LCM and any purification steps in order to already reduce unspecific protein detection by partially digesting plaque-surrounding material. Post-translational modifications (PTMs) such as glycosylation remain difficult to analyze by MS *(Zaia, 2004)* and might have impeded our analysis additionally. Glycosylation is a common PTM applied to cell surface and common extracellular matrix proteins *(Roth, 2002)*, such as Reelin, which shows mainly N-linked carbohydrates *(D'Arcangelo et al., 1997)*. This glycosylation sites might have interfered or even inhibited trypsin digestion, as well as altered the ion mobility in the mass spectrometer. Although, tryptic digestion should have yielded also many unglycosylated peptides of Reelin, one might still use PNGase F (Peptide:N-glycosidase F) to remove all N-linked oligosaccharides, to further increase the amount of Reelin peptides that are available to the mass spectrometer.

3.5 CONCLUDING REMARKS AND FUTURE PERSPECTIVES – BIOLOGICAL RELEVANCE

This current study aimed to establish a protocol to identify the proteins involved in the granular plaque formation. Here, we provided a detailed step by step procedure for the isolation and proteomic analysis of the Reelin positive granular structures.

Although further optimization with respect to sample purity, sample processing and reduction of sample complexity will be required, we were able to confirm for the first time the presence of full-length Reelin and the N-terminal fragment in these deposits by western blotting (WB). These findings verified our immunohistochemical and -electron microscopy findings in aged species (**Fig. 2;** *(Doehner et al., 2010)*). Moreover, WB analysis corroborates the presence of mature and immature APP in the microdissected samples. Though, this does not imply their exclusive presence in the granular deposits. APP and Reelin might derive as well from the surrounding neuropil, or regarding our recent ultrastructural investigations *(Study I (Doehner et al., 2010); Study II)* might derive from neuronal dendritic structures that most likely surround the Reelin positive granules. As previously demonstrated by a few research groups *(Kubo et al., 2002; Utsunomiya-Tate et al., 2000)* it was proposed that Reelin fragments are prone to aggregate. Discovering the N-terminal fragment of Reelin in these dissected granular structures confirmed these previous studies and might indicate that this fragment of Reelin may preferentially oligomerize and aggregate in the extracellular matrix during aging. Furthermore, Hibi and Hattori *(Hibi and Hattori, 2009)* showed that the N-terminal fragment of Reelin is re-secreted into the extracellular space after internalization of the full-length protein and specific proteolysis. After release, the N-terminal fragment does not bind to its receptors anymore *(Hiesberger et al., 1999; Yasui et al., 2007)*, but neither the fate after endocytosis nor the physiological significance of the endocytosis and re-secretion is understood yet. Hence, one might suggest that an excess of the N-terminal fragment of Reelin in the extracellular space leads to its aggregation into the granular structures observed by immunohistochemistry and electron microscopy.

Although Reelin and APP were not detected by MS, data analysis revealed the presence of α-synuclein. It is known that this axonal protein is largely expressed in the neocortex, hippocampus, substantia nigra, thalamus and cerebellum, primarily found in neural tissue,

making up to 1 % of all proteins in the cytosol, but its function is largely unknown *(Iwai et al., 1995)*. Identifying now this particularly protein in the dissected samples, demonstrates on one hand, that the whole process of sample preparation for the proteomic approach is promising and on the other hand supports our immunohistochemical staining and EM data, suggesting a possible involvement of α-synuclein in the granular formation, as well as in axonal dystrophy. Although α-synuclein was identified in the captured samples, it is not fully clear if the protein originated from the granules or from the neuropil which surrounds the structures and came along while microdissecting. To fully elucidate the plaque formation considering as well the surrounding neuropil, plaque free areas need to be isolated and investigated, as the proteome is likely to be different. Therefore, the specific attempt would be to compare the proteome of normal deposit free tissue to the plaque dense areas, which is already highly employed in tumor research *(Guo et al., 2005; Melle et al., 2003; Shekouh et al., 2003*; for review *Mustafa et al., 2008)*. Additional control for deciphering plaque components would be the analysis of dissected tissue obtained from young animals for subsequent comparison with aged animals.

Taken together, these findings indicate that LCM is a practical and precise method for rapid and efficient isolation of specific proteins from tissue for sample pre-purification. Combining LCM subsequently with MS provides a valid approach in studying proteins involved in event of this plaque formation as it permits identification of proteins present in a specific microscopic region with high sensitivity. However, purification of the granules remains a considerable challenge in this approach. Our current proteomic approach involves further technical improvements in order to characterize the plaque components with high fidelity, including the confirmation of the accumulations of several proteolytic APP species, including rodent amyloid-β peptides *(Doehner et al., 2010)*, as well as identification of putative differences in plaque composition between aged PolyI:C and NaCl-exposed subjects. After having achieved an efficient protocol for this approach, a longitutional study would be of high interest to determine proteins involved in the early stages of aggregation, to analyze several types of plaques species, and compare the protein composition relative to their temporal and spatial distribution as well as their morphology: i.e. early vs late, hippocampal vs cortical, granular vs fibrillary plaques in order to characterize the critical initiating factors of plaque formation in distinct brain areas. This proteomic characterization would be expected to reveal important novel information on the nature and abundance of certain proteins during different phases of plaque formation. Furthermore, these results will help to design *in-vitro* studies focusing on the molecular events and protein

interactions that are involved in the early stages of aggregation and initiation of plaque formation. We think that the ability to detect qualitative and quantitative differences from Reelin positive aggregates according to their protein composition at different ages represent an important asset to improve understanding the molecular basis of unique age-related neuropathology in several species.

3.6 ACKNOWLEDGEMENTS

We are grateful to Cornelia Schwerdel, Institute of Pharmacology and Toxicology, UZH, for their excellent technical support and help with histology. Special thanks go to Amrita Madhusudan and Dr. Shiva Tyagarajan, Institute of Pharmacology and Toxicology, UZH for their support and technical assistance with the protein extraction. This work was supported by the SNF Grant Nr. 310 000 – 117806.

3.7 SUPPLEMENT MATERIAL

Full list of detected proteins can be found on the enclosed DVD

4. STUDY IV: REDUCED REELIN EXPRESSION ACCELERATES AMYLOID-β PLAQUE FORMATION AND TAU PATHOLOGY IN TRANSGENIC ALZHEIMER'S DISEASE MICE

Samira Kocherhans[1*], Amrita Madhusudan[1*], Jana Doehner[1*], Karin S. Breu[1], Roger M. Nitsch[2], Jean-Marc Fritschy[1] and Irene Knuesel[1]

[1] Institute of Pharmacology and Toxicology, University of Zurich, Switzerland

[2] Divison of Psychiatry Research, University of Zurich, Switzerland

Published in The Journal of Neuroscience, July 7, 2010 – 30 (27): 9228 – 9240

* These authors contributed equally to this work.

The contribution to this work was a double-immunofluorescence staining to investigate the accelerated aggregation of Aβ as well as its association with the vasculature. These findings were further statistical analyzed by myself.

4.1 ABSTRACT

Besides the fundamental role of the extracellular glycoprotein Reelin in neuronal development and adult synaptic plasticity, alterations in Reelin-mediated signaling have been suggested to contribute to neuronal dysfunction associated with Alzheimer's disease (AD). *In vitro* data revealed a biochemical link between Reelin-mediated signaling, Tau phosphorylation and amyloid precursor protein (APP) processing. To directly address the role of Reelin in amyloid-β plaque and Tau pathology *in vivo*, we crossed heterozygous Reelin knockout mice (*reeler)* with transgenic AD mice to investigate the temporal and spatial AD-like neuropathology. We demonstrate that a reduction in Reelin expression results in enhanced amyloidogenic APP processing, as indicated by the precocious production of amyloid-β peptides, the significant increase in number and size of amyloid-β plaques, as well as age-related aggravation of plaque pathology in double-mutant compared to single AD mutant mice of both sexes. Numerous amyloid-β plaques accumulate in the hippocampal formation and neocortex of double-mutants, precisely in layers with strongest Reelin expression and highest accumulation of Reelin plaques in aged wild type mice. Moreover, concentric accumulations of phosphorylated Tau-positive neurons around amyloid-β plaques were evident in 15 month-old double- versus single-mutant mice. Silver stainings indicated the presence of neurofibrillary tangles, selectively associated with amyloid-β plaques and dystrophic neurites in the entorhinal cortex and hippocampus. Our findings suggest that age-related Reelin aggregation and concomitant reduction in Reelin-mediated signaling plays a proximal role in synaptic dysfunction associated with amyloid-β deposition, sufficient to enhance Tau phosphorylation and tangle formation in the hippocampal formation in aged Reelin-deficient transgenic AD mice.

4.2 INTRODUCTION

Alzheimer's disease (AD) is characterized by progressive cognitive decline and severe neurodegeneration *(Savla and Palmer, 2005)*. Neuropathological hallmarks include neurofibrillary tangles, consisting of hyperphosphorylated Tau *(Grundke-Iqbal et al., 1986)* and senile plaques, mainly composed of amyloid-β peptides *(Glenner and Wong, 1984)*; the amyloidogenic cleavage product of amyloid precursor protein (APP, *(Estus et al., 1992; Haass et al., 1992)*. Non-amyloidogenic cleavage produces fragments with neuroprotective and transcriptional functions *(Furukawa et al., 1996; Gao and Pimplikar, 2001; von Rotz et al., 2004)*. Rare early-onset AD is caused by mutations in *app* and *presenilin1/2* genes, all favoring amyloidogenic APP processing *(Goate et al., 1991; Levy-Lahad et al., 1995; Rogaev et al., 1995b; Sherrington et al., 1995)*. No apparent familial segregation is evident in the frequent late-onset AD cases. Combinations of genetic, such as apolipoprotein E (ApoE) ε4, and non-genetic risk factors likely determine disease predisposition, age-onset, and progression *(Bertram and Tanzi, 2008)*. The effect of ApoEε4 in late-onset AD neuropathology remains to be elucidated. ApoE isoforms bind to neuronal lipoprotein receptors, involved in a variety of brain functions *(Herz, 2009)*, indirectly implicating ApoE receptors in AD pathophysiology. Two, including very-low-density lipoprotein receptor (VLDLR) and ApoE receptor 2 (ApoER2) bind also the extracellular signaling molecule Reelin, a conserved glycoprotein required for neuronal migration and positioning during development *(D'Arcangelo et al., 1995)*. In adult neurons, Reelin-mediated signaling modulates synaptic NMDA receptor activity and is required for learning and memory *(Beffert et al., 2006a, 2005; Chen et al., 1998; Qiu et al., 2006a; Qiu and Weeber, 2007; Weeber et al., 2002)*. Besides its role in synaptic plasticity and mnemonic functions, Reelin-mediated signaling controls several AD-relevant pathways: It inhibits key mediators of Tau phosphorylation *(Beffert et al., 2002, 2004; Hiesberger et al., 1999; Ohkubo et al., 2003)* and decreases amyloidogenic APP processing *in vitro (Hoe and Rebeck, 2008; Hoe et al., 2006)*, potentially mediated by direct Reelin-APP interactions *(Hoe et al., 2009b)*. In AD patients, increased proteolytic Reelin fragments, Reelin depletion in the entorhinal cortex *(Botella-Lopez et al., 2006; Chin et al., 2007; Saez-Valero et al., 2003)*, and significant differences in two *RELN* polymorphisms have been described *(Seripa et al., 2008)*.

We have reported in aged rodents and non-human primates a pronounced reduction of Reelin-expressing interneurons and concomitant accumulation of Reelin in amyloid-like deposits, co-localizing with proteolytic APP fragments and associated with a reduction in basal forebrain

projection neurons that selectively target Reelin-positive hippocampal interneurons *(Doehner et al., 2010; Knuesel et al., 2009; Madhusudan et al., 2009)*. The course and magnitude of the plaque load correlated with cognitive performance and was modulated by exacerbated inflammatory responses and genetic mutations favoring Aβ peptide production *(Knuesel et al., 2009)*. Based on these findings, we hypothesized that reduced Reelin-dependent signaling is a critical upstream factor able to promote amyloidogenic APP processing and Tau hyperphosphorylation. We directly tested this putative association by characterizing AD-like neuropathology in the offspring of transgenic AD mice crossed with heterozygous *reeler* mice in biochemical, histological and immunohistochemical experiments across aging.

4.3 METHODS AND MATERIALS

ANIMALS

All procedures were approved by the local authorities of the Cantonal Veterinary Office in Zurich. All animals were housed in groups of 3 - 4 in an optimized in-house hygiene area (OHB, University of Zurich Irchel, Switzerland) under 12-h day-night cycle and *ad libitum* food and water. Heterozygous Reeler (C57BL/6J-Reln$^{rl\text{-}7J}$/J$^{+/-}$) mice were obtained from Jackson Laboratories, Maine, USA and crossed with transgenic animals expressing the human APP695 gene containing the Swedish (K670N+M671L) and Arctic mutations (E693G) in a C57BL/6 background *(Knobloch et al., 2007b)*. The F1 offspring demonstrated Mendelian inheritance, carrying one of the following genotypes at expected frequencies: *reln*$^{+/+}$*;app*^{wt} (wt, 28.6%), *reln*$^{+/-}$*;app*^{wt} (reln, 26.1%), *reln*$^{+/+}$*;tghapp*$_{swe,arc}$ (app, 27.6%), *reln*$^{+/-}$*;tghapp*$_{swe,arc}$ (reln/app, 17.7%). Genotype determination was done with postmortem tail biopsies using the following primers to detect the mutant *reln* gene product (363 bp): forward 5' TAATCTGTCCTCACTCTGCC 3', and reverse 5' TGCATTAATGTGCAGTGT 3'. The presence of a human 180 bp *app* gene product was confirmed with the following primers: 5' CAGAACTGAACCATTTCAACCGAGC 3' and 5' TCAGTGGGTACCTCCAGCGCCCGA 3'. The number of animals employed in this study is summarized in **Table 1.**

TABLE 1: Animals used

Genotype	Abbreviation	Age	Number/Experiment
Reln$^{+/+}$*; APP*^{wt}	wt	3 mo	4 IHC
		6 mo	5 IHC
		9 mo	6 IHC
Reln$^{+/-}$*; APP*^{wt}	reln	3 mo	4 IHC
		6 mo	4 IHC
		9 mo	9 IHC
Reln$^{+/+}$*; tghAPP*$_{swe,arc}$	app	3 mo	4 IHC
		6 mo	4 IHC
		9 mo	8 IHC/ 8 WB
		15 mo	3 IHC
Reln$^{+/-}$*; tghAPP*$_{swe,arc}$	reln/app	3 mo	4 IHC
		6 mo	4 IHC
		9 mo	8 IHC/8 WB
		15 mo	3 IHC

IHC: Immunohistochemistry, including DAB immunoperoxidase and fluorescence, as well as silver staining; WB: Western blotting and ELISA

MOUSE BRAIN TISSUE PREPARATION

Animals were deeply anesthetized with Nembutal (40 mg/kg i.p.). The tissue was perfusion-fixed and processed as described *(Doehner et al., 2010; Knuesel et al., 2009)*. Random sampled serial sections were collected throughout the hippocampal formation starting at Bregma level -0.85 to -3.5 and stored at -20°C in cryoprotectant solution until immunohistochemical or histological evaluations *(Knuesel et al., 2009)*.

IMMUNOHISTOCHEMISTRY

A 15 min pepsin pretreatment (0.15 mg/ml in 0.2 N HCl at 37°C) was applied to all the free-floating sections for epitope unmasking and reduction of non-specific staining *(Doehner et al., 2010)*. Sections were then briefly washed with phosphate-buffered saline (PBS, pH 7.4) and processed for immunohistochemistry. The following antibodies were used: Mouse anti-rodent Reelin (clone G10, Millipore, Billerica, MA MAB364, 1:1000), rabbit anti-human β-Amyloid (1-40/1-42, Millipore, AB5076, 1:2000), mouse anti-human β-Amyloid (1-17, clone 6E10, Covance, Princeton, NJ, SIG-39320, 1:2000), mouse anti-mouse NeuN (clone A60, Millipore, MAB377, 1:1000), rabbit anti-human phosphorylated Tau (phospho-T205, Abcam, Cambridge, UK, ab4841, 1:1000), rabbit anti-rat α1 syntrophin (polyclonal affinity purified serum, 1:500, *(Haenggi et al., 2005)*, and rat anti-mouse CD68 (AbD Serotec Ltd, Oxford, UK, MCA 341R, 1:2000). After completion of the double-immunofluorescence stainings, GFAP-positive astrocytes were visualized with direct immunofluorescence using Cy3-conjugated rabbit anti-GFAP IgG (kindly provided by Wolfgang Härtig, University of Leipzig, Germany, at 10 µg/ml in Tris buffer, pH 7.4, containing 2 % BSA and 10 % normal rabbit serum). For the nuclear counterstaining, sections were incubated for 5 min in 10 nM SYTOX green™ nucleic acid stain (Invitrogen, Carlsbad, CA) dissolved in PBS. ThioflavinS counterstaining involved 10 min incubation in filtered 1 % aqueous ThioflavinS (Sigma-Aldrich, Buchs, Switzerland) solution at RT, followed by 2 washes for 5 min in 80% EtOH, 5 min wash in 95 % EtOH, and 3 times 5 min washes in distilled water. Brain sections were then air-dried in the dark and mounted with aqueous permanent mounting medium (DAKO, Carpinteria, CA). Double-and triple-immunofluorescence labelings were visualized by confocal microscopy (LSM-710, Zeiss, Jena, Germany) using a 40x (NA 1.3) and sequential acquisition of separate channels. Z-stacks of consecutive optical sections (6 – 12; 512 x 512 pixel, spaced 1 µm in z) were acquired at a magnification of 0.11 - 0.22 µm/pixel. For visual display, Z-sections of all channels were summed and projected in the z dimension (maximal intensity) and merged using the image

analysis software Imaris (Bitplane, Zurich, Switzerland). Cropping of images, adjustments of brightness and contrast were identical for each labeling and done using Adobe Photoshop.

SILVER STAINING

For the detection of dystrophic neurites, extra- and intracellular proteinous aggregates, we used the FD NeuroSilver™ Kit II (FD NeuroTechnologies Inc, Ellicott City, MD). Free-floating perfusion-fixed brain slices (40 μm thick) prepared for normal immunohistochemistry were processes according to the manufacturer's instruction. Control sections obtained from adult wild type mice that received unilateral intrahippocampal injections of kainic acid; a procedure which results in rapid degeneration of hippocampal interneurons and CA1 pyramidal cells *(Knuesel et al., 2002)*, served as controls.

QUANTIFICATION OF REACTIVE ASTROCYTES, MICROGLIA ACTIVATION, AND CO-LOCALIZATION BETWEEN THIOFLAVIN S, α1-SYNTROPHIN, AND Aβ

Quantitative analyses of the immunohistochemical stainings were done on one randomly selected hemisphere and performed blind to the genotype of the animals. Eight single- (GFAP/CD68) or Z-stacks (Aβ/ThioS/α1-syn) of digital images from 6-8 brain sections per genotype and age (n = 4-6) were acquired neocortical areas including LI to LVI, lateral entorhinal cortex, and hippocampus, focusing on the CA1 stratum lacunosum moleculare. Area fractions of the GFAP- or CD68 immunoreactive cells, ThioflavinS-, anti-Aβ–, and anti-α1 syntrophin-IR were quantified using a fixed threshold algorithm of ImageJ software. Co-localization of ThioflavinS and Aβ–immunoreactive signals in amyloid-β plaques in the same brain areas were measured on projected z-sections. Red and green channels were first individually segmented and then analyzed with regard to pixel overlap within outlined plaques using a co-localization plug-in of ImageJ. Signals obtained from the green channel were set as 100%. To examine a putative preferential vascular association of amyloid-β plaques in reln/app mice, we measured using the same approach the degree of pixel co-localization between α1-syntrophin- and Aβ-IR with respect to the ThioflavinS signals, again set as 100%.

Quantification of NeuN-Positive Neurons and Reelin- and Aβ-Positive Plaque Segregation

Quantitative analysis of the neuronal density associated with amyloid-β plaques as well as the Reelin/Aβ plaque segregation in 9 and 15 month old mice were performed on one randomly selected hemisphere in a blinded fashion. Eight single- (NeuN density) or Z-stacks (Reelin/Aβ plaque segregation) digital images from 4 brain sections per genotype and age (n = 6, 9 mo; n = 3, 15 mo) were acquired in the neocortex (motor and somatosensory areas) as well as in the lateral entorhinal cortex. The numerical density of NeuN-positive neurons around plaques was assessed using a threshold algorithm using ImageJ software to individually outline and quantify the number of cells in 512 x 512 pixel images. Co-localization of Reelin- and Aβ–immunoreactive signals in extracellular plaques were measured on projected z-sections in LI of the lateral entorhinal cortex. Red and green channels were first individually segmented and then analyzed with regard to pixel overlap and segregation within outlined individual plaques using the co-localization plug-in of ImageJ. Signals obtained from both channels (Reelin- and Aβ-IR) were calculated as total plaque area and set as 100 %.

Volume Analysis and Quantification of Reelin-Positive and Amyloid-β Plaques

Volumetric analysis was performed with the Mercator software (Explora Nova, LaRochelle, France). Five to seven sections per series were measured per animal. One hemisphere (for plaque analysis) or individual brain areas included in the volumetric assessments in 15 mo-old mice (i.e. neocortex, entorhinal cortex, hippocampus) were delineated with a 2.5x objective (NA 0.075). The volumes were estimated according to the formula $V = \sum A \times t_{nom} \times 1/\text{ssf}$, where $\sum A$ = the summed area of one hemisphere or brain area, t_{nom} = the nominal section thickness of 40 µm, and ssf = the section sampling fraction (1/12). Amyloid-β plaques, classified as either granular or fibrillar based on their morphology, were counted exhaustively and their diameter measured within the neocortical layers I, II-VI, entorhinal and piriform cortex, and hippocampus using a graphic tool of Mercator. Reelin-positive neurons and plaques were counted exhaustively within the outlined hippocampus using the 40x objective (NA 1.3). The total number of neurons (N) and plaques (P) were estimated according to the formula N or $P_{tot} = \sum N$ or $P \times 1/\text{ssf}$, where $\sum N$ or P is the sum of neurons or plaques, respectively.

PROTEIN EXTRACTS AND WESTERN BLOTTING

Dissected hippocampi and neocortex samples (**Table 1**) were sonicated on ice in 10 volumes of RIPA buffer (20 mM Tris, 150 mM NaCl, 1% Triton X100, 1% Na-Deoxycholate, 0.1% SDS) containing protease (Roche, mini complete tablets™) and phosphatase inhibitors (Sigma-Aldrich). Soluble and membrane-associated/insoluble fractions were separated by centrifugation at 20'000 g at 4°C for 20 min. Pellets were resolved in 70% formic acid and neutralized with 8 N NaOH. Total protein concentrations were measured with Bradford assays (BioRad laboratories Inc, Hercules, CA). Protein samples (20 µg) were separated by SDS-PAGE using 10-20% Tris-Tricine gels (Invitrogen, Carlsbad, CA), blotted onto Protran 0.1 µm nitrocellulose (Sigma-Aldrich), and blocked in TBS containing 5% western blocking reagent (Roche) for 10 min - 1 h at RT. All Western blots were run in duplicates for semi-quantitative analysis. Primary antibodies (mouse anti-β-Amyloid [clone 6E10, 1:500], mouse anti-amyloid precursor protein A4 [clone 22C11, Millipore, 1:1000], rabbit anti-human phosphorylated Tau [phospho-T205, 1:1000], rabbit anti-β-actin [A2066, Sigma-Aldrich, 1:15'000]) were incubated over night at 4°C and visualized by the enhanced chemiluminescence reaction (Amersham Biosciences Europe, Freiburg, Germany). Semi-quantitative analyses of the immunoreactive bands were performed on digitalized films using ImageJ software (NIH, Bethesda, MD). Sum pixel brightness values (i.e. integrated density) corrected for non-specific background and equal loading using β-actin as a control were included in the statistical analysis.

ELISA

Human-specific amyloid-β1-40 and 1-42 ELISA microtiter plates were obtained from The Genetics Company (Schlieren, Switzerland) and the assays performed according to the manufacturer's protocol. 50 µl samples of the brain extracts (supernatant, pellet) or blood plasma samples of mutant and wild type mice (**Table 1**) were used and run in duplicates. Following 30 min incubation in the substrate solution (TMB/peroxide mixture), the reaction was stopped and the absorption quantified using the Synergy HT Multi-Mode Microplate Reader (BioTek Instruments Inc, Winooski, VT) measuring the difference at 450 nm and 650 nm.

STATISTICAL ANALYSES

All analyses were performed with the software StatView version 5.0 (Abacus Concepts, Inc., Berkeley, CA). ANOVA with *Age* and *Genotype* as the main between-subjects factors was performed for the immunohistochemical analyses of the GFAP, CD68, NeuN, and Aβ/Reelin

plaque stainings. Fisher's LSD tests were used for post hoc comparisons. Planned comparisons (app vs reln/app) with Mann-Whitney *U* tests were used for the analysis of the total number of plaques estimated separately for each brain region, the volumetric analysis of the hippocampal formation and neocortex at 15 months of age, the levels of full-length APP, sAPP/N-APP, β-stubs, $A\beta_{40}$ and $A\beta_{42}$ (Western blotting and ELISA), full-length Reelin and N-terminal Reelin, phosphoTau (T205), as well as for the size and area fraction of co-localized ThioflavinS and anti-Aβ–, and ThioflavinS and α1-syntrophin-IR, respectively. The two-sample Kolmogorov-Smirnov test was used for comparing plaques size distribution in app and reln/app subjects. One (out of 8) app animal was excluded from the statistical evaluation of the ELISA Aβ42 levels since the measured value was more than 3 SD above the mean. In addition, one 9 mo-old app subject (out of 6) did not show any amyloid-β plaque staining and was therefore excluded for the statistical analysis of the Reelin/Aβ plaque segregation. Statistical significance was set at $p < 0.05$.

4.4 RESULTS

EARLY NEUROPATHOLOGICAL CHANGES IN THE HIPPOCAMPUS OF RELN MICE

We have recently reported a significant aging-associated decline in Reelin expression and concomitant accumulation in amyloid-like plaques, which co-localize with murine proteolytic APP fragments *(Doehner et al., 2010; Knuesel et al., 2009)*. We further showed that this pathology was accompanied by a significant reduction in cholinergic and GABAergic basal forebrain projection neurons, the latter known to selectively target Reelin-positive interneurons in the hippocampus *(Madhusudan et al., 2009)*. Here, we tested whether the impact of reduced Reelin levels in heterozygous Reelin knockout mice (reln) mice correlated with putative accelerated neuropathological changes in the hippocampal formation. The immunohistochemical investigations confirmed the age-dependent reduction in Reelin expression and appearance of Reelin-positive plaques in CA stratum radiatum (sr), lacunosum-moleculare (slm), and dentate gyrus DG molecular layer (ml) in wild type (wt) mice (**Fig. 1A, C**).

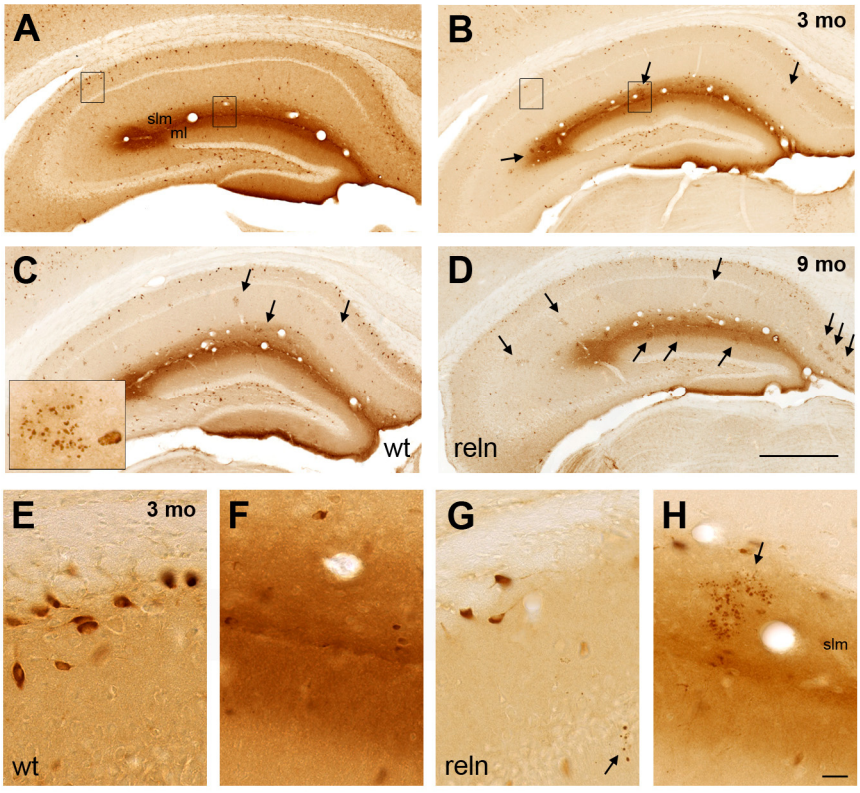

FIGURE 1: Early neuropathological changes in the hippocampus of heterozygous Reeler (reln) mice
Immunoperoxidase labelings of hippocampal brain sections obtained from 3 mo (**A-B, E-H**) and 9 mo (**C, D**) old wild type (wt) and heterozygous Reeler mice (reln). **A, C**) Aging-related reduction in Reelin-IR and concomitant appearance of Reelin-positive plaques (enlarged view in **C**) in the CA1 stratum radiatum, lacunosum-moleculare (slm), and outer molecular layer (ml) of the DG in 9 compared to 3 mo old wt mice. The two boxes in **A** are enlarged in **E** and **F** to show the dense accumulation of Reelin-positive cells in the stratum oriens and the distinct neuropil staining in the slm and ml, respectively; the latter likely representing the extracellular Reelin secreted from perforant path axonal projections. **B**) Reelin-positive plaques are already detectable at 3 months of age in heterozygous Reeler mice. Note the reduction in Reelin-immunoreactive cells in stratum oriens (box in B is enlarged in **G**) and selective enrichment in plaques in the slm (arrow, box in **B** is enlarged in **H**). **D**) Prominent accumulation of Reelin in amyloid-like plaques in the subiculum, slm, and outer ml at 9 months of age. Scale bar: **A, C** = 500 µm; **H** = 20 µm.

Reelin-IR in reln mice was strongly reduced in hippocampal GABAergic interneurons and neuropil compared to wt littermates at all ages investigated (**Fig. 1A-D**). Strikingly, already at 3 months of age, Reelin-positive amyloid-like plaques were seen in the slm of reln mice (**Fig. 1B,** arrows), while the hippocampal formation was devoid of deposits in age-matched littermates (**Fig. 1A, E-F**). In agreement with our previous findings *(Knuesel et al., 2009)*, Reelin-plaques in wt mice appeared only around 9 months (**Fig. 1C**). Statistical evaluation of the stereological estimates of the Reelin plaque density confirmed the significant difference between genotypes at 3 months (**Suppl. Fig. 1A**). At 9 months, however, the plaque density was comparable between wt and reln mice, suggesting a shift in the temporal plaque profile between genotypes and an acceleration of aging-related neuropathological changes in reln versus wt mice (**Suppl. Fig. 1A-B**).

EARLY AMYLOID-β PLAQUE DEPOSITION IN RELN/APP DOUBLE-TRANSGENIC MICE

In order to assess whether reduced Reelin expression is also associated with altered temporal and spatial amyloid-β plaque pathology, we created a mutant mouse line expressing 50 % of the *Reelin* gene product in a transgenic AD background (see methods and materials), referred to as reln/app. Littermate controls were either wild type (wt), heterozygous for Reelin (reln), or transgenic AD mice (app). Immunohistochemical and biochemical experiments were performed across aging, ranging from 3-15 months (**Table 1**). Anti-Aβ immunohistochemistry revealed no fibrillary amyloid-β plaques at 3 months of age independent of the genotype. Likewise, brain sections of 6 month-old wt and reln mice were devoid of fibrillary amyloid-β plaques (data not shown). In line with previous reports *(Knobloch et al., 2007b)*, we found no amyloid-β plaques in the hippocampal formation (**Fig. 2A**) and only very few in the neocortex (max. 1-2 per section) in app mice at 6 months. This was in contrast to reln/app littermates (**Fig. 2B, arrows**), where amyloid-β plaques of different morphologies including fibrillar and granular types (**Fig. 2C**) were evident in the hippocampus and neocortex in all subjects, indicating accelerated amyloid-β plaque formation in Reelin-deficient AD mice. At 9 months, amyloid-β plaques were present in app mice throughout the cortex but largely missing in the hippocampus (**Fig. 2D left, Suppl. Fig. 1C-D**). In reln/app mice, however, the accumulation of granular and fibrillary Aβ-IR was strongly increased; strikingly selective in CA1 slm, DG ml, and piriform/entorhinal cortex layer I (**Fig. 2D right,** arrows, **Suppl. Fig. 1C-D**); notably areas with highest Reelin-IR in wt mice (**Fig. 1A**). Stereological analysis of the plaque load at 9 months revealed a significant increase in plaque size and a corresponding significant increase in the number of large (>75 μm

in diameter) granular and fibrillary plaques in hippocampus and cortical layer I of reln/app compared to app subjects (**Table 2**). In line, the cumulative size distribution revealed a significant shift towards larger plaques (**Suppl. Fig. 1E-H**, D_{max} ranging from 0.18-0.37, KS-test), despite comparable numerical densities of small (>25 μm) and medium sized plaques (25-75 μm) between genotypes (**Table 2**).

TABLE 2: Stereological estimates of amyloid-β plaques in 9-month-old single and double transgenic AD mice

			app	reln/app	*p*
Hippocampus	granular	small	175 ± 84	224 ± 81	0.35
		medium	125 ± 45	249 ± 69	0.15
		large	0 ± 0	11 ± 4**	0.01
	fibrillar	small	434 ± 161	1014 ± 313	0.15
		medium	247 ± 82	604 ± 175	0.20
		large	3 ± 2	38 ± 17*	0.04
Cortex Layer I	granular	small	127 ± 57	158 ± 49	0.35
		medium	87 ± 31	194 ± 53	0.15
		large	0 ± 0	6 ± 3	0.08
	fibrillar	small	514 ± 183	1142 ± 316	0.16
		medium	297 ± 86	600 ± 136	0.10
		large	5 ± 4	39 ± 17*	0.04
Cortex Layer II-VI	granular	small	106 ± 42	105 ± 50	0.82
		medium	79 ± 32	114 ± 26	0.38
		large	3 ± 2	6 ± 5	0.99
	fibrillar	small	382 ± 130	960 ± 279	0.11
		medium	243 ± 91	543 ± 113	0.06
		large	21 ± 13	42 ± 11	0.12

Values are presented as mean (± SEM) for the quantification of the estimated number of granular and fibrillary amyloid-β plaques, classified as either small (<25 μm), medium (25 – 75 μm), or large (>75 μm in diameter), and expressed as total number in the given brain area of app and reln/app (n=8) subjects. Plaque counts in the hippocampus were performed along its entire septo-temporal axis; numerical estimates in the cortex included the piriform, lateral entorhinal, as well as the neocortex. No fibrillary amyloid-β plaques were detected in wt and reln littermates.

We also observed some strikingly large fibrillary and granular plaques in cortical layers II-VI (**Suppl. Fig. 1C-D**); however, the overall number, mean size, as well as the cumulative size distribution of amyloid-β plaques were not different between genotypes in these cortical layers. At 15 months, amyloid-β plaque density further increased and remained significantly higher in reln/app as compared to app mice throughout the hippocampal formation and cortex (**Fig. 2E**).

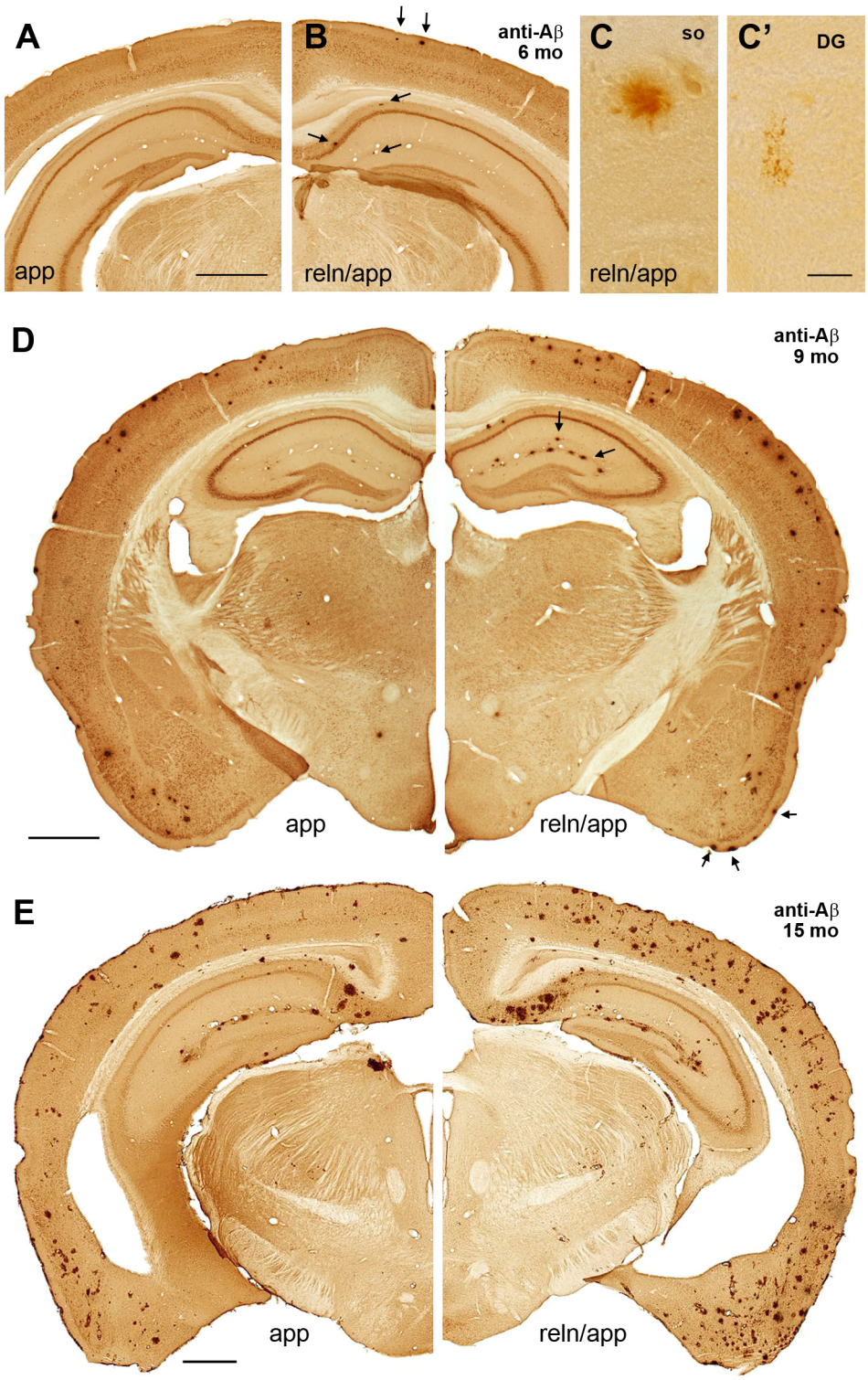

FIGURE 2: Early and accelerated amyloid-plaque deposition in reln/app double-transgenic mice
Representative images of coronal brain sections taken from 6- (**A-C**), 9- (**D**) and 15 month-old single mutant (app) and double-mutant (reln/app) mice (**E**) processed for anti-amyloid-β immunoperoxidase stainings. **A**) No amyloid-β plaque deposition was detected in single transgenic AD mice at 6 months. **B**) In contrast, numerous amyloid-β plaques were evident in both hippocampus and cortex of reln/app mice at this age. **C**) Typical dense-core fibrillar plaque in the CA1 stratum oriens (so). **C'**) Granular Aβ plaque, potentially representing precursor amyloid deposits in the DG molecular layer. **D**) Representative images of half-brain sections of a single- (left) and double-mutant (right) mouse processed for immunoperoxidase staining using 6E10 monoclonal anti-Aβ antibody. Note the increase in plaques size and the prominent layer-specific localization of amyloid-β plaques in the CA1 lacunosum-

At this age, app mice also showed amyloid-□ plaques in the subiculum and CA1 slm, most prominently seen in the temporal pole of the hippocampus. However, in reln/app mice these layers were almost completely covered by amyloid-□-IR along the entire septal-temporal axis. Moreover, signs of massively enlarged ventricles and a distinct shrinkage in cortical thickness were evident in reln/app mice at 15 months (3/3). Quantitative volumetric analysis of the hippocampus (along its entire septo-temporal axis) and cortex (including piriform, entorhinal, motor and somatosensory areas) revealed a significant volume reduction in 15 mo old reln/app (hip: 10.1 ± 1.5 mm^3; ctx 28.3 ± 1.5 mm^3) compared to app mice (hip: 13.8 ± 1.1 mm^3; p = 0.029, ctx 33.3 ± 1.5 mm^3; p = 0.017). Volumetric reductions in the whole hippocampal formation of reln/app mice approached a difference of -26% compared to app; whereas neocortical areas were less affected (-9%). The ventricle enlargement in the posterior part was also significantly larger in reln/app compared to app (+11.8%, p = 0.049, Mann-Whitney U test, values are mean ± SD). Altogether, these results indicate that a reduction in Reelin expression significantly accelerates A□ deposition and promotes neurodegeneration in aged transgenic AD mice.

INCREASED INFLAMMATORY RESPONSES IN DOUBLE-TRANSGENIC MICE

Neurodegeneration is tightly linked to inflammation, a process that is characterized by the presence of activated microglia and reactive astrocytes around amyloid-β plaques and increased levels of inflammatory mediators *(Wyss-Coray, 2006)*. To test whether the accelerated formation and size increase of amyloid-β plaques in double-mutant mice were accompanied by enhanced inflammatory changes, we used markers for activated microglia (CD68) and astrocytes (GFAP) combined with anti-Aβ or -Reelin immunohistochemistry (**Fig. 3A-F**). In line with the amyloid-β pathology, GFAP- and CD68-IR in hippocampus and cortex at 6 months were only moderately higher in reln and reln/app compared to wt and app mice (**Fig. 3G-H**). In contrast, at 9 months of age, both astrocytes and microglia levels were significantly enhanced in reln/app mice compared to app subjects and revealed a pronounced association with amyloid-β as well as Reelin-positive plaques in cortex and hippocampus (**Fig. 3C, F**). Interestingly, despite the presence of amyloid-β plaques in app mice, the levels of GFAP- and CD68-IR were moderate and not different from wt

moleculare and piriform cortex layer I (arrows) of reln/app mice. **E**) Representative brain sections of an app (left) and reln/app (right) mouse at 15 months showing the further aggravated plaque load in reln/app mice as compared to app subjects. Note the ventricular enlargement and reduced cortical thickness in reln/app brains, indicative of progressive neurodegeneration. Scale bars: **A, D, E** = 500 μm, **C** = 20 μm.

littermates (**Fig. 3G-H**), suggesting that the abnormal activation of microglia and astrocytes due to the exacerbated amyloid-β plaque pathology in reln/app mice.

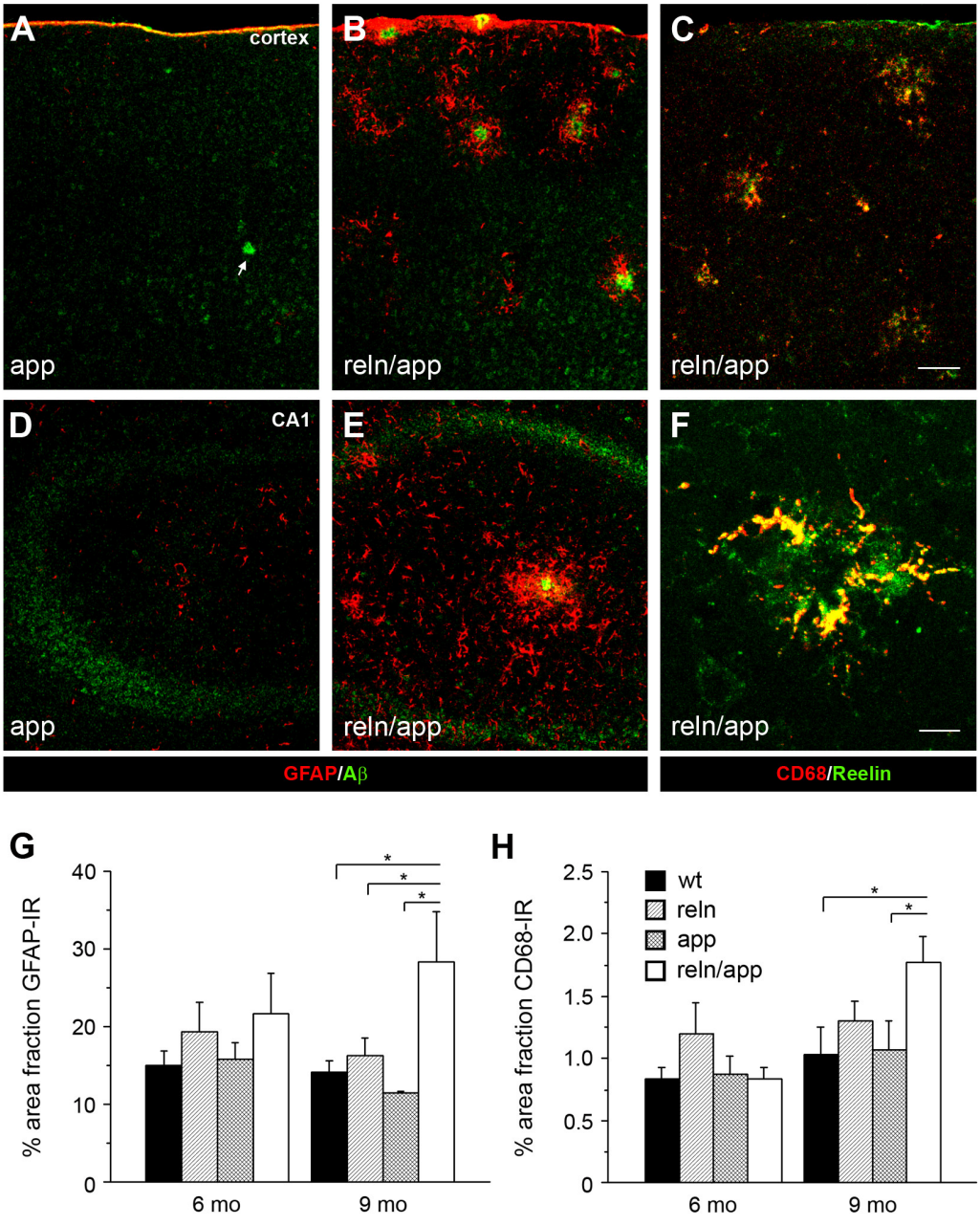

FIGURE 3: Increased inflammatory responses in reln/app double-transgenic mice
Low magnification images of double-immunofluorescence staining of cortical (**A-C**) and hippocampal (**D-F**) brain sections obtained from 9 month old single-mutant app and double-mutant reln/app mice. **A-B, D-E**) Pronounced increase in GFAP-positive astrocytes (red) selectively associated with amyloid-β plaques (anti-$A\beta_{1\text{-}40/42}$ antibody, green) was found in reln/app compared to app subjects. **C, F**) A similar increase in reactive microglia was evident in the neocortex (**C**) and hippocampus (**F**) of 9 mo reln/app mice. Note the selective accumulation of CD68-positive microglia (red) with Reelin-immunoreactive plaques (green). **G**) Quantification of the area fraction of GFAP immunoreactive astrocytes revealed a main effect of *Genotype* ($F_{3,20} = 4.4$, $p = 0.016$) and significant differences between reln/app *vs* wt ($p = 0.022$), reln/app *vs* reln ($p = 0.043$), and reln/app *vs* app ($p = 0.010$) at 9 months of age. **H**) Similar differences emerged between reln/app *vs* wt ($p = 0.039$) and reln/app *vs* app ($p = 0.046$) subjects for the CD68 area fraction. Values are given as mean ± SEM. *$p < 0.05$ (comparison to reln/app subjects), statistical significance based on Fisher's LSD *post hoc* analysis. Scale bars: **C** = 50 µm, **F** = 10 µm.

AGGRAVATED AMYLOID-β PLAQUE PATHOLOGY IN RELN/APP MICE

To investigate further the progression of reactive astrocytes, amyloid-β and Reelin-IR in reln/app mice, we performed high magnification confocal imaging of triple-labeled brain sections of 6, 9 and 15 month-old mice. We found a prominent elevation in GFAP-IR surrounding granular amyloid-β plaques in reln/app mice across aging that was accompanied by a significant enlargement of individual granules and increased co-localization between amyloid-β and Reelin-IR in granular plaques (**Suppl. Fig. 2A-B**). In contrast, granular plaque pathology in app subjects was much less pronounced, as indicated by the moderate GFAP-, Aβ- and Reelin-IR in CA1 area at 9 months of age (**Suppl. Fig. 2C**).

Fibrillary Aβ plaques in 6 month-old reln/app mice were already densely surrounded by astrocytes, particularly prominent in the hippocampus, pointing again to the advanced stage in amyloid-β plaques formation (**Suppl. Fig. 2E**). A similar pattern was seen in the neocortex; however, astrogliosis was muss less advanced compared to the hippocampal formation (**Suppl. Fig. 2D**). Interestingly, prominent Reelin-IR was associated with fibrillary plaques, correlating with their size and showing partial co-localization with Aβ (**Suppl. Fig. 2E,** arrows), again a feature being much less pronounced in app as compared to the reln/app subjects. At 9 months of age, Reelin-IR further increased in area and intensity, most prominently in fibrillary plaques in the cortex and CA1 slm (**Fig. 4**) of reln/app mice, whereas plaque pathology in app littermates resembled the pattern seen in 6 mo reln/app mice (**Fig. 4A, Suppl. Fig. 2D**). Moreover, Reelin-positive plaques appeared to segregate from amyloid-β plaques in hippocampus and cortex of reln/app but not age-matched app mice (**Fig. 4H**). Quantitative analysis of the area covered by Reelin- and Aβ plaques confirmed the increase in Reelin-IR in extracellular deposits (**Suppl. Fig. 3**) and revealed a significantly lower overlap and higher levels of segregation between Reelin- and Aβ-IR in extracellular plaques in reln/app as compared to app mice. These results point to a potential bi-directional facilitation of aggregation between Reelin and amyloid-β peptides. At 15 months, the further increase in plaque pathology in reln/app mice was mirrored by a selective reduction in neuronal density, accompanied by a massive coverage by activated astrocytes and microglia occupying the neuropil surrounding amyloid-β deposits (**Fig. 4M-O**), a phenomenon likely underlying the volumetric reductions of cortical areas measured in reln/app mice at this age (**Fig. 2E**). In app littermates, no evidence for a significant reduction in neuronal numbers in the vicinity of amyloid-β plaques was evident (**Fig. 4K**) and, correspondingly, glia activation was not as high as in double-mutants (**Fig. 4J**). Quantitative evaluation of the neuronal

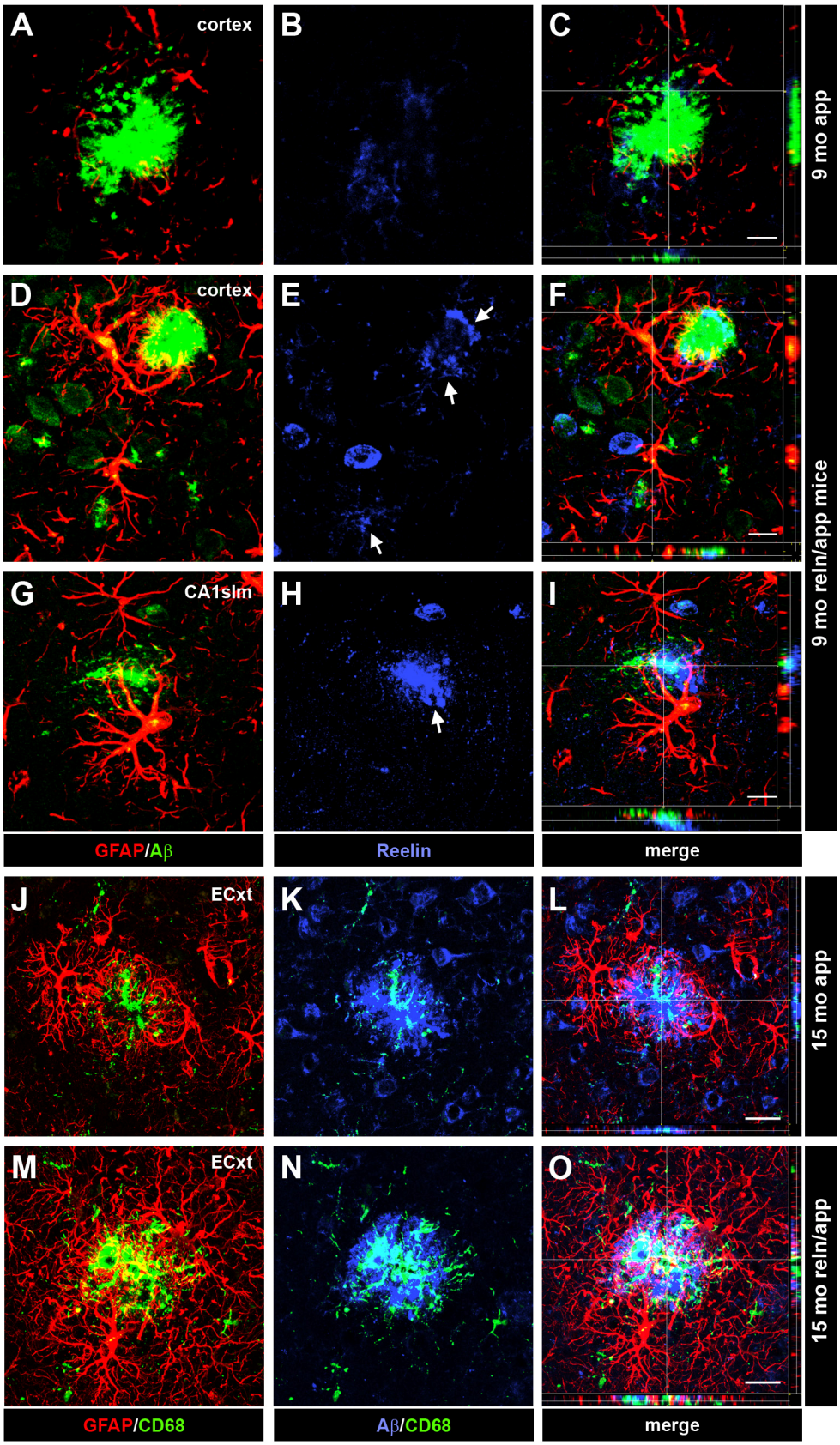

FIGURE 4: Aggravation and segregation of Reelin and amyloid-β plaques pathology in the hippocampus and cortex of 9 and 15 mo old double-mutant reln/app mice

A-I) Triple-immunofluorescence stainings using Cy3-GFAP (red), anti-$A\beta_{1\text{-}40/42}$ (green) and anti-Reelin (blue) antibodies on cortical (**A-F**) and hippocampal (**G-I**) brain sections of 9 month-old app (**A-C**) and reln/app mice (**D-I**). In the double-mutants, amyloid-β plaques were densely surrounded and tightly associated with reactive

density around amyloid-β plaques using NeuN-immunohistochemistry supported this observation and revealed a significant reduction in NeuN-positive neurons in reln/app versus app subjects (**Suppl. Fig. 4A-D**), suggesting that the reduction in Reelin-mediated signaling and the elevation in inflammatory markers significantly contribute to progressive neurodegeneration in aged reln/app mice.

INCREASE IN AMYLOIDOGENIC APP PROCESSING AND INSOLUBLE Aβ SPECIES IN DOUBLE-MUTANTS

In vitro data revealed reduced amyloidogenic APP processing in the presence of Reelin in the culture medium *(Hoe et al., 2006)*. To test whether the aggravation in amyloid-β plaque pathology was accompanied by enhanced production and increased Aβ-peptide levels, we performed Western blot analysis and ELISA of SDS-soluble and insoluble; formic acid extracted fractions of hippocampal and cortical brain lysates of app and reln/app mice. In the soluble fraction, enhanced amyloidogenic APP processing in reln/app vs app was evident, as indicated by the presence of Aβ species and the increase in β-secretase-cleaved APP ectodomains (sAPP) and C-terminal fragments (β-stubs) in the hippocampus of reln/app mice as compared to app subjects (**Fig. 5A-D**). Semi-quantitative analysis of the immunoreactive bands in the soluble fractions revealed significantly higher levels of β-stubs and sAPP in the double-mutants as compared to the single transgenic AD mutants (**Fig. 5B-D**). Surprisingly, we also observed elevated levels of a N-terminal APP fragment, inversely correlating with the expression levels of full-length Reelin (**Fig. 5C, G**), further confirming that reduction in Reelin expression alters proteolytic processing of APP. The insoluble fractions of both hippocampal and cortical brain lysates of reln/app mice contained substantial amounts of Aβ species (**Fig. 5E**). Quantitative analysis using ELISA confirmed this observation and revealed significant increases in insoluble Aβ40 and Aβ42 peptides in both hippocampus and cortex in reln/app compared to app littermates (**Fig. 5F**). Altogether, these results suggest that reduction in Reelin increases Aβ levels by favoring amyloidogenic APP processing and by promoting aggregation of Aβ peptides in the neuropil of the hippocampus and cortex.

---

astrocytes, whereas in app subjects only moderate astrogliosis was evident. Note the intense Reelin-IR associated with fibrillary amyloid-β plaques (**B** vs **E**, arrows) and their striking segregation from Aβ deposits (**H**, arrow) in the CA1 slm in reln/app as compared to app subjects. **J-O**) Aggravation of the micro- and astrogliosis in reln/app mice at 15 months of age was particularly prominent in the entorhinal cortex (ECtx). Note the reduction in APP-expressing neurons in the aged double- (**N**) vs single-mutants (**K**). Scale bars: **C, F, I** = 10 μm; **L, O** = 20 μm.

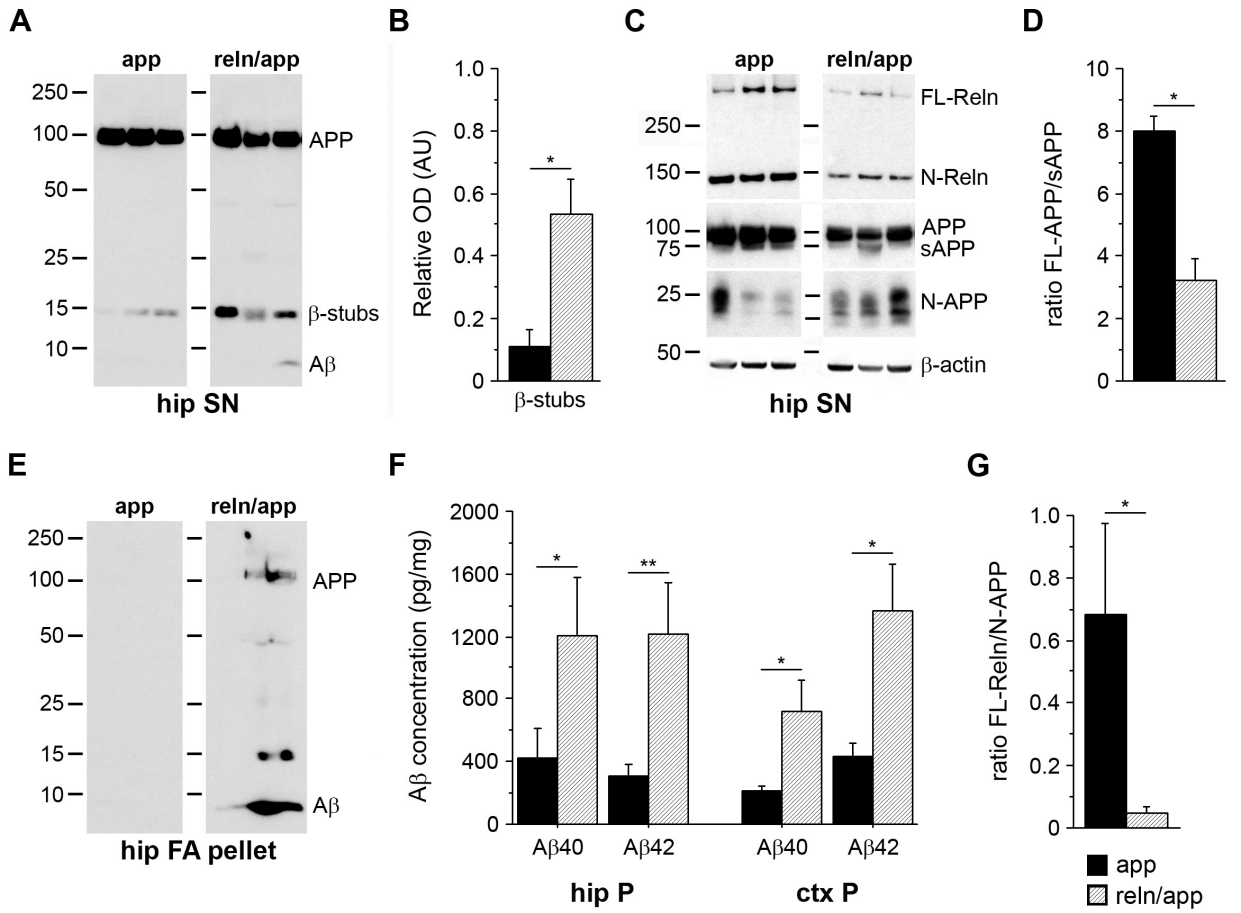

FIGURE 5: Increase in amyloidogenic APP processing and insoluble Aβ levels in double-mutant reln/app mice **A**) Representative western blots of the SDS-soluble supernatant (SN) derived from hippocampal brain lysates of 9 month-old mice using anti-Aβ (6E10) antibodies. **B**) Semi-quantitative analysis involving densitometry of the immunoreactive β-cleaved C-terminal APP fragments (β-stubs), run in duplicates, corrected for non-specific background and equal loading using β-actin as control, revealed a significant increase in reln/app as compared to app ($p = 0.049$; n = 4). Soluble Aβ-levels were very low, but clearly detectable in samples of reln/app subjects. **C**) Representative western blots using anti-Reelin (G10) antibody recognizing both full-length (FL-Reln) and the N-terminal 180 kDa fragment (N-Reln). The N-terminal-specific APP antibody (22C11) antibody recognized besides full-length APP (FL-APP) and the soluble α- or β-secretase-cleaved APP ectodomain (sAPP) a short N-terminal fragment, presumably representing N-APP. **D**) Statistical analysis of the densitometrical measurements of FL-APP and sAPP-immunoreactive fragments revealed a significant difference between genotypes as indicated by the reduced FL-APP/sAPP ratio in reln/app as compared to app subjects ($p = 0.033$, n = 4). In addition, a marked shift towards higher N-APP-immunoreactive fragments in 9 mo old reln/app mice was evident, as demonstrated by the significant reduction in the FL-Reelin/N-APP ratio (G, $p = 0.034$, n = 4). **E**) Representative western blots using anti-Aβ (6E10) antibodies of SDS-insoluble fractions (pellet) of hippocampal brain lysates, which was resuspended in formic acid (FA). **F**) Quantitative analysis using ELISA with Aβ40- and Aβ42-specific antibodies revealed a significant increase in Aβ peptides in the insoluble fractions of reln/app compared to app littermates in the hippocampus (Aβ40, $p = 0.021$; Aβ42, $p = 0.046$) and neocortex (Aβ40, $p = 0.016$; Aβ42, $p = 0.016$; n = 7-8). Values are expressed as fraction of total protein content and given as mean ± SEM. *$p < 0.05$; statistical significance based on Mann-Whitney *U* test.

To investigate further the accelerated aggregation state, we compared the density of fibrillary Aβ species between genotypes using ThioflavinS staining in combination with anti-Aβ immunohistochemistry (6E10). In addition, we employed an antibody against α1-syntrophin, a marker for astrocytic endfeet, to investigate a putative preferential association of Aβ plaques

with cerebral perivasculature. In agreement with our biochemical measurements, we detected a significant increase in the number and size of ThioflavinS-positive fibrillary aggregates in all brain areas investigated, including neocortical and hippocampal formation in reln/app vs app subjects (**Fig. 6A-C**).

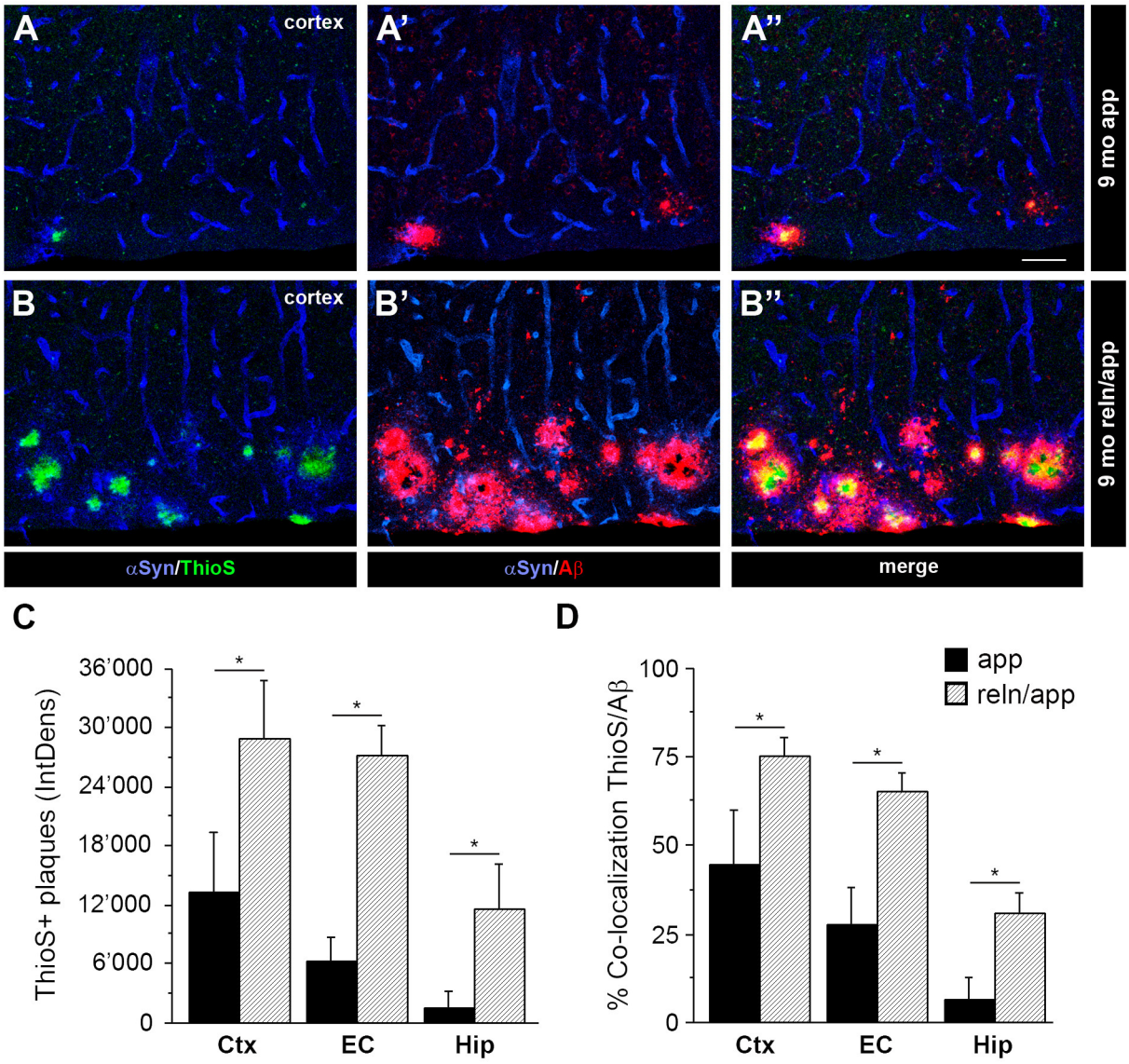

FIGURE 6: Increase in ThioflavinS-positive amyloid-β plaques in reln/app mice in neocortex and hippocampal formation

Double-immunofluorescence using anti-Aβ (6E10, red) and anti-α1-syntrophin (α-Syn, blue) antibodies combined with ThioflavinS counterstaining (green) were performed to investigate the fibrillary amyloid-β plaque load in both neuropil and cerebral vasculature in 9 mo-old app (**A**) and reln/app mice (**B**). Note the increase in ThioflavinS signals concomitantly with the anti-Aβ-IR in the outer layers of the neocortex. **C**) Densitometric analysis of the brightness and surface area covered by ThioflavinS-positive signals in the neocortical layers I-VI (Ctx), lateral entorhinal cortex (EC), and dorsal and ventral hippocampus (Hip). **D**) Quantification of the pixel overlap between the green ThioflavinS-positive signals and red anti-Aβ immunoreactive staining, averaged from measurements of 8 images (512x512 pixel in size) per animal and brain region (n = 4 per genotype) acquired in the areas indicated. Values are given as mean ± SEM. **p* < 0.05; statistical significance based on Mann-Whitney *U* test. Scale bar = 50 µm.

Moreover, the area covered by Aβ- and Thioflavin S-positive signals in these brain regions was significantly larger in reln/app as compared to app mice (**Fig. 6D**), supporting the view that the reduction in Reelin expression facilitates and accelerates the formation of fibrillary Aβ species. No difference with respect to neuropil vs vascular amyloidosis was found between genotypes (all $p > 0.6$), indicating that the increase in Aβ plaque deposition in reln/app mice was not associated with a preferential increase in β-amyloid angiopathy.

ABUNDANT DYSTROPHIC NEURITES AND ELEVATION OF PHOSPHO-TAU IN AGED RELN/APP MICE

Besides direct binding to APP and modulating its proteolytic processing *(Hoe et al., 2006, 2009b)*, Reelin-mediated signaling inhibits key mediators of Tau phosphorylation *(Beffert et al., 2002, 2004; Hiesberger et al., 1999; Ohkubo et al., 2003)*. We therefore reasoned that genetic reduction in Reelin expression – in addition to favoring amyloidogenic APP processing - might promote hyperphosphorylation of Tau and facilitate the formation of neurofibrillary tangles in aged subjects. We therefore performed biochemical and immunohistochemical analysis to assess the levels of phospho-Tau using an antibody raised against phosphoT205 across aging. In young and adult brain tissue, highest phospho-Tau levels can be detected in axonal projections throughout the brain, particularly prominent in mossy fibers and terminals in stratum lucidum of the CA3 area (data not shown). At 9 months of age, biochemical analyses revealed a significant elevation of phospho-Tau levels in hippocampal and cortical brain lysates of reln/app compared to app mice (**Suppl. Fig. 4E-G**), confirming that Reelin-mediated signaling in aged subjects remains a major modulator of Tau phosphorylation as described during neurodevelopment *(Beffert et al., 2002; Brich et al., 2003)*. In line with these biochemical data, several neurons with distinct anti-phospho-Tau signals in the soma were detectable, sparsely distributed in plaque-dense areas in the hippocampal formation and neocortex in 9 month old reln/app but not in app mice (data not shown). At 15 months of age, a striking concentric accumulation of phospho-Tau-positive cells selectively associated with amyloid-β plaques was evident in reln/app. High-magnification confocal microscopy revealed a distinct anti-phospho-Tau-IR enriched in neuronal somata and dendrites (**Fig. 7B,** arrow, inset). Littermate app mice at the same age showed some anti-phospho-Tau-IR, however, this was largely restricted to extrasomatic sites, likely representing axonal localization (**Fig. 7A,** inset).

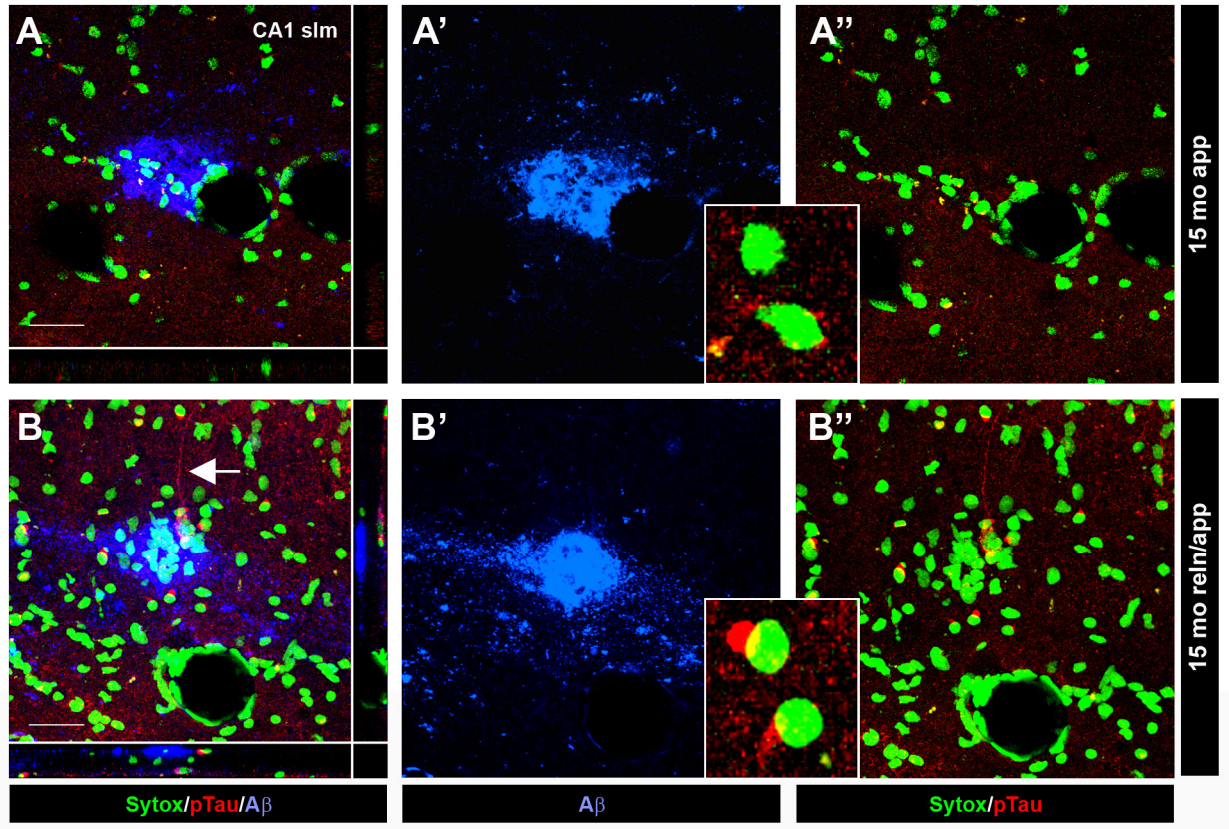

FIGURE 7: Selective association of anti-phospho-Tau immunoreactivity in plaque-dense areas within CA1 slm
A-B) Double-immunofluorescence using anti-phospho-T205 (red) and anti-Aβ (6E10, blue) antibodies combined with SytoxGreen™ nuclear counterstaining to investigate the relationship between amyloid-β plaque and Tau pathology in app (**A**) and reln/app (**B**) at 15 months of age. **A**) Representative amyloid-β plaque in the CA1 slm of app mice with a dense core and some diffuse anti-Aβ-IR surrounding it. In line with the immunoperoxidase stainings, anti-phospho-Tau-IR in app subjects was readily detectable in the neuropil but no evidence for any enrichment in cells surrounding the plaques was found (inset in **A**). **B**) Anti-amyloid-β-IR covered large areas within the core and surrounding areas of plaques in the CA1slm of reln/app mice. Note the selective fibrillary enrichment of anti-phospho-Tau signals in the cytoplasm (inset) and dendrites (arrow) of neurons selectively associated with amyloid plaques. The distinct spatial distribution of the amyloid-β and Tau pathology is also evident on the xz and yz view at the bottom and right side of the image. Scale bars in **A, B** = 30 µm.

Typically, the area surrounding the plaques also contained pronounced anti-amyloid-β-IR in reln/app compared to app mice at 15 months (**Fig. 8A'-B'**), suggesting that hyperphosphorylation of Tau in soma and dendrites is selectively promoted around amyloid-β plaques, potentially mediated by reduced Reelin and elevated non-fibrillary Aβ levels, and/or glia cells and their secreted inflammatory cytokines.

A highly similar picture emerged using immunoperoxidase labelings. Both cortical and hippocampal neurons associated with amyloid-β plaques in reln/app but not app mice showed strong somatic anti-phospho-Tau-IR (**Fig. 8A-B,** inset). Interestingly, some of them stood out by the presence of distinct phospho-Tau aggregates, suggestive of degenerating neurons (**Fig. 8C,** inset). This was also evident in the hippocampus, particularly prominent in the CA1 slm and sr

where we detected typical tangle-like structures (**Fig. 7D,** inset), indicating the presence of neurofibrillary depositions in aged double-mutants. To confirm the presence of this typical AD-like neuropathological hallmark and to assess putative neurodegeneration associated with amyloid-β plaques, we performed also Gallyas silver staining. At 9 months of age, no indication of neurodegenerative processes nor tangle-like aggregates were evident in reln/app and app mice (data not shown). At 15 months, selectively in reln/app subjects, brightfield microscopy revealed the presence of distinct silver precipitates selectively associated with amyloid-β plaques, which likely represent dystrophic neurites (**Fig. 8F-G**). This feature was most prominently seen in the entorhinal cortex, accompanied by densely labeled cell bodies and neurites surrounding the plaques in the double-mutants but not app mice (**Fig. 8E**). In line with the anti-phospho-Tau immunohistochemistry, individual silver stained intracellular aggregates were detected in the entorhinal cortex of reln/app mice within the dystrophic compartment, suggesting the presence of neurofibrillary tangles selectively associated with amyloid-β plaques in aged Reelin-deficient AD mice.

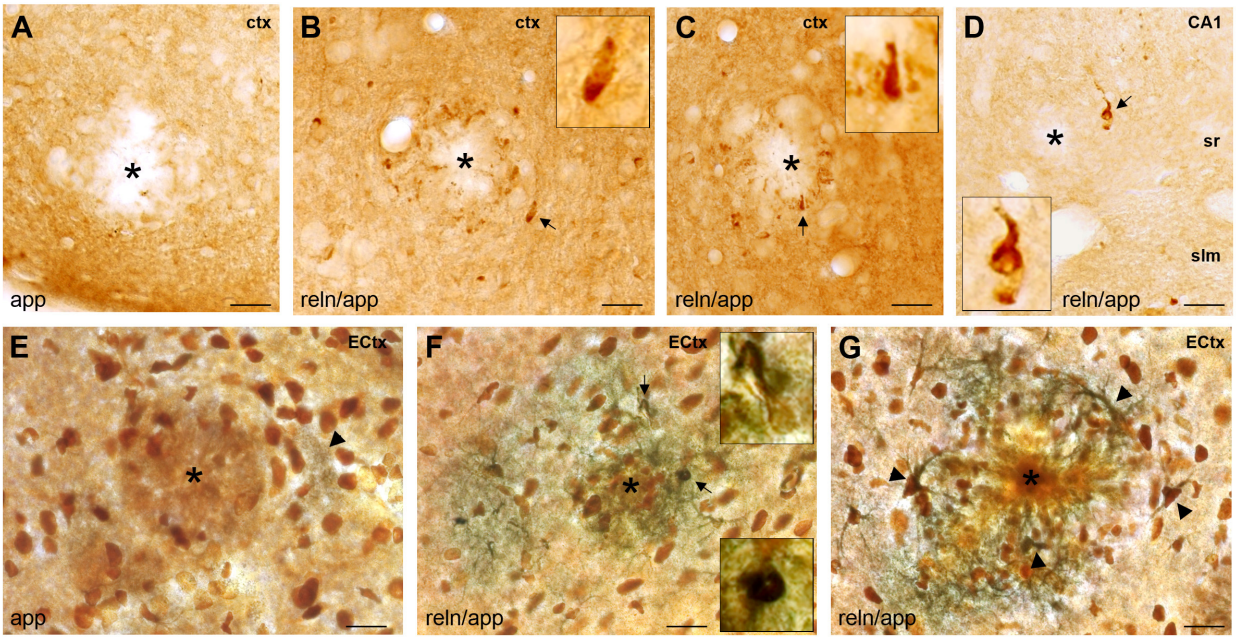

FIGURE 8: Concentric accumulations of phospho-Tau-positive neurons and neurofibrillary tangles around amyloid-β plaques in 15 mo old reln/app mice
Representative images of brain sections obtained from app (**A, E**) and reln/app mice (**B-D,F-G**) processed for immunoperoxidase staining using anti-phospho-T205 antibody (**A-D**) or silver staining (**E-G**). **A**) In app subjects, uniform phospho-Tau-IR was evident in the cortical neuropil, indicative of axonal localization. No particular enrichment was seen in the vicinity of amyloid-β plaques, recognized by their lack of phospho-Tau-IR (asterisk). **B-C**) In reln/app mice, strongly stained phospho-Tau-positive neurons were evident around amyloid-β plaques in neocortical areas (insets). **D**) In the hippocampus of reln/app mice, a similar pattern was evident in close vicinity to plaques; some neurons appeared dystrophic, strongly suggestive of tangle-like intraneuronal accumulations (inset in **D**). **E**) Silver staining revealed some dark precipitates (arrowhead) in the vicinity of large plaques (asterisk) in the entorhinal cortex of app mice. **F**) In contrast, dense silver precipitates surrounding amyloid-β plaques, indicative of

Altogether, the findings indicate that a genetic reduction in Reelin expression accelerates the production of amyloidogenic Aβ peptides which results in earlier plaque formation and an age-related aggravation of the pathology including early signs of neurodegeneration in hippocampal formation and cortex of AD mice that is accompanied by elevated phospho-Tau levels and neurofibrillary tangle formation in aged subjects.

dystrophic neurites, were very prominent in reln/app mice. In addition, black-labeled intraneuronal aggregates, likely representing neurofibrillary tangles, were seen in neurons associated with these plaques (arrows, enlarged in the insets). **G**) Representative image of a large amyloid-β plaque in the entorhinal cortex of a reln/app mouse, showing a concentric pattern of silver stained cells, likely representing degenerating neurons in the vicinity of plaques (arrowheads). Scale bars = 20 μm.

4.5 DISCUSSION

The present study provides convergent immunohistochemical and biochemical evidence that a genetic reduction in Reelin expression favors amyloidogenic APP processing *in vivo;* resulting in precocious formation and age-related aggravation of amyloid-β plaque pathology, accompanied by concentric accumulation of phospho-Tau-positive neurons, neurofibrillary tangles, and neurodegeneration in the hippocampal formation. The animal model thereby unites for the first time amyloid-β plaque and Tau pathology in a temporal and spatial pattern that closely recapitulates the progression of AD neuropathology in humans *(Braak and Braak, 1996)*, importantly in the absence of *tau* mutations. Further, it complements several previous studies involving genetic studies *(Brich et al., 2003) in vitro* experiments *(Hoe et al., 2006)*, and *in vivo* neuronal survival assays *(Beffert et al., 2006b)* demonstrating that dysfunctional Reelin-mediated signaling through ApoER2 acts as a critical upstream modulator of amyloidogenic APP processing, Tau hyperphosphorylation and neuronal survival, presumed to underlie AD-associated neuropathology.

Our comprehensive investigations across aging revealed a significantly accelerated extracellular Aβ neuropathology in Reelin-deficient AD mice; indicated by the presence of amyloid-β plaques in hippocampus and neocortex as early as 6 months. Littermate app mice were virtually devoid of amyloid-β deposits at this age, in line with the original report *(Knobloch et al., 2007b)*. At 9 and 15 months, pathology was further aggravated in reln/app mice, resulting in a striking redistribution and selective accumulation of Aβ plaques in entorhinal projection areas, precisely corresponding to areas where Reelin-IR is enriched in extracellular plaques in reln but not app littermates (**Fig. 1-2**). Moreover, we detected numerous Aβ plaques in layer I of the entorhinal, piriform and neocortex, again in areas with strong Reelin expression in young and Reelin plaque depositions in aged subjects *(Knuesel et al., 2009)*. Aβ plaques were also significantly larger in these areas in double- as compared to single-mutants, affecting both granular (presumable non-fibrillary, soluble deposits) as well as fibrillary plaques (**Table 2, Fig. 2, 6, Suppl. Fig. 1E-H**). Biochemical investigations using SDS-soluble fractions of hippocampal and cortical lysates revealed significant decrease in full-length APP and concomitant increases in β-secretase-cleaved APP ectodomains (sAPPβ), C-terminal fragments (β-stubs), and Aβ peptides (**Fig. 5**), indicating elevated amyloidogenic APP processing, in line with previous *in vitro* data *(Hoe and Rebeck, 2008; Hoe et al., 2006)*. Western blotting and quantitative ELISA of formic acid-extracted hippocampal and cortical brain lysates revealed also significantly higher levels of

insoluble Aβ40/42 peptides in reln/app compared to app littermates (**Fig. 5**), confirming that reduced Reelin levels, potentially by altering APP trafficking, membrane insertion and favoring β-secretase cleavage *(Hoe et al., 2006)*, enhances Aβ production. It is further conceivable that reduction in Reelin-signaling promotes APP endocytosis due to reduced binding of the central Reelin domain to the N-terminus of APP *(Hoe et al., 2009b)*. This scenario fits with previous data showing preferential APP β-secretase cleavage in endocytic vesicles *(Hoe et al., 2009b; Rajendran et al., 2006, 2008)*, in line with the reported endosomal localization and pH optimum of β-secretase activity *(Vassar et al., 1999)*.

Besides the role of reduced Reelin-mediated signaling on amyloidogenic APP processing, our data also suggest a direct effect on Aβ aggregation. We show that a reduction in Reelin expression favors its own aggregation, as demonstrated by the significantly earlier but highly conserved Reelin plaque pathology *(Knuesel et al., 2009)* in reln compared to wt mice (**Fig. 1**). Thus, it is conceivable that both reduced Reelin-dependent signaling promoting Aβ production as well as Reelin-aggregation by providing a nucleation site for aggregation-prone peptides, results in aggravation of the amyloid-β plaque phenotype. Indeed, we observe an overlap between Reelin and amyloid-β plaques in LI of the entorhinal cortex and perforant path axonal projection sites where the two selectively associate and partially co-localize in granular and fibrillary plaques (**Fig. 4, Suppl. Fig. 2**). Interestingly, we also detected a segregation of Reelin-IR from Aβ-positive fibrillary plaques in aged reln/app mice, indicating that aggregation of Reelin itself aggravates in the vicinity of amyloid-β plaques and reactive glia. This phenomenon was again more prominent in the hippocampal formation compared to neocortical regions, confirming the increased vulnerability of this brain area with respect to AD-like neuropathology. A reciprocal effect is also conceivable; with Aβ peptides promoting Reelin aggregation. Support for this hypothesis has been recently provided by *(Botella-Lopez et al., 2010)* demonstrating that amyloid-β peptides can alter Reelin processing and glycosylation; critical modifications demonstrated to be required for proper Reelin-mediated signaling *(Jossin et al., 2007; Koch et al., 2002; Lambert de Rouvroit et al., 1999)*, and potentially involved in abnormal oligomerization and aggregation of Reelin *(Kubo et al., 2002; Utsunomiya-Tate et al., 2000; Yasui et al., 2007)*.

Difference in plaque pathology between genotypes was also associated with distinct inflammatory responses in reln/app versus app mice. Our investigations of reactive glia revealed a significant aging-related increase in GFAP- and CD68-IR, tightly intermingled with amyloid-β plaques in reln/app mice (**Fig. 3-4, Suppl. Fig. 2**). In contrast, Aβ plaques were detected without

or weak GFAP/CD68-IR in app littermates (**Fig. 3**). In line with the biochemical data, these findings support our interpretation of a significantly more aggravated and advanced fibrillary plaque pathology in aged reln/app compared to app mice. This is in agreement with immunohistochemical studies examining the brains of AD patients *(McGeer et al., 1987)*, as well as with numerous studies using different animal models of AD *(El Khoury and Luster, 2008)*, demonstrating that microglia accumulation in senile plaques is an integral part of AD pathogenesis. Our data also fit with recent findings showing that the phenotype of accumulating microglia changes as AD-like pathology progresses in tgAPP-PS1 mice *(Hickman et al., 2008)*; from a protective, Aβ-clearing role during early phases to a enhanced production in inflammatory cytokine and loss in Aβ-clearing capabilities during later disease phases. Furthermore, it is conceivable that, in addition to dysfunctional Reelin signaling, pro-inflammatory cytokines including interferon-γ, TNF-α and interleukin-1, shown to be secreted from glia *(Hickman et al., 2008)* and demonstrated to be involved in β-secretase up-regulation *(Yamamoto et al., 2007)* and γ-secretase-mediated APP cleavage APP *(Liao et al., 2004b)*. The elevated release of pro-inflammatory cytokines by Aβ-activated glia is also expected to promote neurodegenerative processes *(Blurton-Jones and Laferla, 2006; Chiarini et al., 2006)*. On the other hand, neurodegeneration in turn strongly promotes gliosis. Indeed, at 15 months, amyloid-β plaque pathology was accompanied by striking and significant reduction in neuronal density, accompanied by strong astrogliosis and dystrophic neurites surrounding the plaques in reln/app, whereas app littermates showed only very mild signs of plaque-associated neurodegeneration (**Fig. 8**). Moreover, a significant ventricular enlargement and shrinkage of cortical areas, mostly affecting the hippocampal formation, was evident in double- compared to single-mutants (**Fig. 2**), indicating that reduced Reelin levels by promoting Aβ plaque deposition and inflammatory responses, result in neurodegeneration in aged subjects. A potential molecular mechanisms has been recently provided by the findings that signaling through a spliced isoform of the Reelin receptor ApoER2 is essential for protection against neuronal cell loss during normal aging *(Beffert et al., 2006b)*, pointing to an exciting mechanistic link between Reelin deficiency and neurodegeneration through dysfunctional ApoER2 signaling. On the other hand, we cannot rule out completely that subtle neuroanatomical changes occurring in reln mice may contribute to the observed neuropathology in reln/app mice. However, considering that we did not detect statistical differences in volume and neuronal density between genotypes up to 9 months of age, we consider this putative confounding factor as unlikely.

Another striking effect accompanying these neuropathological changes was the concentric accumulation of phospho-Tau-positive neurons around senile plaques in reln/app mice (**Fig. 7-8**), supporting previous genetic interaction studies demonstrating a critical role of Reelin-mediated signaling via Dab1 phosphorylation in inhibiting Tau hyperphosphorylation *(Brich et al., 2003)*. Interestingly, while neocortical neurons contained mainly cytoplasmic anti-phospho-Tau-IR, distinct tangle-like structures were found in the hippocampal formation (Figure 8), in line with the more advanced plaque pathology in this brain region in double- *vs* single-mutants. Silver staining revealed the presence of neurofibrillary tangle-like structures, selectively associated with dystrophic neurites surrounding the plaques in the entorhinal cortex, importantly in non-transgenic *Tau* mutants. The temporal and spatial aspects of the neuropathology supports the critical upstream role of dysfunctional Reelin-mediated signaling that is sufficient to accelerate amyloid-β peptide production in the hippocampal formation, which in turn promotes Tau phosphorylation and tangle formation, selectively in plaque- and glia-dense areas. This is in line with the current hypothesis of a upstream role of Aβ species with respect to Tau pathology *(Hardy and Selkoe, 2002; Selkoe, 2000; Walsh and Selkoe, 2004)* and with the findings from postmortem AD tissue showing a distinct temporal and spatial progression of the neuropathology in humans *(Braak and Braak, 1996)*.

In conclusion, the data revealed for the first time *in vivo* that reduced expression of Reelin has a significant effect on amyloidogenic APP processing and amyloid-β plaque deposition as well as neurofibrillary tangle formation in the hippocampal formation of aged transgenic AD mice with a genetic reduction in the *reeler* gene. Considering that Reelin is also an important modulator of adult NMDA receptor-mediated neurotransmission and synaptic plasticity *(Beffert et al., 2006a; Chen et al., 2005; Qiu and Weeber, 2007; Qiu et al., 2006b; Weeber et al., 2002)* a stronger decline than normally seen during aging is expected to trigger a cascade of downstream events, resulting in the shift from non-amyloidogenic to amyloidogenic pathways, accompanied by immunological changes, Tau hyperphosphorylation and neurofibrillary tangle formation, that presumably underlie the progressive neurodegeneration and cognitive decline associated with late-onset AD.

4.6 ACKNOWLEDGEMENTS

The present study was supported by Hartmann Müller Foundation (IK), SNF Grant Nr. 310000-117806 (IK) and Swiss National Competence Center in Neural Plasticity and Repair (NCCR; IK, RN). We are extremely grateful to Corinne Sidler and Cornelia Schwerdel for their excellent technical support; and to Kofi Kyere for animal husbandry and care.

4.7 SUPPLEMENT MATERIAL

Supplement Figures can be found on the enclosed DVD.

IV. GENERAL DISCUSSION

In this thesis we investigated the ultrastructural and proteomic properties of the aging-related Reelin-positive clustered structures in the hippocampal formation of wild type mice. After comprehensive immunohistochemical investigations, immuno-electron microscopy (IEM) was employed to further characterize the ultrastructural properties of the Reelin-positive deposits, their potential association with cellular organelles, and to confirm the preliminary findings of the formation of fibrillary deposits following prenatal brain infection with the viral mimic PolyI:C. These studies were further complemented by the determination of the biochemical compositions of these extracellular deposits in order to identify the proteins that are enriched in this area and potentially involved in the early stages of aggregation. We further aimed to decipher the putative association of Reelin and its functional signaling in AD-like pathology. Therefore, we investigated transgenic AD mice with reduced Reelin levels by biochemical and immunohistochemical methods. In the following section the main results of the 4 chapters obtained will be briefly summarized:

1) A new and optimized immunohistochemical protocol was developed involving a stringent protease pretreatment which markedly enhanced Reelin-IR. Surprisingly, this allowed for the first time the specific detection of variable forms of murine APP in these particular structures. Ultrastructurally, the Reelin granules appeared to be of extracellular and fibrillary origin.
2) Additional investigation at the subcellular level revealed striking new insights into granule morphology as well as its putative origin. Here, we have evidence that the granular structure likely originates from axonal varicosities, indicative of being an intracellular phenomenon. Moreover, ultrastructural investigation of prenatal immune challenged mice with the viral mimic PolyI:C revealed significant morphological differences in size and the elevated presence of organelles, namely mitochondria, in these fibrillary granular structures.
3) We were establishing a protocol for proteomic analysis combining laser capture microdissection with highly sensitive mass spectrometric analysis of the Reelin-positive deposits. However, although further optimization with respect to sample purity, sample processing and reduction of sample complexity will be required, we were able to confirm for the first time the enrichment of full-length Reelin and the N-terminal fragment in these

deposits by western blotting, verifying our immunohistochemical and –electron microscopy findings in aged species

4) We confirmed *in vivo* previous *in vitro* data, that a reduced Reelin expression aggravates amyloid pathology by altering APP processing and elevates Tau pathology in transgenic AD mice. We further provide biochemical evidence that alterations in Reelin expression and in its signaling critical modulates APP processing and Tau pathology.

These data provide strong evidence and support previous investigations *(Knuesel et al., 2009)* that Reelin itself aggregates during aging, reflecting potential alterations in subcellular trafficking and its proteolytic processing.

WHERE THE REELIN-POSITIVE AGGREGATES APPEAR – EVIDENCE OF AN INTRACELLULAR ORIGIN

In the adult brain, Reelin is expressed by GABAergic interneurons that are dispersed throughout the forebrain, as well as by glutamatergic pyramidal neurons in layer II of the entorhinal cortex, olfactory mitral cells and cerebellar granule cells *(Abraham and Meyer, 2003; Abraham et al., 2004; Alcantara et al., 1998; Baloyannis, 2005; Chin et al., 2007; Knuesel et al., 2009; Lacor et al., 2000; Miettinen et al., 2005; Pappas et al., 2003; Pesold et al., 1998a; Ramos-Moreno et al., 2006)*. These are also the layers where Reelin accumulation in the form of the granular clusters occurs throughout aging, accompanied by loss of Reelin expressing cells *(Knuesel et al., 2009)*, going in line with the observation of high Reelin-IR after birth and in young adults, but declining in the course of adult life *(Perez-Garcia et al., 2001)*. The Reelin-expressing neurons in layer II of the entorhinal cortex project via the perforant path to the hippocampus *(Muraoka et al., 2007; Steward and Scoville, 1976; Witter and Groenewegen, 1984)*, involving axonal transport of Reelin to the stratum lacunosum moleculare (slm) as well as the outer molecular layer (ml) of the hippocampal formation. This is in agreement with the contribution of Reelin to synaptic plasticity *(Weeber et al., 2002)* as well as the detection of high levels of Reelin-IR in these layers. Interestingly, the described Reelin deposits mainly appear in the *slm* and *sr* region of the CA1 hippocampal region. Importantly, the entorhinal cortex, the basal forebrain and the hippocampus - core structures playing a critical role in encoding, storage and retrieval of episodic memory and being crucial for learning and cognitive abilities*(Qiu and Weeber, 2007)*; reviewed in *(Eichenbaum, 2004)*) - are primarily affected by the neuropathology of AD *(Braak and Braak, 1991)*. One would suggest that the Reelin aggregates are related to axonal structures

terminating in these regions. This gives already rise to the assumption that Reelin aggregation putatively reflecting a consequence of axonal degeneration, an event playing a major role in the neuropathology and/or development of AD. The deposits may serve as seeding points for amyloid deposition. It may, however also represent a protective mechanism for keeping toxic substances away from neurons. This further supports the observations that there is a considerable variability in quantity of the Reelin deposits throughout aging.

Regarding our 3D-EM studies *(Study II),* there is strong evidence that the granular structures are not simply round and ovoid individual structures, that they are interconnected representing dendritic and/or axonal projections; indicative of an intracellular origin. This is further supported by our biochemical findings reporting the presence of several proteins, especially of intracellular origin, within or associated with the Reelin-positive deposits (*(Knuesel et al., 2009), Study III*). Supporting, the work of Derer and Goffinet *(Derer et al., 2001)* and another recent paper by the group of Phelps *(Kubasak et al., 2004)* suggest that Reelin is likely to be secreted from varicose axons. These swelling-like structures might in turn represent a budding event of degenerative material formed in the axon – likely as a consequence of abnormal Reelin processing - which then gets removed and form the described granules. This is strongly supported by our own ultrastructural findings as well the positive immunostaining of Reelin and myelin basic protein after prenatal PolyI:C exposure *(Study II)*. Potential disruption of the myelin sheaths on the axons likely due to PolyI:C-induced inflammation might trigger alterations in axonal transport in these subjects or further, might lead to axonal degeneration, explaining the increased density of clustered Reelin-positive deposits in these mice. The increased production of phosphorylated Tau due to PolyI:C *(unpublished data)* support these findings, as phosphorylation of Tau yields its detachment from microtubules and delocalization to somadodendritic compartments *(Ballatore et al., 2007; Ittner et al., 2010)* affecting in turn the stability and integrity of axons. This might be an explanation for the increased appearance of Reelin-positive granules in the immune challenged mice. Another paper describing axonal swellings due to disturbed autophagy *(Lee et al., 2011)* supports our hypothesis that the aggregation of Reelin into clustered granules might derive from inappropriate clearance of the protein. It is known that maturation of autophagolysosomes is inhibited in neurodegenerative diseases, resulting in swellings along dystrophic neurites. This is suggestive, that PolyI:C likely triggers this insufficiency of autophagosome formation and/or disruption of the autophagy system in the normal wild type mice and therefore results in elevated Reelin plaque load. A failure in autophagy, a defending process for clearing altered/dead organelles and protein aggregates, would accelerate the loss of

cellular integrity, ultimately leading to neuronal degeneration. It can be assumed that the formation of these clusters is a sign of a neurodegenerative event in the aging brain, going in line with the finding of similar structures in the aging brain obtained by other research groups *(Akiyama et al., 2000; Jucker and Ingram, 1994; Nakamura et al., 1995)*. This is further supported by our ultrastructural investigations as well as silver stainings that the aggregates itself likely represent degeneration on its own *(Study II)*. Further support for the granules being degenerative came from one recent study demonstrating Periodic acid Schiff (PAS) positive granules in proximal axons in the spinal cord and sciatic nerves in a model of infantile neuroaxonal dystrophy (INAD) *(Beck et al., 2011)*. Interestingly, they were positive for a mitochondrial outer membrane marker, but negative for the inner mitochondrial membrane, suggestive that these detected spheroids originate from degenerating mitochondria. This abnormal mitochondrial collapse gave rise to a focal disappearance of the axonal cytoskeleton, resulting in axonal swellings due to mitochondrial release of cytochrome c and reactive oxygen species (ROS), possibly yielding to axonal degeneration. Further, these structures are significantly increased in the axonal distal part in the late clinical stage. This phenomenon might likely be applicable to our ultrastructural as well our immunohistochemical findings, where Reelin-positive granules may appear from neuronal protrusions *(Study II)*. Also findings of degenerating organelles in the granules investigated in our lab by EM might be potential degenerating mitochondria as described in *(Beck et al., 2011)*. This data suggest that our investigated Reelin-positive granules originate from degeneration of presynaptic membranes at axonal terminals.

However, more approaches, concerning different stainings for several markers already mentioned above, a complete 3D reconstruction of the granular substructure as well as a longitudinal study throughout aging have to be accomplished, to precisely determine the granular origin.

CORRELATION BETWEEN REELIN AGGREGATES AND AD

A current precise cause and cure of AD remains still elusive. Although the amyloid hypothesis *(Hardy and Selkoe, 2002)*, postulating that Aβ is the pivotal cause of AD, dominated the research field of the disease, as highly supported by many genetic and biochemical data, there is growing evidence that Aβ is unlikely to be the exclusive initiating factor in the AD etiology *(for review see Herrup, 2010; Pimplikar, 2009)*. Necessarily, finding other contributing factors and/or mechanisms contributing to the pathology of AD beside Aβ would fill gaps in our

knowledge of the etiology of the disease and reconcile the findings that cannot be explained exclusively by the amyloid cascade hypothesis. Impairment in Reelin processing and/or signaling as well the formation of the Reelin-positive plaques may facilitate or initiate AD progression. Several groups have already found a strong impact of Reelin in the pathology of AD by either negatively regulating Tau phosphorylation *(Hiesberger et al., 1999; Ohkubo et al., 2003; Trommsdorff et al., 1999)* or by altering APP processing *(Hoe et al., 2006, 2009b)*. These are just a few of several more studies conducting this potential involvement. Moreover, genetic evidence is given by a study *(Kramer et al., 2010)* revealing the RELN locus as one of the putative risk factors in AD. To the best of our knowledge, our data were the first describing Aβ aggregation in normal aging wild type mice *(Study I (Doehner et al., 2010))*. Findings show the presence of Aβ or APP fragments in the formation of the granular Reelin-positive deposits, as well as fibrillary Aβ deposition as seen in human in close vicinity of the granular aggregates, indicating that similar aging-related pathophysiological changes occur in aged rodents. With the collection of antibodies used, we could rule out the presence of full-length APP, however, we have not deciphered yet which type of APP ectodomains or which proteolytic fragments of APP are present in these plaques. Recent investigations by the group of Pelegri *(Del Valle et al., 2010)* report also the appearance of Aβ in similar clustered granular structures in the hippocampal formation of SAMP8 mice, mice which are also lacking transgenic interference, supporting our findings in normal aged wild type mice *(Study I (Doehner et al., 2010))*. They even used specific antibodies for Aβ, binding only to cleaved ends, likely indicating, that in fact the Aβ peptide is present in the clustered granules. Nevertheless, based on these findings as well as the recent data of *(Hoe et al., 2009a; Nikolaev et al., 2009)*, further investigations using specific antibodies binding to the different cleaved sites of the proteolytic APP fragments need to be accomplished to clearly identify the type of APP fragments as well as the interaction of Reelin and the N-terminal fragment of APP in young and aged wild type mice. Further, several other studies show that similar granular clusters are also co-localizing with Tau, MAP2 and syndecan-2, components which are also found in senile plaques in AD *(Del Valle et al., 2010; Kern et al., 2011; Manich et al., 2011)*, supporting the hypothesis of Reelin aggregation being a seeding site for other aggregation prone proteins. On the other hand these findings are also supporting the fact that either altered Reelin signaling and/or processing and its subsequent aggregation correlates with axonal degeneration. Besides the studies performed here, this is further supported by a previous study conducted in our lab *(Madhusudan et al., 2009)* centering around the hypothesis that early accumulations of Reelin deposits in the projection areas of

subcortical neurons could impair the integrity of axonal terminals, potentially resulting in degeneration of cholinergic neurons in the basal forebrain, known to be early affected in AD.

In order to identify the putative neurotoxic factors within these extracellular Reelin aggregates, we initiated a proteomic approach to investigate their composition as well as temporal and spatial progression. Using this approach we expected to confirm the presence of Reelin and potentially also its proteolytic fragments in these extracellular deposits and answer whether there is an association of proteolytic APP fragments and Reelin in wild type mice. Further, this study might decipher where these granules originate from. Unfortunately, the keratin contamination and the low amount of the sample were major limitations in the proteomic analysis of the microdissected Reelin granules. Although, careful and even successful efforts were made in the second MS experiment, we still failed to detect any Reelin peptides in these samples. However, this does not indicate that Reelin was not present in the sample and that the protocol is not working properly. It needs to be stressed that a comprehensive analysis especially of such complex mixtures with low abundance of the required protein are still very challenging tasks and should not be underestimated. Note, that for several reasons already discussed *(Kuster et al., 2005; Mallick et al., 2007)*, it is not the case that only the presence of a protein in a small sample implies the readily observation of its peptides in proteomic analysis; in the most cases only a single peptide might be observed for many proteins. Although, we failed to detect the target protein, the protocol seems already very promising, and future studies should be accomplished with a much higher amount of captured sample and simplifying the composition of the mixture by additional purification steps discussed already previously. For future proteomic studies, we believe that the ability to detect qualitative and quantitative differences from the plaques according to their appearance rate in immune challenged mice compared to the control represent an important asset to understand better the molecular basis of this plaque formation as well its association in the pathology of neurodegenerative diseases. One further perspective, which should be considered in this proteomic approach, would be to study post-translational modifications (PTMs, like glycosylation) in the immune challenged mice compared to the NaCl exposed control. It is likely that Reelin glycosylation changes due to this immune challenge and might be a cause of the accelerated and increased plaque load in these mice. This would go in line with the recently addressed putative link between abnormal Reelin levels and AD pathogenesis *(Botella-Lopez et al., 2006, 2010; Saez-Valero et al., 2003)*. They report altered glycosylation of Reelin as well as a preferential up-regulation of the N-terminal 180 kDa Reelin fragment in the CSF and frontal cortex of AD patients, whereas full-length and other proteolytic

fragments of Reelin remained unaltered in control and AD subjects *(Botella-Lopez et al., 2006)*. Another recent study showed that the N-terminal fragment of Reelin can be generated within the endosomes after internalization of the full-length form *(Hibi and Hattori, 2009)*, pointing to the possibility that in AD patients the endosomal recycling and re-secretion of this fragment into the extracellular space could also be significantly affected, likely indicating that the N-terminal fragments may preferentially oligomerize and aggregate in the extracellular matrix during aging after an abnormal increase. Indeed, our biochemical investigations confirmed that these Reelin deposits contain besides the full-length form also considerable amounts of N-terminal Reelin fragments *(Study III)*. However, why Reelin starts to aggregate and which precise molecular mechanism potentially connects altered Reelin signaling to the pathology of AD has not been deciphered yet. To directly test the role of Reelin in AD pathophysiology, we crossed heterozygous *reeler* mice into a transgenic AD background *(Knobloch et al., 2007b)* to investigate the effect of reduced Reelin-mediated signaling on Aβ plaque and NFT formation, as well as neurodegenerative processes *(Study IV (Kocherhans et al., 2010))*. We could provide the first *in vivo* support that dysfunctional Reelin-mediated signaling is a critical upstream modulator of amyloidogenic APP processing and Tau hyperphosphorylation, both likely contributing to progressive neurodegeneration observed in Reelin-deficient AD mice. Altogether, these observations add to our understanding of the putative molecular mechanisms that underlie the pathogenesis of AD. Reduced Reelin-dependent signaling during aging appears as crucial driving force able to shift APP processing from non-amyloidogenic to amyloidogenic forms *in vivo*. Moreover, alterations in the proteolytic cleavage of Reelin might be a potential factor impairing Reelin signaling and causing several downstream effects being possibly involved in the etiology of AD. Cleavage of Reelin impairs the formation of dimers and therefore the correct binding to its receptors *(Kohno et al., 2009; Kubo et al., 2002; Strasser et al., 2004)*, consequently impairing the signaling cascade and formation of aggregates as Reelin fragments are more prone to aggregation *(Kubo et al., 2002)*. As already mentioned in the introduction we recently found that tPA is a potential protease cleaving Reelin at the C-terminal site *(D. Krstic, unpublished data),* which in turn is known to be susceptible to aggregate *(Nakano et al., 2007)*. Importantly, tPA-mediated cleavage of Reelin potentially impairs the interaction with its receptors, resulting in less precise induction of its signaling cascades *(Hibi and Hattori, 2009; Nakano et al., 2007)* as well reduction in the internalization rate of ApoER2 with Reelin *(D. Krstic, unpublished data)*. In line, a second protease involved in the cleavage of Reelin was found, namely ADAMTS-4, indicating a dominant N-terminal cleavage compared to the

cleavage at the C-terminal *(D. Krstic, unpublished data)*. This would further support the hypothesis that the granular structures are mainly formed from N-terminal fragments of Reelin. Alterations in either the more likely intracellular processing or the exocytosis of the N-terminus *(Hibi and Hattori, 2009)* are a likely explanation for the intracellular aggregation of Reelin as shown by EM *(Study II)*. These accumulations potentially get cleaned through axonal transport, supporting our findings of Reelin and/or this particular fibrillary structure in these neuritic processes *(Study II)*.

THE ROLE OF INFLAMMATION IN THE NEUROPATHOLOGY - PERSPECTIVES

Studies performed by us and many other labs have provided exciting new insights into the function of Reelin-mediated signaling in synaptic function in the adult and aging brain. However, the molecular mechanisms how this developmental signaling pathway regulates directly or indirectly AD-associated pathophysiological processes remains to be fully elucidated. Moreover, many of the studies including ours have employed transgenic AD mice that model the genetic, early-onset form of the disease. Though, the majority of patients suffer from the age-associated, late-onset form of AD. Furthermore, several recent studies describe an active involvement of the immune system in the etiology of sporadic AD *(Akiyama et al., 2000; McGeer and McGeer, 2002; Wyss-Coray, 2006)*, and that peripheral infections potential drive the pathophysiology of this disease *(Schmidt et al., 2002)*. The question, therefore, is: can the investigations of dysfunctional Reelin-mediated signaling in normal aged wild type mice provide us some insights into the molecular mechanisms of late-onset AD? In other words, is an impaired Reelin-mediated signaling sufficient to induce AD-like neuropathological changes in aged wild type rodents that would allow us to study putative early disease-relevant pathophysiological alterations in a more physiological context?

Our recent experimental approach might provide first support for this hypothesis: (1) We have demonstrated that a systemic administration of the cytokine releaser and viral mimic PolyI:C in mice provides convincing support to the link between maternal infection during pregnancy and behavioral and neurochemical abnormalities in the adult offspring *(Meyer et al., 2005; Shi et al., 2003; Zuckerman et al., 2003)*. We have recently provided the first evidence that a prenatal immune challenge during late gestation results in significant acceleration of aging-associated neuropathological alterations in non-transgenic wild type mice. This involved reduced Reelin expression levels, precocious accumulation of Reelin-positive deposits, as well as long-term

alterations in inflammatory modulators *(Knuesel et al., 2009)*, suggesting inflammatory cytokines as putative regulators of Reelin expression, proteolytic processing, and/or signaling. This goes in line with our ultrastructural investigations, demonstrating that immune challenged mice (PolyI:C) showed a trend towards larger granule size accompanied by an increased association with mitochondria, highly indicative of an intracellular origin, supported by biochemical findings. (2) The application of our adapted immunohistochemical protocol involving protease-pretreatment allowed for the first time the detection of murine proteolytic APP fragments in extracellular amyloid-like *plaques (Study I (Doehner et al., 2010)),* indicating that the experimental conditions contribute more strongly to the observed lack in amyloid deposition in aged rodents than anticipated. (3) In addition, we recently found that a viral like immune challenge at a critical time point during gestation is sufficient to cause long term alterations in the brain leading to the development of pathological features characteristic for AD as elevated processing of APP and increased Tau phosphorylation. This was accompanied by Tau delocalization, and an overproduction of inflammatory cytokines (Il-1β, Il-6, Il-10; TNF-α) *(unpublished data, (Madhusudan et al.)),* the same cytokines which are increased in the brains of AD patients *(Mrak and Griffin, 2005)*. Further impact of PolyI:C on Reelin processing and signaling was given by biochemical approaches showing altered Reelin-fragment levels compared to normal wild type mice *(unpublished data).* Interestingly, this induction triggered the onset of such pathology in non-transgenic animals. This data support strongly the involvement of neuroinflammation in the onset and progression of the late-onset form of the disease, being likely a causative factor. This suggests that an inflammation early in life can already sense the brain to develop AD, maybe due to the altered cytokine levels, which later might cause alteration in Reelin processing and signaling, as well as in APP processing.

Our studies demonstrate that normal wild type mice are a very useful and accessible model system to gain insights into the development of the sporadic form of the disease. Therefore, the combination of these experimental paradigms presented in this thesis is expected to provide a potent way to address aging-associated neuropathology in non-transgenic mice or rats.

CONCLUSION

Accumulating evidence indicates that the same Reelin-mediated signaling pathway required for proper early neurodevelopmental processes is equally relevant for the regulation of adult neuronal function and plasticity. Both a decline and overproduction of Reelin in adulthood is

associated with abnormal synaptic function, indicating an important homeostatic regulation of this extracellular glycoprotein *(for review (Doehner and Knuesel, 2010))*. Our investigations showed for the first time that aging across species is accompanied by a reduction in Reelin expression, accompanied by a highly selective layer-specific accumulation of Reelin-positive amyloid-like plaques.

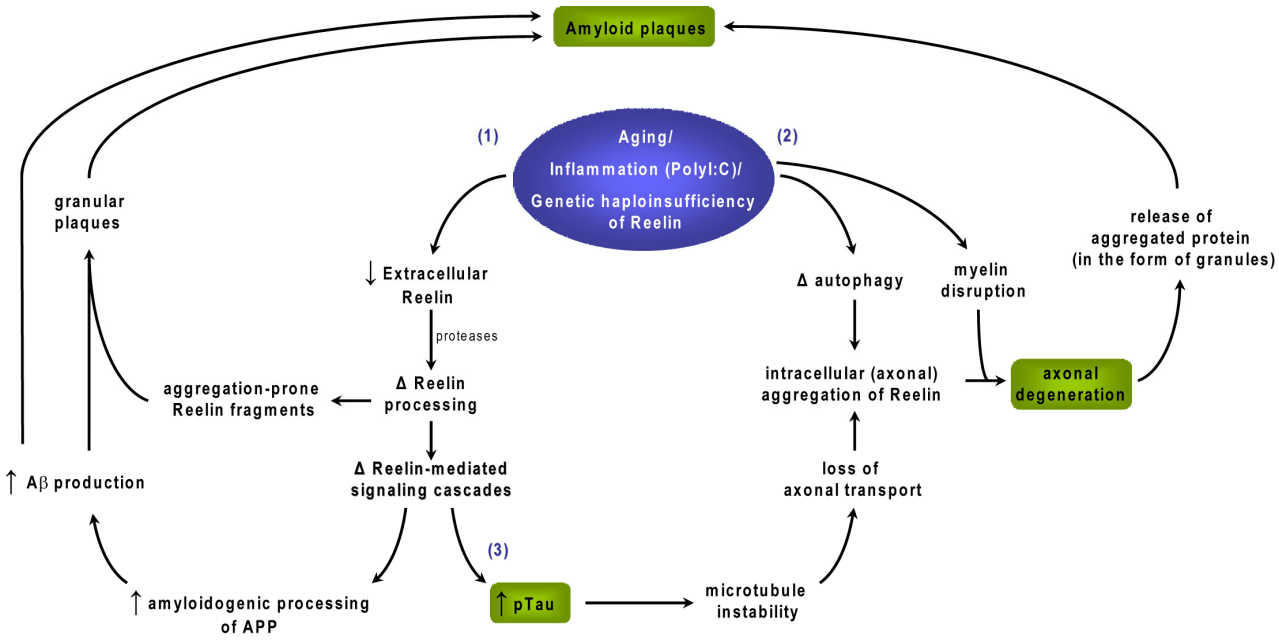

FIGURE 1: Hypothetical model representing the link between Reelin, its alterations and the influence of inflammation in the pathogenesis of AD. During aging, a pronounced decrease in Reelin expression accompanied by accumulation of Reelin deposits has been reported. There are three potential and partially interconnected hypotheses how altered Reelin could potentially contribute to the pathogenesis of AD: (1) Due to the aging-associated decrease in Reelin expression and alterations in extracellular Reelin processing, Reelin starts to form granular deposits, which possibly serve as a seeding site for Aβ and other potential aggregation-prone proteins, ultimately leading to the formation of amyloid plaques. Further, alterations in Reelin processing cause changes in the Reelin-mediated signaling cascade which favors amyloidogenic APP processing and results in an increase in Aβ production, with that facilitating the accumulation of the peptides in granular deposits or in amyloid plaques. (2) Experimental evidence supports the hypothesis that Reelin aggregates are of intracellular origin. This might be caused by age-related impairments in autophagy alterations as well as in alterations in the myelin sheath structure, potentially related to axonal swellings accompanying improper clearance of organelles and misfolded or abnormally processed proteins, including Reelin. This in turn is expected to result in axonal degeneration and release of the accumulated proteins into the neuropil; an alternative way to provide a seeding site for amyloid plaque formation. (3) Elevated Tau phosphorylation due to deficiency in Reelin signaling leads to microtubule instability and therefore inefficient and poorly coordinated axonal transport constituting an additional detrimental factor underlying axonal degeneration. Alterations in all these different pathways provide a strong link between dysfunctional Reelin signaling and pathophysiological processes characteristic for AD (green boxes). Alterations due to early inflammation or genetic reduction of Reelin aggravate and accelerate these changes potentially underlying the shift from normal to pathological brain aging.

Taken together, the presented findings so far provide important information regarding putative temporal processes underlying the transition from normal to pathological aging, including an intracellular and abnormal aggregation of Reelin, possibly leading to neurodegeneration, which gets accelerated by a prenatal peripheral immune challenge (PolyI:C), and increased Aβ~ and Tau pathology due to haploinsufficiency of Reelin. Combining the results presented in this work with the recent findings in our lab the following model can be proposed (**Fig. 1**), pointing to Reelin as a prospective missing link in the development of neuropathological changes in the etiology of AD. Comprehensive ultrastructural and immunohistochemical characterizations indicate that Reelin, likely by self-aggregating into abnormal oligomeric or protofibrillary deposits during aging, is also able to induce or result from degenerative axonal varicosities that selectively terminate in plaque dense areas within the hippocampal formation. These findings give evidence that the Reelin-positive granules are of intracellular origin, and not exclusively extracellular as first expected. It is likely that other aggregation-prone proteins that accumulate and associate with these deposits further contribute to the degenerative processes investigated. Healthy and cognitively normal subjects are normally able to sufficiently clear and degrade these deposits, whereas cognitively impaired aged mice failed to do so *(Knuesel et al., 2009)*. This might be indicative of alterations in the autophagy system as well as altered axonal transport processes. Autophagy pathway changes may also occur due to systemic inflammation, potentially explaining the higher plaque load in the PolyI:C exposed animals with concomitant appearance of mitochondria in these granular structures. Reduced Reelin, as well as inflammation, are likely able to trigger AD-like pathophysiological processes including increased APP processing and hyperphosphorylation of Tau (pTau). Increased levels of pTau in turn lead to the destabilization of axonal processes as well as the transport system, which possibly results in the appearance of Reelin aggregates in the axons. Altogether, these correlations potentially contribute to progressive neurodegeneration in aged individuals, as well providing a seeding point for aggregation prone proteins, major characteristic phenomena in the etiology of AD. We suggest that dysfunction in Reelin-mediated signaling and/or processing, either due to early inflammation events or genetic reduction of Reelin, represents an important driving force able to induce a shift from normal to pathological aging.

REFERENCES

Abraham, H. and G. Meyer (2003). Reelin-expressing neurons in the postnatal and adult human hippocampal formation. Hippocampus, 13 (6): 715-727.

Abraham, H., C.G. Perez-Garcia and G. Meyer (2004). p73 and Reelin in Cajal-Retzius cells of the developing human hippocampal formation. Cereb Cortex, 14 (5): 484-495.

Adams, M.O. (1984). Alzheimer's disease: the human response. Conn Med, 48 (7): 437-439.

Aebersold, R. and M. Mann (2003). Mass spectrometry-based proteomics. Nature, 422 (6928): 198-207.

Ahram, M., M.J. Flaig, J.W. Gillespie, P.H. Duray, W.M. Linehan, D.K. Ornstein, S. Niu, Y. Zhao, E.F. Petricoin, 3rd and M.R. Emmert-Buck (2003). Evaluation of ethanol-fixed, paraffin-embedded tissues for proteomic applications. Proteomics, 3 (4): 413-421.

Akiyama, H., M. Kameyama, I. Akiguchi, H. Sugiyama, T. Kawamata, H. Fukuyama, H. Kimura, M. Matsushita and T. Takeda (1986). Periodic acid-Schiff (PAS)-positive, granular structures increase in the brain of senescence accelerated mouse (SAM). Acta Neuropathol (Berl), 72 (2): 124-129.

Akiyama, H., S. Barger, S. Barnum, B. Bradt, J. Bauer, G.M. Cole, N.R. Cooper, P. Eikelenboom, M. Emmerling, B.L. Fiebich, et al. (2000). Inflammation and Alzheimer's disease. Neurobiol Aging, 21 (3): 383-421.

Alcantara, S., M. Ruiz, G. D'Arcangelo, F. Ezan, L. de Lecea, T. Curran, C. Sotelo and E. Soriano (1998). Regional and cellular patterns of reelin mRNA expression in the forebrain of the developing and adult mouse. J Neurosci, 18 (19): 7779-7799.

Alder, N. (1953). On the nature, origin and distribution of the corpora amylacea of the brain with observations on some new staining reactions. J Ment Sci, 99 (417): 689-697.

Aoki, M., I. Volkmann, L.O. Tjernberg, B. Winblad and N. Bogdanovic (2008). Amyloid beta-peptide levels in laser capture microdissected cornu ammonis 1 pyramidal neurons of Alzheimer's brain. Neuroreport, 19 (11): 1085-1089.

Apweiler, R., M.J. Martin, C. O'Donovan, M. Magrane, Y. Alam-Faruque, R. Antunes, D. Barrell, B. Bely, M. Bingley, D. Binns, et al. (2010). The Universal Protein Resource (UniProt) in 2010. Nucleic Acids Research, 38 D142-D148.

Ard, M.D. and R.P. Bunge (1988). Heparan sulfate proteoglycan and laminin immunoreactivity on cultured astrocytes: relationship to differentiation and neurite growth. J Neurosci, 8 (8): 2844-2858.

Armstrong, D.M., L.B. Hersh and F.H. Gage (1988). Morphologic alterations of cholinergic processes in the neocortex of aged rats. Neurobiol Aging, 9 (2): 199-205.

Armstrong, R.A. (2006). Plaques and tangles and the pathogenesis of Alzheimer's disease. Folia Neuropathol, 44 (1): 1-11.

Arnaud, L., B.A. Ballif and J.A. Cooper (2003). Regulation of protein tyrosine kinase signaling by substrate degradation during brain development. Mol Cell Biol, 23 (24): 9293-9302.

Ball, H.J., B. McParland, C. Driussi and N.H. Hunt (2002). Isolating vessels from the mouse brain for gene expression analysis using laser capture microdissection. Brain Res Brain Res Protoc, 9 (3): 206-213.

Ballatore, C., V.M. Lee and J.Q. Trojanowski (2007). Tau-mediated neurodegeneration in Alzheimer's disease and related disorders. Nat Rev Neurosci, 8 (9): 663-672.

Baloyannis, S.J. (2005). Morphological and morphometric alterations of Cajal-Retzius cells in early cases of Alzheimer's disease: a Golgi and electron microscope study. Int J Neurosci, 115 (7): 965-980.

Bar, I., C. Lambert De Rouvroit, I. Royaux, D.B. Krizman, C. Dernoncourt, D. Ruelle, M.C. Beckers and A.M. Goffinet (1995). A YAC contig containing the reeler locus with preliminary characterization of candidate gene fragments. Genomics, 26 (3): 543-549.

Baumeister, W., R. Grimm and J. Walz (1999). Electron tomography of molecules and cells. Trends Cell Biol, 9 (2): 81-85.

Beck, G., Y. Sugiura, K. Shinzawa, S. Kato, M. Setou, Y. Tsujimoto, S. Sakoda and H. Sumi-Akamaru (2011). Neuroaxonal Dystrophy in Calcium-Independent Phospholipase A2{beta} Deficiency Results from Insufficient Remodeling and Degeneration of Mitochondrial and Presynaptic Membranes. J Neurosci, 31 (31): 11411-11420.

Beffert, U., G. Morfini, H.H. Bock, H. Reyna, S.T. Brady and J. Herz (2002). Reelin-mediated signaling locally regulates protein kinase B/Akt and glycogen synthase kinase 3beta. J Biol Chem, 277 (51): 49958-49964.

Beffert, U., E.J. Weeber, G. Morfini, J. Ko, S.T. Brady, L.H. Tsai, J.D. Sweatt and J. Herz (2004). Reelin and cyclin-dependent kinase 5-dependent signals cooperate in regulating neuronal migration and synaptic transmission. J Neurosci, 24 (8): 1897-1906.

Beffert, U., E.J. Weeber, A. Durudas, S. Qiu, I. Masiulis, J.D. Sweatt, W.P. Li, G. Adelmann, M. Frotscher, R.E. Hammer, et al. (2005). Modulation of synaptic plasticity and memory by Reelin involves differential splicing of the lipoprotein receptor Apoer2. Neuron, 47 (4): 567-579.

Beffert, U., A. Durudas, E.J. Weeber, P.C. Stolt, K.M. Giehl, J.D. Sweatt, R.E. Hammer and J. Herz (2006a). Functional dissection of Reelin signaling by site-directed disruption of Disabled-1 adaptor binding to apolipoprotein E receptor 2: distinct roles in development and synaptic plasticity. J Neurosci, 26 (7): 2041-2052.

Beffert, U., F. Nematollah Farsian, I. Masiulis, R.E. Hammer, S.O. Yoon, K.M. Giehl and J. Herz (2006b). ApoE receptor 2 controls neuronal survival in the adult brain. Curr Biol, 16 (24): 2446-2452.

Belichenko, P.V., D.M. Vogt Weisenhorn, J. Myklossy and M.R. Celio (1995). Calretinin-positive Cajal-Retzius cells persist in the adult human neocortex. Neuroreport, 6 (14): 1869-1874.

Bertram, L. and R.E. Tanzi (2008). Thirty years of Alzheimer's disease genetics: the implications of systematic meta-analyses. Nat Rev Neurosci, 9 (10): 768-778.

Bertram, L. and R.E. Tanzi (2009). Genome-wide association studies in Alzheimer's disease. Hum Mol Genet, 18 (R2): R137-145.

Bertram, L., C.M. Lill and R.E. Tanzi (2010). The genetics of Alzheimer disease: back to the future. Neuron, 68 (2): 270-281.

Binder, L.I., A. Frankfurter and L.I. Rebhun (1985). The distribution of tau in the mammalian central nervous system. J Cell Biol, 101 (4): 1371-1378.

Bird, T.D. (2008). Genetic aspects of Alzheimer disease. Genet Med, 10 (4): 231-239.

Bliss, T.V. and T. Lomo (1973). Long-lasting potentiation of synaptic transmission in the dentate area of the anaesthetized rabbit following stimulation of the perforant path. J Physiol, 232 (2): 331-356.

Blurton-Jones, M. and F.M. Laferla (2006). Pathways by which Abeta facilitates tau pathology. Curr Alzheimer Res, 3 (5): 437-448.

Bock, H.H., Y. Jossin, P. Liu, E. Forster, P. May, A.M. Goffinet and J. Herz (2003). Phosphatidylinositol 3-kinase interacts with the adaptor protein Dab1 in response to Reelin signaling and is required for normal cortical lamination. J Biol Chem, 278 (40): 38772-38779.

Bock, H.H., Y. Jossin, P. May, O. Bergner and J. Herz (2004). Apolipoprotein E receptors are required for reelin-induced proteasomal degradation of the neuronal adaptor protein Disabled-1. J Biol Chem, 279 (32): 33471-33479.

Borrell, V., J.A. Del Rio, S. Alcantara, M. Derer, A. Martinez, G. D'Arcangelo, K. Nakajima, K. Mikoshiba, P. Derer, T. Curran, et al. (1999). Reelin regulates the development and synaptogenesis of the layer-specific entorhino-hippocampal connections. J Neurosci, 19 (4): 1345-1358.

Borrell, V., L. Pujadas, S. Simo, D. Dura, M. Sole, J.A. Cooper, J.A. Del Rio and E. Soriano (2007). Reelin and mDab1 regulate the development of hippocampal connections. Mol Cell Neurosci, 36 (2): 158-173.

Botella-Lopez, A., F. Burgaya, R. Gavin, M.S. Garcia-Ayllon, E. Gomez-Tortosa, J. Pena-Casanova, J.M. Urena, J.A. Del Rio, R. Blesa, E. Soriano, et al. (2006). Reelin expression and glycosylation patterns are altered in Alzheimer's disease. Proc Natl Acad Sci U S A, 103 (14): 5573-5578.

Botella-Lopez, A., I. Cuchillo-Ibanez, T. Cotrufo, S.S. Mok, Q.X. Li, M.S. Barquero, M. Dierssen, E. Soriano and J. Saez-Valero (2010). Beta-amyloid controls altered Reelin expression and processing in Alzheimer's disease. Neurobiol Dis, 37 (3): 682-691.

Braak, H. and E. Braak (1991). Neuropathological stageing of Alzheimer-related changes. Acta Neuropathol, 82 (4): 239-259.

Braak, H. and E. Braak (1996). Evolution of the neuropathology of Alzheimer's disease. Acta Neurol Scand Suppl, 165 3-12.

Brich, J., F.S. Shie, B.W. Howell, R. Li, K. Tus, E.K. Wakeland, L.W. Jin, M. Mumby, G. Churchill, J. Herz, et al. (2003). Genetic modulation of tau phosphorylation in the mouse. J Neurosci, 23 (1): 187-192.

Brunden, K.R., J.Q. Trojanowski and V.M. Lee (2009). Advances in tau-focused drug discovery for Alzheimer's disease and related tauopathies. Nat Rev Drug Discov, 8 (10): 783-793.

Caughey, B. and P.T. Lansbury (2003). Protofibrils, pores, fibrils, and neurodegeneration: separating the responsible protein aggregates from the innocent bystanders. Annu Rev Neurosci, 26 267-298.

Chai, X., E. Forster, S. Zhao, H.H. Bock and M. Frotscher (2009). Reelin stabilizes the actin cytoskeleton of neuronal processes by inducing n-cofilin phosphorylation at serine3. J Neurosci, 29 (1): 288-299.

Chameau, P., D. Inta, T. Vitalis, H. Monyer, W.J. Wadman and J.A. van Hooft (2009). The N-terminal region of reelin regulates postnatal dendritic maturation of cortical pyramidal neurons. Proc Natl Acad Sci U S A, 106 (17): 7227-7232.

Chang, W.P., G. Koelsch, S. Wong, D. Downs, H. Da, V. Weerasena, B. Gordon, T. Devasamudram, G. Bilcer, A.K. Ghosh, et al. (2004). In vivo inhibition of Abeta production by memapsin 2 (beta-secretase) inhibitors. J Neurochem, 89 (6): 1409-1416.

Chen, H.J., M. Rojas-Soto, A. Oguni and M.B. Kennedy (1998). A synaptic Ras-GTPase activating protein (p135 SynGAP) inhibited by CaM kinase II. Neuron, 20 (5): 895-904.

Chen, Y., U. Beffert, M. Ertunc, T.S. Tang, E.T. Kavalali, I. Bezprozvanny and J. Herz (2005). Reelin modulates NMDA receptor activity in cortical neurons. J Neurosci, 25 (36): 8209-8216.

Chen, Y., M.S. Durakoglugil, X. Xian and J. Herz (2010). ApoE4 reduces glutamate receptor function and synaptic plasticity by selectively impairing ApoE receptor recycling. Proc Natl Acad Sci U S A, 107 (26): 12011-12016.

Cheng, A.L., W.G. Huang, Z.C. Chen, F. Peng, P.F. Zhang, M.Y. Li, F. Li, J.L. Li, C. Li, H. Yi, et al. (2008). Identification of novel nasopharyngeal carcinoma biomarkers by laser capture microdissection and proteomic analysis. Clin Cancer Res, 14 (2): 435-445.

Chiarini, A., I. Dal Pra, J.F. Whitfield and U. Armato (2006). The killing of neurons by beta-amyloid peptides, prions, and pro-inflammatory cytokines. Ital J Anat Embryol, 111 (4): 221-246.

Chin, J., C.M. Massaro, J.J. Palop, M.T. Thwin, G.Q. Yu, N. Bien-Ly, A. Bender and L. Mucke (2007). Reelin depletion in the entorhinal cortex of human amyloid precursor protein transgenic mice and humans with Alzheimer's disease. J Neurosci, 27 (11): 2727-2733.

Cleary, J.P., D.M. Walsh, J.J. Hofmeister, G.M. Shankar, M.A. Kuskowski, D.J. Selkoe and K.H. Ashe (2005). Natural oligomers of the amyloid-beta protein specifically disrupt cognitive function. Nat Neurosci, 8 (1): 79-84.

Cooper, J.A. (2008). A mechanism for inside-out lamination in the neocortex. Trends Neurosci, 31 (3): 113-119.

Corder, E.H., A.M. Saunders, W.J. Strittmatter, D.E. Schmechel, P.C. Gaskell, G.W. Small, A.D. Roses, J.L. Haines and M.A. Pericak-Vance (1993). Gene dose of apolipoprotein E type 4 allele and the risk of Alzheimer's disease in late onset families. Science, 261 (5123): 921-923.

Corsetti, V., G. Amadoro, A. Gentile, S. Capsoni, M.T. Ciotti, M.T. Cencioni, A. Atlante, N. Canu, T.T. Rohn, A. Cattaneo, et al. (2008). Identification of a caspase-derived N-terminal tau fragment in cellular and animal Alzheimer's disease models. Mol Cell Neurosci, 38 (3): 381-392.

Courtes, S., J. Vernerey, L. Pujadas, K. Magalon, H. Cremer, E. Soriano, P. Durbec and M. Cayre (2011). Reelin controls progenitor cell migration in the healthy and pathological adult mouse brain. PLoS One, 6 (5): e20430.

Crockett, D.K., Z. Lin, C.P. Vaughn, M.S. Lim and K.S. Elenitoba-Johnson (2005). Identification of proteins from formalin-fixed paraffin-embedded cells by LC-MS/MS. Lab Invest, 85 (11): 1405-1415.

Curran, S., J.A. McKay, H.L. McLeod and G.I. Murray (2000). Laser capture microscopy. Mol Pathol, 53 (2): 64-68.

D'Arcangelo, G., G.G. Miao, S.C. Chen, H.D. Soares, J.I. Morgan and T. Curran (1995). A protein related to extracellular matrix proteins deleted in the mouse mutant reeler. Nature, 374 (6524): 719-723.

D'Arcangelo, G., K. Nakajima, T. Miyata, M. Ogawa, K. Mikoshiba and T. Curran (1997). Reelin is a secreted glycoprotein recognized by the CR-50 monoclonal antibody. J Neurosci, 17 (1): 23-31.

D'Arcangelo, G., R. Homayouni, L. Keshvara, D.S. Rice, M. Sheldon and T. Curran (1999). Reelin is a ligand for lipoprotein receptors. Neuron, 24 (2): 471-479.

Dahlgren, K.N., A.M. Manelli, W.B. Stine, Jr., L.K. Baker, G.A. Krafft and M.J. LaDu (2002). Oligomeric and fibrillar species of amyloid-beta peptides differentially affect neuronal viability. J Biol Chem, 277 (35): 32046-32053.

de Bergeyck, V., K. Nakajima, C. Lambert de Rouvroit, B. Naerhuyzen, A.M. Goffinet, T. Miyata, M. Ogawa and K. Mikoshiba (1997). A truncated Reelin protein is produced but not secreted in the 'Orleans' reeler mutation (Reln[rl-Orl]). Brain Res Mol Brain Res, 50 (1-2): 85-90.

Deguchi, K., K. Inoue, W.E. Avila, D. Lopez-Terrada, B.A. Antalffy, C.C. Quattrocchi, M. Sheldon, K. Mikoshiba, G. D'Arcangelo and D.L. Armstrong (2003). Reelin and disabled-1 expression in developing and mature human cortical neurons. J Neuropathol Exp Neurol, 62 (6): 676-684.

Del Rio, J.A., B. Heimrich, V. Borrell, E. Forster, A. Drakew, S. Alcantara, K. Nakajima, T. Miyata, M. Ogawa, K. Mikoshiba, et al. (1997). A role for Cajal-Retzius cells and reelin in the development of hippocampal connections. Nature, 385 (6611): 70-74.

Del Valle, J., J. Duran-Vilaregut, G. Manich, G. Casadesus, M.A. Smith, A. Camins, M. Pallas, C. Pelegri and J. Vilaplana (2010). Early amyloid accumulation in the hippocampus of SAMP8 mice. J Alzheimers Dis, 19 (4): 1303-1315.

Denk, W. and H. Horstmann (2004). Serial block-face scanning electron microscopy to reconstruct three-dimensional tissue nanostructure. PLoS Biol, 2 (11): e329.

Derer, P., M. Derer and A. Goffinet (2001). Axonal secretion of Reelin by Cajal-Retzius cells: evidence from comparison of normal and Reln(Orl) mutant mice. J Comp Neurol, 440 (2): 136-143.

Deverman, B.E. and P.H. Patterson (2009). Cytokines and CNS development. Neuron, 64 (1): 61-78.

Doehner, J. and I. Knuesel (2010). Reelin-mediated signaling during normal and pathological forms of aging. Aging and Disease, 1 (1): 12-29.

Doehner, J., A. Madhusudan, U. Konietzko, J.M. Fritschy and I. Knuesel (2010). Co-localization of Reelin and proteolytic AbetaPP fragments in hippocampal plaques in aged wild-type mice. J Alzheimers Dis, 19 (4): 1339-1357.

Dooley, N.P., S. Gauthier and H.D. Durham (1992). Antibody to beta-amyloid precursor protein recognizes an intermediate filament-associated protein in Alzheimer's and control fibroblasts. J Neurosci Res, 33 (1): 60-67.

Duit, S., H. Mayer, S.M. Blake, W.J. Schneider and J. Nimpf (2010). Differential functions of ApoER2 and very low density lipoprotein receptor in Reelin signaling depend on differential sorting of the receptors. J Biol Chem, 285 (7): 4896-4908.

Dunn, B.M. (2002). Structure and mechanism of the pepsin-like family of aspartic peptidases. Chem Rev, 102 (12): 4431-4458.

Durakoglugil, M.S., Y. Chen, C.L. White, E.T. Kavalali and J. Herz (2009). Reelin signaling antagonizes beta-amyloid at the synapse. Proc Natl Acad Sci U S A, 106 (37): 15938-15943.

Eichenbaum, H. (2004). Hippocampus: cognitive processes and neural representations that underlie declarative memory. Neuron, 44 (1): 109-120.

El Khoury, J. and A.D. Luster (2008). Mechanisms of microglia accumulation in Alzheimer's disease: therapeutic implications. Trends Pharmacol Sci, 29 (12): 626-632.

Emmert-Buck, M.R., R.F. Bonner, P.D. Smith, R.F. Chuaqui, Z. Zhuang, S.R. Goldstein, R.A. Weiss and L.A. Liotta (1996). Laser capture microdissection. Science, 274 (5289): 998-1001.

Estus, S., T.E. Golde, T. Kunishita, D. Blades, D. Lowery, M. Eisen, M. Usiak, X.M. Qu, T. Tabira, B.D. Greenberg, et al. (1992). Potentially amyloidogenic, carboxyl-terminal derivatives of the amyloid protein precursor. Science, 255 (5045): 726-728.

Falconer, D.S. (1951). Two new mutants "trembler" and "reeler" with neurological actions in the house mouse. J Genet, 50 192-201.

Fend, F., M.R. Emmert-Buck, R. Chuaqui, K. Cole, J. Lee, L.A. Liotta and M. Raffeld (1999). Immuno-LCM: laser capture microdissection of immunostained frozen sections for mRNA analysis. Am J Pathol, 154 (1): 61-66.

Fernandez-Medarde, A., A. Porteros, J. de las Rivas, A. Nunez, J.J. Fuster and E. Santos (2007). Laser microdissection and microarray analysis of the hippocampus of Ras-GRF1 knockout mice reveals gene expression changes affecting signal transduction pathways related to memory and learning. Neuroscience, 146 (1): 272-285.

Fiala, J.C. (2007). Mechanisms of amyloid plaque pathogenesis. Acta Neuropathol, 114 (6): 551-571.

Fiala, J.C., M. Feinberg, A. Peters and H. Barbas (2007). Mitochondrial degeneration in dystrophic neurites of senile plaques may lead to extracellular deposition of fine filaments. Brain Struct Funct, 212 (2): 195-207.

Förster, E., H.H. Bock, J. Herz, X. Chai, M. Frotscher and S. Zhao (2010). Emerging topics in Reelin function. Eur J Neurosci, 1-8.

Forster, E., A. Tielsch, B. Saum, K.H. Weiss, C. Johanssen, D. Graus-Porta, U. Muller and M. Frotscher (2002). Reelin, Disabled 1, and beta 1 integrins are required for the formation of the radial glial scaffold in the hippocampus. Proc Natl Acad Sci U S A, 99 (20): 13178-13183.

Forster, E., Y. Jossin, S. Zhao, X. Chai, M. Frotscher and A.M. Goffinet (2006). Recent progress in understanding the role of Reelin in radial neuronal migration, with specific emphasis on the dentate gyrus. Eur J Neurosci, 23 (4): 901-909.

Fowler, C.J., A. Wiberg, L. Oreland, J. Marcusson and B. Winblad (1980). The effect of age on the activity and molecular properties of human brain monoamine oxidase. J Neural Transm, 49 (1-2): 1-20.

Fox, C.H., F.B. Johnson, J. Whiting and P.P. Roller (1985). Formaldehyde fixation. J Histochem Cytochem, 33 (8): 845-853.

Frotscher, M. (1998). Cajal-Retzius cells, Reelin, and the formation of layers. Curr Opin Neurobiol, 8 (5): 570-575.

Frotscher, M., X. Chai, H.H. Bock, C.A. Haas, E. Forster and S. Zhao (2009). Role of Reelin in the development and maintenance of cortical lamination. J Neural Transm, 116 (11): 1451-1455.

Frotscher, M., C.A. Haas and E. Forster (2003). Reelin controls granule cell migration in the dentate gyrus by acting on the radial glial scaffold. Cereb Cortex, 13 (6): 634-640.

Fung, J., D. Frost, A. Chakrabartty and J. McLaurin (2004). Interaction of human and mouse Abeta peptides. J Neurochem, 91 (6): 1398-1403.

Furukawa, K., B.L. Sopher, R.E. Rydel, J.G. Begley, D.G. Pham, G.M. Martin, M. Fox and M.P. Mattson (1996). Increased activity-regulating and neuroprotective efficacy of alpha-secretase-derived secreted amyloid precursor protein conferred by a C-terminal heparin-binding domain. J Neurochem, 67 (5): 1882-1896.

Gao, Y. and S.W. Pimplikar (2001). The gamma -secretase-cleaved C-terminal fragment of amyloid precursor protein mediates signaling to the nucleus. Proc Natl Acad Sci U S A, 98 (26): 14979-14984.

Giannakopoulos, P., P.R. Hof, J.P. Michel, J. Guimon and C. Bouras (1997). Cerebral cortex pathology in aging and Alzheimer's disease: a quantitative survey of large hospital-based geriatric and psychiatric cohorts. Brain Res Brain Res Rev, 25 (2): 217-245.

Giunta, B., F. Fernandez, W.V. Nikolic, D. Obregon, E. Rrapo, T. Town and J. Tan (2008). Inflammaging as a prodrome to Alzheimer's disease. J Neuroinflammation, 5 51.

Glabe, C.G. (2008). Structural classification of toxic amyloid oligomers. J Biol Chem, 283 (44): 29639-29643.

Glenner, G.G. and C.W. Wong (1984). Alzheimer's disease: initial report of the purification and characterization of a novel cerebrovascular amyloid protein. Biochem Biophys Res Commun, 120 (3): 885-890.

Goate, A., M.C. Chartier-Harlin, M. Mullan, J. Brown, F. Crawford, L. Fidani, L. Giuffra, A. Haynes, N. Irving, L. James, et al. (1991). Segregation of a missense mutation in the amyloid precursor protein gene with familial Alzheimer's disease. Nature, 349 (6311): 704-706.

Goffinet, A.M. (1984). Events governing organization of postmigratory neurons: studies on brain development in normal and reeler mice. Brain Res, 319 (3): 261-296.

Gold, P.E. (2003). Acetylcholine modulation of neural systems involved in learning and memory. Neurobiol Learn Mem, 80 (3): 194-210.

Goldsworthy, S.M., P.S. Stockton, C.S. Trempus, J.F. Foley and R.R. Maronpot (1999). Effects of fixation on RNA extraction and amplification from laser capture microdissected tissue. Mol Carcinog, 25 (2): 86-91.

Gonzalez-Billault, C., J.A. Del Rio, J.M. Urena, E.M. Jimenez-Mateos, M.J. Barallobre, M. Pascual, L. Pujadas, S. Simo, A.L. Torre, R. Gavin, et al. (2005). A role of MAP1B in Reelin-dependent neuronal migration. Cereb Cortex, 15 (8): 1134-1145.

Gottfries, C.G. (1990). Neurochemical aspects on aging and diseases with cognitive impairment. J Neurosci Res, 27 (4): 541-547.

Gotthardt, M., M. Trommsdorff, M.F. Nevitt, J. Shelton, J.A. Richardson, W. Stockinger, J. Nimpf and J. Herz (2000). Interactions of the low density lipoprotein receptor gene family with cytosolic adaptor and scaffold proteins suggest diverse biological functions in cellular communication and signal transduction. J Biol Chem, 275 (33): 25616-25624.

Gotz, J., F. Chen, J. van Dorpe and R.M. Nitsch (2001). Formation of neurofibrillary tangles in P301l tau transgenic mice induced by Abeta 42 fibrils. Science, 293 (5534): 1491-1495.

Gralle, M. and S.T. Ferreira (2007). Structure and functions of the human amyloid precursor protein: the whole is more than the sum of its parts. Prog Neurobiol, 82 (1): 11-32.

Grathwohl, S.A., R.E. Kalin, T. Bolmont, S. Prokop, G. Winkelmann, S.A. Kaeser, J. Odenthal, R. Radde, T. Eldh, S. Gandy, et al. (2009). Formation and maintenance of Alzheimer's disease beta-amyloid plaques in the absence of microglia. Nat Neurosci, 12 (11): 1361-1363.

Gray, B.C., Z. Siskova, V.H. Perry and V. O'Connor (2009). Selective presynaptic degeneration in the synaptopathy associated with ME7-induced hippocampal pathology. Neurobiol Dis, 35 (1): 63-74.

Grundke-Iqbal, I., K. Iqbal, Y.C. Tung, M. Quinlan, H.M. Wisniewski and L.I. Binder (1986). Abnormal phosphorylation of the microtubule-associated protein tau (tau) in Alzheimer cytoskeletal pathology. Proc Natl Acad Sci U S A, 83 (13): 4913-4917.

Guidotti, A., J. Auta, J.M. Davis, V. Di-Giorgi-Gerevini, Y. Dwivedi, D.R. Grayson, F. Impagnatiello, G. Pandey, C. Pesold, R. Sharma, et al. (2000). Decrease in reelin and glutamic acid decarboxylase67 (GAD67) expression in schizophrenia and bipolar disorder: a postmortem brain study. Arch Gen Psychiatry, 57 (11): 1061-1069.

Guo, J., T.J. Colgan, L.V. DeSouza, M.J. Rodrigues, A.D. Romaschin and K.W. Siu (2005). Direct analysis of laser capture microdissected endometrial carcinoma and epithelium by matrix-assisted laser desorption/ionization mass spectrometry. Rapid Commun Mass Spectrom, 19 (19): 2762-2766.

Haass, C., E.H. Koo, A. Mellon, A.Y. Hung and D.J. Selkoe (1992). Targeting of cell-surface beta-amyloid precursor protein to lysosomes: alternative processing into amyloid-bearing fragments. Nature, 357 (6378): 500-503.

Haass, C. and D.J. Selkoe (2007). Soluble protein oligomers in neurodegeneration: lessons from the Alzheimer's amyloid beta-peptide. Nat Rev Mol Cell Biol, 8 (2): 101-112.

Hack, I., S. Hellwig, D. Junghans, B. Brunne, H.H. Bock, S. Zhao and M. Frotscher (2007). Divergent roles of ApoER2 and Vldlr in the migration of cortical neurons. Development, 134 (21): 3883-3891.

Haenggi, T., M.C. Schaub and J.M. Fritschy (2005). Molecular heterogeneity of the dystrophin-associated protein complex in the mouse kidney nephron: differential alterations in the absence of utrophin and dystrophin. Cell Tissue Res, 319 (2): 299-313.

Haenggi, T. and J.M. Fritschy (2006). Role of dystrophin and utrophin for assembly and function of the dystrophin glycoprotein complex in non-muscle tissue. Cell Mol Life Sci, 63 (14): 1614-1631.

Hardy, J. and D.J. Selkoe (2002). The amyloid hypothesis of Alzheimer's disease: progress and problems on the road to therapeutics. Science, 297 (5580): 353-356.

Hartley, D.M., D.M. Walsh, C.P. Ye, T. Diehl, S. Vasquez, P.M. Vassilev, D.B. Teplow and D.J. Selkoe (1999). Protofibrillar intermediates of amyloid beta-protein induce acute electrophysiological changes and progressive neurotoxicity in cortical neurons. J Neurosci, 19 (20): 8876-8884.

Hellwig, S., I. Hack, J. Kowalski, B. Brunne, J. Jarowyj, A. Unger, H.H. Bock, D. Junghans and M. Frotscher (2011). Role for Reelin in neurotransmitter release. J Neurosci, 31 (7): 2352-2360.

Herrup, K. (2010). Reimagining Alzheimer's disease--an age-based hypothesis. J Neurosci, 30 (50): 16755-16762.

Herz, J. and Y. Chen (2006). Reelin, lipoprotein receptors and synaptic plasticity. Nat Rev Neurosci, 7 (11): 850-859.

Herz, J. (2009). Apolipoprotein E receptors in the nervous system. Curr Opin Lipidol, 20 (3): 190-196.

Hibi, T. and M. Hattori (2009). The N-terminal fragment of Reelin is generated after endocytosis and released through the pathway regulated by Rab11. FEBS Lett, 583 (8): 1299-1303.

Hickman, S.E., E.K. Allison and J. El Khoury (2008). Microglial dysfunction and defective beta-amyloid clearance pathways in aging Alzheimer's disease mice. J Neurosci, 28 (33): 8354-8360.

Hiesberger, T., M. Trommsdorff, B.W. Howell, A. Goffinet, M.C. Mumby, J.A. Cooper and J. Herz (1999). Direct binding of Reelin to VLDL receptor and ApoE receptor 2 induces tyrosine phosphorylation of disabled-1 and modulates tau phosphorylation. Neuron, 24 (2): 481-489.

Hilbich, C., B. Kisters-Woike, J. Reed, C.L. Masters and K. Beyreuther (1991a). Aggregation and secondary structure of synthetic amyloid beta A4 peptides of Alzheimer's disease. J Mol Biol, 218 (1): 149-163.

Hilbich, C., B. Kisters-Woike, J. Reed, C.L. Masters and K. Beyreuther (1991b). Human and rodent sequence analogs of Alzheimer's amyloid beta A4 share similar properties and can be solubilized in buffers of pH 7.4. Eur J Biochem, 201 (1): 61-69.

Hilbich, C., U. Monning, C. Grund, C.L. Masters and K. Beyreuther (1993). Amyloid-like properties of peptides flanking the epitope of amyloid precursor protein-specific monoclonal antibody 22C11. J Biol Chem, 268 (35): 26571-26577.

Hirotsune, S., T. Takahara, N. Sasaki, K. Hirose, A. Yoshiki, T. Ohashi, M. Kusakabe, Y. Murakami, M. Muramatsu, S. Watanabe, et al. (1995). The reeler gene encodes a protein with an EGF-like motif expressed by pioneer neurons. Nat Genet, 10 (1): 77-83.

Hirtz, D., D.J. Thurman, K. Gwinn-Hardy, M. Mohamed, A.R. Chaudhuri and R. Zalutsky (2007). How common are the "common" neurologic disorders? Neurology, 68 (5): 326-337.

Hoe, H.S., T.S. Tran, Y. Matsuoka, B.W. Howell and G.W. Rebeck (2006). Dab1 and Reelin effects on APP and ApoEr2 trafficking and processing. J Biol Chem, 281 (46): 35176-35185.

Hoe, H.S. and G.W. Rebeck (2008). Regulated proteolysis of APP and ApoE receptors. Mol Neurobiol, 37 (1): 64-72.

Hoe, H.S., Z. Fu, A. Makarova, J.Y. Lee, C. Lu, L. Feng, A. Pajoohesh-Ganji, Y. Matsuoka, B.T. Hyman, M.D. Ehlers, et al. (2009a). The effects of amyloid precursor protein on postsynaptic composition and activity. J Biol Chem, 284 (13): 8495-8506.

Hoe, H.S., K.J. Lee, R.S. Carney, J. Lee, A. Markova, J.Y. Lee, B.W. Howell, B.T. Hyman, D.T. Pak, G. Bu, et al. (2009b). Interaction of reelin with amyloid precursor protein promotes neurite outgrowth. J Neurosci, 29 (23): 7459-7473.

Hollingworth, P., D. Harold, R. Sims, A. Gerrish, J.C. Lambert, M.M. Carrasquillo, R. Abraham, M.L. Hamshere, J.S. Pahwa, V. Moskvina, et al. (2011). Common variants at ABCA7, MS4A6A/MS4A4E, EPHA1, CD33 and CD2AP are associated with Alzheimer's disease. Nat Genet, 43 (5): 429-435.

Homayouni, R., D.S. Rice, M. Sheldon and T. Curran (1999). Disabled-1 binds to the cytoplasmic domain of amyloid precursor-like protein 1. J Neurosci, 19 (17): 7507-7515.

Hong, S.E., Y.Y. Shugart, D.T. Huang, S.A. Shahwan, P.E. Grant, J.O. Hourihane, N.D. Martin and C.A. Walsh (2000). Autosomal recessive lissencephaly with cerebellar hypoplasia is associated with human RELN mutations. Nat Genet, 26 (1): 93-96.

Hoozemans, J.J., R. Veerhuis, J.M. Rozemuller and P. Eikelenboom (2006). Neuroinflammation and regeneration in the early stages of Alzheimer's disease pathology. Int J Dev Neurosci, 24 (2-3): 157-165.

Howell, B.W., L.M. Lanier, R. Frank, F.B. Gertler and J.A. Cooper (1999). The disabled 1 phosphotyrosine-binding domain binds to the internalization signals of transmembrane glycoproteins and to phospholipids. Mol Cell Biol, 19 (7): 5179-5188.

Hsieh, H., J. Boehm, C. Sato, T. Iwatsubo, T. Tomita, S. Sisodia and R. Malinow (2006). AMPAR removal underlies Abeta-induced synaptic depression and dendritic spine loss. Neuron, 52 (5): 831-843.

Hutchinson, R.W., A.G. Cox, C.W. McLeod, P.S. Marshall, A. Harper, E.L. Dawson and D.R. Howlett (2005). Imaging and spatial distribution of beta-amyloid peptide and metal ions in Alzheimer's plaques by laser ablation-inductively coupled plasma-mass spectrometry. Anal Biochem, 346 (2): 225-233.

Hwang, S.I., J. Thumar, D.H. Lundgren, K. Rezaul, V. Mayya, L. Wu, J. Eng, M.E. Wright and D.K. Han (2007). Direct cancer tissue proteomics: a method to identify candidate cancer biomarkers from formalin-fixed paraffin-embedded archival tissues. Oncogene, 26 (1): 65-76.

Impagnatiello, F., A.R. Guidotti, C. Pesold, Y. Dwivedi, H. Caruncho, M.G. Pisu, D.P. Uzunov, N.R. Smalheiser, J.M. Davis, G.N. Pandey, et al. (1998). A decrease of reelin expression as a putative vulnerability factor in schizophrenia. Proc Natl Acad Sci U S A, 95 (26): 15718-15723.

Irino, S. and J. Fujita (1994). [Granulomatous pneumonitis]. Ryoikibetsu Shokogun Shirizu, (4): 972-974.

Ittner, L.M., Y.D. Ke, F. Delerue, M. Bi, A. Gladbach, J. van Eersel, H. Wolfing, B.C. Chieng, M.J. Christie, I.A. Napier, et al. (2010). Dendritic function of tau mediates amyloid-beta toxicity in Alzheimer's disease mouse models. Cell, 142 (3): 387-397.

Iwai, A., E. Masliah, M. Yoshimoto, N. Ge, L. Flanagan, H.A. de Silva, A. Kittel and T. Saitoh (1995). The precursor protein of non-A beta component of Alzheimer's disease amyloid is a presynaptic protein of the central nervous system. Neuron, 14 (2): 467-475.

Jain, E., A. Bairoch, S. Duvaud, I. Phan, N. Redaschi, B.E. Suzek, M.J. Martin, P. McGarvey and E. Gasteiger (2009). Infrastructure for the life sciences: design and implementation of the UniProt website. BMC Bioinformatics, 10 136.

Jarrett, J.T., E.P. Berger and P.T. Lansbury, Jr. (1993). The carboxy terminus of the beta amyloid protein is critical for the seeding of amyloid formation: implications for the pathogenesis of Alzheimer's disease. Biochemistry, 32 (18): 4693-4697.

Jarrett, J.T. and P.T. Lansbury, Jr. (1993). Seeding "one-dimensional crystallization" of amyloid: a pathogenic mechanism in Alzheimer's disease and scrapie? Cell, 73 (6): 1055-1058.

Jellinger, K. and P. Riederer (1984). Dementia in Parkinson's disease and (pre) senile dementia of Alzheimer type: morphological aspects and changes in the intracerebral MAO activity. Adv Neurol, 40 199-210.

Johann, D.J., J. Rodriguez-Canales, S. Mukherjee, D.A. Prieto, J.C. Hanson, M. Emmert-Buck and J. Blonder (2009). Approaching solid tumor heterogeneity on a cellular basis by tissue proteomics using laser capture microdissection and biological mass spectrometry. J Proteome Res, 8 (5): 2310-2318.

Jones, A., P. Kulozik, A. Ostertag and S. Herzig (2009). Common pathological processes and transcriptional pathways in Alzheimer's disease and type 2 diabetes. J Alzheimers Dis, 16 (4): 787-808.

Jossin, Y., N. Ignatova, T. Hiesberger, J. Herz, C. Lambert de Rouvroit and A.M. Goffinet (2004). The central fragment of Reelin, generated by proteolytic processing in vivo, is critical to its function during cortical plate development. J Neurosci, 24 (2): 514-521.

Jossin, Y. and A.M. Goffinet (2007). Reelin signals through phosphatidylinositol 3-kinase and Akt to control cortical development and through mTor to regulate dendritic growth. Mol Cell Biol, 27 (20): 7113-7124.

Jossin, Y., L. Gui and A.M. Goffinet (2007). Processing of Reelin by embryonic neurons is important for function in tissue but not in dissociated cultured neurons. J Neurosci, 27 (16): 4243-4252.

Jucker, M. and D.K. Ingram (1994). Age-related fibrillar material in mouse brain. Assessing its potential as a biomarker of aging and as a model of human neurodegenerative disease. Ann N Y Acad Sci, 719 238-247.

Jucker, M., L.C. Walker, L.J. Martin, C.A. Kitt, H.K. Kleinman, D.K. Ingram and D.L. Price (1992). Age-associated inclusions in normal and transgenic mouse brain. Science, 255 (5050): 1443-1445.

Jucker, M., L.C. Walker, H. Kuo, M. Tian and D.K. Ingram (1994a). Age-related fibrillar deposits in brains of C57BL/6 mice. A review of localization, staining characteristics, and strain specificity. Mol Neurobiol, 9 (1-3): 125-133.

Jucker, M., L.C. Walker, P. Schwarb, J. Hengemihle, H. Kuo, A.D. Snow, F. Bamert and D.K. Ingram (1994b). Age-related deposition of glia-associated fibrillar material in brains of C57BL/6 mice. Neuroscience, 60 (4): 875-889.

Jucker, M. and D.K. Ingram (1997). Murine models of brain aging and age-related neurodegenerative diseases. Behav Brain Res, 85 (1): 1-26.

Kamenetz, F., T. Tomita, H. Hsieh, G. Seabrook, D. Borchelt, T. Iwatsubo, S. Sisodia and R. Malinow (2003). APP processing and synaptic function. Neuron, 37 (6): 925-937.

Keller, A., A.I. Nesvizhskii, E. Kolker and R. Aebersold (2002). Empirical statistical model to estimate the accuracy of peptide identifications made by MS/MS and database search. Anal Chem, 74 (20): 5383-5392.

Keller, A., J. Eng, N. Zhang, X.J. Li and R. Aebersold (2005). A uniform proteomics MS/MS analysis platform utilizing open XML file formats. Mol Syst Biol, 1 2005 0017.

Kerjan, G. and J.G. Gleeson (2007). A missed exit: Reelin sets in motion Dab1 polyubiquitination to put the break on neuronal migration. Genes Dev, 21 (22): 2850-2854.

Kern, D.S., K.N. Maclean, H. Jiang, E.Y. Synder, J.R. Sladek, Jr. and K.B. Bjugstad (2011). Neural stem cells reduce hippocampal tau and reelin accumulation in aged Ts65Dn Down syndrome mice. Cell Transplant, 20 (3): 371-379.

Kim, J., J.M. Basak and D.M. Holtzman (2009). The role of apolipoprotein E in Alzheimer's disease. Neuron, 63 (3): 287-303.

Klyubin, I., D.M. Walsh, C.A. Lemere, W.K. Cullen, G.M. Shankar, V. Betts, E.T. Spooner, L. Jiang, R. Anwyl, D.J. Selkoe, et al. (2005). Amyloid beta protein immunotherapy neutralizes Abeta oligomers that disrupt synaptic plasticity in vivo. Nat Med, 11 (5): 556-561.

Knobloch, M., M. Farinelli, U. Konietzko, R.M. Nitsch and I.M. Mansuy (2007a). Abeta oligomer-mediated long-term potentiation impairment involves protein phosphatase 1-dependent mechanisms. J Neurosci, 27 (29): 7648-7653.

Knobloch, M., U. Konietzko, D.C. Krebs and R.M. Nitsch (2007b). Intracellular Abeta and cognitive deficits precede beta-amyloid deposition in transgenic arcAbeta mice. Neurobiol Aging, 28 (9): 1297-1306.

Knuesel, I., V. Riban, R.A. Zuellig, M.C. Schaub, R.M. Grady, J.R. Sanes and J.M. Fritschy (2002). Increased vulnerability to kainate-induced seizures in utrophin-knockout mice. Eur J Neurosci, 15 (9): 1474-1484.

Knuesel, I., M. Nyffeler, C. Mormede, M. Muhia, U. Meyer, S. Pietropaolo, B.K. Yee, C.R. Pryce, F.M. LaFerla, A. Marighetto, et al. (2009). Age-related accumulation of Reelin in amyloid-like deposits. Neurobiol Aging, 30 (5): 697-716.

Knuesel, I. (2010). Reelin-mediated signaling in neuropsychiatric and neurodegenerative diseases. Prog Neurobiol,

Koch, S., V. Strasser, C. Hauser, D. Fasching, C. Brandes, T.M. Bajari, W.J. Schneider and J. Nimpf (2002). A secreted soluble form of ApoE receptor 2 acts as a dominant-negative receptor and inhibits Reelin signaling. Embo J, 21 (22): 5996-6004.

Kocherhans, S., A. Madhusudan, J. Doehner, K.S. Breu, R.M. Nitsch, J.M. Fritschy and I. Knuesel (2010). Reduced Reelin expression accelerates amyloid-beta plaque formation and tau pathology in transgenic Alzheimer's disease mice. J Neurosci, 30 (27): 9228-9240.

Kohno, S., T. Kohno, Y. Nakano, K. Suzuki, M. Ishii, H. Tagami, A. Baba and M. Hattori (2009). Mechanism and significance of specific proteolytic cleavage of Reelin. Biochem Biophys Res Commun, 380 (1): 93-97.

Konietzko, U. (2011). AICD Nuclear Signaling and its Possible Contribution to Alzheimer's Disease. Curr Alzheimer Res, in press.

Kramer, P.L., H. Xu, R.L. Woltjer, S.K. Westaway, D. Clark, D. Erten-Lyons, J.A. Kaye, K.A. Welsh-Bohmer, J.C. Troncoso, W.R. Markesbery, et al. (2010). Alzheimer disease pathology in cognitively healthy elderly: A genome-wide study. Neurobiol Aging,

Kubasak, M.D., R. Brooks, S. Chen, S.A. Villeda and P.E. Phelps (2004). Developmental distribution of reelin-positive cells and their secreted product in the rodent spinal cord. J Comp Neurol, 468 (2): 165-178.

Kubo, K., K. Mikoshiba and K. Nakajima (2002). Secreted Reelin molecules form homodimers. Neurosci Res, 43 (4): 381-388.

Kuo, H., D.K. Ingram, L.C. Walker, M. Tian, J.M. Hengemihle and M. Jucker (1996). Similarities in the age-related hippocampal deposition of periodic acid-schiff-positive granules in the senescence-accelerated mouse P8 and C57BL/6 mouse strains. Neuroscience, 74 (3): 733-740.

Kuster, B., M. Schirle, P. Mallick and R. Aebersold (2005). Scoring proteomes with proteotypic peptide probes. Nat Rev Mol Cell Biol, 6 (7): 577-583.

Lacor, P.N., D.R. Grayson, J. Auta, I. Sugaya, E. Costa and A. Guidotti (2000). Reelin secretion from glutamatergic neurons in culture is independent from neurotransmitter regulation. Proc Natl Acad Sci U S A, 97 (7): 3556-3561.

Lacor, P.N., M.C. Buniel, L. Chang, S.J. Fernandez, Y. Gong, K.L. Viola, M.P. Lambert, P.T. Velasco, E.H. Bigio, C.E. Finch, et al. (2004). Synaptic targeting by Alzheimer's-related amyloid beta oligomers. J Neurosci, 24 (45): 10191-10200.

Lamar, C.H., E.J. Hinsman and C.K. Henrikson (1976). Alterations in the hippocampus of aged mice. Acta Neuropathol (Berl), 36 (4): 387-391.

Lambert de Rouvroit, C., V. de Bergeyck, C. Cortvrindt, I. Bar, Y. Eeckhout and A.M. Goffinet (1999). Reelin, the extracellular matrix protein deficient in reeler mutant mice, is processed by a metalloproteinase. Exp Neurol, 156 (1): 214-217.

Lambert de Rouvroit, C. and A.M. Goffinet (1998). The reeler mouse as a model of brain development. Adv Anat Embryol Cell Biol, 150 1-106.

Lambert, M.P., A.K. Barlow, B.A. Chromy, C. Edwards, R. Freed, M. Liosatos, T.E. Morgan, I. Rozovsky, B. Trommer, K.L. Viola, et al. (1998). Diffusible, nonfibrillar ligands derived from Abeta1-42 are potent central nervous system neurotoxins. Proc Natl Acad Sci U S A, 95 (11): 6448-6453.

Lambert, J.C., S. Heath, G. Even, D. Campion, K. Sleegers, M. Hiltunen, O. Combarros, D. Zelenika, M.J. Bullido, B. Tavernier, et al. (2009). Genome-wide association study identifies variants at CLU and CR1 associated with Alzheimer's disease. Nat Genet, 41 (10): 1094-1099.

Lee, S., Y. Sato and R.A. Nixon (2011). Lysosomal proteolysis inhibition selectively disrupts axonal transport of degradative organelles and causes an Alzheimer's-like axonal dystrophy. J Neurosci, 31 (21): 7817-7830.

Lee, V.M., M. Goedert and J.Q. Trojanowski (2001). Neurodegenerative tauopathies. Annu Rev Neurosci, 24 1121-1159.

Leemhuis, J., E. Bouche, M. Frotscher, F. Henle, L. Hein, J. Herz, D.K. Meyer, M. Pichler, G. Roth, C. Schwan, et al. (2010). Reelin signals through apolipoprotein E receptor 2 and Cdc42 to increase growth cone motility and filopodia formation. J Neurosci, 30 (44): 14759-14772.

Leighton, S.B. (1981). SEM images of block faces, cut by a miniature microtome within the SEM - a technical note. Scan Electron Microsc, (Pt 2): 73-76.

Levy-Lahad, E., W. Wasco, P. Poorkaj, D.M. Romano, J. Oshima, W.H. Pettingell, C.E. Yu, P.D. Jondro, S.D. Schmidt, K. Wang, et al. (1995). Candidate gene for the chromosome 1 familial Alzheimer's disease locus. Science, 269 (5226): 973-977.

Lewis, J., D.W. Dickson, W.L. Lin, L. Chisholm, A. Corral, G. Jones, S.H. Yen, N. Sahara, L. Skipper, D. Yager, et al. (2001). Enhanced neurofibrillary degeneration in transgenic mice expressing mutant tau and APP. Science, 293 (5534): 1487-1491.

Li, Y., L. Liu, S.W. Barger and W.S. Griffin (2003). Interleukin-1 mediates pathological effects of microglia on tau phosphorylation and on synaptophysin synthesis in cortical neurons through a p38-MAPK pathway. J Neurosci, 23 (5): 1605-1611.

Liao, L., D. Cheng, J. Wang, D.M. Duong, T.G. Losik, M. Gearing, H.D. Rees, J.J. Lah, A.I. Levey and J. Peng (2004a). Proteomic characterization of postmortem amyloid plaques isolated by laser capture microdissection. J Biol Chem, 279 (35): 37061-37068.

Liao, Y.F., B.J. Wang, H.T. Cheng, L.H. Kuo and M.S. Wolfe (2004b). Tumor necrosis factor-alpha, interleukin-1beta, and interferon-gamma stimulate gamma-secretase-mediated cleavage of amyloid precursor protein through a JNK-dependent MAPK pathway. J Biol Chem, 279 (47): 49523-49532.

Liesi, P., S. Kaakkola, D. Dahl and A. Vaheri (1984). Laminin is induced in astrocytes of adult brain by injury. Embo J, 3 (3): 683-686.

Liu, W.S., C. Pesold, M.A. Rodriguez, G. Carboni, J. Auta, P. Lacor, J. Larson, B.G. Condie, A. Guidotti and E. Costa (2001). Down-regulation of dendritic spine and glutamic acid decarboxylase 67 expressions in the reelin haploinsufficient heterozygous reeler mouse. Proc Natl Acad Sci U S A, 98 (6): 3477-3482.

Lu, Q., N. Murugesan, J.A. Macdonald, S.L. Wu, J.S. Pachter and W.S. Hancock (2008). Analysis of mouse brain microvascular endothelium using immuno-laser capture microdissection coupled to a hybrid linear ion trap with Fourier transform-mass spectrometry proteomics platform. Electrophoresis, 29 (12): 2689-2695.

Lucin, K.M. and T. Wyss-Coray (2009). Immune activation in brain aging and neurodegeneration: too much or too little? Neuron, 64 (1): 110-122.

Lugli, G., J.M. Krueger, J.M. Davis, A.M. Persico, F. Keller and N.R. Smalheiser (2003). Methodological factors influencing measurement and processing of plasma reelin in humans. BMC Biochem, 4 9.

Luterman, J.D., V. Haroutunian, S. Yemul, L. Ho, D. Purohit, P.S. Aisen, R. Mohs and G.M. Pasinetti (2000). Cytokine gene expression as a function of the clinical progression of Alzheimer disease dementia. Arch Neurol, 57 (8): 1153-1160.

Lyon, M., G. Rushton, J.A. Askari, M.J. Humphries and J.T. Gallagher (2000). Elucidation of the structural features of heparan sulfate important for interaction with the Hep-2 domain of fibronectin. J Biol Chem, 275 (7): 4599-4606.

Madhusudan, A., D. Krstic, J. Doehner, P. Vogel, C. Imhof, A. Manalastas, M. Hilfiker, S. Pfister, C. Schwerdel, F. LaFerla, et al. Systemic immune challenges trigger and drive Alzheimer-like neuropathology in mice. Submitted to Nature.

Madhusudan, A., C. Sidler and I. Knuesel (2009). Accumulation of reelin-positive plaques is accompanied by a decline in basal forebrain projection neurons during normal aging. Eur J Neurosci, 30 (6): 1064-1076.

Malenka, R.C. (2003). The long-term potential of LTP. Nat Rev Neurosci, 4 (11): 923-926.

Mallick, P., M. Schirle, S.S. Chen, M.R. Flory, H. Lee, D. Martin, J. Ranish, B. Raught, R. Schmitt, T. Werner, et al. (2007). Computational prediction of proteotypic peptides for quantitative proteomics. Nat Biotechnol, 25 (1): 125-131.

Mandybur, T.I., I. Ormsby and F.P. Zemlan (1989). Cerebral aging: a quantitative study of gliosis in old nude mice. Acta Neuropathol (Berl), 77 (5): 507-513.

Manich, G., C. Mercader, J. del Valle, J. Duran-Vilaregut, A. Camins, M. Pallas, J. Vilaplana and C. Pelegri (2011). Characterization of amyloid-beta granules in the hippocampus of SAMP8 mice. J Alzheimers Dis, 25 (3): 535-546.

Mann, J.J., M. Stanley, S. Gershon and M. Rossor (1980). Mental symptoms in Huntington's disease and a possible primary aminergic neuron lesion. Science, 210 (4476): 1369-1371.

Martin, R., A. Gutierrez, A. Penafiel, M. Marin-Padilla and A. de la Calle (1999). Persistence of Cajal-Retzius cells in the adult human cerebral cortex. An immunohistochemical study. Histol Histopathol, 14 (2): 487-490.

Martinez-Cerdeno, V., M.J. Galazo, C. Cavada and F. Clasca (2002). Reelin immunoreactivity in the adult primate brain: intracellular localization in projecting and local circuit neurons of the cerebral cortex, hippocampus and subcortical regions. Cereb Cortex, 12 (12): 1298-1311.

Martinez-Cerdeno, V., M.J. Galazo and F. Clasca (2003). Reelin-immunoreactive neurons, axons, and neuropil in the adult ferret brain: evidence for axonal secretion of reelin in long axonal pathways. J Comp Neurol, 463 (1): 92-116.

Matsuki, T., A. Pramatarova and B.W. Howell (2008). Reduction of Crk and CrkL expression blocks reelin-induced dendritogenesis. J Cell Sci, 121 (Pt 11): 1869-1875.

Mayeux, R., M.X. Tang, D.M. Jacobs, J. Manly, K. Bell, C. Merchant, S.A. Small, Y. Stern, H.M. Wisniewski and P.D. Mehta (1999). Plasma amyloid beta-peptide 1-42 and incipient Alzheimer's disease. Ann Neurol, 46 (3): 412-416.

McGeer, P.L., S. Itagaki, H. Tago and E.G. McGeer (1987). Reactive microglia in patients with senile dementia of the Alzheimer type are positive for the histocompatibility glycoprotein HLA-DR. Neurosci Lett, 79 (1-2): 195-200.

McGeer, P.L., M. Schulzer and E.G. McGeer (1996). Arthritis and anti-inflammatory agents as possible protective factors for Alzheimer's disease: a review of 17 epidemiologic studies. Neurology, 47 (2): 425-432.

McGeer, P.L. and E.G. McGeer (2002). Local neuroinflammation and the progression of Alzheimer's disease. J Neurovirol, 8 (6): 529-538.

McLean, C.A., R.A. Cherny, F.W. Fraser, S.J. Fuller, M.J. Smith, K. Beyreuther, A.I. Bush and C.L. Masters (1999). Soluble pool of Abeta amyloid as a determinant of severity of neurodegeneration in Alzheimer's disease. Ann Neurol, 46 (6): 860-866.

McMaster, K.R., J.M. Powers, G.R. Hennigar, Jr., H.J. Wohltmann and G.H. Farr, Jr. (1979). Nervous system involvement in type IV glycogenosis. Arch Pathol Lab Med, 103 (3): 105-111.

Melle, C., G. Ernst, B. Schimmel, A. Bleul, S. Koscielny, A. Wiesner, R. Bogumil, U. Moller, D. Osterloh, K.J. Halbhuber, et al. (2003). Biomarker discovery and identification in laser microdissected head and neck squamous cell carcinoma with ProteinChip technology, two-dimensional gel electrophoresis, tandem mass spectrometry, and immunohistochemistry. Mol Cell Proteomics, 2 (7): 443-452.

Meyer, G. and A.M. Goffinet (1998). Prenatal development of reelin-immunoreactive neurons in the human neocortex. J Comp Neurol, 397 (1): 29-40.

Meyer, U., J. Feldon, M. Schedlowski and B.K. Yee (2005). Towards an immuno-precipitated neurodevelopmental animal model of schizophrenia. Neurosci Biobehav Rev, 29 (6): 913-947.

Meyer, U., M. Nyffeler, A. Engler, A. Urwyler, M. Schedlowski, I. Knuesel, B.K. Yee and J. Feldon (2006). The time of prenatal immune challenge determines the specificity of inflammation-mediated brain and behavioral pathology. J Neurosci, 26 (18): 4752-4762.

Meyer, U., M. Nyffeler, S. Schwendener, I. Knuesel, B.K. Yee and J. Feldon (2008a). Relative prenatal and postnatal maternal contributions to schizophrenia-related neurochemical dysfunction after in utero immune challenge. Neuropsychopharmacology, 33 (2): 441-456.

Meyer, U., M. Nyffeler, B.K. Yee, I. Knuesel and J. Feldon (2008b). Adult brain and behavioral pathological markers of prenatal immune challenge during early/middle and late fetal development in mice. Brain Behav Immun, 22 (4): 469-486.

Mi, H., B. Lazareva-Ulitsky, R. Loo, A. Kejariwal, J. Vandergriff, S. Rabkin, N. Guo, A. Muruganujan, O. Doremieux, M.J. Campbell, et al. (2005). The PANTHER database of protein families, subfamilies, functions and pathways. Nucleic Acids Res, 33 (Database issue): D284-288.

Miettinen, R., A. Riedel, G. Kalesnykas, H.P. Kettunen, J. Puolivali, H. Soininen and T. Arendt (2005). Reelin-immunoreactivity in the hippocampal formation of 9-month-old wildtype mouse: effects of APP/PS1 genotype and ovariectomy. J Chem Neuroanat, 30 (2-3): 105-118.

Mikkonen, M., H. Soininen and A. Pitkanen (1997). Distribution of parvalbumin-, calretinin-, and calbindin-D28k-immunoreactive neurons and fibers in the human entorhinal cortex. J Comp Neurol, 388 (1): 64-88.

Miravalle, L., M. Calero, M. Takao, A.E. Roher, B. Ghetti and R. Vidal (2005). Amino-terminally truncated Abeta peptide species are the main component of cotton wool plaques. Biochemistry, 44 (32): 10810-10821.

Mitsuno, S., M. Takahashi, T. Gondo, Y. Hoshii, N. Hanai, T. Ishihara and M. Yamada (1999). Immunohistochemical, conventional and immunoelectron microscopical characteristics of periodic acid-Schiff-positive granules in the mouse brain. Acta Neuropathol, 98 (1): 31-38.

Morfini, G.A., M. Burns, L.I. Binder, N.M. Kanaan, N. LaPointe, D.A. Bosco, R.H. Brown, Jr., H. Brown, A. Tiwari, L. Hayward, et al. (2009). Axonal transport defects in neurodegenerative diseases. J Neurosci, 29 (41): 12776-12786.

Morimura, T., M. Hattori, M. Ogawa and K. Mikoshiba (2005). Disabled1 regulates the intracellular trafficking of reelin receptors. J Biol Chem, 280 (17): 16901-16908.

Morris, M., S. Maeda, K. Vossel and L. Mucke (2011). The many faces of tau. Neuron, 70 (3): 410-426.

Motoi, Y., M. Itaya, H. Mori, Y. Mizuno, T. Iwasaki, H. Hattori, S. Haga and K. Ikeda (2004). Apolipoprotein E receptor 2 is involved in neuritic plaque formation in APP sw mice. Neurosci Lett, 368 (2): 144-147.

Mrak, R.E. and W.S. Griffin (2005). Glia and their cytokines in progression of neurodegeneration. Neurobiol Aging, 26 (3): 349-354.

Muraoka, D., Y. Katsuyama, S. Kikkawa and T. Terashima (2007). Postnatal development of entorhinodentate projection of the Reeler mutant mouse. Dev Neurosci, 29 (1-2): 59-72.

Muresan, Z. and V. Muresan (2004). A phosphorylated, carboxy-terminal fragment of beta-amyloid precursor protein localizes to the splicing factor compartment. Hum Mol Genet, 13 (5): 475-488.

Mustafa, D., J.M. Kros and T. Luider (2008). Combining laser capture microdissection and proteomics techniques. Methods Mol Biol, 428 159-178.

Naj, A.C., G. Jun, G.W. Beecham, L.S. Wang, B.N. Vardarajan, J. Buros, P.J. Gallins, J.D. Buxbaum, G.P. Jarvik, P.K. Crane, et al. (2011). Common variants at MS4A4/MS4A6E, CD2AP, CD33 and EPHA1 are associated with late-onset Alzheimer's disease. Nat Genet, 43 (5): 436-441.

Nakamura, S., I. Akiguchi, N. Seriu, K. Ohnishi, M. Takemura, M. Ueno, H. Tomimoto, T. Kawamata, J. Kimura and M. Hosokawa (1995). Monoamine oxidase-B-positive granular structures in the hippocampus of aged senescence-accelerated mouse (SAMP8). Acta Neuropathol, 90 (6): 626-632.

Nakano, Y., T. Kohno, T. Hibi, S. Kohno, A. Baba, K. Mikoshiba, K. Nakajima and M. Hattori (2007). The extremely conserved C-terminal region of Reelin is not necessary for secretion but is required for efficient activation of downstream signaling. J Biol Chem, 282 (28): 20544-20552.

Narindrasorasak, S., D. Lowery, P. Gonzalez-DeWhitt, R.A. Poorman, B. Greenberg and R. Kisilevsky (1991). High affinity interactions between the Alzheimer's beta-amyloid precursor proteins and the basement membrane form of heparan sulfate proteoglycan. J Biol Chem, 266 (20): 12878-12883.

Nesvizhskii, A.I., A. Keller, E. Kolker and R. Aebersold (2003). A statistical model for identifying proteins by tandem mass spectrometry. Anal Chem, 75 (17): 4646-4658.

Nikolaev, A., T. McLaughlin, D.D. O'Leary and M. Tessier-Lavigne (2009). APP binds DR6 to trigger axon pruning and neuron death via distinct caspases. Nature, 457 (7232): 981-989.

Niu, S., A. Renfro, C.C. Quattrocchi, M. Sheldon and G. D'Arcangelo (2004). Reelin promotes hippocampal dendrite development through the VLDLR/ApoER2-Dab1 pathway. Neuron, 41 (1): 71-84.

Niu, S., O. Yabut and G. D'Arcangelo (2008). The Reelin signaling pathway promotes dendritic spine development in hippocampal neurons. J Neurosci, 28 (41): 10339-10348.

Nixon, R.A. (2007). Autophagy, amyloidogenesis and Alzheimer disease. J Cell Sci, 120 (Pt 23): 4081-4091.

Nixon, R.A., J. Wegiel, A. Kumar, W.H. Yu, C. Peterhoff, A. Cataldo and A.M. Cuervo (2005). Extensive involvement of autophagy in Alzheimer disease: an immuno-electron microscopy study. J Neuropathol Exp Neurol, 64 (2): 113-122.

Nyffeler, M., U. Meyer, B.K. Yee, J. Feldon and I. Knuesel (2006). Maternal immune activation during pregnancy increases limbic GABAA receptor immunoreactivity in the adult offspring: implications for schizophrenia. Neuroscience, 143 (1): 51-62.

Nyffeler, M., W.N. Zhang, J. Feldon and I. Knuesel (2007). Differential expression of PSD proteins in age-related spatial learning impairments. Neurobiol Aging, 28 (1): 143-155.

Ogawa, M., T. Miyata, K. Nakajima, K. Yagyu, M. Seike, K. Ikenaka, H. Yamamoto and K. Mikoshiba (1995). The reeler gene-associated antigen on Cajal-Retzius neurons is a crucial molecule for laminar organization of cortical neurons. Neuron, 14 (5): 899-912.

Ohkubo, N., Y.D. Lee, A. Morishima, T. Terashima, S. Kikkawa, M. Tohyama, M. Sakanaka, J. Tanaka, N. Maeda, M.P. Vitek, et al. (2003). Apolipoprotein E and Reelin ligands modulate tau phosphorylation through an apolipoprotein E receptor/disabled-1/glycogen synthase kinase-3beta cascade. Faseb J, 17 (2): 295-297.

Okun, E., K.J. Griffioen and M.P. Mattson (2011). Toll-like receptor signaling in neural plasticity and disease. Trends Neurosci, 34 (5): 269-281.

Pappas, G.D., V. Kriho and C. Pesold (2001). Reelin in the extracellular matrix and dendritic spines of the cortex and hippocampus: a comparison between wild type and heterozygous reeler mice by immunoelectron microscopy. J Neurocytol, 30 (5): 413-425.

Pappas, G.D., V. Kriho, W.S. Liu, L. Tremolizzo, G. Lugli and J. Larson (2003). Immunocytochemical localization of reelin in the olfactory bulb of the heterozygous reeler mouse: an animal model for schizophrenia. Neurol Res, 25 (8): 819-830.

Parachikova, A., M.G. Agadjanyan, D.H. Cribbs, M. Blurton-Jones, V. Perreau, J. Rogers, T.G. Beach and C.W. Cotman (2007). Inflammatory changes parallel the early stages of Alzheimer disease. Neurobiol Aging, 28 (12): 1821-1833.

Park, T.J. and T. Curran (2008). Crk and Crk-like play essential overlapping roles downstream of disabled-1 in the Reelin pathway. J Neurosci, 28 (50): 13551-13562.

Parlato, R., A. Rosica, V. Cuccurullo, L. Mansi, P. Macchia, J.D. Owens, J.F. Mushinski, M. De Felice, R.F. Bonner and R. Di Lauro (2002). A preservation method that allows recovery of intact RNA from tissues dissected by laser capture microdissection. Anal Biochem, 300 (2): 139-145.

Patel, V., B.L. Hood, A.A. Molinolo, N.H. Lee, T.P. Conrads, J.C. Braisted, D.B. Krizman, T.D. Veenstra and J.S. Gutkind (2008). Proteomic analysis of laser-captured paraffin-embedded tissues: a molecular portrait of head and neck cancer progression. Clin Cancer Res, 14 (4): 1002-1014.

Patterson, P.H. (2009). Immune involvement in schizophrenia and autism: etiology, pathology and animal models. Behav Brain Res, 204 (2): 313-321.

Paxinos, G. and K. Franklin (2001). The mouse brain in stereotaxic coordinates. Academic Press, Second Edition

Pedrioli, P.G., J.K. Eng, R. Hubley, M. Vogelzang, E.W. Deutsch, B. Raught, B. Pratt, E. Nilsson, R.H. Angeletti, R. Apweiler, et al. (2004). A common open representation of mass spectrometry data and its application to proteomics research. Nat Biotechnol, 22 (11): 1459-1466.

Penner, J.D. and A.S. Brown (2007). Prenatal infectious and nutritional factors and risk of adult schizophrenia. Expert Rev Neurother, 7 (7): 797-805.

Perez-Costas, E., M. Melendez-Ferro, Y. Santos, R. Anadon, M.C. Rodicio and H.J. Caruncho (2002). Reelin immunoreactivity in the larval sea lamprey brain. J Chem Neuroanat, 23 (3): 211-221.

Perez-Garcia, C.G., F.J. Gonzalez-Delgado, M.L. Suarez-Sola, R. Castro-Fuentes, J.M. Martin-Trujillo, R. Ferres-Torres and G. Meyer (2001). Reelin-immunoreactive neurons in the adult vertebrate pallium. J Chem Neuroanat, 21 (1): 41-51.

Perry, V.H. and V. O'Connor (2010). The role of microglia in synaptic stripping and synaptic degeneration: a revised perspective. ASN Neuro, 2 (5):

Pesold, C., F. Impagnatiello, M.G. Pisu, D.P. Uzunov, E. Costa, A. Guidotti and H.J. Caruncho (1998a). Reelin is preferentially expressed in neurons synthesizing gamma-aminobutyric acid in cortex and hippocampus of adult rats. Proc Natl Acad Sci U S A, 95 (6): 3221-3226.

Pesold, C., M.G. Pisu, F. Impagnatiello, D.P. Uzunov and H.J. Caruncho (1998b). Simultaneous detection of glutamic acid decarboxylase and reelin mRNA in adult rat neurons using in situ hybridization and immunofluorescence. Brain Res Brain Res Protoc, 3 (2): 155-160.

Peters, A., S. Palay and H. Webster (1991). The fine structure of the nervous system: Neurons and their supporting cells. Oxford University Press, Third Edition

Peters, A. (2002). Structural changes in the normally aging cerebral cortex of primates. Prog Brain Res, 136 455-465.

Pimplikar, S.W. (2009). Reassessing the amyloid cascade hypothesis of Alzheimer's disease. Int J Biochem Cell Biol, 41 (6): 1261-1268.

Price, D.L., L.J. Martin, S.S. Sisodia, M.V. Wagster, E.H. Koo, L.C. Walker, V.E. Koliatsos and L.C. Cork (1991). Aged non-human primates: an animal model of age-associated neurodegenerative disease. Brain Pathol, 1 (4): 287-296.

Pujadas, L., A. Gruart, C. Bosch, L. Delgado, C.M. Teixeira, D. Rossi, L. de Lecea, A. Martinez, J.M. Delgado-Garcia and E. Soriano (2010). Reelin regulates postnatal neurogenesis and enhances spine hypertrophy and long-term potentiation. J Neurosci, 30 (13): 4636-4649.

Qiu, S., K.M. Korwek, A.R. Pratt-Davis, M. Peters, M.Y. Bergman and E.J. Weeber (2006a). Cognitive disruption and altered hippocampus synaptic function in Reelin haploinsufficient mice. Neurobiol Learn Mem, 85 (3): 228-242.

Qiu, S., L.F. Zhao, K.M. Korwek and E.J. Weeber (2006b). Differential reelin-induced enhancement of NMDA and AMPA receptor activity in the adult hippocampus. J Neurosci, 26 (50): 12943-12955.

Qiu, S. and E.J. Weeber (2007). Reelin signaling facilitates maturation of CA1 glutamatergic synapses. J Neurophysiol, 97 (3): 2312-2321.

Querfurth, H.W. and F.M. LaFerla (2010). Alzheimer's disease. N Engl J Med, 362 (4): 329-344.

Quintanilla, R.A., D.I. Orellana, C. Gonzalez-Billault and R.B. Maccioni (2004). Interleukin-6 induces Alzheimer-type phosphorylation of tau protein by deregulating the cdk5/p35 pathway. Exp Cell Res, 295 (1): 245-257.

Rabilloud, T. (1990). Mechanisms of protein silver staining in polyacrylamide gels: a 10-year synthesis. Electrophoresis, 11 (10): 785-794.

Rabilloud, T. (1992). A comparison between low background silver diammine and silver nitrate protein stains. Electrophoresis, 13 (7): 429-439.

Rajendran, L., M. Honsho, T.R. Zahn, P. Keller, K.D. Geiger, P. Verkade and K. Simons (2006). Alzheimer's disease beta-amyloid peptides are released in association with exosomes. Proc Natl Acad Sci U S A, 103 (30): 11172-11177.

Rajendran, L., A. Schneider, G. Schlechtingen, S. Weidlich, J. Ries, T. Braxmeier, P. Schwille, J.B. Schulz, C. Schroeder, M. Simons, et al. (2008). Efficient inhibition of the Alzheimer's disease beta-secretase by membrane targeting. Science, 320 (5875): 520-523.

Ramos-Moreno, T., M.J. Galazo, C. Porrero, V. Martinez-Cerdeno and F. Clasca (2006). Extracellular matrix molecules and synaptic plasticity: immunomapping of intracellular and secreted Reelin in the adult rat brain. Eur J Neurosci, 23 (2): 401-422.

Ramsey, H.J. (1965). Ultrastructure Of Corpora Amylacea. J Neuropathol Exp Neurol, 24 25-39.

Reddy, S.S., T.E. Connor, E.J. Weeber and W. Rebeck (2011). Similarities and differences in structure, expression, and functions of VLDLR and ApoER2. Mol Neurodegener, 6 30.

Rice, D.S. and T. Curran (2001). Role of the reelin signaling pathway in central nervous system development. Annu Rev Neurosci, 24 1005-1039.

Riedel, A., R. Miettinen, J. Stieler, M. Mikkonen, I. Alafuzoff, H. Soininen and T. Arendt (2003). Reelin-immunoreactive Cajal-Retzius cells: the entorhinal cortex in normal aging and Alzheimer's disease. Acta Neuropathol, 106 (4): 291-302.

Riederer, P., C. Konradi, V. Schay, E. Kienzl, G. Birkmayer, W. Danielczyk, E. Sofic and M.B. Youdim (1987). Localization of MAO-A and MAO-B in human brain: a step in understanding the therapeutic action of L-deprenyl. Adv Neurol, 45 111-118.

Roberson, E.D., B. Halabisky, J.W. Yoo, J. Yao, J. Chin, F. Yan, T. Wu, P. Hamto, N. Devidze, G.Q. Yu, et al. (2011). Amyloid-beta/Fyn-induced synaptic, network, and cognitive impairments depend on tau levels in multiple mouse models of Alzheimer's disease. J Neurosci, 31 (2): 700-711.

Roberson, E.D., K. Scearce-Levie, J.J. Palop, F. Yan, I.H. Cheng, T. Wu, H. Gerstein, G.Q. Yu and L. Mucke (2007). Reducing endogenous tau ameliorates amyloid beta-induced deficits in an Alzheimer's disease mouse model. Science, 316 (5825): 750-754.

Roberts, R.C., L. Xu, J.K. Roche and B. Kirkpatrick (2005). Ultrastructural localization of reelin in the cortex in post-mortem human brain. J Comp Neurol, 482 (3): 294-308.

Rodriguez, A.S., B.H. Espina, V. Espina and L.A. Liotta (2008). Automated laser capture microdissection for tissue proteomics. Methods Mol Biol, 441 71-90.

Rodriguez, M.A., C. Pesold, W.S. Liu, V. Kriho, A. Guidotti, G.D. Pappas and E. Costa (2000). Colocalization of integrin receptors and reelin in dendritic spine postsynaptic densities of adult nonhuman primate cortex. Proc Natl Acad Sci U S A, 97 (7): 3550-3555.

Rogaev, E.I., E.A. Rogaeva and P. Dzhordzh-Khislop (1995a). [Direct detection of loci with pathologic trinucleotide repeats in diseases with anticipation]. Genetika, 31 (4): 578-582.

Rogaev, E.I., R. Sherrington, E.A. Rogaeva, G. Levesque, M. Ikeda, Y. Liang, H. Chi, C. Lin, K. Holman, T. Tsuda, et al. (1995b). Familial Alzheimer's disease in kindreds with missense mutations in a gene on chromosome 1 related to the Alzheimer's disease type 3 gene. Nature, 376 (6543): 775-778.

Roth, J. (2002). Protein N-glycosylation along the secretory pathway: relationship to organelle topography and function, protein quality control, and cell interactions. Chem Rev, 102 (2): 285-303.

Ryle, A.P. and C.A. Auffret (1979). The specificity of some pig and human pepsins towards synthetic peptide substrates. Biochem J, 179 (1): 247-249.

Saez-Valero, J., M. Costell, M. Sjogren, N. Andreasen, K. Blennow and J.M. Luque (2003). Altered levels of cerebrospinal fluid reelin in frontotemporal dementia and Alzheimer's disease. J Neurosci Res, 72 (1): 132-136.

Salminen, A., J. Ojala, A. Kauppinen, K. Kaarniranta and T. Suuronen (2009). Inflammation in Alzheimer's disease: amyloid-beta oligomers trigger innate immunity defence via pattern recognition receptors. Prog Neurobiol, 87 (3): 181-194.

Sassoe-Pognetto, M., H. Wassle and U. Grunert (1994). Glycinergic synapses in the rod pathway of the rat retina: cone bipolar cells express the alpha 1 subunit of the glycine receptor. J Neurosci, 14 (8): 5131-5146.

Savla, G.N. and B.W. Palmer (2005). Neuropsychology in Alzheimer's disease and other dementia research. Curr Opin Psychiatry, 18 (6): 621-627.

Schad, M., M.S. Lipton, P. Giavalisco, R.D. Smith and J. Kehr (2005). Evaluation of two-dimensional electrophoresis and liquid chromatography--tandem mass spectrometry for tissue-specific protein profiling of laser-microdissected plant samples. Electrophoresis, 26 (14): 2729-2738.

Schellenberg, G.D. (1995). Genetic dissection of Alzheimer disease, a heterogeneous disorder. Proc Natl Acad Sci U S A, 92 (19): 8552-8559.

Schmechel, D.E., A.M. Saunders, W.J. Strittmatter, B.J. Crain, C.M. Hulette, S.H. Joo, M.A. Pericak-Vance, D. Goldgaber and A.D. Roses (1993). Increased amyloid beta-peptide deposition in cerebral cortex as a consequence of apolipoprotein E genotype in late-onset Alzheimer disease. Proc Natl Acad Sci U S A, 90 (20): 9649-9653.

Schmidt, R., H. Schmidt, J.D. Curb, K. Masaki, L.R. White and L.J. Launer (2002). Early inflammation and dementia: a 25-year follow-up of the Honolulu-Asia Aging Study. Ann Neurol, 52 (2): 168-174.

Scicchitano, M.S., D.A. Dalmas, R.W. Boyce, H.C. Thomas and K.S. Frazier (2009). Protein extraction of formalin-fixed, paraffin-embedded tissue enables robust proteomic profiles by mass spectrometry. J Histochem Cytochem, 57 (9): 849-860.

Selkoe, D.J. (2000). Toward a comprehensive theory for Alzheimer's disease. Hypothesis: Alzheimer's disease is caused by the cerebral accumulation and cytotoxicity of amyloid beta-protein. Ann N Y Acad Sci, 924 17-25.

Selkoe, D.J. (2002). Alzheimer's disease is a synaptic failure. Science, 298 (5594): 789-791.

Seripa, D., M.G. Matera, M. Franceschi, A. Daniele, A. Bizzarro, M. Rinaldi, F. Panza, V.M. Fazio, C. Gravina, G. D'Onofrio, et al. (2008). The RELN locus in Alzheimer's disease. J Alzheimers Dis, 14 (3): 335-344.

Shacka, J.J., K.A. Roth and J. Zhang (2008). The autophagy-lysosomal degradation pathway: role in neurodegenerative disease and therapy. Front Biosci, 13 718-736.

Shankar, G.M., B.L. Bloodgood, M. Townsend, D.M. Walsh, D.J. Selkoe and B.L. Sabatini (2007). Natural oligomers of the Alzheimer amyloid-beta protein induce reversible synapse loss by modulating an NMDA-type glutamate receptor-dependent signaling pathway. J Neurosci, 27 (11): 2866-2875.

Shankar, G.M., S. Li, T.H. Mehta, A. Garcia-Munoz, N.E. Shepardson, I. Smith, F.M. Brett, M.A. Farrell, M.J. Rowan, C.A. Lemere, et al. (2008). Amyloid-beta protein dimers isolated directly from Alzheimer's brains impair synaptic plasticity and memory. Nat Med, 14 (8): 837-842.

Shekouh, A.R., C.C. Thompson, W. Prime, F. Campbell, J. Hamlett, C.S. Herrington, N.R. Lemoine, T. Crnogorac-Jurcevic, M.W. Buechler, H. Friess, et al. (2003). Application of laser capture microdissection combined with two-dimensional electrophoresis for the discovery of differentially regulated proteins in pancreatic ductal adenocarcinoma. Proteomics, 3 (10): 1988-2001.

Sheng, J.G., R.A. Jones, X.Q. Zhou, J.M. McGinness, L.J. Van Eldik, R.E. Mrak and W.S. Griffin (2001). Interleukin-1 promotion of MAPK-p38 overexpression in experimental animals and in Alzheimer's disease: potential significance for tau protein phosphorylation. Neurochem Int, 39 (5-6): 341-348.

Sheng, J.G., S.G. Zhu, R.A. Jones, W.S. Griffin and R.E. Mrak (2000). Interleukin-1 promotes expression and phosphorylation of neurofilament and tau proteins in vivo. Exp Neurol, 163 (2): 388-391.

Sherrington, R., E.I. Rogaev, Y. Liang, E.A. Rogaeva, G. Levesque, M. Ikeda, H. Chi, C. Lin, G. Li, K. Holman, et al. (1995). Cloning of a gene bearing missense mutations in early-onset familial Alzheimer's disease. Nature, 375 (6534): 754-760.

Shevchenko, A., H. Tomas, J. Havlis, J.V. Olsen and M. Mann (2006). In-gel digestion for mass spectrometric characterization of proteins and proteomes. Nat Protoc, 1 (6): 2856-2860.

Shi, L., S.H. Fatemi, R.W. Sidwell and P.H. Patterson (2003). Maternal influenza infection causes marked behavioral and pharmacological changes in the offspring. J Neurosci, 23 (1): 297-302.

Shivers, B.D., C. Hilbich, G. Multhaup, M. Salbaum, K. Beyreuther and P.H. Seeburg (1988). Alzheimer's disease amyloidogenic glycoprotein: expression pattern in rat brain suggests a role in cell contact. Embo J, 7 (5): 1365-1370.

Siebert, J.R. and D.J. Osterhout (2011). Oligodendroglial cells express and secrete reelin. Anat Rec (Hoboken), 294 (5): 759-763.

Simone, N.L., R.F. Bonner, J.W. Gillespie, M.R. Emmert-Buck and L.A. Liotta (1998). Laser-capture microdissection: opening the microscopic frontier to molecular analysis. Trends Genet, 14 (7): 272-276.

Snow, A.D., H. Mar, D. Nochlin, K. Kimata, M. Kato, S. Suzuki, J. Hassell and T.N. Wight (1988). The presence of heparan sulfate proteoglycans in the neuritic plaques and congophilic angiopathy in Alzheimer's disease. Am J Pathol, 133 (3): 456-463.

Snow, A.D. and T.N. Wight (1989). Proteoglycans in the pathogenesis of Alzheimer's disease and other amyloidoses. Neurobiol Aging, 10 (5): 481-497.

Snyder, E.M., Y. Nong, C.G. Almeida, S. Paul, T. Moran, E.Y. Choi, A.C. Nairn, M.W. Salter, P.J. Lombroso, G.K. Gouras, et al. (2005). Regulation of NMDA receptor trafficking by amyloid-beta. Nat Neurosci, 8 (8): 1051-1058.

Stagliano, N.E., A.J. Carpino, J.S. Ross and M. Donovan (2001). Vascular gene discovery using laser capture microdissection of human blood vessels and quantitative PCR. Ann N Y Acad Sci, 947 344-349.

Stanfield, B.B. and W.M. Cowan (1979a). The development of the hippocampus and dentate gyrus in normal and reeler mice. J Comp Neurol, 185 (3): 423-459.

Stanfield, B.B. and W.M. Cowan (1979b). The morphology of the hippocampus and dentate gyrus in normal and reeler mice. J Comp Neurol, 185 (3): 393-422.

Steiner, H., R. Fluhrer and C. Haass (2008). Intramembrane proteolysis by gamma-secretase. J Biol Chem, 283 (44): 29627-29631.

Steward, O. and S.A. Scoville (1976). Cells of origin of entorhinal cortical afferents to the hippocampus and fascia dentata of the rat. J Comp Neurol, 169 (3): 347-370.

Stewart, J.M., L. Gera, D.C. Chan, E.T. Whalley, W.L. Hanson and J.S. Zuzack (1997). Potent, long-acting bradykinin antagonists for a wide range of applications. Can J Physiol Pharmacol, 75 (6): 719-724.

Stockinger, W., C. Brandes, D. Fasching, M. Hermann, M. Gotthardt, J. Herz, W.J. Schneider and J. Nimpf (2000). The reelin receptor ApoER2 recruits JNK-interacting proteins-1 and -2. J Biol Chem, 275 (33): 25625-25632.

Strasser, V., D. Fasching, C. Hauser, H. Mayer, H.H. Bock, T. Hiesberger, J. Herz, E.J. Weeber, J.D. Sweatt, A. Pramatarova, et al. (2004). Receptor clustering is involved in Reelin signaling. Mol Cell Biol, 24 (3): 1378-1386.

Strittmatter, W.J., A.M. Saunders, D. Schmechel, M. Pericak-Vance, J. Enghild, G.S. Salvesen and A.D. Roses (1993). Apolipoprotein E: high-avidity binding to beta-amyloid and increased frequency of type 4 allele in late-onset familial Alzheimer disease. Proc Natl Acad Sci U S A, 90 (5): 1977-1981.

Su, J.H., B.J. Cummings and C.W. Cotman (1992). Localization of heparan sulfate glycosaminoglycan and proteoglycan core protein in aged brain and Alzheimer's disease. Neuroscience, 51 (4): 801-813.

Suetsugu, S., T. Tezuka, T. Morimura, M. Hattori, K. Mikoshiba, T. Yamamoto and T. Takenawa (2004). Regulation of actin cytoskeleton by mDab1 through N-WASP and ubiquitination of mDab1. Biochem J, 384 (Pt 1): 1-8.

Sugiyama, H., J.A. Hainfellner, H. Lassmann, S. Indravasu and H. Budka (1993). Uncommon types of polyglucosan bodies in the human brain: distribution and relation to disease. Acta Neuropathol, 86 (5): 484-490.

Switzer, R.C., 3rd, C.R. Merril and S. Shifrin (1979). A highly sensitive silver stain for detecting proteins and peptides in polyacrylamide gels. Anal Biochem, 98 (1): 231-237.

Takahara, T., T. Ohsumi, J. Kuromitsu, K. Shibata, N. Sasaki, Y. Okazaki, H. Shibata, S. Sato, A. Yoshiki, M. Kusakabe, et al. (1996). Dysfunction of the Orleans reeler gene arising from exon skipping due to transposition of a full-length copy of an active L1 sequence into the skipped exon. Hum Mol Genet, 5 (7): 989-993.

Thal, D.R., E. Capetillo-Zarate, K. Del Tredici and H. Braak (2006). The development of amyloid beta protein deposits in the aged brain. Sci Aging Knowledge Environ, 2006 (6): re1.

Thomas, P.D., A. Kejariwal, M.J. Campbell, H. Mi, K. Diemer, N. Guo, I. Ladunga, B. Ulitsky-Lazareva, A. Muruganujan, S. Rabkin, et al. (2003). PANTHER: a browsable database of gene products organized by biological function, using curated protein family and subfamily classification. Nucleic Acids Res, 31 (1): 334-341.

Townsend, M., G.M. Shankar, T. Mehta, D.M. Walsh and D.J. Selkoe (2006). Effects of secreted oligomers of amyloid beta-protein on hippocampal synaptic plasticity: a potent role for trimers. J Physiol, 572 (Pt 2): 477-492.

Trommsdorff, M., J.P. Borg, B. Margolis and J. Herz (1998). Interaction of cytosolic adaptor proteins with neuronal apolipoprotein E receptors and the amyloid precursor protein. J Biol Chem, 273 (50): 33556-33560.

Trommsdorff, M., M. Gotthardt, T. Hiesberger, J. Shelton, W. Stockinger, J. Nimpf, R.E. Hammer, J.A. Richardson and J. Herz (1999). Reeler/Disabled-like disruption of neuronal migration in knockout mice lacking the VLDL receptor and ApoE receptor 2. Cell, 97 (6): 689-701.

Tueting, P., E. Costa, Y. Dwivedi, A. Guidotti, F. Impagnatiello, R. Manev and C. Pesold (1999). The phenotypic characteristics of heterozygous reeler mouse. Neuroreport, 10 (6): 1329-1334.

Utsunomiya-Tate, N., K. Kubo, S. Tate, M. Kainosho, E. Katayama, K. Nakajima and K. Mikoshiba (2000). Reelin molecules assemble together to form a large protein complex, which is inhibited by the function-blocking CR-50 antibody. Proc Natl Acad Sci U S A, 97 (17): 9729-9734.

Van Dooren, T., D. Muyllaert, P. Borghgraef, A. Cresens, H. Devijver, I. Van der Auwera, S. Wera, I. Dewachter and F. Van Leuven (2006). Neuronal or glial expression of human apolipoprotein e4 affects parenchymal and vascular amyloid pathology differentially in different brain regions of double- and triple-transgenic mice. Am J Pathol, 168 (1): 245-260.

Vassar, R., B.D. Bennett, S. Babu-Khan, S. Kahn, E.A. Mendiaz, P. Denis, D.B. Teplow, S. Ross, P. Amarante, R. Loeloff, et al. (1999). Beta-secretase cleavage of Alzheimer's amyloid precursor protein by the transmembrane aspartic protease BACE. Science, 286 (5440): 735-741.

Vaughan, D.W. and A. Peters (1981). The structure of neuritic plaque in the cerebral cortex of aged rats. J Neuropathol Exp Neurol, 40 (4): 472-487.

Ventruti, A., T.M. Kazdoba, S. Niu and G. D'Arcangelo (2011). Reelin deficiency causes specific defects in the molecular composition of the synapses in the adult brain. Neuroscience, 189 32-42.

von Eggeling, F., C. Melle and G. Ernst (2007). Microdissecting the proteome. Proteomics, 7 (16): 2729-2737.

von Rotz, R.C., B.M. Kohli, J. Bosset, M. Meier, T. Suzuki, R.M. Nitsch and U. Konietzko (2004). The APP intracellular domain forms nuclear multiprotein complexes and regulates the transcription of its own precursor. J Cell Sci, 117 (Pt 19): 4435-4448.

Walsh, D.M., I. Klyubin, J.V. Fadeeva, W.K. Cullen, R. Anwyl, M.S. Wolfe, M.J. Rowan and D.J. Selkoe (2002). Naturally secreted oligomers of amyloid beta protein potently inhibit hippocampal long-term potentiation in vivo. Nature, 416 (6880): 535-539.

Walsh, D.M. and D.J. Selkoe (2004). Deciphering the molecular basis of memory failure in Alzheimer's disease. Neuron, 44 (1): 181-193.

Wang, Z., B. Wang, L. Yang, Q. Guo, N. Aithmitti, Z. Songyang and H. Zheng (2009). Presynaptic and postsynaptic interaction of the amyloid precursor protein promotes peripheral and central synaptogenesis. J Neurosci, 29 (35): 10788-10801.

Washburn, M.P., D. Wolters and J.R. Yates, 3rd (2001). Large-scale analysis of the yeast proteome by multidimensional protein identification technology. Nat Biotechnol, 19 (3): 242-247.

Watanabe, M., M. Fukaya, K. Sakimura, T. Manabe, M. Mishina and Y. Inoue (1998). Selective scarcity of NMDA receptor channel subunits in the stratum lucidum (mossy fibre-recipient layer) of the mouse hippocampal CA3 subfield. Eur J Neurosci, 10 (2): 478-487.

Weeber, E.J., U. Beffert, C. Jones, J.M. Christian, E. Forster, J.D. Sweatt and J. Herz (2002). Reelin and ApoE receptors cooperate to enhance hippocampal synaptic plasticity and learning. J Biol Chem, 277 (42): 39944-39952.

Weiss, K.H., C. Johanssen, A. Tielsch, J. Herz, T. Deller, M. Frotscher and E. Forster (2003). Malformation of the radial glial scaffold in the dentate gyrus of reeler mice, scrambler mice, and ApoER2/VLDLR-deficient mice. J Comp Neurol, 460 (1): 56-65.

Wilson, K.E., R. Marouga, J.E. Prime, D.P. Pashby, P.R. Orange, S. Crosier, A.B. Keith, R. Lathe, J. Mullins, P. Estibeiro, et al. (2005). Comparative proteomic analysis using samples obtained with laser microdissection and saturation dye labelling. Proteomics, 5 (15): 3851-3858.

Wirths, O., G. Multhaup, C. Czech, V. Blanchard, G. Tremp, L. Pradier, K. Beyreuther and T.A. Bayer (2001). Reelin in plaques of beta-amyloid precursor protein and presenilin-1 double-transgenic mice. Neurosci Lett, 316 (3): 145-148.

Witter, M.P. and H.J. Groenewegen (1984). Laminar origin and septotemporal distribution of entorhinal and perirhinal projections to the hippocampus in the cat. J Comp Neurol, 224 (3): 371-385.

Wyss-Coray, T. (2006). Inflammation in Alzheimer disease: driving force, bystander or beneficial response? Nat Med, 12 (9): 1005-1015.

Yamada, T., H. Sasaki, H. Furuya, T. Miyata, I. Goto and Y. Sakaki (1987). Complementary DNA for the mouse homolog of the human amyloid beta protein precursor. Biochem Biophys Res Commun, 149 (2): 665-671.

Yamamoto, M., T. Kiyota, M. Horiba, J.L. Buescher, S.M. Walsh, H.E. Gendelman and T. Ikezu (2007). Interferon-gamma and tumor necrosis factor-alpha regulate amyloid-beta plaque deposition and beta-secretase expression in Swedish mutant APP transgenic mice. Am J Pathol, 170 (2): 680-692.

Yasui, N., T. Nogi, T. Kitao, Y. Nakano, M. Hattori and J. Takagi (2007). Structure of a receptor-binding fragment of reelin and mutational analysis reveal a recognition mechanism similar to endocytic receptors. Proc Natl Acad Sci U S A, 104 (24): 9988-9993.

Yu, W.H., A.M. Cuervo, A. Kumar, C.M. Peterhoff, S.D. Schmidt, J.H. Lee, P.S. Mohan, M. Mercken, M.R. Farmery, L.O. Tjernberg, et al. (2005). Macroautophagy--a novel Beta-amyloid peptide-generating pathway activated in Alzheimer's disease. J Cell Biol, 171 (1): 87-98.

Zaia, J. (2004). Mass spectrometry of oligosaccharides. Mass Spectrom Rev, 23 (3): 161-227.

Zellner, M., M. Veitinger and E. Umlauf (2009). The role of proteomics in dementia and Alzheimer's disease. Acta Neuropathol, 118 (1): 181-195.

Zhang, Y., R. McLaughlin, C. Goodyer and A. LeBlanc (2002). Selective cytotoxicity of intracellular amyloid beta peptide1-42 through p53 and Bax in cultured primary human neurons. J Cell Biol, 156 (3): 519-529.

Zheng, H., M. Jiang, M.E. Trumbauer, D.J. Sirinathsinghji, R. Hopkins, D.W. Smith, R.P. Heavens, G.R. Dawson, S. Boyce, M.W. Conner, et al. (1995). beta-Amyloid precursor protein-deficient mice show reactive gliosis and decreased locomotor activity. Cell, 81 (4): 525-531.

Zuckerman, L., M. Rehavi, R. Nachman and I. Weiner (2003). Immune activation during pregnancy in rats leads to a postpubertal emergence of disrupted latent inhibition, dopaminergic hyperfunction, and altered limbic morphology in the offspring: a novel neurodevelopmental model of schizophrenia. Neuropsychopharmacology, 28 (10): 1778-1789.

ABBREVIATIONS

ABC	Ammonium bi-carbonate
ACN	Acetonitrile
AD	Alzheimer's disease
AICD	APP intracellular domain
ApoE	Apolipoprotein E
ApoER2	Apolipoprotein E Receptor 2
APP	Amyloid precursor protein
Aβ	Amyloid-β
CA	Cornu ammonis
CDK5	Cyclin-dependent kinase 5
CID	Collision induced dissociation
CNS	Central Nervous System
CR	Cajal-Retzius
Dab1	Disabled-1
DOC	Sodium Deoxycholate
DTT	dithiothreitol
EM	Electron Microscopy
EOAD	Early-onset Alzheimer's disease
FA	formic acid
FDR	False discovery rate
GABA	γ-aminobutyric acid
GD17	gestation day 17
GFAP	Glial fibrillary acidic protein
GSK3β	Glycogen synthase kinase 3β
GWAS	genome wide association studies
HSPG	heparan sulfate proteoglycan
HPLC	High performance liquid chromatography
IAA	iodoacetamide
IEM	Immuno-electron microscopy
IHC	Immunohistochemistry
IR	Immunoreactivity
kDa	Kilo Dalton
LCM	laser capture microdissection
LOAD	late-onset Alzheimer's disease
LMD	Laser microdissection
LTP	long-term potentiation
ml	molecular layer
MS	Mass spectrometry
NFT	Neurofibrillary tangle
NGS	Normal goat serum
PB	Phosphate buffer
PBS	Phosphate buffered saline
PG	polyglycogen
PI3K	phosphatidylinositol 3-kinase
PolyI:C	polyriboinosinic-polyribocytidilic acid
PSEN	presenilins
pTau	hyperphosphorylated Tau
RIPA	radioimmunoprecipitation assay buffer
RP	Reversed phase
RT	room temperature
SB	Sample buffer
SDS-PAGE	sodium dodecyl sulfate polyacrylamide gel electrophoresis
SFK	Src family tyrosine kinase
slm	stratum lacunosum moleculare
sr	stratum radiatum
TBS	Tris-buffered saline
TCEP	tris-2-carboxyethyl-phosphine
TFA	trifluoroacetic acid
TPP	Trans Proteomic Pipeline
WB	Western blot
WT	wild type
VLDLR	very-low-density lipoprotein receptor

CURRICULUM VITAE

PERSONAL DATA:

Surname:	DÖHNER
First Name:	Jana
Date of Birth:	February 8th, 1982
Nationality:	German

EDUCATION:

10/2007 – 11/2011	**PhD thesis:** Institute of Pharmacology and Toxicology, University of Zurich, Zurich Switzerland Supervision: PD Dr. Irene Knuesel, Prof. Dr. Jean-Marc Fritschy Title: "Morphological and Biochemical Characterization of Reelin-Amyloid Deposition in the Aging Mouse Brain" Affiliation to the PhD program in Neuroscience of the Center for Neuroscience, Zurich (ZNZ)
10/2000 - 09/2006	**Studies in Bio-Process-Engineering** at the University of Technology Dresden, Dresden, Germany Degree: Dipl. Ing. for Bioprocess Engineering Diploma Thesis: University of Calgary (Faculty of Medicine), Calgary, Canada Supervision: Prof. Dr. Matthias Amrein; Prof. Dr. Thomas Bley Title: "Proteome Analysis at the Cellular, Sub-cellular and Nano-scale Level, Initial Experiments"
09/1992-07/2000	**Comprehensive secondary school**; „Gymnasium Albert-Schweitzer" in Limbach-Oberfrohna, Germany Abitur

PUBLICATIONS

INVITED TALKS

USGEB Meeting 2011 (Zürich, Switzerland): *"Aging enhances co-association of Reelin and amyloid-beta immunoreactivity in rodent and human brain tissue"*

ORIGINAL ARTICLES

Doehner Jana, Madhusudan Amrita, Konietzko Uwe, Fritschy Jean-Marc and Knuesel Irene. *Co-Localization of Reelin and Proteolytic AbetaPP Fragments in Hippocampal Plaques in Aged Wild-Type Mice.* J Alzheimers Dis 2010, 19:1339-57.

Jana Doehner and Irene Knuesel. *Reelin-mediated Signaling during Normal and Pathological Forms of Aging*. Aging and Disease 2010, 1(1): 2-11.

Kocherhans Samira*, Madhusdan Amrita*, **Doehner Jana***, Breu Karin S., Nitsch Roger M., Fritschy Jean-Marc and Knuesel Irene. *Reduced Reelin expression accelerates amyloid-beta plaque formation and tau pathology in transgenic Alzheimer's disease mice*. J Neurosci 2010, 30(27):9228-40. (* = equal contribution)

Amrita Madhusudan*, Dimitrije Krstic*, **Jana Doehner**, Prisca Vogel, Claudine Imhof, Abigail Manalastas, Martina Hilfiker, Sandra Pfister, Cornelia Schwerdel, Frank LaFerla, Irene Knuesel. *Systemic immune challenges trigger and drive Alzheimer-like neuropathology in mice.* Submitted to Nature. (* = equal contribution)

ABSTRACTS

Jana Döhner, Samira Kocherhans, Urs Meyer, Corinne Sidler, Jean-Marc Fritschy, Irene Knuesel (2008). *Enhancing Reelin immunoreactivity by partial pepsin digestion: a tool for analyzing amyloid-like deposits in normal and pathological aging.* 6th Forum of European Neuroscience (FENS), Geneva, Switzerland

Jana Döhner, Jean-Marc Fritschy and Irene Knüsel (2008). *Reelin amyloid-like deposits in the aged brain of wild-type mice: A causative role in the pathogenesis of Alzheimer's disease?* Annual Meeting of the society of Neuroscience (SfN), Washington DC, USA

Jana Döhner, Jean-Marc Fritschy and Irene Knüsel (2009). *Reelin-positive plaques co-localize with murine amyloid-beta in the hippocampus of aged wild-type mice.* Swiss Society of Neuroscience (SSN) Annual Meeting, Fribourg, Switzerland

Jana Doehner, Amrita Madhusudan, Tina Notter, Jean-Marc Fritschy and Irene Knuesel (2010). *Enhanced Reelin and amyloid-beta immunoreactivity in postmortem rodent and human brain tissue following stringent protease pretreatment.* 7th Forum of European Neuroscience (FENS), Amsterdam, Netherlands

Jana Doehner, Amrita Madhusudan, Tina Notter, and Irene Knuesel (2010). *Aging enhances co-association of Reelin and amyloid-beta immunoreactivity in human and rodent brain tissue.* Annual Meeting of the society of Neuroscience (SfN), San Diego, CA, USA

Jana Doehner, Tina Notter, Dimitrije Krstic, Manuela Neumann and Irene Knuesel (2011). *Co-association of Reelin and amyloid-b immunoreactivity in rodent and human tissue is enhanced in the aged brain.* 10th International Conference on Alzheimer's and Parkinson's Diseases (AD/PD), Barcelona, Spain.